

ISSN 1980-9743

Soils and Rocks

Soils and Rocks

An International Journal of Geotechnical
and Geoenvironmental Engineering

Volume 40, N. 3

AB
—
MS



Volume 40, N. 3
September-December 2017

2017

**Soils and Rocks is an International Journal of Geotechnical and
Geoenvironmental Engineering published by**

**ABMS - Brazilian Association for Soil Mechanics and Geotechnical Engineering
Av. Queiroz Filho, 1700 - Torre A Sky, Sala 106 - Vila Hamburguesa
05319-000, São Paulo, SP
Brazil**

**SPG - Portuguese Geotechnical Society
LNEC, Avenida do Brasil, 101
1700-066 Lisboa
Portugal**



Issue Date: December 2017

Issue: 400 copies and 800 online-distributed copies

Manuscript Submission: For review criteria and manuscript submission information, see Instructions for Authors at the end.

Disclaimer: The opinions and statements published in this journal are solely the author's and not necessarily reflect the views or opinions of the publishers (ABMS and SPG). The publishers do not accept any liability arising in any way from the opinions, statements and use of the information presented.

Copyright: Authors and ABMS-Brazilian Society for Soil Mechanics and Geotechnical Engineering

SOILS and ROCKS

An International Journal of Geotechnical and Geoenvironmental Engineering

Editor Paulo Scarano Hemsí - Aeronautics Institute of Technology, Brazil

Co-editor José Couto Marques - University of Porto, Portugal

Executive Board

Waldemar Coelho Hachich
University of São Paulo, Brazil
António Topa Gomes
University of Porto, Portugal

Gustavo Ferreira Simões
Federal University of Minas Gerais, Brazil
Rafaela Cardoso
University of Lisbon, Portugal

Associate Editors

H. Einstein
MIT, USA
John A. Hudson
Imperial College, UK
Kenji Ishihara
University of Tokyo, Japan
Michele Jamiolkowski
Studio Geotecnico Italiano, Italy
Willy A. Lacerda
COPPE/UFRJ, Brazil

E. Maranha das Neves
Lisbon Technical University, Portugal
Nielen van der Merve
University of Pretoria, South Africa
Paul Marinos
NTUA, Greece
James K. Mitchell
Virginia Tech., USA
Lars Persson
SGU, Sweden

Harry G. Poulos
University of Sidney, Australia
Niek Rengers
ITC, The Netherlands
Fumio Tatsuoka
Tokyo University of Science, Japan
Luiz González de Vallejo
UCM, Spain
Roger Frank
ENPC-Cermes, France

Editorial Board Members

Roberto F. Azevedo
Federal University of Viçosa, Brazil
Milton Kanji
University of São Paulo, Brazil
Kátia Vanessa Bicalho
Federal University of Espírito Santo, Brazil
Omar Y. Bitar
IPT, Brazil
Lázaro V. Zuquette
University of São Paulo at São Carlos, Brazil
Fabio Taioli
University of São Paulo, Brazil
Tarcisio Celestino
University of São Paulo at São Carlos, Brazil
Edmundo Rogério Esquível
University of São Paulo at São Carlos, Brazil
Nilo C. Consoli
Federal Univ. Rio Grande do Sul, Brazil
Sandro S. Sandroni
Consultant, Brazil
Sérgio A.B. Fontoura
Pontifical Catholic University, Brazil
Ennio M. Palmeira
University of Brasília, Brazil
Luciano Décourt
Consultant, Brazil
Façal Massad
University of São Paulo, Brazil
Marcus Pacheco
University of the State of Rio de Janeiro, Brazil
Paulo Maia
University of Northern Rio de Janeiro, Brazil
Renato Cunha
University of Brasília, Brazil

Orencio Monje Vilar
University of São Paulo at São Carlos, Brazil
Maria Eugenia Boscov
University of São Paulo, Brazil
Eda Freitas de Quadros
BGTECH, Brazil
Tácio de Campos
Pontifical Catholic University of Rio de Janeiro, Brazil
Richard J. Bathurst
Royal Military College of Canada
Robert Mair
University of Cambridge, UK
Serge Leroueil
University of Laval, Canada
Mario Manassero
Politécnico di Torino, Italy
Luis Valenzuela
Consultant, Chile
Jorge G. Zornberg
University of Texas/Austin, USA
Andrew Whittle
MIT, USA
Pierre Bérest
LCPC, France
Peter Kaiser
Laurentian University, Canada
He Manchao
CUMT, China
Teruo Nakai
Nagoya Inst. Technology, Japan
Claudio Olalla
CEDEX, Spain
Frederick Baynes
Baynes Geologic Ltd., Australia

R. Kerry Rowe
Queen's University, Canada
R. Jonathan Fannin
University of British Columbia, Canada
Laura Caldeira
LNEC, Portugal
António S. Cardoso
University of Porto, Portugal
José D. Rodrigues
Consultant, Portugal
António G. Coelho
Consultant, Portugal
Luís R. Sousa
University of Porto, Portugal
Rui M. Correia
LNEC, Portugal
João Marcelino
LNEC, Portugal
António C. Mineiro
University of Lisbon, Portugal
António P. Cunha
LNEC, Portugal New
António G. Correia
University of Minho, Portugal
Carlos D. Gama
Lisbon Technical University, Portugal
José V. Lemos
LNEC, Portugal
Nuno Grossmann
LNEC, Portugal
Luís L. Lemos
University of Coimbra, Portugal
Ricardo Oliveira
COBA, Portugal

“Ad hoc” Reviewers (2017)

Alexandre Duarte Gusmão
UPE, Brazil
Alessander C.M. Kormann
UFPR, Brazil
Adilson do Lago Leite
UFOP, Brazil
Antonio Thomé
UPF, Brazil
Antônio Topa Gomes
FEUP, Portugal
Arsenio Negro Jr.
Bureau, Brazil
Anna Luíza M. Ayres da Silva
USP-Poli, Brazil
Bernadete Ragoni Danziger
UERJ, Brazil
Brajá Das
California State Univ., USA
Carlos Emmanuel Ribeiro Lautenschläger
PUC-Rio, Brazil
Castorina Vieira
FEUP, Portugal
Celeste Jorge
LNEC, Portugal
Celso Lima
FEUP/Portugal
Celso Romanel
PUC-RJ, Brazil
Christianne de Lyra Nogueira
UFOP, Brazil
Claudio Michael Wolle
USP-Poli, Brazil
Denise Gerscovich
UERJ, Brazil
Delma de Mattos Vidal
ITA, Brazil
Edgar Odebrecht
Geofoma, Brazil
Eurípedes Vargas
PUC-RJ, Brazil
Edmundo Rogério Esquivel
USP-S.Carlos, Brazil
Eda Quadros
BGTECH, Brazil
Eduardo Fortunato
LNEC, Portugal
Ennio Marques Palmeira
UnB, Brazil
Façal Massad
USP-Poli, Brazil
Fernando Saboya Albuquerque Jr.
UNF, Brazil
Filipe Telmo Jeremias
LNEC, Portugal
Frederico Falconi
ZF, Brazil
Giulliana Mondelli
UFABC, Brazil

Gisleine Coelho de Campos
IPT, Brazil
Gregório Luis Silva Araújo
UnB, Brazil
Hui Xu
China Univ. Mining & Technology, China
Hossein Soltani-Jigheh
Azarbaijan Shahid Madani Univ., Iran
Heraldo Nunes Pitanga
UFV, Brazil
Heraldo Luiz Giacheti
USP-S.Carlos, Brazil
He Manchao
China Univ. Mining & Technology, China
Ian Schumann Martins
UFRJ, Brazil
José Tadeu Balbo
USP-Poli, Brazil
José Maria de Barros
IPT, Brazil
José Jorge Nader
USP-Poli, Brazil
José Eduardo Quintanilha Menezes
FEUP, Portugal
José Leitão Borges
FEUP, Portugal
Jaime Domingos Marzionna
Engeos, Brazil
João Marcos Vaillant
CEFET-MG, Brazil
João Bilé Serra
LNEC, Portugal
Jorge Almeida e Souza
Univ. Coimbra, Portugal
Jorge Carvalho
FEUP, Portugal
Kátia Vanessa Bicalho
UFES, Brazil
Lúcio Flávio de Souza Villar
UFMG, Brazil
Luís Ribeiro e Souza
FEUP, Portugal
Larissa de Brum Passini
UFPR, Brazil
Luís Lemos
Univ. Coimbra, Portugal
Luciano Décourt
LD Eng. Consult., Brazil
Luiz Guilherme F.S. de Mello
Vectior, Brazil
Marcelo Monteiro da Rocha
USP, Brazil
Maurício Ehrlich
UFRJ, Brazil
Manuel Matos Fernandes
FEUP, Portugal
Maurício M. Sales
UFG, Brazil

Maria de Lurdes Lopes
FEUP, Portugal
Mafalda Laranjo
Inst. Politécnico de Viana do Castelo, Portugal
Maria Cláudia Barbosa
UFRJ, Brazil
Maria Giovana Parizzi
UFMG, Brazil
Michéle Dal Toe Casagrande
PUC-RJ, Brazil
Marcia Maria dos Anjos Mascarenhas
UFG, Brazil
Nuno Raposo
Inst. Politécnico de Viseu, Portugal
Nuno M. da Costa Guerra
Univ. Nova de Lisboa, Portugal
Nuno Cristelo
Univ. de Trás-os-Montes e Alto Douro, Portugal
Nilo Cesar Consoli
UFRGS, Brazil
Natália de Souza Correia
UFSCAR, Brazil
Orencio Monje Vilar
USP-S. Carlos, Brazil
Patricia Romão
UFG, Brazil
Paulo José Rocha Albuquerque
Unicamp, Brazil
Paulo José da Venda Oliveira
Univ. Coimbra, Portugal
Paul Mayne
GA Tech, USA
Pedro Guedes de Melo
Consulgeo, Portugal
Roberto Francisco Azevedo
UFV, Brazil
Roberto Quental Coutinho
UFPE, Brazil
Rodolfo Moreda Mendes
CEMADEN, Brazil
Rafaela Cardoso
IST, Portugal
Renato Pinto da Cunha
UnB, Brazil
Sara Rios
FEUP, Portugal
Saulo Batista de Oliveira
VOTORANTIM, Brazil
Sussumu Niyama
Tecnum, Brazil
Sérgio A. Barreto da Fontoura
PUC-RJ, Brazil
Thiago Luiz Coelho Morandini
CEFET-MG, Brazil
Tácio Mauro Pereira de Campos
PUC-RJ, Brazil
Vivian Silveira dos Santos Bardini
UNESP, Brazil
Willy Alvarenga Lacerda
UFRJ, Brazil

Soils and Rocks publishes papers in English in the broad fields of Geotechnical Engineering, Engineering Geology and Geoenvironmental Engineering. The Journal is published in April, August and December. Subscription price is US\$ 90.00 per year. The journal, with the name “Solos e Rochas”, was first published in 1978 by the Graduate School of Engineering, Federal University of Rio de Janeiro (COPPE-UFRJ). In 1980 it became the official magazine of the Brazilian Association for Soil Mechanics and Geotechnical Engineering (ABMS), acquiring the national character that had been the intention of its founders. In 1986 it also became the official Journal of the Brazilian Association for Engineering Geology and the Environment (ABGE) and in 1999 became the Latin American Geotechnical Journal, following the support of Latin-American representatives gathered for the Pan-American Conference of Guadalajara (1996). In 2007 the journal acquired the status of an international journal under the name of Soils and Rocks, published by the Brazilian Association for Soil Mechanics and Geotechnical Engineering (ABMS), Brazilian Association for Engineering Geology and the Environment (ABGE) and Portuguese Geotechnical Society (SPG). In 2010, ABGE decided to publish its own journal and left the partnership.

Soils and Rocks

1978,	1 (1, 2)
1979,	1 (3), 2 (1,2)
1980-1983,	3-6 (1, 2, 3)
1984,	7 (single number)
1985-1987,	8-10 (1, 2, 3)
1988-1990,	11-13 (single number)
1991-1992,	14-15 (1, 2)
1993,	16 (1, 2, 3, 4)
1994-2010,	17-33 (1, 2, 3)
2011,	34 (1, 2, 3, 4)
2012-2016,	35-39 (1, 2, 3)
2017,	40 (1, 2, 3)

ISSN 1980-9743

CDU 624.131.1

SOILS and ROCKS

An International Journal of Geotechnical and Geoenvironmental Engineering

Publication of**ABMS - Brazilian Association for Soil Mechanics and Geotechnical Engineering****SPG - Portuguese Geotechnical Society****Volume 40, N. 3, September-December 2017****Table of Contents***MANUEL ROCHA LECTURE**Stress History of Soils from Cone Penetration Tests*

P.W. Mayne

203

*ARTICLES**Stabilised Soil Layers Enhancing Performance of Transverse-Loaded Flexible Piles
on Lightly Bonded Residual Soils*

N.C. Consoli, V.P. Faro, F. Schnaid, R.B. Born

219

Anchored Retaining Walls in Granite Residual Soils I – Parametric Study

N. Raposo, A.T. Gomes, M.M. Fernandes

229

Anchored Retaining Walls in Granite Residual Soils II. A Method for Preliminary Design

N. Raposo, A.T. Gomes, M.M. Fernandes

243

*Influence of Traverse Velocity and Pump Pressure on the Efficiency
of Abrasive Waterjet for Rock Cutting*

P.B. Arab, T.B. Celestino

255

*Rainfall Effects on Pore Pressure Changes in a Coastal Slope of the Serra do Mar
in Santa Catarina*

A.A.M. González, L.B. Passini, A.C.M. Kormann

263

Development of a Cyclic Simple Shear Apparatus

M.B. Corte, L. Festugato, N.C. Consoli

279

The Undrained Strength of Soft Clays Determined from Unconventional and Conventional Tests

S.G.F.P. Lemos, P.J.M. Pires

291

Manuel Rocha Lecture



Manuel Rocha (1913-1981) was honoured by the Portuguese Geotechnical Society with the establishment of the Lecture Series bearing his name in 1984.

Having completed the Civil Engineering Degree at the Technical University of Lisbon (1938) he did post-graduate training at MIT. He was the driving force behind the creation of the research team in Civil Engineering that would lead to the foundation of the National Laboratory for Civil Engineering (LNEC), in Lisbon. He was Head of LNEC from 1954 to 1974 and led it to the cutting edge of research in Civil Engineering.

His research work had great impact in the area of concrete dams and rock mechanics. He was the 1st President of the International Society for Rock Mechanics and organized its 1st Congress in Lisbon (1966). He did consultancy work in numerous countries. He was Honorary President of the Portuguese Geotechnical Society, having promoted with great commitment the cooperation between Portugal and Brazil in the area of Civil Engineering, and member of the National Academy of Sciences of the USA. Recognized as a brilliant researcher, scientist and professor, with a sharp, discerning intellect allied to a prodigious capacity for work and management, he was truly a man of many talents.



The 2017 Manuel Rocha Lecturer was Prof. Dr. **Paul W. Mayne**, P.E., Ph.D., a professor of Civil & Environmental Engineering at the Georgia Institute of Technology. With 41 years in geotechnical engineering, Paul's expertise is in the areas of geotechnical site characterization, including cone, piezocone, dilatometer, and seismic tests with applications to foundation systems and ground modification. He has given invited lectures internationally and provides CPT workshops & short courses around the world. Of recent, he completed the 2007 Manual on Cone Penetration Testing (Synthesis 368: www.trb.org), SOA-1: Geomaterial Behavior & Testing at the 17th ICSMGE in Egypt in 2009, ASCE SOA lecture on in-situ testing (GeoOakland 2012), the 2013 Jennings Lecture in South Africa, 16th Sowers Lecture (2013), James Hoover Distinguished Lecture at Iowa State Univ. (2014), invited keynote lecture at CPT' 14, 2014 Hal Hunt Lecture at the 39th Annual DFI Conference, invited keynote lecture at ISC-5 Brisbane (2016), and the Nonveiller lecture in Zagreb (2016). Dr. Mayne is an active member of ASCE, TRB, DFI, ADSC, CGS, USUCGER, and ISSMGE. He served as the chair of the international committee on in-situ testing (TC 102) from 2000-2013 and as the ISSMGE Vice President for North America from 2013-2017. Of additional note, Paul has worked as a consultant on recent projects in Australia, Virginia, Washington, South Carolina, Ontario, Puerto Rico, Alabama, Georgia, Belgium, North Carolina, and Alaska. He is married with one daughter and plays bass guitar.

Soils and Rocks
v. 40, n. 3

Stress History of Soils from Cone Penetration Tests

P.W. Mayne

Abstract. Stress history is an important measurement in soils as it affects strength, stability, stiffness, and flow characteristics. The evaluation of the in-situ preconsolidation stress, or effective yield stress, from the results of piezocone penetration tests allows for an economical and expedient means to profile the stress history of clays, sands, and mixed soil types on geotechnical projects. The methodology is based on a derived analytical cavity expansion - critical state solution for clays and statistical inversion of data from calibration chamber tests on sands. Applications are given for case studies involving clay, silt, and sand where laboratory consolidation tests provide benchmark values for the stress history. Since yield stress demarcates contractive vs. dilative soil behavior, extended uses in screening soil susceptibility for concerns involving flow and cyclic liquefaction are also presented.

Keywords: clay, cone penetration, overconsolidation, piezocone, preconsolidation, sand, stress history, yield stress.

1. Introduction

The stress history of soils is a significant and important measure of its behavior in terms of stability, strength, deformational characteristics, and pore pressure behavior. The effective yield stress (σ_{vy}'), or preconsolidation stress ($\sigma_p' = P_c' = \sigma_{vmax}'$), represents the demarcation between normally-consolidated (NC) states and overconsolidated (OC) response. It also distinguishes the porewater pressures generated during shear which can either be positive or negative, and the volumetric strain characteristics that can be contractive or dilative.

Traditionally, the preconsolidation stress was defined as the maximum past stress that had been physically and mechanically applied to the soil, such as due to overburden erosion or glaciation. The more general term of effective yield stress ($\sigma_{vy}' = \sigma_p'$) has been recommended (*e.g.*, Leroueil & Barbosa 2000; Jardine *et al.*, 2003) since many other geological and environmental processes can result in a quasi-preconsolidation effect, such as ageing, cyclic loading, desiccation, repeated wetting-drying, groundwater changes, alternating freezing-thawing, bio-chemical bonding, etc.

2. Effective Yield Stress

The effective preconsolidation stress or yield stress of soils is best determined through a series of one-dimensional consolidation tests performed on undisturbed samples taken at different elevations in soil formation. A firm knowledge of the local engineering geology and terrain helps to put the stress history profile in a best perspective (Locat *et al.*, 2003). Figure 1 shows an example consolidation test conducted on a specimen of silty clay taken from a depth of 6.5 m at a highway embankment site in Evergreen, North Carolina ($w = 70.8\%$, $LL = 44\%$, $PI = 19\%$). Results are plotted in terms of void ratio (e) vs. log of effective ver-

tical stress (σ_v'), with a calculated in-situ effective overburden stress of $\sigma_{vo}' = 43$ kPa.

Using the classical construction technique from Casagrande (1936), a most probable magnitude of effective yield stress $\sigma_p' = 80$ kPa is determined. Following the orange dashed line, a minimum estimate of 65 kPa and maximum estimate of 90 kPa can also be extracted. Beyond this procedure, some 30 different graphical methods have been developed for the evaluation of σ_p' from consolidation test data (Ku & Mayne 2013).

The preconsolidation stress can be presented in dimensionless terms using a normalized form called the overconsolidation ratio (OCR), or the more generalized yield stress ratio (YSR), which is defined by:

$$YSR = \frac{\sigma_p'}{\sigma_{vo}'} \quad (1)$$

The yield stress and YSR affect the behavior of soils and the magnitude of many geoparameters. A partial listing of the influence and significance of σ_p' and YSR is given in Table 1.

Another convenient parameter for representation of soil stress history is the yield stress difference, YSD, which is defined (Locat *et al.*, 2003):

$$YSD = (\sigma_p' - \sigma_{vo}') \quad (2)$$

The advantage of the YSD is that it is constant with depth for soil deposits that have become preconsolidated by erosion, glaciation, and/or excavation, where in contrast, the magnitude of YSR decreases with depth (Mayne 2007b). For soils that have a quasi-preconsolidation effect due to ageing, a constant YSR with depth is observed.

While oedometer and consolidometer tests will remain the benchmark for determining stress history profiles, there are often cases when “undisturbed” samples are diffi-

Paul W. Mayne, Ph.D., Professor, Civil & Environmental Engineering, Georgia Institute of Technology, 790 Atlantic Drive, 30332-0355 Atlanta, GA, USA. e-mail: paul.mayne@ce.gatech.edu.
Invited Lecture, no discussions.
DOI: 10.28927/SR.403203

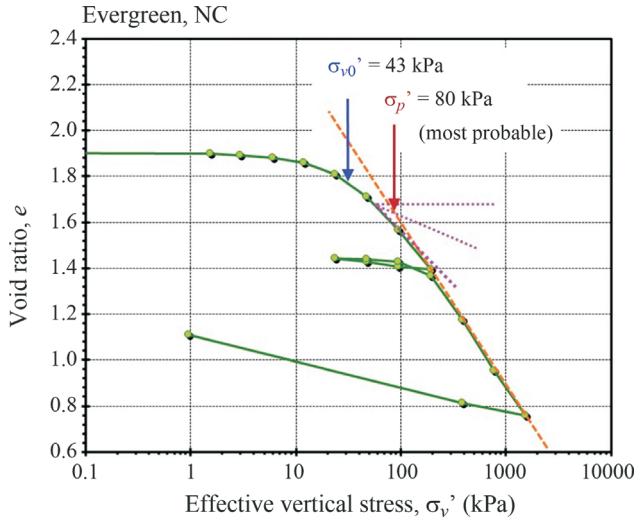


Figure 1 - Post-processing consolidation test results on clay from Evergreen, North Carolina for evaluating yield stress.

cult to procure because of the silty to sandy nature of the ground, inevitable sample disturbance, ageing and storage effects, and stress relief, as well as the expense and necessary time required for laboratory testing. Therefore, it has become of great interest and motivation in seeking in-situ test based methods to evaluate stress history profiles of soils, specifically using the cone penetration test (CPT) and piezocone (CPTu). These acquired data can be used to complement the laboratory program and fill in gaps between sampling depths and locations.

The interpretation of a full suite of geoparameters using CPT and CPTu is detailed elsewhere (Robertson 2009; Schnaid 2010; Mayne 2015).

3. Analytical SCE-CSSM Model for CPTU in Clays

A hybrid analytical model for piezocone penetration in clays was developed from Spherical Cavity Expansion

(SCE) theory and Critical State Soil Mechanics (CSSM), as detailed by Mayne (1991, 2005) and Chen & Mayne (1994). The SCE-CSSM formulation provides for separate evaluations for the YSR in terms of the net cone resistance ($q_{net} = q_t - \sigma_{vo}$) and/or the measured excess porewater pressure ($\Delta u = u_2 - u_0$):

$$YSR = 2 \left[\frac{\frac{q_t - \sigma_{vo}}{\sigma'_{vo}}}{M \left[\frac{2}{3} (\ln I_R + 1) + \frac{\pi}{4} + \frac{1}{2} \right]} \right]^{\frac{1}{\Lambda}} \quad (3)$$

$$YSR = 2 \left[\frac{\frac{\Delta u}{\sigma'_{vo}} - 1}{\frac{2}{3} M \ln(I_R) - 1} \right]^{\frac{1}{\Lambda}} \quad (4)$$

where $M = 6 \sin \phi' / (3 - \sin \phi')$ = frictional envelope in Cambridge University type $q - p'$ space, $I_R = G/s_u$ = undrained rigidity index, G = shear modulus, s_u = undrained shear strength, and $\Lambda = 1 - C_s/C_c$ = plastic volumetric strain potential, with C_s = recompression or swelling index, and C_c = virgin compression index. The value of $\Lambda \approx 0.8$ for most clays (Ladd & DeGroot 2003).

For soft to firm clays, the shear-component of porewater pressures is small (< 20%) of the total measured porewater pressures (Baligh 1986; Burns & Mayne 2002). Thus, neglecting that component, Eq. (4) can be reduced without much error to:

$$YSR = 2 \left[\frac{\frac{\Delta u}{\sigma'_{vo}}}{\frac{2}{3} M \ln(I_R)} \right]^{\frac{1}{\Lambda}} \quad (5)$$

Finally, by combining Eqs. (3) and (4), a third estimate of OCR can be formulated in terms of effective cone

Table 1 - Importance of yield stress and $YSR = \sigma_p' / \sigma_{vo}'$ on soil behavior and geoparameters.

Geoparameter or behavioral facet	Relevance
Degree of overconsolidation	Separates normally-consolidated (NC) and overconsolidated (OC) regions
Settlement analysis	Demarcates recompression from virgin compression on consolidation: $e - \log \sigma_v'$
Undrained shear strength	$s_u / \sigma_{vo}' = 1/2 \sin \phi' YSR^\Lambda$ where $\Lambda = 1 - C_s/C_c$ and ϕ' = friction angle
Geostatic lateral stress	$K_0 = (1 - \sin \phi') YSR^{\sin \phi'}$
Porewater pressures	Skempton's parameter A_f
Anchors the yield surface	Constitutive soil models
Elastic soil moduli	E' and E_u
Small-strain stiffness	$G_{max} = F(e) p' YSR^k$ where $F(e)$ = void ratio function p' = effective stress and k = plasticity effect
Screening for flow liquefaction of soils	Alternate to state parameter (ψ) separating contractive vs. dilative response
Screening for cyclic liquefaction potential	Supplement to CSR and CRR

resistance ($q_E = q_t - u_2$) that removes the reliance on rigidity index (I_R):

$$\text{YSR} = 2 \left[\frac{1}{1.95M + 1} \left(\frac{q_t - u_2}{\sigma'_{vo}} \right) \right]^{\frac{1}{\Lambda}} \quad (6)$$

The above equations can be simplified from power law expressions to form linear equations for evaluating effective yield stress in intact clays. Adopting a value $\Lambda = 1$, the three CPTu formulae given by Eqs. (3), (5), and (6) are reduced to:

$$\sigma'_p = \frac{q_t - \sigma_{vo}}{M(1 + \frac{1}{3} \ln I_R)} \quad (7)$$

$$\sigma'_p = \frac{u_2 - u_0}{\frac{1}{3} M \ln I_R} \quad (8)$$

$$\sigma'_p = \frac{q_t - u_2}{0.957M + 0.5} \quad (9)$$

3.1. Case study – Hartford, Connecticut

Geotechnical investigations for a five-story hotel in Hartford, Connecticut included soil borings and series of seismic piezocone tests (SCPTu) for settlement and bearing capacity analyses of shallow spread footings. The site is located adjacent to the Connecticut River and a representative SCPTu is shown in Fig. 2. The profile indicates an upper 11.5 m thick sand stratum underlain by a firm clay that extends to about 26 m. Lab data from the nearby Bissell Bridge are available (Long *et al.*, 1978), with a summary of drained and undrained triaxial compression tests indicating

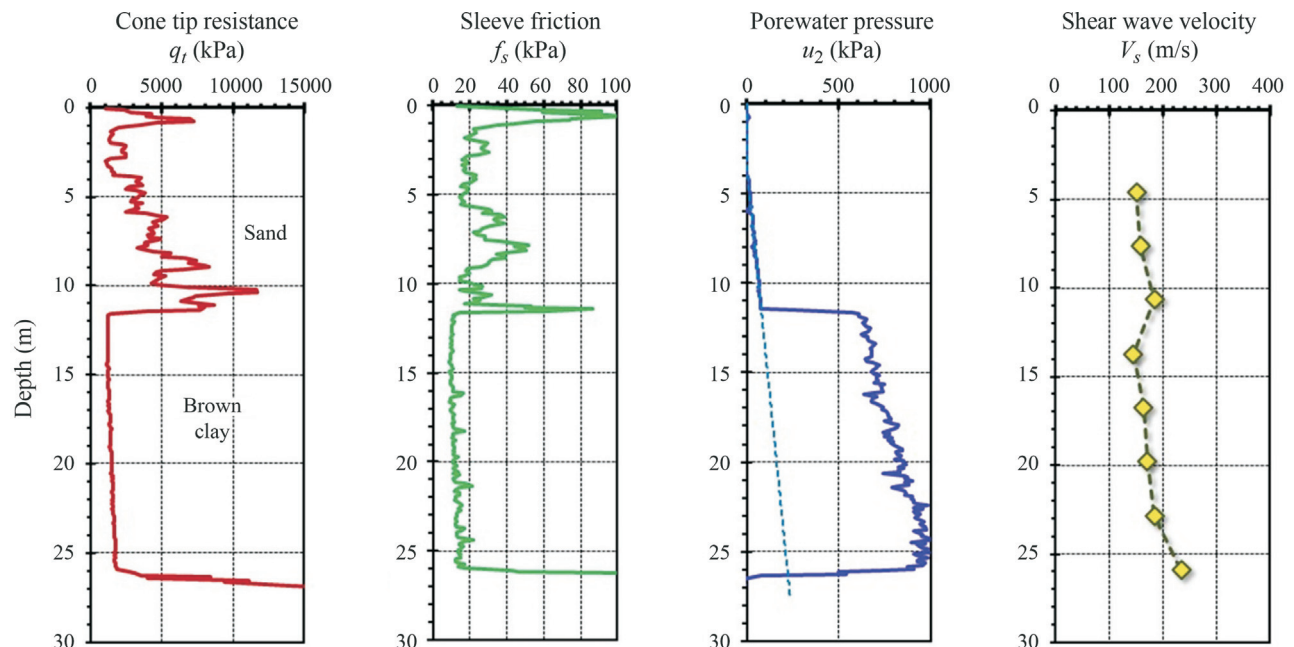


Figure 2 - Representative seismic piezocone sounding at site in Hartford, Connecticut.

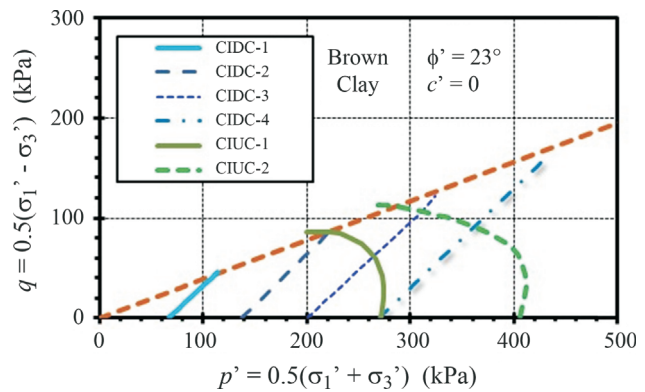


Figure 3 - Effective stress paths for CIDC and CIUC tests on brown clay at Bissell Bridge, Hartford, Connecticut (data from Long *et al.*, 1978).

an effective stress friction angle $\phi' = 23^\circ$ for the brown clay, as presented in Fig. 3. The SCPTu results can be used to estimate the rigidity of the clay (G taken at 50% of strength) from a recent formulation developed by Krage *et al.* (2014):

$$(I_R)_{50} = \frac{1.81G_0}{(q_{net})^{0.75} (\sigma'_{vo})^{0.25}} \quad (10)$$

where $G_0 = \rho_t V_s^2$ is the small-strain shear modulus and ρ_t = total soil mass density. For the current data, an average value of $I_R = 127$ was obtained.

Using Eqs. (7), (8), and (9) with $\phi' = 23^\circ$ and $I_R = 127$ gives the three separate and corresponding profiles of yield stress and YSR shown in Fig. 4. These agree well with the results of one-dimensional consolidation tests reported by Long *et al.* (1978).

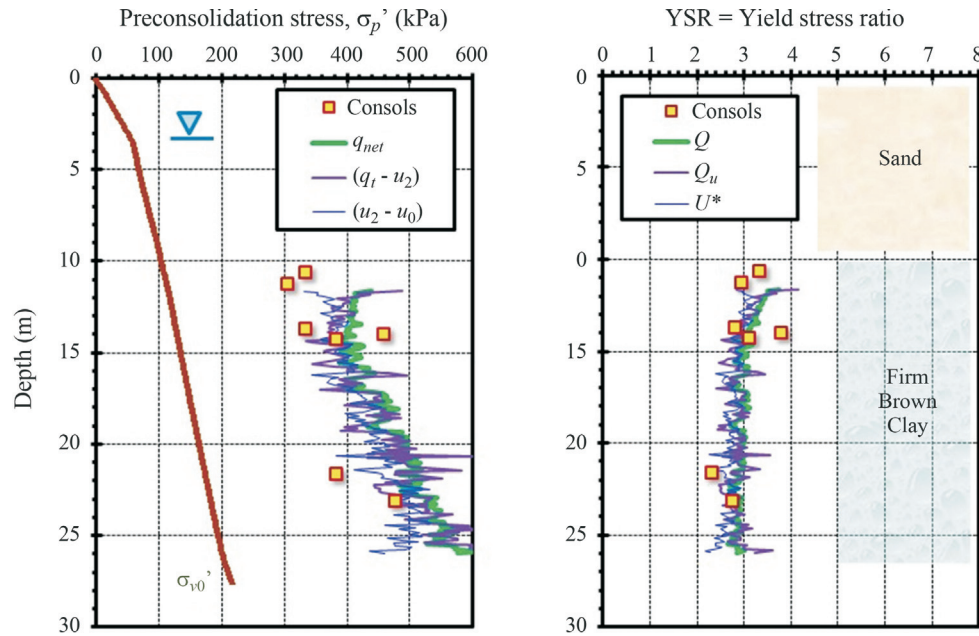


Figure 4 - Profiles of effective yield stress and YSR from consolidation tests and SCPTu at Hartford site.

3.2. Yield stresses from CPTU in soft inorganic clays

The full range for measured effective stress friction angle of natural clays is in the range $17^\circ \leq \phi' \leq 43^\circ$ (Diaz-Rodriguez *et al.*, 1992). A review of triaxial data from 453 clays indicates a mean $\phi' = 28.6^\circ$ with standard deviation S.D. $\pm 5.0^\circ$ (Mayne 2013). Ranges of the rigidity index are much larger, yet the SCE-CSSM expressions are a function of $\ln(I_R)$, so much more forgiving in exactitude. Shear modulus is highly nonlinear from the nondestructive range at G_0 to intermediate values at medium strains (G) and low values at peak strength (Viana da Fonseca *et al.*, 2011). Full ranges of laboratory-measured rigidity indices for soft clays is reported as: $40 \leq I_R \leq 600$ that decreases with increasing YSR (Casey *et al.*, 2016). A default value is often taken as $I_R = 100$ (*e.g.*, Teh & Houlsby 1991).

For intact inorganic clays of low sensitivity and low OCR < 3 , the SCE-CSSM expressions can be further simplified for practical use by adopting characteristic values of $\phi' = 30^\circ$ and $I_R = 100$ (Mayne 2001, 2005):

$$\sigma'_p = 0.33(q_t - \sigma_{v0}) \quad (11)$$

$$\sigma'_p = 0.54(u_2 - u_0) \quad (12)$$

$$\sigma'_p = 0.60(q_t - u_2) \quad (13)$$

Of course, these coefficients should be adjusted based on local geologies and site-specific geomaterials, where possible.

These relationships have been studied for a wide variety of clays, including statistical studies involving: 206 different sites (Chen & Mayne 1996); 22 sites in Canada (Demers & Leroueil 2002); 17 Norwegian clays (Karlsrud *et al.*, 2005); as well as individual sites, *e.g.*, Pisa, Italy

(Jamiolkowski & Pepe 2001); Costa Rica (Eller *et al.*, 2014). Results from Swedish clays give similar values however the coefficients appear to trend with plasticity index (Larsson & Mulabdic 1991; Larsson & Åhnberg 2005), whereas the study involving clays of eastern Canada did not show such a trend (Demers & Leroueil 2002).

3.3. Soft clay at Torp, Sweden

For soft intact clays, it is warranted to utilize all three equations, as redundancy can be helpful in geotechnical site characterization. If the three methods show consensus, then this helps to validate a “well-behaved” clay and encourages further use of these relationships in the geological setting. An illustrative application of all three solutions given by Eqs. (11), (12), and (13) is given in Fig. 5 for a soft clay site in Torp, Sweden (Larsson & Åhnberg 2003). The estimated profiles of σ'_p and YSR from the CPTu-estimates compare well with the rather large set of consolidation test results at this site.

If the three methods show disparities, then a closer examination and scrutiny of the laboratory and/or field data may be warranted, perhaps providing justification that additional testing and investigation should be conducted. If unusual mineralogy exists in the soil (*i.e.*, calcite, diatoms, forams, etc.), it may be possible to re-tune these equations for the particular geologic formation attributes (*e.g.*, Mayne 2005).

In highly sensitive or structured clays, it has been recognized that Eq. (11) gives a slight underprediction in the σ'_p profile, while a serious overestimation occurs with Eq. (12) and a large underestimate when using Eq. (13). For clays with a very pronounced strain-softening after peak in

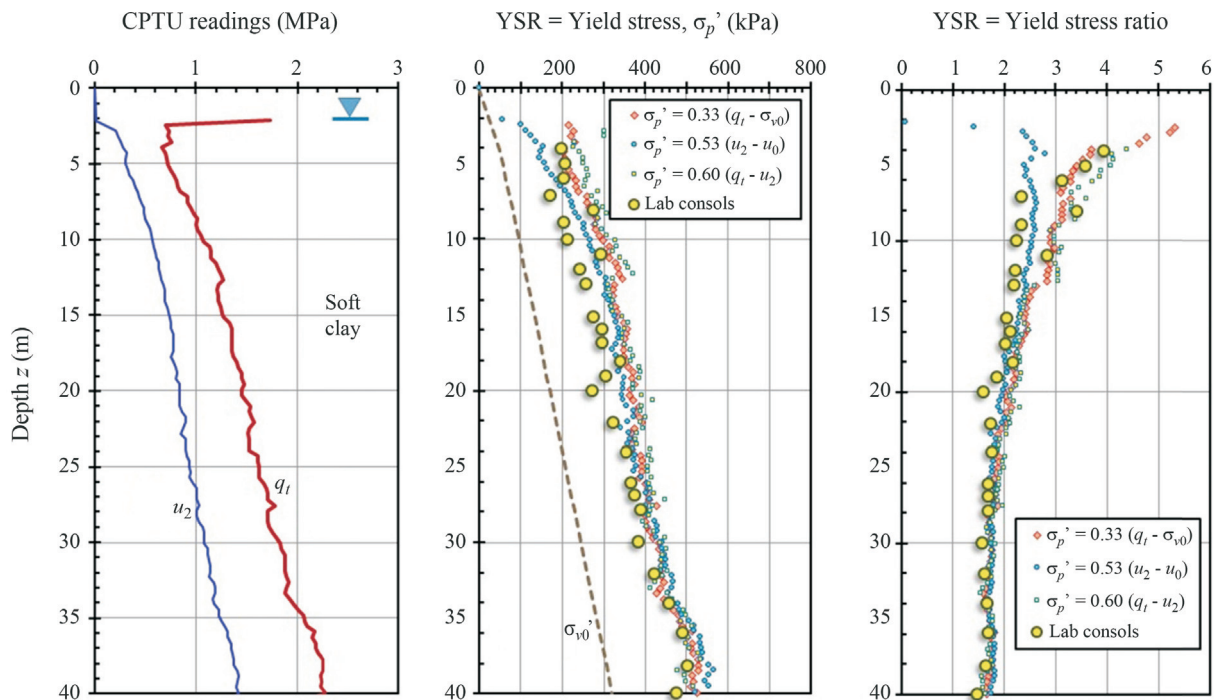


Figure 5 - CPTu data and YSR evaluations for Torp clay, Sweden (data from Larsson & Åhlberg 2003).

their stress-strain-strength behavior, a modified SCE-CSSM is available (Agaiby & Mayne 2018).

3.4. Yield stresses in organic clays using CPTu

The fitted coefficients in Eqs. (11), (12), and (13) for a number of soft organic clays in Brazil are reportedly quite different (Coutinho & Bello 2014). For instance, $0.125 q_{net}$ and $0.154 q_E$ are recommended (Baroni & Almeida 2017). This may reflect either a higher operational value of friction angle and/or rigidity index than the above adopted “characteristic” values used in the SCE-CSSM solution, or perhaps can be related to the organic content and mineralogy of these clays. An adjustment for the coefficients is necessary for the organic sulfide clays of Sweden (Larsson *et al.*, 2007). Here, the normal coefficients (0.33, 0.53, 0.60) are better fitted with values (0.22, 0.68, 0.28).

In lieu of adjusting the coefficients, an alternative approach to addressing σ_p' in organic clays is offered in the Section 5 of this paper.

4. Yield Stress Evaluation in Sand from CPT

A statistical review of over 626 calibration chamber tests on 26 different clean sands of silica and quartz constituency has been compiled (Mayne 2001). By inversion, this study determined relationships between the measured net cone resistance (q_{net}) and the applied stress state, including effective vertical stress (σ_{vc}'), lateral stress ratio ($K_0 = \sigma_{vc}'/\sigma_{vc}'$), and induced OCR, as summarized in Fig. 6. A direct expression for evaluating the YSR in clean sands is given by (Mayne 2005):

$$YSR = \frac{0.192 \left(\frac{q_{net}}{\sigma_{atm}} \right)^{0.22}}{(1 - \sin \phi') \left(\frac{\sigma'_{vo}}{\sigma_{atm}} \right)^{0.31}} \left[\frac{1}{\sin \phi' - 0.27} \right] \quad (14)$$

Taking a characteristic value of friction angle $\phi' = 35.5^\circ$ for clean sands, Eq. (14) reduces to the linear format:

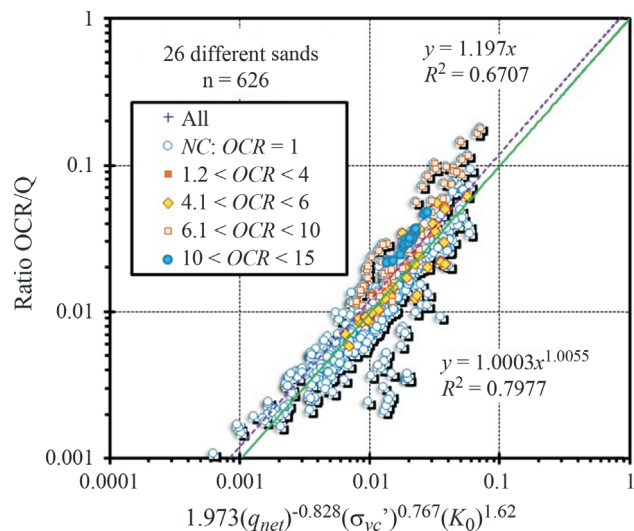


Figure 6 - Inversion relationship from CPT chamber tests on 26 different quartz-silica sands.

$$\sigma'_p = 0.08 q_{net}^{0.7} \sigma_{am}^{0.3} \tag{15}$$

Using SI units, the reference stress is $\sigma_{am} = 1 \text{ bar} = 100 \text{ kPa}$, therefore Eq. (15) further diminishes to the even simpler expression:

$$\sigma'_p = 0.32 q_{net}^{0.7} \text{ (units of kPa)} \tag{16}$$

which bears an uncanny resemblance to the expression for clay given by Eq. (11). As shown by Fig. 7, the simplified approach for clean sands compares well with the more rig-

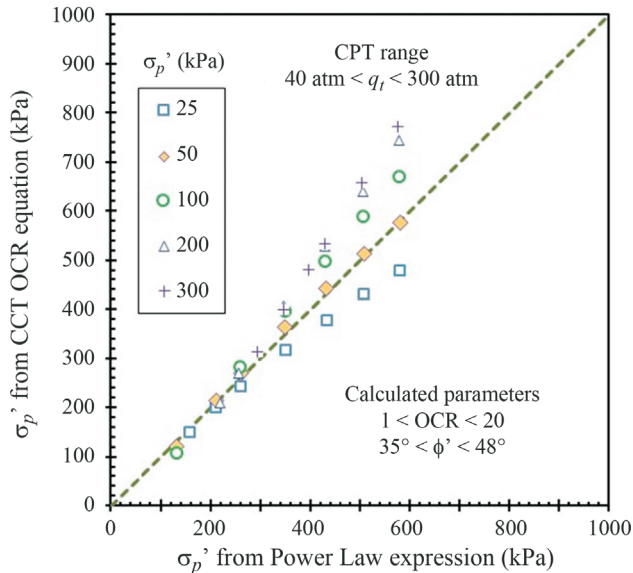


Figure 7 - Comparison of yield stress of sands from statistical algorithm and simplified solution.

orous algorithm given by Eq. (14) for the specified ranges of ϕ' , stress level (σ'_{vc}), and normalized cone resistance. For high stress levels and high values of ϕ' , the simplified approach will underpredict the yield stresses.

4.1. Case study from Blessington Sand Site, Ireland

The aforementioned approach can be applied to a case study involving dense OC sands in Blessington, Ireland (Doherty *et al.*, 2012). The site is used by Univ. College Dublin for offshore pile research (Gavin *et al.*, 2013). The glacially-derived dense fine sands have an in-place relative density around 100% and mean particle size: $0.10 < D_{50} \text{ (mm)} < 0.15 \text{ mm}$. Mineralogies include a predominance of quartz with calcite component, and subsets of feldspar, mica, and kaolinite fractions.

Measured cone tip resistances from 4 CPT soundings at the test site are presented in Fig. 8a. Samples of the sand were procured using sonic drilling methods that were later tested in the laboratory consolidometer to define the yield stress (σ'_p) per Casagrande method. The interpreted profiles of yield stress from the simplified CPT approach are shown in Fig. 8b along with a comparison to the lab reference values, with good agreement evident.

5. Generalized Profiling of YSR by CPT

For the general case of evaluating effective yield stress in all soil types, Fig. 9 provides a compilation of data from a variety of natural formations, including sands, silts, clays, and mixed geomaterials. The independent expres-

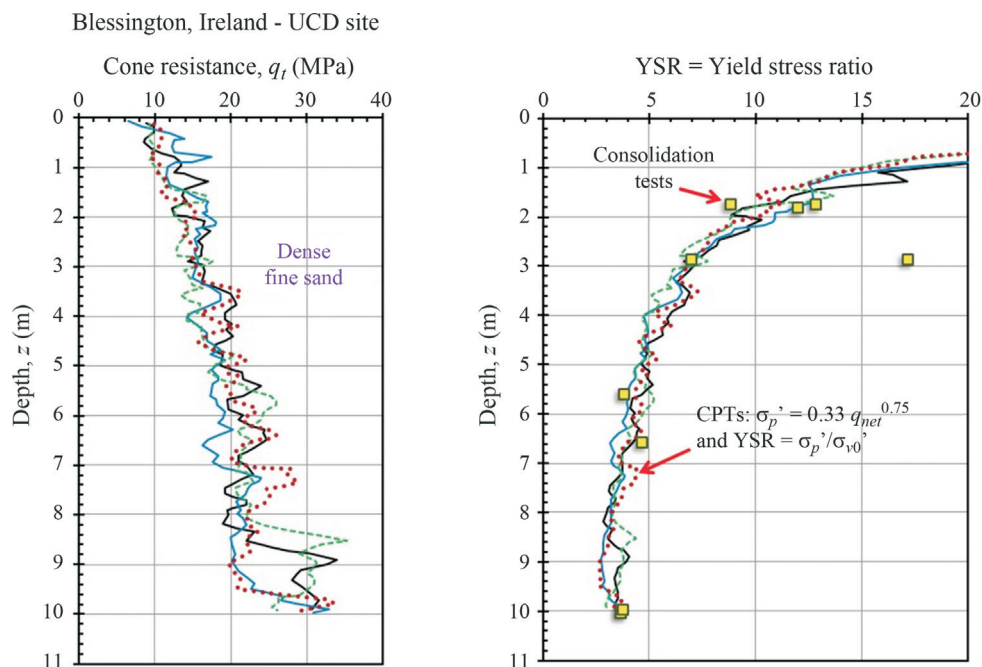


Figure 8 - Profiles of cone resistance and yield stress ratio in dense overconsolidated sands at Blessington, Ireland (data from Doherty *et al.*, 2012).

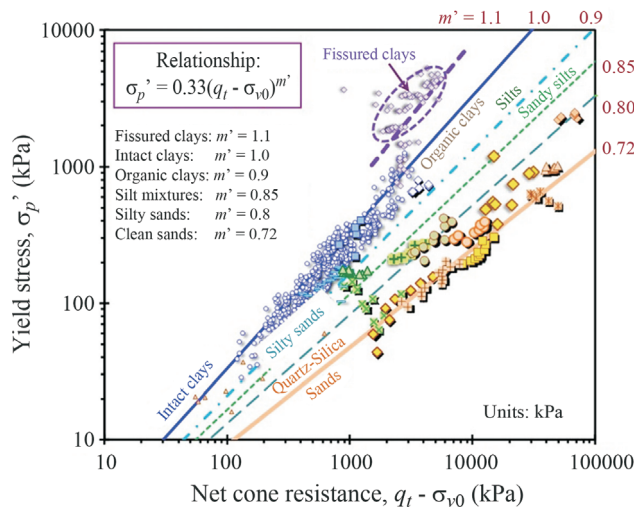


Figure 9 - Yield stress vs. net cone resistance for wide range of geomaterials (after Mayne, Coop, Springman, Huang, and Zornberg 2009).

sions for clays and sands can be united to provide the general format:

$$\sigma'_p = 0.33(q_t - \sigma_{v0})^{m'} \left(\frac{\sigma_{atm}}{100} \right)^{1-m'} \quad (17)$$

where the exponent m' increases with fines content and decreases with mean grain size. Specifically, the value of $m' \approx 0.72$ in clean quartz sands, 0.8 in silty sands, 0.85 in silts, and is 1.0 in intact clays of low sensitivity. It may even take on values of 1.1+ in fissured geomaterials. If only SI units are used (kPa), the form simply becomes:

$$\sigma'_p = 0.33(q_t - \sigma_{v0})^{m'} \quad (\text{in kPa}) \quad (18)$$

For soft organic clays, it appears the exponent takes on value of around $m' = 0.9 \pm 0.1$, thus site-specific calibrations will be required when working with these soils. As indicated in Section 3.5, an alternate approach is to adopt $m' = 1$ and employ a lower coefficient.

5.1. Yield stress exponent from CPT material index

The CPT material index I_c is used to evaluate soil behavioral type from cone penetrometer readings in natural soil formations (e.g., Riyis & Giacheti 2017), mine tailings (Schnaid *et al.*, 2014), and soil liquefaction assessment (Rodrigues *et al.*, 2016). Details are given by (Robertson 2009) where the index is determined by:

$$I_c = \sqrt{(3.47 - \log Q_m)^2 + (1.22 + \log F)^2} \quad (19)$$

where Q_m = normalized cone resistance that is defined by:

$$Q_m = \frac{q_t - \sigma_{v0}}{\left(\frac{\sigma'_{v0}}{\sigma_{atm}} \right)^n} \quad (20)$$

and the normalized sleeve friction (F) is determined from:

$$F(\%) = \frac{100f_s}{q_t - \sigma_{v0}} \quad (21)$$

The exponent “ n ” varies from 1 in intact clays to around 0.5 in sands. It is specifically determined from (Robertson 2009):

$$n = 0.381I_c + 0.05 \left(\frac{\sigma'_{v0}}{\sigma_{atm}} \right) - 0.05 \leq 1.0 \quad (22)$$

Thus, an iterative solution is needed to find I_c . In terms of soil classification, sands are identified when $I_c < 2.05$ while clays are found when $I_c > 2.95$. Intermediate soil types to these values include sandy mixtures and silty mixtures that are separated at $I_c = 2.60$, which is also the threshold for soil behavior: *i.e.*, drained when $I_c < 2.60$ and undrained when $I_c > 2.60$.

The material index I_c also provides a means of quantifying the magnitude of the yield stress exponent m' for the automatic CPT profiling of σ'_p in homogeneous soils, heterogeneous deposits, mixed geomaterials, and stratified formations. Figure 10 shows the trend between m' and CPT index (I_c) given by:

$$m' = 1 - \frac{0.28}{1 + \left(\frac{I_c}{2.65} \right)^{25}} \quad (23)$$

Where possible, the interpreted σ'_p results should be cross-checked and validated with other information, such as the results from one-dimensional consolidation tests on high-quality undisturbed samples, as well as the geologic stress history. In certain cases, additional results and corroboration may be obtained by running other in-situ tests, such as the flat plate dilatometer test (DMT) and/or vane shear test (VST), as discussed elsewhere (Schnaid 2009).

5.2. British Columbia

A representative SCPTu sounding shows a stratified soil profile from the Golden Ears Bridge south of Vancouver, British Columbia in Fig. 11 (Niazi *et al.*, 2010). The profile indicates silty to sandy layers that occupy the upper 40 m and overlie deeper deposits of clays to sensitive clays that extend to at least 95 m below grade. The sand-clay demarcation is evident from the change in porewater pressures readings at around 40 m, as well as the CPT material index profile shown in Fig. 12. Yet despite the abrupt transitions from silts to sands to clays, the post-processing of the CPT data in these geologically-related Holocene units

shows a consistent and gradual yield stress profile indicating lightly-overconsolidated sediments with low YSRs. Although no lab consolidation tests were available, estimated

yield stresses from shear wave velocity measurements (Mayne 2005) confirm the low values of $YSR \approx 1.5$, as shown by Fig. 12.

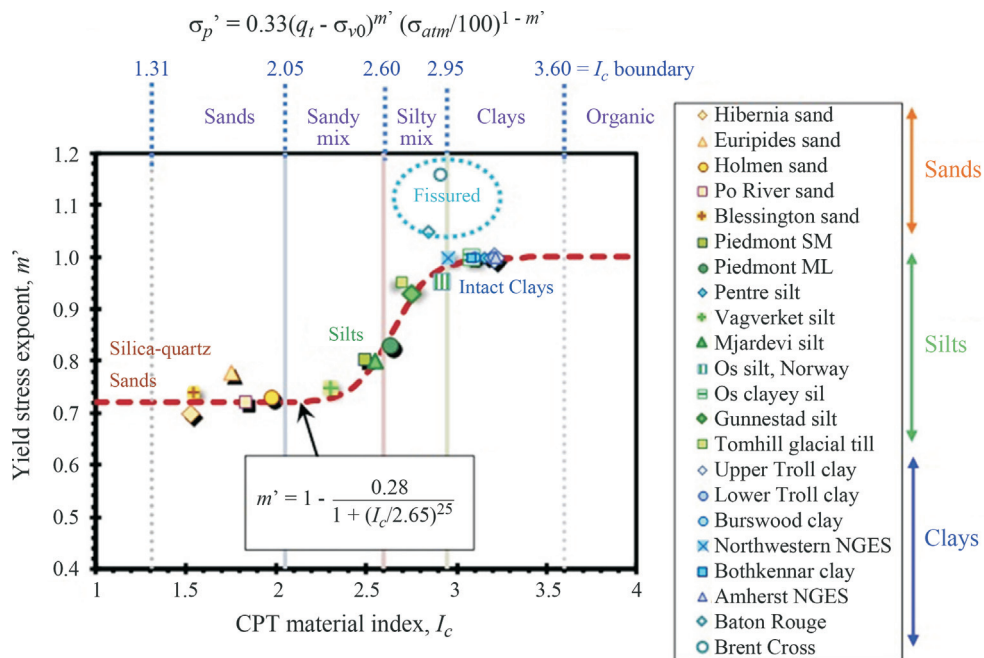


Figure 10 - Exponent m' for yield stress evaluation vs. CPT material index in non-cemented quartz-silica sands and inorganic clays of low sensitivity.

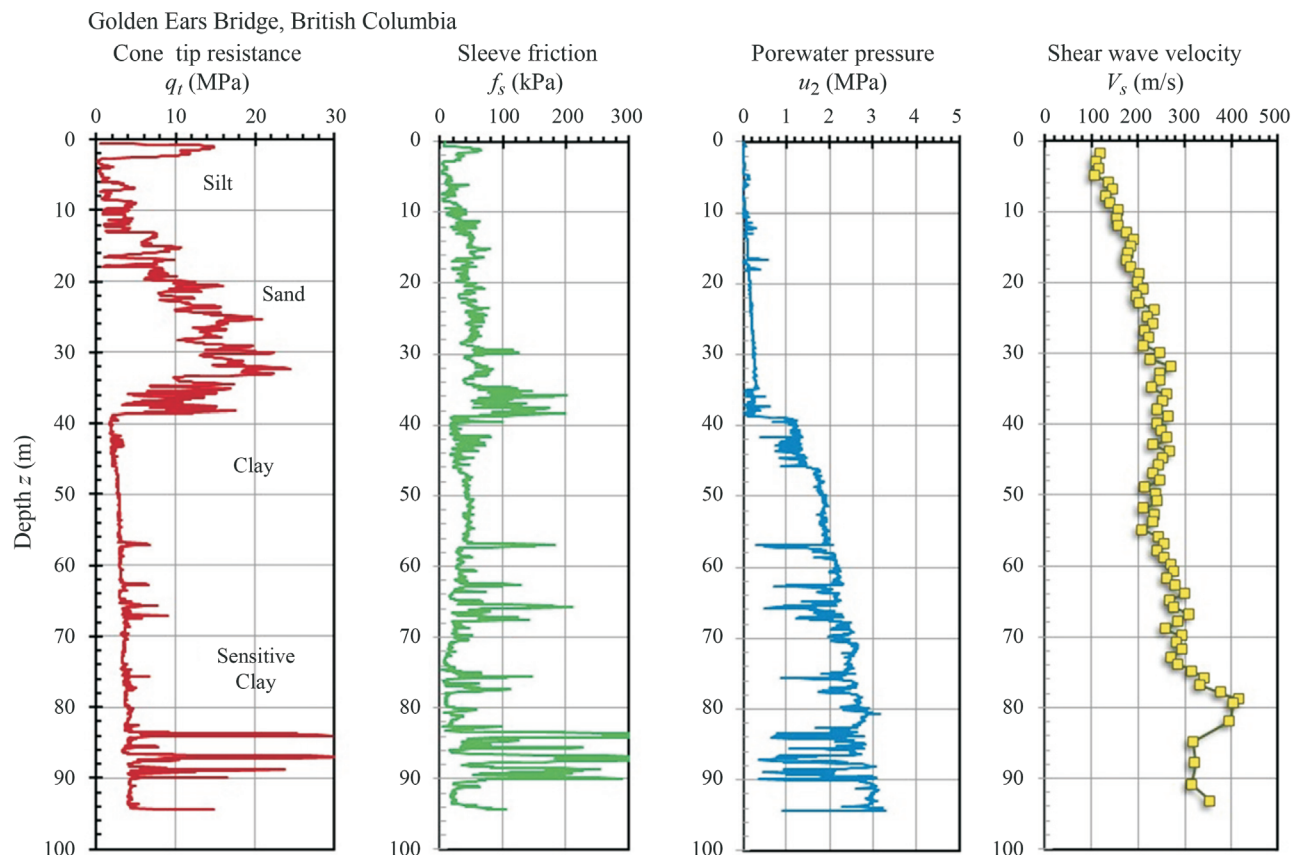


Figure 11 - Representative SCPTu at Golden Ears Bridge, BC (Niazi *et al.*, 2010).

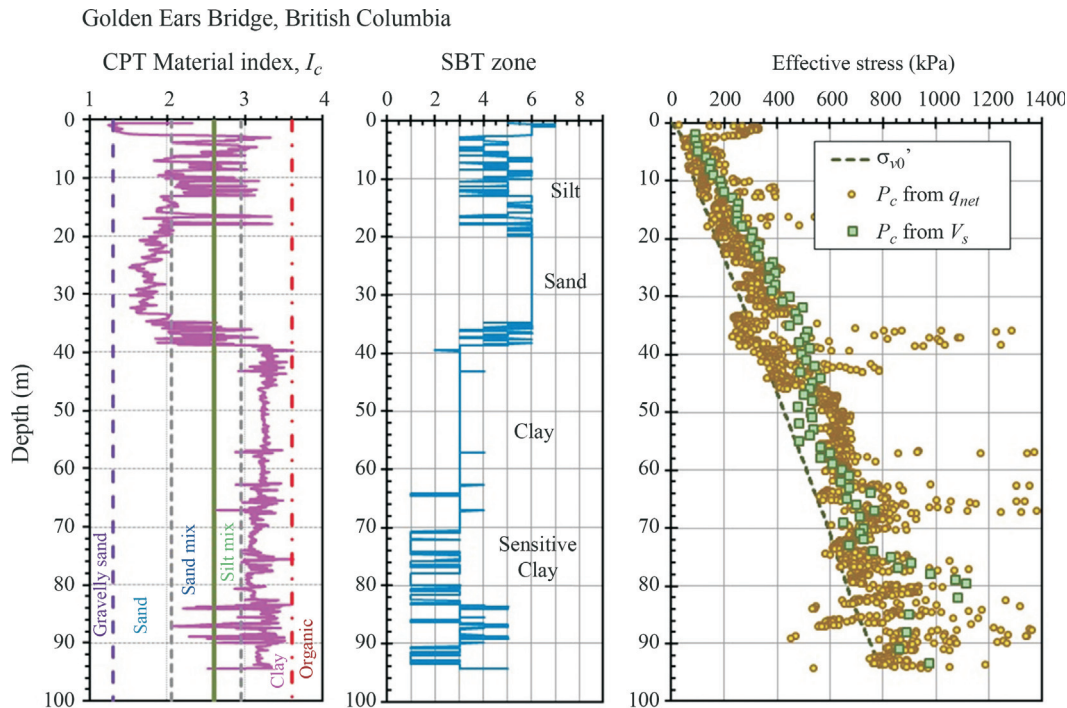


Figure 12 - Interpreted profiles at Golden Ears Bridge: (a) CPT material index; (b) soil behavioral type; and (c) effective yield stresses.

6. Soil Liquefaction

Two primary concerns in soil dynamics include: (a) flow liquefaction associated with mine tailings and dam stability; and (b) cyclic liquefaction caused by earthquakes. For both topics, critical state soil mechanics (CSSM) provides a rational and useful framework for the understanding and evaluation of soils that are prone to liquefaction (Viana da Fonseca 2011).

The approach to using CSSM for flow and cyclic liquefaction in sands has been via use of the state parameter: $\psi = e_0 - e_{CSL}$, where e_0 = initial in-situ void ratio and e_{CSL} = void ratio at critical state for constant effective stress (Jefferies & Been 2006; Idriss & Boulanger 2008). Sands that are prone to liquefaction are contractive and have a characteristic $\psi > 0$, while in contrast, dilative sands are not so susceptible and exhibit $\psi < 0$. The value of $\psi = 0$ is therefore a theoretical screening value, however, often a threshold $\psi = -0.05$ has been adopted for practical purposes and conservative benchmark (Robertson 2010).

While ψ works well, the methodology can be alternatively represented in terms of YSR just as effectively. Herein, we shall explore its vantages within a simplified version of CSSM (Mayne *et al.*, 2009; Holtz *et al.*, 2011). As presented in Fig. 13, the critical state line (CSL) can be represented in terms of ψ as a drained stress path, or alternatively as an equivalent YSR, termed YSR_{CSL} . In fact, YSR and ψ have been interrelated through their compressibility parameters (C_c, C_s) and frictional properties (ϕ'), as shown by Been *et al.* (1988) and Plewes *et al.* (1992).

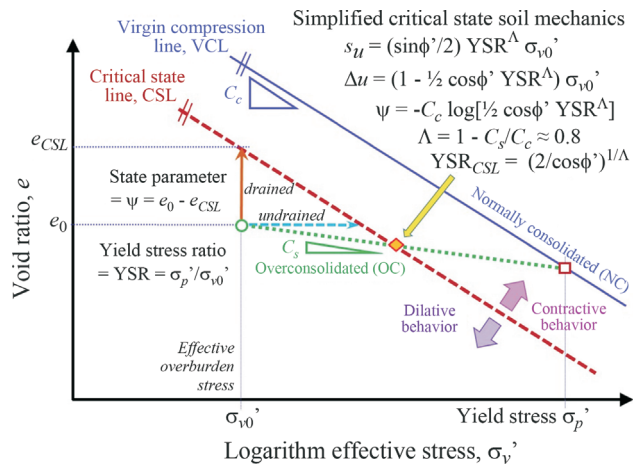


Figure 13 - Simplified critical state soil mechanics and definition of state parameter.

For the mode of simple shear, simplified CSSM provides the magnitude of excess porewater pressures during undrained shearing:

$$\Delta u = (1 - \frac{1}{2} \cos \phi' \cdot YSR^\Lambda) \sigma'_{v0} \quad (24)$$

For clays, a characteristic value of $\Lambda = 0.80 \pm 0.10$ is well recognized (Ladd & DeGroot, 2003). Compressibility parameters for various sands were reviewed by Been *et al.* (1987) including Monterey, Ticino, Hokksund, Ottawa, Reid Bedford, and Hilton Mines. The measured C_c and C_s values indicate an overall mean $\Lambda = 0.790$ with S.D. = 0.164 (n = 24) for these sands. Thus, the value of

$\Lambda = 0.80$ can be considered characteristic for soils in general.

The boundary separating contractive and dilative soil behavior is defined when $\Delta u = 0$ during undrained shear. The corresponding YSR at critical state is then calculated as:

$$YSR_{CSL} = \left(\frac{2}{\cos \phi'} \right)^{\frac{1}{\Lambda}} \quad (25)$$

Analogous to the ψ threshold, this YSR_{CSL} becomes the threshold for identifying contractive unstable soils from those that are dilative and rather stable (Mayne *et al.*, 2017). In fact, Robertson (2012) suggested that a $YSR = 4$ was a reasonable threshold for this purpose.

For purposes of calculating the yield stress ratio at the critical state, the following equations can be recommended for the effective friction angle (Mayne 2007a):

when $I_c < 2.6$,

$$\phi' = 17.6^\circ + 11.0^\circ \log(Q_m)$$

when $I_c > 2.6$,

$$\phi' = 29.5^\circ B_q^{0.121} [0.256 + 0.336 B_q + \log(Q_m)]$$

6.1. Flow liquefaction example - tailings

At a gold mine facility (site A) in western USA, results from the processing of a representative CPTu sound-

ing in tailings comprised of sandy silts are presented in Fig. 14 (Been *et al.*, 2012). Adjacent soil borings with sampling, and laboratory testing indicated that most recovered samples had fines contents (FC) ranging from 45% to 75%, generally $FC > 50\%$. Per the Unified Soil Classification System (USCS), these tailings are predominantly low-plasticity sandy silts (ML) with clay fractions (CF < 0.002 mm) less than 10%. In addition to the q_t profile in Fig. 14a, the soil behavioral type classification system using the CPT material index (I_c) is shown in Fig. 14b, indicating primarily silty mixtures with mixed sandy zones, in agreement with the borings and lab results.

The interpreted yield stresses are generally just above the current effective overburden stresses, thus these geomaterials are normally- to lightly-overconsolidated (NC to LOC). At depths > 3 m, Fig. 14c shows the YSR profiles are generally below 3 and thus contractive over the rest of the sounding to 22 m. This agrees well with the more elaborate CPT analysis for state parameter (Been *et al.*, 2012) shown in Fig. 14d, clearly showing a $\psi > -0.05$ over most of the profile.

6.2. Cyclic liquefaction example - Christchurch

The same procedure using a threshold YSR_{CSL} to separate contractive vs. dilative soils can be implemented for screening cyclic liquefaction susceptibility (Mayne & Styler 2018).

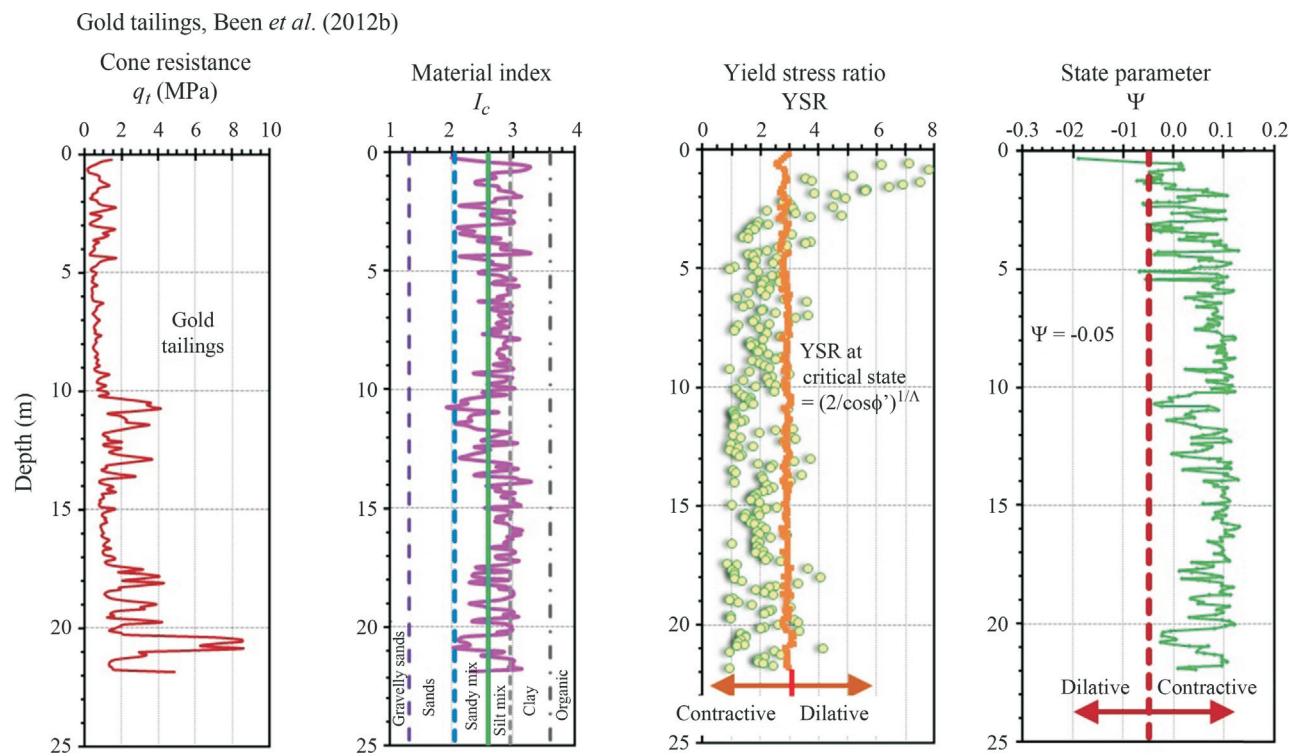


Figure 14 - Flow liquefaction evaluation in gold tailings with profiles: (a) cone resistance, (b) CPT material index, (c) threshold YSR approach, and (d) state parameter (data from Been *et al.*, 2012).

A selected liquefaction case study at Site 19 in Brighton, a suburb of Christchurch, New Zealand that had experienced damages during the 2010-2011 sequences of large earthquakes will be used for illustration. Full details on the liquefaction site are given in Green *et al.* (2014) and a quick summary of the post-processing of the CPTu sounding is presented in Fig. 15. The measured cone tip resistance (q_t) is shown in Fig. 15a with corresponding soil behavior type by CPT index I_c given in Fig. 15b, indicating primarily sands over the 14 m profile, with a shallow silty sand to sandy silt evident in the 2 to 3 m depth range.

Using the YSR_{CSL} threshold clearly shows contractive soil layer in the 2-3 m depths and a thicker critical layer from 6 to 10.5 m. A full cyclic stress-based liquefaction analysis was performed for this site using the standard procedures (Robertson & Wride 1998; Youd *et al.*, 2001). This approach involves a number of steps, including: (a) evaluating of the cyclic stress ratio, CSR; (b) adoption of a threshold triggering curve termed the cyclic resistance ratio, CRR; (c) calculating the stress-normalized cone resistance, Q_m ; (d) evaluating CPT index, I_c ; (e) correcting the cone resistance to an equivalent value for clean sands, designated: Q_{m-cs} based on estimated fines content: $Q_{m-cs} = K_c Q_m$. For this site, a moment magnitude $M_w = 6.2$ and peak ground acceleration $PGA = 0.35$ g were used in the standard liquefaction procedures to determine the level of ground shaking (*i.e.*, CSR) and the calculated Q_{m-cs} profile provided the available soil resistance. This determined the relative profiles of $CSR_{7.5}$ and $CRR_{7.5}$ as shown in Fig. 15d. Green *et al.* (2014) identified sand layer 1 as the critical

layer, yet the analyses also showed a thinner and shallower sandy layer that has a high probability of liquefaction. For both layers, the threshold YSR approach clearly recognizes these two sand layers as contractive. Those layers match well with the layers identified by the more rigorous and detailed post-processing procedures.

6.3. Flow liquefaction analysis at Neves Corvo mine, Portugal

Results from CPT and laboratory testing in copper and copper-tin mine tailings at the Neves Corvo mine in southern Portugal are reported by Been *et al.* (2002). Sounding CPT-001 has been post-processed to look at the flow liquefaction potential in these fine-grained tailings, as presented in Fig. 16. The tailings are a special paste fill with cement added to increase stability. Results are shown for the following: (a) cone tip resistance, (b) material index according to Robertson (2009), (c) YSR and threshold value at CSL; (d) state parameter per the Jefferies & Been (2006) type analysis reported by Been *et al.* (2002). For the latter, a zone from 4 to 18 m is indicated to be contractive based on the ψ criterion. Using the YSR criterion, however, a much larger zone of tailings can be considered contractive.

7. Conclusions

A generalized approach to profiling yield stresses in soils from cone penetration tests has been developed from three primary sources: (a) analytical cavity expansion - critical state solution for clays; (b) database of large calibration chamber tests on sands; (c) field and lab data from world-

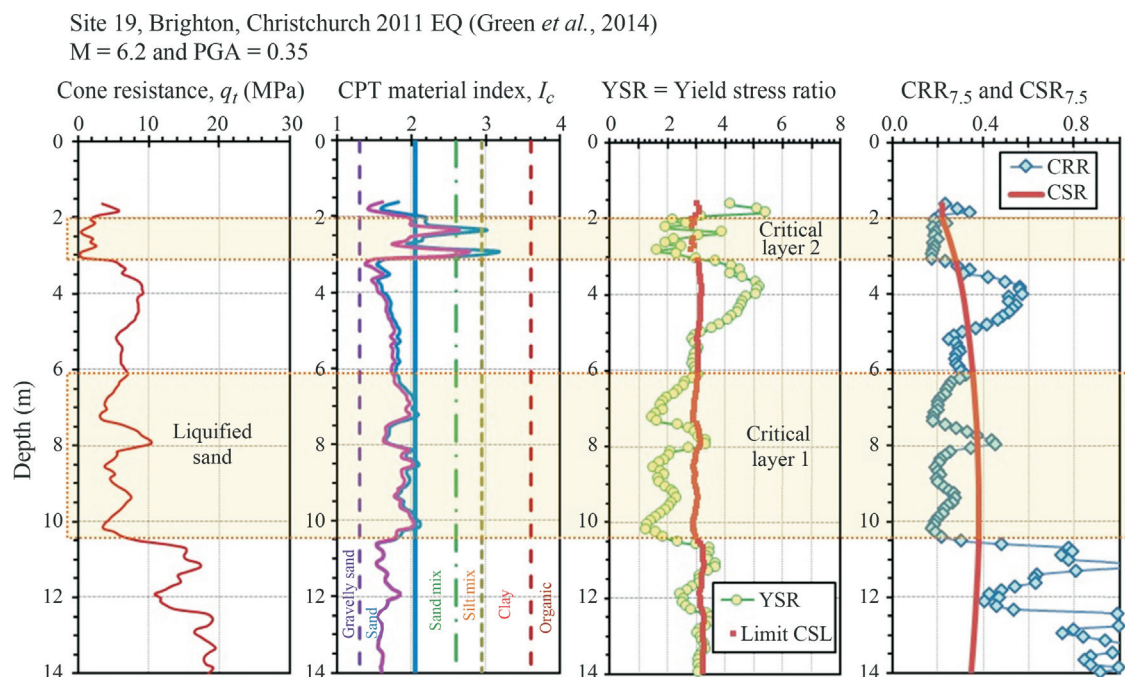


Figure 15 - Cyclic liquefaction case study in natural sands at Site 19, Brighton, Christchurch with profiles: (a) cone resistance, (b) CPT material index, (c) threshold YSR approach, and (d) traditional CRR-CSR comparison (data from Green *et al.*, 2014).

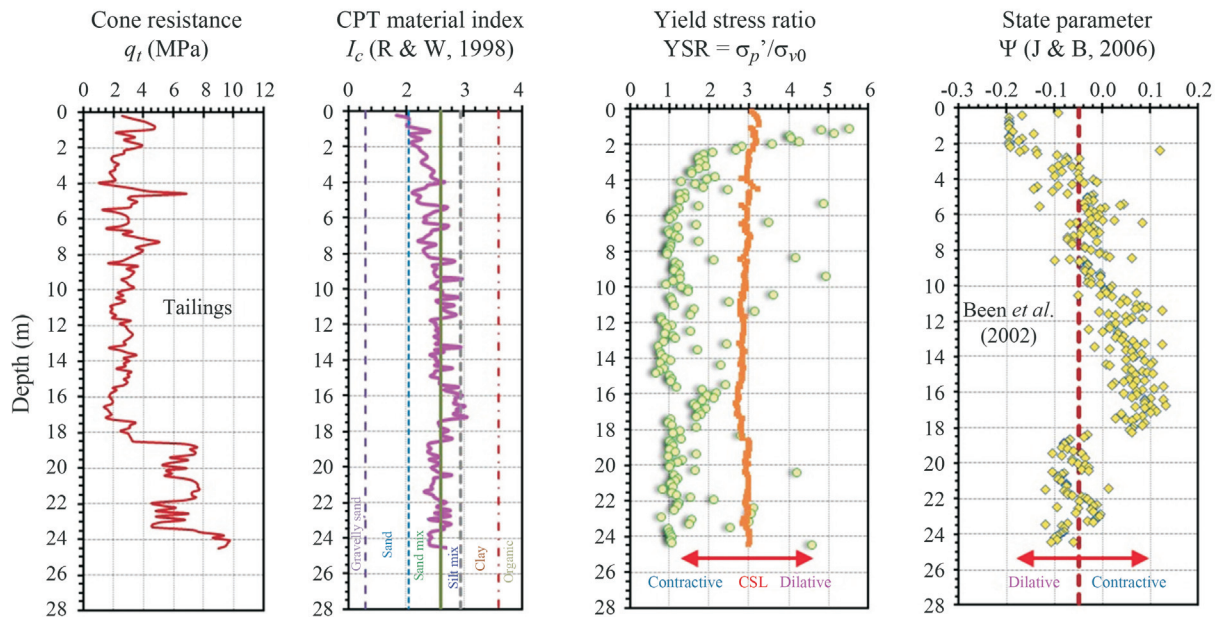
CPT-001 Neves Corvo Tailings, Portugal (Been *et al.*, 2002)

Figure 16 - Flow liquefaction analysis in copper tailings in southern Portugal with profiles: (a) cone resistance, (b) CPT material index, (c) threshold YSR approach, and (d) state parameter (Note: CPT data and interpreted ψ from Been *et al.*, 2002).

wide sites for verification and geoparameter backfitting. In SI units of kilopascal, the yield stress is evaluated simply from $\sigma_p' = 0.33(q_{net}')^m$ where the exponent m' tracks well with CPT material index, I_c . The yield stress ratio ($YSR = \sigma_p' / \sigma_{v0}'$) demarcates the sorting of normally-consolidated and overconsolidated soils, thus used extensively in embankment and foundation settlement analyses. The YSR also affects the normalized undrained shear strength (s_u / σ_{v0}'), porewater pressures during shear ($\Delta u / \sigma_{v0}'$), soil stiffness (e.g., E_u , G_{max}), as well as the initial state (K_0). Moreover, YSR within a critical state framework can be used to distinguish contractive and dilative soil behavior, thus find application in problems involving flow and cyclic liquefaction.

Acknowledgments

The author appreciates the support of ConeTec Investigations of Richmond, British Columbia and Minnesota Department of Transportation in St. Paul in research activities on cone penetration testing.

References

- Agaiby, S. & Mayne, P.W. (2018). Modified SCE-CSSM solution for CPTu soundings in sensitive clays. Paper in preparation. Civil & Environmental Engineering, Georgia Tech.
- Baligh, M.M. (1986). Undrained deep penetration: Pore pressures. *Geotechnique*, 36(4):487-501.
- Baroni, M. & Almeida, M.S.S. (2017). Compressibility and stress history of very soft organic clays. *Proc. Inst. Civ. Eng. – Geotechnical Engineering*, 170(2):148-160.

- Been, K.; Jefferies, M.G.; Crooks, J.H.A. & Rothenburg, L. (1987). The cone penetration test in sands: Part II, general inference of state. *Geotechnique*, 37(3):285-299.
- Been, K.; Crooks, J.H.A. & Jefferies, M.G. (1988). Interpretation of Material State From the CPT in Sands and Clays. *Penetration Testing in the U.K.* Thomas Telford, London, pp. 215-220.
- Been, K.; Brown, E.T. & Hepworth, N. (2002). Liquefaction potential of paste fill at Neves Corvo mine, Portugal. *Mining Technology*, 111(1):47-58.
- Been, K.; Romero, S.; Obermeyer, J. & Hebler, G. (2012). Determining in-situ state of sand and silt tailings from the CPT. *Proc. 12th Tailings and Mine Wastes*, Keystone, Colorado State University.
- Burns, S.E. & Mayne, P.W. (2002). Analytical cavity expansion-critical state model for piezocone dissipation in fine-grained soils. *Soils & Foundations*, 42(2):131-137.
- Casagrande, A. (1936). The determination of the preconsolidation load and its practical significance. *Proc. 1st Intl. Conf. on Soil Mechanics & Foundation Engineering*, Harvard Univ., Cambridge, v. 3, pp. 60-64.
- Casey, B.; Germaine, J.T.; Abdulhadi, N.O.; Kontopoulos, N.S. & Jones, C.A. (2016). Undrained Young's modulus of fine-grained soils. *J. Geotechnical & Geoenvironmental Engineering*, 1090-0241/04015070.
- Chen, B.S.-Y. & Mayne, P.W. (1994). Profiling the Overconsolidation Ratio of Clays by Piezocone Tests. Report GIT-CEEGEO-94-1 to National Science Foundation by Georgia Tech Research Corp., Atlanta, 280 p. Download at <http://geosystems.ce.gatech.edu/Faculty/Mayne>.

- Chen, B.S-Y. and Mayne, P.W. (1996). Statistical relationships between piezocone measurements and stress history of clays. *Canadian Geotechnical J.*, 33(3):488-498.
- Coutinho, R.Q. & Bello, M.I.M.C.V. (2014). Geotechnical characterization of Suape soft clays, Brazil. *Soils & Rocks*, 37(3):257-276.
- Demers, D. & Leroueil, S. (2002). Evaluation of preconsolidation pressure and the overconsolidation ratio from piezocone tests of clay deposits in Quebec. *Canadian Geotechnical Journal*, 39(1):174-192.
- Diaz-Rodriguez, J.A.; Leroueil, S. & Alem n, J.D. (1992). Yielding of Mexico City clay and other natural clays. *Journal of Geotechnical Engineering*, 118(7):981-995.
- Doherty, P.; Kirwan, L.; Gavin, K. & Igoe, D. (2012). Soil properties at the UCD geotechnical research site at Blessington. *Proc. Bridge and Concrete Research in Ireland*, Dublin Institute of Technology and Trinity College Dublin, p. 499-504.
- Eller, J.M.; McCullough, N.J.; Vargas-Herrera, L.A. & Coto-Loría, M. (2014). Role of CPTu in design of large Atlantic port terminal in Costa Rica. *Proc. 3rd IS Cone Penetration Testing*, Las Vegas, pp. 1129-1138.
- Gavin, K., Cadogan, D., Tolooiyan, A. & Casey, P. (2013). The base resistance of non-displacement piles in sand. Part I. *Proc. ICE – Geotechnical Engineering*, 166(6):540-548.
- Green, R.A.; Cubrinovski, M.; Cox, B.; Wood, C.; Wotherspoon, L.; Bradley, B. & Maurer, B. (2014). Select liquefaction case histories from the 2010-2011 Canterbury earthquake sequence. *Earthquake Spectra*, 30(1):131-153.
- Holtz, R.D.; Kovacs, W.D. & Sheehan, T.C. (2011). *An Introduction to Geotechnical Engineering*, Second Edition. Pearson Publishing, Upper Saddle River, 864 p.
- Idriss, I.M. & Boulanger, R.W. (2008), *Soil Liquefaction during Earthquakes*. Earthquake Engineering Research Institute, Monograph 12, EERI MNO-12, Oakland, 266 p.
- Jamiolkowski, M. & Pepe, M.C. (2001). Vertical yield stress of Pisa clay from piezocone tests. *Journal of Geotechnical & Geoenvironmental Engineering*, 127(10):893-897.
- Jardine, R.J.; Smith, P.R. & Nicholson, D.P. (2003). Properties of the soft Holocene Thames estuary clay from Queensborough, Kent. In: *Characterisation and Engineering Properties of Natural Soils*. Swets & Zeitlinger, Lisse, v. 1, pp. 599-643.
- Jefferies, M. & Been, K. (2006). *Soil Liquefaction: A Critical State Approach*. Taylor and Francis Group, London, 480 p.
- Karlsrud, K.; Lunne, T.; Kort, D.A. & Strandvik, S. (2005). CPTU correlations for clays. *Proc. 16th International Conference on Soil Mechanics and Geotechnical Engineering*, Osaka, v. 2, pp. 693-702.
- Krage, C.P.; Broussard, N.S. & DeJong, J.T. (2014). Estimating rigidity index based on CPT measurements. *Proc. 3rd Intl. Symposium on Cone Penetration Testing, CPT'14*, Las Vegas, www.cpt14.com.
- Ku, T. & Mayne, P.W. (2013). Yield stress history evaluated from paired in-situ shear moduli of different modes. *Engineering Geology*, 152(1):122-132.
- Ladd, C.C. & DeGroot, D.J. (2003). Recommended practice for soft ground site characterization. *Soil & Rock America 2003*. *Proc. 12th Pan American Conference*, MIT, Verlag Glückauf Publishing, Essen, v. 1, pp. 3-57.
- Larsson, R. & Mulabdic, M. (1991). *Piezocone Tests in Clay*. SGI Report 42. Swedish Geotechnical Institute, Linköping, 240 p.
- Larsson, R. & Åhnberg, H. (2003). Long-term effects of excavations at crests of slopes. *SGI Report 61*. Swedish Geotechnical Institute, Linköping, 372 p.
- Larsson, R. & Åhnberg, H. (2005). On the evaluation of undrained shear strength and preconsolidation pressure from common field tests in clays. *Canadian Geotechnical Journal*, 42(4):1221-1231.
- Larsson, R.; Westerberg, B.; Albing, D.; Knutsson, S. & Carlsson, E. (2007). *Sulfidjord*. SGI Report 69. Swedish Geotechnical Institute, Linköping, 138 p.
- Leroueil, S. & Barbosa, P.S. de A. (2000). Combined effect of fabric, bonding, and partial saturation on yielding of soils. *Proc. Unsaturated Soils for Asia*, Balkema, Rotterdam, pp. 527-532.
- Locat, J.; Tanaka, H.; Tan, T.S.; Dasari, G.R. & Lee, H. (2003). Natural soils: Geotechnical behavior and geological knowledge. *Proc. Characterisation & Engineering Properties of Natural Soils*. Swets & Zeitlinger, Lisse, v. 1, pp. 3-28.
- Long, R.P.; Healy, K.A. & Carey, P.J. (1978). Final report: Field consolidation of varved clay. *Univ. Connecticut Report JHR 78-113*, Project 70-3 to Connecticut Dept. of Transportation, 162 p.
- Mayne, P.W. (1991). Determination of OCR in clays by piezocone tests using cavity expansion and critical state concepts. *Soils and Foundations*, 31(2):65-76.
- Mayne, P.W. (2001). Stress-strain-strength-flow parameters from enhanced in-situ tests. *Proc. International Conference on In-Situ Measurement of Soil Properties & Case Histories*, Bali, Indonesia, pp. 27-47.
- Mayne, P.W. (2005). Integrated ground behavior: In-situ and lab tests. Deformation characteristics of geomaterials. *Proc. IS Lyon'03*, Taylor & Francis Group, London, v. 2, pp. 155-177.
- Mayne, P.W. (2007a). *Synthesis 368: Cone Penetration Testing*. NCHRP, Transportation Research Board, National Academy Press, Washington, DC, 118 p. www.trb.org.
- Mayne, P.W. (2007b). In-situ test calibrations for evaluating soil parameters, characterization & engineering pro-

- properties of natural soils. Proc. Singapore 2006, Taylor & Francis Group, London, v. 3, pp. 1602-1652.
- Mayne, P.W.; Coop, M.R.; Springman, S.; Huang, A-B. & Zornberg, J. (2009). SOA-1: Geomaterial behavior and testing. Proc. 17th Intl. Conf. Soil Mechanics & Geotechnical Engrg. ICSMGE, Alexandria, Millpress/IOS Press Rotterdam, v. 4, pp. 2777-2872.
- Mayne, P.W. (2013). Updating our geotechnical curricula via a balanced approach of in-situ, laboratory, and geophysical testing of soil. Proc. 61st Annual Geotechnical Conference, Minnesota Geotechnical Society, University of Minnesota, St. Paul, pp. 65-86.
- Mayne, P.W. (2015). Keynote lecture: In-situ geocharacterization of soils in the year 2016 and beyond. Advances in Soil Mechanics: Geotechnical Synergy. Proc. PCSMGE, Buenos Aires. IOS Press, Amsterdam, v. 5, pp. 139-161.
- Mayne, P.W.; Styler, M.; Woeller, D.J. & Sharp, J. (2017). Identifying contractive soils by CPT material index for flow liquefaction concerns. Proc. GeoOttawa - 70th Canadian Geotechnical Conference, Canadian Geotechnical Society: www.cgs.ca.
- Mayne, P.W. & Styler, M. (2018). Soil liquefaction evaluation using CPT yield stress profiles and simplified critical state soil mechanics. Proc. Geotechnical Earthquake Engineering and Soil Dynamics V, Austin, TX.
- Niazi, F.; Mayne, P.W. & Woeller, D. (2010). Evaluating drilled shaft O-cell response at Golden Ears Bridge from in-situ seismic cone tests. The Art of Foundation Engineering Practice. Proc. Volume in Honor of Clyde Baker (GSP 198), ASCE, Reston, Virginia, pp. 452-469.
- Plewes, H.D.; Davies, M.P. & Jefferies, M.G. (1992). CPT-based screening procedure for evaluating liquefaction susceptibility. Proc. 45th Canadian Geotechnical Conference, Paper 4, Toronto, Canadian Geotech Society: www.cgs.ca.
- Riyis, M.T. & Giacheti, H.L. (2017). Resistivity piezocone in the conceptual site model definition. Soils & Rocks, 40(2):93-107.
- Robertson, P.K. & Wride, C.E. (1998). Evaluating cyclic liquefaction potential using the cone penetration test. Canadian Geotechnical J., 35(3):442-459.
- Robertson, P.K. (2009). Interpretation of cone penetration tests: A unified approach. Canadian Geotechnical Journal, 46(11):1337-1355.
- Robertson, P.K. (2010). Evaluation of flow liquefaction and liquefied strength using the cone penetration test. J. Geotechnical & Geoenvironmental Engineering, 136(6):842-853.
- Robertson, P.K. (2012). The James K. Mitchell Lecture: Interpretation of in-situ tests - Some insights. Proc. Geotechnical & Geophysical Site Characterization 4, Pernambuco, Taylor & Francis Group, London, v. 1, pp. 3-24.
- Rodrigues, C.; Amoroso, S.; Cruz, N. & Viana da Fonseca, A. (2016). Liquefaction assessment CPTu tests in a site in south Portugal. Geotechnical & Geophysical Site Characterization 5 (ISC-5), Australian Geomechanics Society, v. 1, pp. 633-638.
- Schnaid, F. (2009). In Situ Testing in Geomechanics – The Main Tests. Taylor & Francis, London and New York, 352 p.
- Schnaid, F.; Nierwinski, H.P.; Bedin, J. & Odebrecht, E. (2014). On the characterization and classification of bauxite tailings. Soils & Rocks, 37(3):277-284.
- Teh, C.I. & Houlsby, G.T. (1991). An analytical study of the cone penetration test in clay. Geotechnique, 41(1):17-34.
- Viana da Fonseca, A.; Coop, M.R.; Fahey, M. & Consoli, N.C. (2011). The interpretation of conventional and non-conventional laboratory tests for challenging geotechnical problem. Proc. IS Deformation Characteristics of Geomaterials, Seoul, v. 1, pp. 84-119.
- Youd, T.L., Idriss, I., Andrus, R.D., Arango, I., Castro, G., Christian, J.T., Dobry, R., Finn, W.D.L., Harder Jr., L.F., Hynes, M.E., Ishihara, K., Koester, J.P., Liao, S.S.C., Marcuson III, W.F., Martin, J.R., Mitchell, J.K., Moriwaki, Y., Power, M.S., Robertson, P.K., Seed, R.B. & Stokoe, K.H. (2001). Liquefaction Resistance of Soils: Summary Report from the 1996 NCEER and 1998 NCEER/NSF Workshops on Evaluation of Liquefaction Resistance of Soils. Journal of Geotechnical and Geoenvironmental Engineering, 127(10):817-833.

Articles

Soils and Rocks
v. 40, n. 3

Stabilised Soil Layers Enhancing Performance of Transverse-Loaded Flexible Piles on Lightly Bonded Residual Soils

N.C. Consoli, V.P. Faro, F. Schnaid, R.B. Born

Abstract. A set of crosswise-loaded flexible piles was tested in binder stabilised top sand layers embedded in lightly bonded residual soil. Slope indicators were used to measure horizontal displacements in free-headed flexible piles during all loading stages. The geometry of the cement stabilised top sand layer surrounding the piles varied from about 2 to 4 times the pile diameter and 0.1 to 0.3 times the pile length. Experimental outcomes present an important enhancement in the performance of the flexible piles under transverse load when a cement stabilised sand layer replaces top residual soil, increasing bearing capacity and reducing maximum horizontal displacements at any given working load. At large horizontal displacements (close to failure), a linear relation is observed between the lateral load and the total lateral area compressing the natural soil around the pile. This evidence helps identifying the pile-soil interaction mechanism and provides sound normalization for test results, both considered necessary steps towards the development of a design concept for predicting lateral pile response.

Keywords: flexible piles, residual soil, top soil stabilisation, lateral load, pile field-testing.

1. Introduction

The performance of piles subjected to lateral loads is known to be mainly controlled by the properties of the soil near the surface (Simons and Menzies, 1975; Poulos and Davis, 1980; Verruijt & Kooijman, 1989; Basu *et al.*, 2009; Faro *et al.*, 2015). It is for this reason that Simons and Menzies (1975) suggest being beneficial to replace poor surface soils by compacted gravel. Poulos & Davis (1980) presented an overview of methods conceived to increase the lateral resistance of piles by increasing the dimensions and/or stiffness of the piles near the ground surface. These methods comprise the use of sand or gravel fills, the insertion of wings around the pile (only near the surface), concrete collars, mortar and even short piers or beams surrounding the piles.

For analysing laterally loaded piles in a layered elastic continuum, numerical methods were used (*e.g.* Verruijt & Kooijman, 1989). Basu *et al.* (2009) supported the development of an analytic framework for assessing the response of transversally loaded piles in multi-layered elastic soils. Higgins *et al.* (2013) analysed laterally loaded pile performance using the Fourier FEM and two-layer elastic soil with constant modulus within each layer.

Field-tests in laterally loaded piles were carried out by Cintra (1981), Miguel (1996), Del Pino Jr *et al.* (2002)

and Almeida *et al.* (2011) in a lateritic soil profile in order to establish values of coefficient of soil reaction. Consoli *et al.* (2016) subjected long piles to transversal load in residual soil sites and found out that lightly bonded soil might not be analysed as sedimentary fine-grained soils once the pile-soil interaction is analysed. Ferreira *et al.* (2006) and Miranda Jr. (2006) performed lateral load tests on different pile types, including omega screw piles, continuous flight auger piles, bored piles, and small diameter drilled shaft (root piles). Those tests were performed with soil in natural condition, flooded, and also with a cemented soil top layer. Conclusions pointed to a gain of approximately five times in the soil reaction coefficient due to the cemented soil layer. Rollins *et al.* (2010) performed full-scale lateral load tests on a pile group in clay before and after construction of soil mixing and jet grouting walls on either side of the pile group. According to the authors, both soil mixing and jet grouting provided significant increase in the transverse load of pile clusters. Although these results provide important insights to pile design, there is no established method to estimate the lateral load vs. lateral displacement response of a pile embedded in cement-treated soil and subjected to lateral load. The response ought to take into consideration the lateral resistance of the adjacent soil, especially the near-surface soil type that controls the load-displacement performance of the pile (Faro, 2014; Faro *et al.*, 2015).

Nilo Cesar Consoli, Full Professor, Ph.D., Departamento de Engenharia Civil, Universidade Federal do Rio Grande do Sul, Porto Alegre, RS, Brazil. e-mail: consoli@ufrgs.br.

Vitor Pereira Faro, Associate Professor, D.Sc., Departamento de Construção Civil, Universidade Federal do Paraná, Curitiba, PR, Brazil. e-mail: vpfaro@ufpr.br.

Fernando Schnaid, Emeritus Professor, Ph.D., Departamento de Engenharia Civil, Universidade Federal do Rio Grande do Sul, Porto Alegre, RS, Brazil. e-mail: fernando@ufrgs.br.

Ricardo Bergan Born, Ph.D. Student, M.Sc., Departamento de Engenharia Civil, Universidade Federal do Rio Grande do Sul, Porto Alegre, RS, Brazil. e-mail: born@ufrgs.br.

Submitted on December 20, 2016; Final Acceptance on September 21, 2017; Discussion open until April 30, 2018.

DOI: 10.28927/SR.403219

In the present research, an attempt is made to extend these early views by interpreting results of crosswise load tests carried out in flexible piles embedded in lightly bonded residual soil with binder-stabilised top sand layers considering distinctive thicknesses and diameters around piles. Different improved top layers geometries were tested under a particular diameter-to-length ratio and, based on these results, an attempt is made to normalize data in order to help the elaboration of design methods. This follows studies of shallow foundations bearing in cement treated layers (Thomé *et al.*, 2005; Consoli *et al.*, 2008, 2009) and plate anchors subjected to pullout loads (Consoli *et al.*, 2013), as well as short rigid piles embedded in cement treated soils subjected to lateral load (Faro *et al.*, 2015).

It is important to recall that residual soils are a product of rocks *in situ* weathering. According to Leroueil & Vaughan (1990) and Blight (1990), stress history has little influence on residual soil properties since both the crystallisation associated with the formation of mother rocks and the precipitation of mineral cells create interparticle bonding. The porous cemented structure leads to distinctive geotechnical characteristics that are quite different from those of transported soils with similar densities and grain size distribution. According to Consoli *et al.* (1998), prestressing lightly bonded residual soils produces substantial damage to the cemented structure with considerable reduction in initial soil stiffness. According to the same authors, it is important to notice that the result of prestressing slightly bonded residual soils contrasts with ordinary patterns produced by overconsolidation in which soil stiffness is expected to increase along with increasing maximum past mean consolidation stress.

2. Soil Features

The present investigation reports data from transversally loaded piles in cement treated sand layers embedded in lightly bonded residual soil. Subsequently to pile execution and previously to the compaction of the cement-stabilized top sand layers, the local soil was removed according to the volumetric geometry of the cement treated soil layer to be built.

Appropriate sand-cement mixing and compaction are essential factors for the suitable performance of the pile system. For assessment between attained field compaction and laboratory referential values, field water content, density and compression strength were measured thoroughly. In overall terms, the backfill control indicated a homogeneous mass with the characteristic values presented herein.

2.1. Homogeneous lightly bonded residual soil stratum

In situ cone penetration (CPT) tests were carried out to establish the main features of the studied residual soil site. Typical chart showing variations of CPT data up to 20 m depth (see Fig. 1) indicates a homogeneous residual soil stratum in which slight variations on cone tip strength

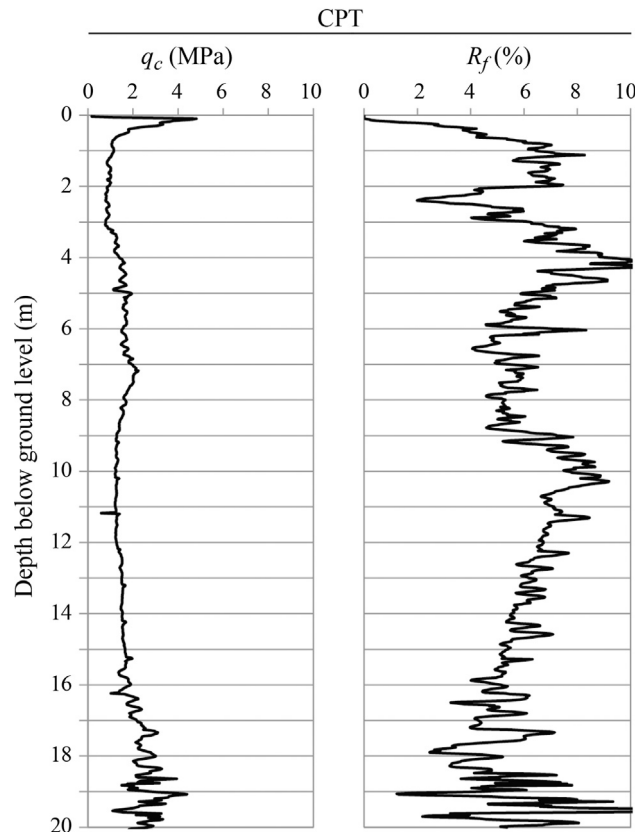


Figure 1 - CPT soil profile to a depth of 20 m.

(q_c) are attributed to weathering progression, a usual characteristic of residual soil sites. According to USCS, the residual soil was ranked as low plasticity clay (CL). The dry unit weight was around 12.1 kN/m^3 and the water table was found at about 10 m depth. Saturated drained triaxial tests were carried out in specimens collected at about 1.0 m depth and tests included measurement of strains using Hall-effect sensors (Clayton & Khattrush, 1986). Deviator stress - axial strain and volumetric strain - axial strain triaxial curves are presented in Fig. 2 considering confining stresses of 20, 60 and 100 kPa. Indication of soil bonding was obtained by testing specimens in drained triaxial compression, following experience of Consoli *et al.* (1998) in residual soil site. The stress-strain curve with smallest confining stress (20 kPa) shows high stiffness at small strains and perfectly plastic behaviour at larger strains. Increasing isotropic confining stresses from 20 kPa to 60 kPa and 100 kPa, soil stiffness is reduced at small strains due to bonding degradation (breakage of bonds) (Leroueil & Vaughan, 1990; Consoli *et al.*, 1998, 2000) and strain-hardening behaviour is observed at larger strains. Isotropic yielding occurs at a stress greater than 20 kPa and lower than 60 kPa. Volumetric strains were contractile in all studied confining stresses, increasing their maximum values with increasing confining stress. Effective friction angle of 29.5° and effective cohesion intercept of 24.0 kPa were

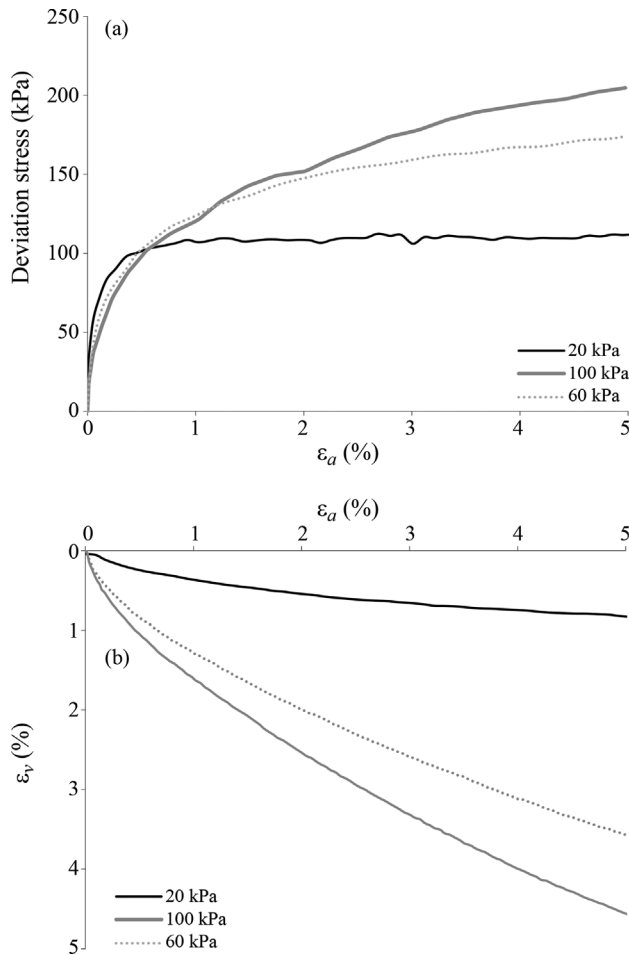


Figure 2 - Saturated drained triaxial tests of lightly bonded residual soil at confined stresses of 20, 60 and 100 kPa.

computed after triaxial test (see Fig. 3 for Mohr-Coulomb failure envelope) results. Oedometric yielding (according to Casagrande’s graphical procedure) occurs at approximately 81 kPa (see Fig. 4) and unconfined compressive strength was nearly 51.2 kPa. Initial shear modulus (G_0) of about 50 MPa was determined after seismic dilatometer testing. Saturated hydraulic conductivity [obtained using a flexible wall permeameter following ASTM D 5084 (ASTM, 2016)] is relatively high at 1.5×10^{-5} m/s, when compared to hydraulic conductivity of alluvial clays. Different from alluvial soils with analogous particle grain sizes, residual soils are a product of *in situ* weathering, which reduces unit weight, increases hydraulic conductivity and exhibit parent rock characteristics (interparticle bonding), typical of cohesive-frictional materials.

Lastly, initial matric suction measurements carried out with the Imperial College suction probe are lower than 5 kPa, the soil does not exhibit collapse response (Medero *et al.*, 2007) and therefore the lateral load-displacement response of piles in this lightly bonded residual soil is essentially dependent on the bonded structure.

2.2. Cement stabilised top sand layer

The cement stabilised top sand layer was made in a gyratory drum blender, mixing uniform fine Osorio sand previously studied by Consoli *et al.* (2010, 2011, 2012a, 2012b) and Consoli (2014), type III high early strength Portland cement (7% by weight of dry soil) and 10% water content. Strata of the sand-cement blends were constructed

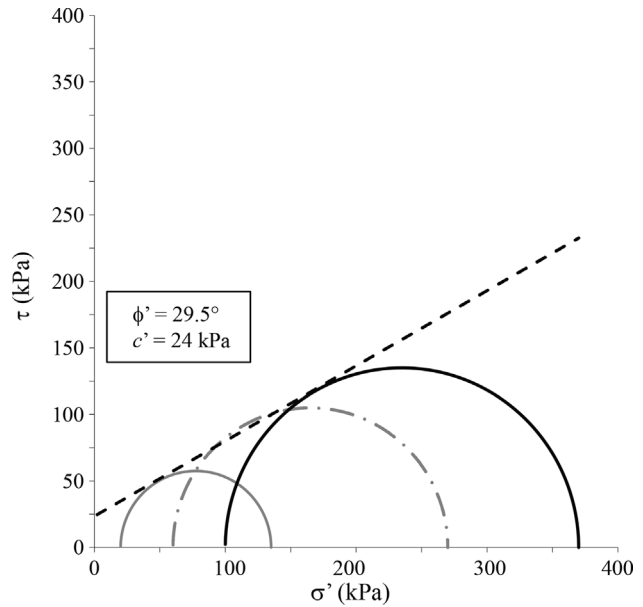


Figure 3 - Mohr-Coulomb failure envelope considering drained triaxial tests of lightly bonded residual soil at confined stresses of 20, 60 and 100 kPa.

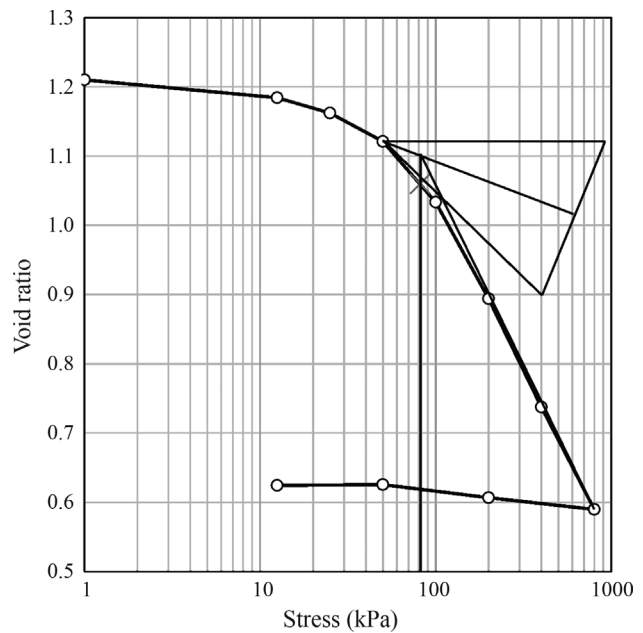


Figure 4 - Oedometric test result for lightly bonded residual soil with Casagrande’s graphical procedure to obtain oedometric yield stress.

in successive sub layers, 10 cm thick each, using a vibratory plate to reach a dry unit weight of 16.0 kN/m^3 . The sand-cement backfills stayed curing during 14 days previously to piles being transversally loaded. Unconfined compression tests carried out on specimens cured for 14 days produced strength of roughly 1.0 MPa. Effective cohesion intercept of 346 kPa and effective friction angle of 38.3° were determined in triaxial tests.

3. Field Testing Program

Piles were excavated with rotating auger at the experimental site portrayed above and reinforced with carbon steel tee rails 75 AS section designation (ASTM, 2010) alongside the whole length (steel tee rail used in present research in a 400-mm concrete shaft has a equivalent behaviour of a 3% - regarding shaft cross section - steel conventional cage reinforcement). Bored piles were made with concrete of uniaxial strength of about 15 MPa and transversally loaded pile tests were performed at the field testing site using 2 indistinguishable symmetrical piles in an appropriate reaction arrangement where a single pile reacts alongside another. Hence, it was concurrently feasible to have both pile reaction and test repeatability. A photo of the scheme containing the hydraulic jack horizontally positioned amid 2 steel cylinders and 2 adjusted load cells (cell capacity of 500 kN with a resolution of 2.5 kN), reacting against the top of 2 symmetrically placed piles, is presented in Fig. 5. Details of the transverse loading test schematic general plan view are shown in Fig. 6a and cross-sectional view in Fig. 6b. Most piles had a PVC pipeline in the interior to measure their horizontal displacements along the pile length during all loading stages using a slope indicator. Besides, two linear displacement transducers with resolution of 0.01 mm and 50 mm travel were used for measurement of horizontal displacements at about 100 mm above the surface of cement-stabilized sand. It is important to em-

phasize that close to the final stage of the gauges, they were reset at the end of the loading stage, allowing horizontal displacement measurements larger than 50 mm. Procedures for carrying out the transverse-loaded pile tests are in accord with ASTM D 3966 (ASTM, 2013). The transverse load was applied in cumulative equal increments of not

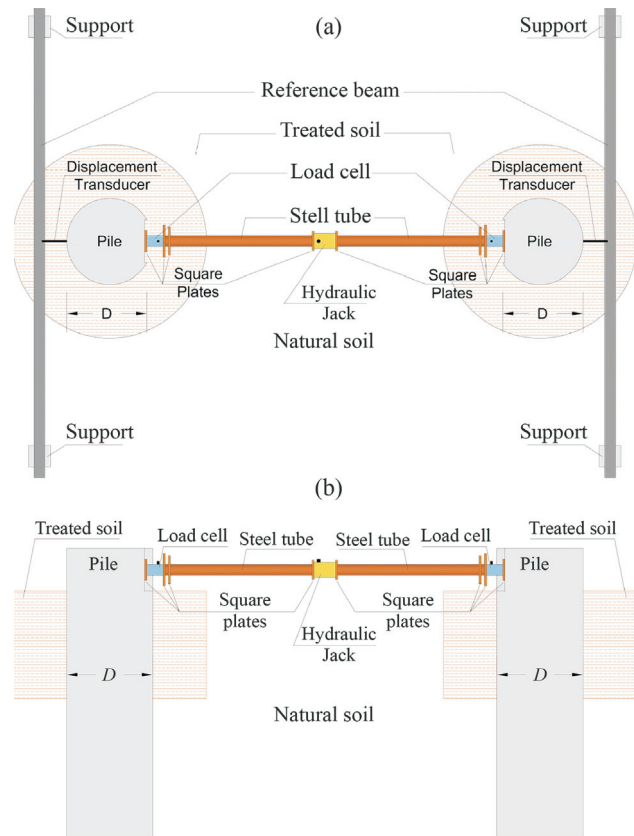


Figure 6 - Transverse loading tests schematic (a) general plan view and (b) cross-sectional view.



Figure 5 - General overview of reaction system used.

more than 1/10 of the estimated ultimate capacity. Following every transverse load increment, the required period to stabilize the displacements was expended. In agreement with Brazilian standard NBR 12131 (ABNT, 2006), every increment was sustained for at least 30 min until the following criterion [Eq. (1)] was reached:

$$L_n - L_{n-1} \leq 0.05(L_n - L_1) \tag{1}$$

where L_n is the LVDT reading at a specified time interval t , L_{n-1} the LVDT reading immediately prior to L_n , and L_1 the first reading of the stage of loading taken just following stage loading application.

Tried piles are $L = 8$ m long and $D = 0.4$ m diameter showing $L/D = 20$, characterising the behaviour of a free-headed flexible pile that deflects in the direction of the applied load. Besides piles inserted directly in residual soil stratum, a sequence of tests was carried out on piles embedded in cement stabilised top sand backfill layers of distinct volumes encompassing the piles. Cement stabilised top sand layers have treated diameter (D_{cem}) varying from 2 to 4 times the pile diameter (D) and treated depth (L_{cem}) varying from 0.1 to 0.3 times the pile length (L). Table 1 presents the geometry of field tests carried out on cement stabilised top sand layers. To identify each lateral load test, the following notation was used: $cem_x D_yL$, where “cem” denotes the top cement stabilised sand; “x” is D_{cem}/D ratio and “y” the L_{cem}/L ratio.

4. Test Results

4.1. Transverse load - displacement response

Typical horizontal load vs. horizontal displacements (measured 100 mm above ground by displacement transducer) of piles with stabilized backfill with dimensions corresponding to $L_{cem} = 0.2L$ and $D_{cem} = 3D$ and $4D$ are presented in Figure 7. Unloading and reloading cycles demonstrated that the system response is nonlinear elastic-plastic in all unload-reload cycles, with irrecoverable horizontal displacements clearly observed. All cycles also exhibit a strong hysteretic response.

Inclinometer probes were used for determining horizontal displacement d vs. depth profiles during lateral pile load tests. Since two piles are reacting against each other, two sets of results from two identical symmetrical piles were obtained, as illustrated in Fig. 8 for natural residual soil at horizontal loads corresponding to 20 kN (about elastic range), 40 kN (working load) and 60 kN (close to failure). Measured d vs. pile depths show very similar trends, presenting sound reproducibility at the three applied horizontal loads. Figure 9 presents an additional example for a pile embedded in treated ground ($D_{cem} = 4D$ and $L_{cem} = 0.1L$) for loads of up to 260 kN. Displacements are shown to increase with increasing lateral loads to a depth of approximately 0.3 times the pile diameter; below this depth displacements are negligible. Displacements measured at

Table 1 - Specific data of each laterally loaded test and their notation.

Notation	Cement content (%)	Depth of cemented backfill [L_{cem}] (m)	Diameter of cemented backfill [D_{cem}] (m)	L_{cem}/L	D_{cem}/D	Cemented backfill volume (m^3)	Lateral load for an horizontal displacement of 25 mm at the top of the pile (kN)
Natural	-	-	-	-	-	-	50
Cem_2D_0.1L	7	0.8	0.8	0.1	2	0.30	140
Cem_3D_0.1L	7	0.8	1.2	0.1	3	0.80	155
Cem_3D_0.2L	7	1.6	1.2	0.2	3	1.61	200
Cem_4D_0.1L	7	0.8	1.6	0.1	4	1.51	255
Cem_4D_0.2L	7	1.6	1.6	0.2	4	3.02	260
Cem_4D_0.3L	7	2.4	1.6	0.3	4	4.52	300

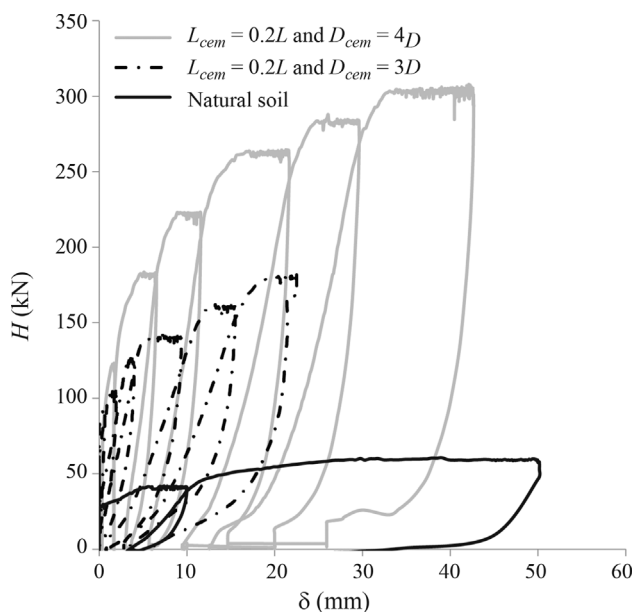


Figure 7 - Horizontal load vs. horizontal displacement curves for natural residual soil and cement stabilized sand backfill in different testing geometries ($L_{cem} = 0.2L$ and $D_{cem} = 3D$ and $4D$).

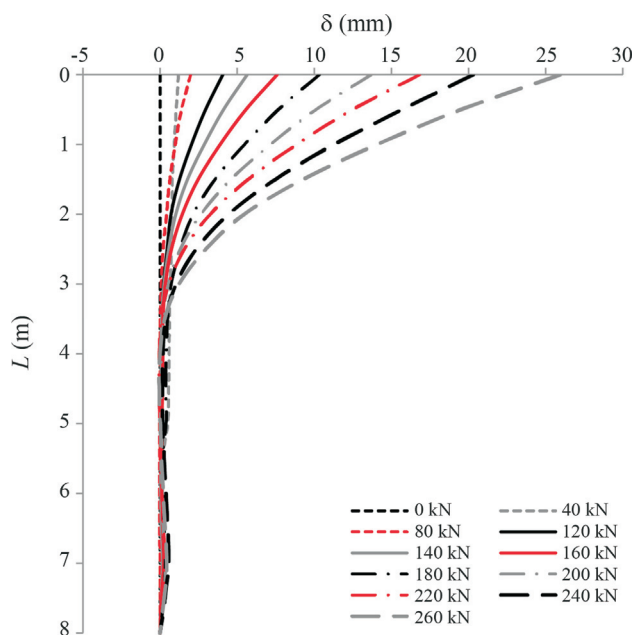


Figure 9 - Horizontal displacement vs. depth curves (considering horizontal loads up to 260 kN) for top cemented sand backfill with improved diameter $D_{cem} = 4D$ and improved depth $L_{cem} = 0.1L$.

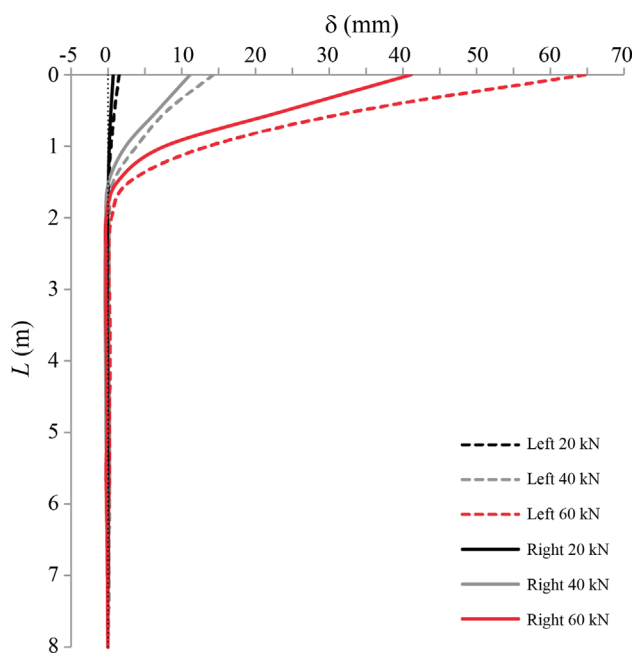


Figure 8 - Horizontal displacement vs. pile depth profiles (at horizontal loads of 20 kN, 40 kN and 60 kN) for two identical symmetrical piles in natural residual soil.

the surface by displacement transducers and inclinometer probe are of the same order. As an example, considering the horizontal load of 80 kN and 120 kN, the slope indicator reads 2.0 mm and 4.1 mm, while the external linear displacement reads 1.7 mm and 4.2 mm, respectively.

Figure 10 shows that, for the horizontal load of 60 kN, the pile in natural residual soil reaches an average 50 mm

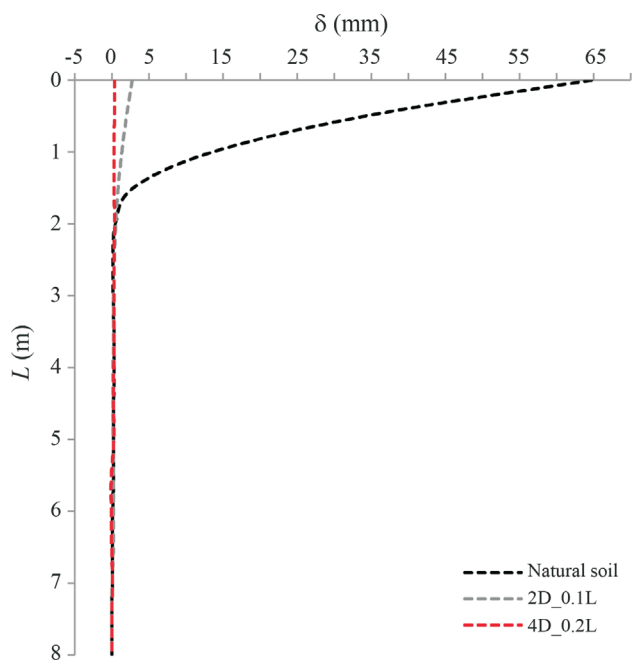


Figure 10 - Horizontal displacement vs. depth curves for top cemented sand backfill with distinct improved geometries considering a lateral load of 60 kN.

maximum displacement. Considering the influence of the cement stabilized improved geometry, it can be seen that, for the top cemented sand backfill with improved diameter $D_{cem} = 2D$ and improved depth $L_{cem} = 0.1L$ (consisting of 0.3 m^3 of cemented stabilised sand), the displacement for the horizontal load of 60 kN reduces to about 2.7 mm and,

with $D_{cem} = 4D$ and $L_{cem} = 0.2L$ (consisting of 3.0 m^3 of cemented stabilised sand - about 10 times the previous stabilised volume), a further reduction to around 0.4 mm is verified.

Figure 11 shows that, for the horizontal load of 120 kN, for the top cemented sand backfill with improved diameter $D_{cem} = 2D$ and improved depth $L_{cem} = 0.1L$ (consisting in 0.3 m^3 of cemented stabilised sand), the maximum displacement is above 10 mm, reducing to 6 mm with increasing improved diameter $D_{cem} = 3D$ and improved depth $L_{cem} = 0.2L$ (consisting in 1.6 m^3 of cemented stabilised sand). Increasing the diameter to $D_{cem} = 4D$ and reducing the improved depth to $L_{cem} = 0.1L$ (consisting in 1.5 m^3 of cemented stabilised sand), the maximum displacement reduces to 4.1 mm, further reducing to 2.6 mm with $D_{cem} = 4D$ and $L_{cem} = 0.2L$ (consisting in 3.0 m^3 of cemented stabilised sand).

5. Analysis

Before analysing results of pile lateral loading, it is important to recall that all tested piles were reinforced to yield at large load stages. The depth of the structural yield point was monitored by inclinometer measurements and was later confirmed by pile exhumation. Under this condition, maximum mobilized lateral resistance is determined as the soil reaction net of the earth pressures integrated along the pile shaft down to the critical embedment depth (*i.e.* down to the depth of yielding). Below the yield point, the piles experience virtually no lateral displacements.

A summary of the lateral load capacity of all tested piles is given in Table 1, taking the horizontal displacement

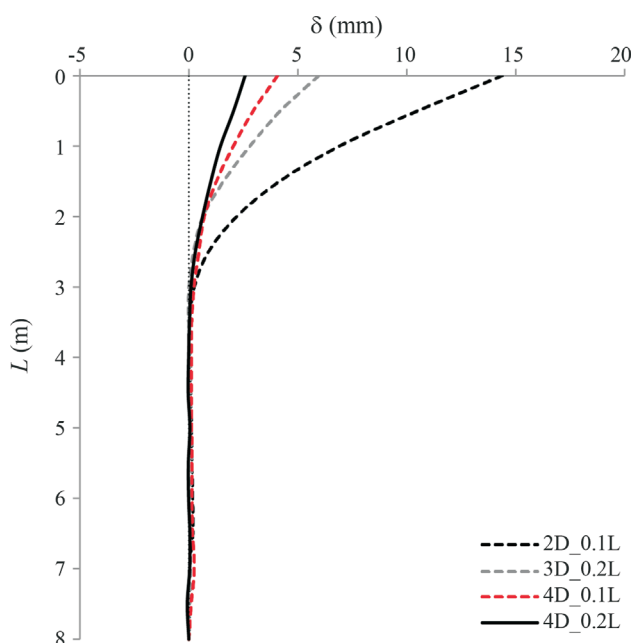


Figure 11 - Horizontal displacement vs. depth curves for top cemented sand backfill with distinct improved geometries considering a lateral load of 120 kN.

of 25 mm at the top of the pile as a reference value. From measured data, it can be observed that horizontal loads increase 180% and 410%, from 50 kN to 140 kN and 255 kN, respectively, for pile in the natural soil to $D_{cem} = 2D$ and $D_{cem} = 4D$, both considering the improved depth of $L_{cem} = 0.1L$ (consisting in a volume of cemented stabilised sand increasing from 0.3 m^3 to 1.5 m^3).

Figure 12 illustrates propagation of cracks in both natural ground and cemented layer when loading reaches more than 80% of transverse bearing capacity. A series of small cracks appear in the natural ground due to the compressive stress generated by the continued horizontal displacement of the cement-treated soil shaft system. It can be observed that about half the circular perimeter of the treated soil compresses the natural soil from the beginning of loading to failure and that the direction of cracks predominantly follows the direction of the pile movement.

These observed ground conditions allow an interaction mechanism to be postulated and, ultimately, a design concept to be developed. The improved ground is considered as a mass of high stiffness that moves as a solid block, compressing the less stiff natural soil (in the present study the actual stiffness of the improved ground is about 10 to 15 times that of the natural ground). It follows that ultimate bearing capacity should then be calculated as the theoretical maximum average contact pressure that can be supported without failure by the natural ground, *i.e.* the lightly structured natural ground near the surface controls the foundation horizontal resistance, since the pile and the improved ground act as one body that works in distributing the applied load only.

The second important aspect is the realization that lateral bearing capacity is not dictated by the mobilization of passive earth pressure developed at the onset of shear failure produced by pile movement, as often assumed in geotechnical design of foundations and earth structures. In lightly cemented soils, the failure model is associated to punching shear failure mechanisms which are accom-

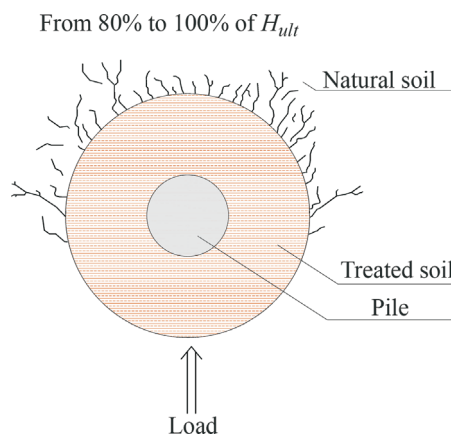


Figure 12 - Top view of failure mechanisms (cracking) on the top cement stabilized sand backfills.

plished by poorly defined shear planes, with soil zones beyond the perimeter of the loaded area being little affected. Following the basic modes of cracking displacements shown in Figure 12, the pile-soil interaction characterizes a typical punching phenomenon that comprises the origination of a series of small cracks ahead of the loaded area that, at a given applied load, exhibit brittle response and rapid fracture propagation. Pile displacements induced deformations, combined with localized volumetric strains and crack propagation, produce the breakage of the natural soil cement bonds and, at this stage, the pile reaches its maximum bearing capacity.

With the recognition that the yield stresses controlling the cemented bonds may govern the characteristic lateral bearing capacity of composite ground foundations, the results from *in situ* load tests can be further analysed. The full set of results is presented in Fig. 13, in which the lateral load ($H_{25\text{ mm}}$) measured at the ground surface displacement of 25 mm (Table 1) is plotted against the lateral area pressing natural soil [mobilized at the pile shaft (A_{mob})] including the cemented treated superficial layer. In natural ground, A_{mob} is calculated as half the pile perimeter times the critical embedment depth (L_{crit}) of approximately 2.0 m (see horizontal displacements at Fig. 8), whereas in treated ground, A_{mob} is calculated as half the circular perimeter of the treated soil multiplied by improved depth plus half the pile perimeter times the remainder of pile length till reaching critical embedment depth (L_{crit}) (equal to 3 m in present case - see horizontal displacements in Fig. 9), which clearly define the maximum pile length mobilized by applied horizontal loads. The actual value of L_{crit} for each pile is obtained as the

depth in which horizontal displacement is smaller than 0.1 mm. As observed in Fig. 13, a linear relationship ($R^2 = 0.87$) is achieved between $H_{25\text{ mm}}$ and A_{mob} , [see Eq. (2)] including tests on piles with and without superficial ground treatment. Despite the scatter, always considered as a natural occurrence in residual soils (Schnaid & Huat 2012), there is evidence that horizontal load increases linearly with increasing mobilized area pressing natural ground.

$$H_{\text{at } 25\text{ mm}} \text{ (kN)} = 53.82 A_{\text{mob}} \text{ (m}^2\text{)} \quad (2)$$

This evidence is regarded as an indication of mobilization and mechanism associated to horizontal load transfer, which is a simple summation of pressures generated in front of both pile and cemented ground areas, despite the difference in stiffness of these materials. As a matter of fact, the constant of Eq. (2) is representative of the yielding pressure that is obtained after oedometric test, which gives an experimental evidence that the response of laterally loaded piles is actually governed by the yield stresses characterizing bond breakages in lightly cemented ground.

It is worth noticing that Consoli *et al.* (2006) have shown that there is a direct relation between isotropic yield stress and the unconfined compressive strength for lightly cemented soils. In the present case, isotropic yielding occurs at a stress greater than 20 kPa and lower than 60 kPa and the unconfined compressive strength is 51.2 kPa, both in the range of the field pressure $\frac{H_{\text{at } 25\text{ mm}}}{A_{\text{mob}}} = 53.82 \text{ kPa}$

that causes failure by lateral punching. The oedometric yield stress of 81 kPa is somehow larger than the field pressure causing failure by punching. So, for practical purposes, in order to establish the maximum transverse load, the designer should request determination of the unconfined compressive strength and/or isotropic yield stress (or even oedometric yield stress) of the lightly bonded residual soil and estimate the lateral area (A_{mob}) pressing natural soil (calculated as half the circular perimeter of the treated soil multiplied by improved depth plus half the pile perimeter times the remainder of pile length till reaching critical embedment depth of long flexible piles). In a conservative first approach, A_{mob} could consider only half of the circular perimeter of the improved area times the improved depth.

6. Conclusions

Some conclusions can be drawn from the data presented in this technical paper:

- The response of transversally loaded piles is essentially governed by the yield stresses characterizing bond breakages in lightly cemented ground;
- The cement stabilised top soil layers considerably improve the behaviour of free-headed flexible piles submitted to transverse loads. The reduction of horizontal displacements under a service load is a direct function of the increase in the cement treated soil layer;

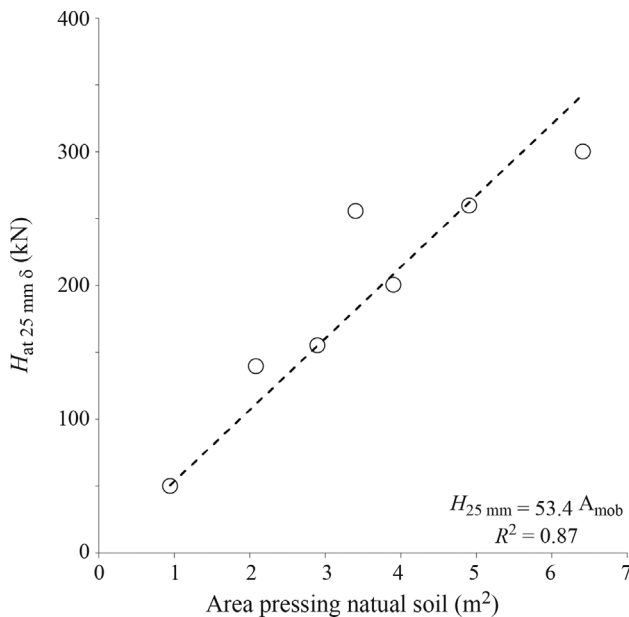


Figure 13 - Lateral loading for 25 mm horizontal displacement $H_{25\text{ mm}}$ vs. area under compression (mobilized area pressing natural ground A_{mob}).

- A linear relationship is obtained between the maximum lateral load $H_{25\text{ mm}}$ and the mobilized soil compression area (A_{mob}) ahead of the pile and the treated ground.
- In order to establish the failure transverse load, the designer should determine the unconfined compressive strength and/or isotropic yield stress (alternatively oedometric yield stress) of the lightly bonded residual soil and estimate the lateral area pressing natural soil (calculated as half the circular perimeter of the treated soil multiplied by improved depth plus half the pile perimeter times the remainder of pile length till reaching critical embedment depth of long flexible piles).

Acknowledgments

The authors desire to state their gratitude to PRONEX FAPERGS/CNPq 12/2014 (grant number 16/2551-0000469-2) and CNPq (Projects Produtividade em Pesquisa & INCT-REAGEO) for the support to the research group.

References

- ABNT (2006). Piles - Static Load Test, NBR 12131, Rio de Janeiro, Brazil (in Portuguese).
- Almeida, M.A., Miguel, M.G. & Teixeira, S.H.C. (2011). Horizontal bearing capacity of piles in a lateritic soil. *Journal of Geotechnical and Geoenvironmental Engineering*, ASCE, 137(1):59-69.
- ASTM (2010). Standard Specification for Carbon Steel Tee Rails, A1-00. American Society for Testing and Materials, Philadelphia, 7 p.
- ASTM (2013). Standard Test Method for Deep Foundations Under Lateral Load, D 3966, American Society for Testing and Materials, Philadelphia, 18 p.
- ASTM (2016). Standard Test Methods for Measurement of Hydraulic Conductivity of Saturated Porous Materials Using a Flexible Wall Permeameter, D5084. American Society for Testing and Materials, Philadelphia, 24 p.
- Basu, D.; Salgado, R. & Prezzi, M. (2009). A continuum-based model for analysis of laterally loaded piles in layered soils. *Géotechnique*, 59(2):127-140.
- Blight, G.E. (1990). Construction in tropical soils. Proc. 2nd International Conference on Tropical Soils, v. 2, pp. 449-467.
- Cintra, J.C.A. (1981). Uma Análise de Provas de Carga Lateral em Estacas e Comparação com os Métodos da Teoria de Reação Horizontal do Solo. Dissertação de Mestrado, Universidade de São Paulo.
- Clayton, C.R.I. & Khatrush, S.A. (1986). A new device for measuring local axial strain on triaxial specimens. *Géotechnique*, 36(4):593-597.
- Consoli, N.C. (2014). A method proposed for the assessment of failure envelopes of cemented sandy soils. *Engineering Geology*, 169:61-68.
- Consoli, N.C.; Schnaid, F. & Milititsky, J. (1998). Interpretation of plate load tests on residual soil site. *Journal of Geotechnical and Geoenvironmental Engineering*, 124(9):857-867.
- Consoli, N.C.; Rotta, G.V. & Prietto, P.D.M. (2000). Influence of cured under stress on the triaxial response of cemented soils. *Géotechnique*, 50(1):99-105.
- Consoli, N.C.; Rotta, G.V. & Prietto, P.D.M. (2006). Yielding-compressibility-strength relationship for an artificially cemented soil cured under stress. *Géotechnique*, 56(1):69-72.
- Consoli, N.C.; Thomé, A.; Donato, M. & Graham, J. (2008). Loading tests on compacted soil - bottom ash - carbide lime layers. *Proceedings of the Institute of Civil Engineers, Geotechnical Engineering*, 161(1):29-38.
- Consoli, N.C.; Dalla Rosa, F. & Fonini, A. (2009). Plate load tests on cemented soil layers overlaying weaker soil. *Journal of Geotechnical and Geoenvironmental Engineering*, ASCE, 135(12):1846-1856.
- Consoli, N.C.; Cruz, R.C.; Floss, M.F. & Festugato L. (2010). Parameters controlling tensile and compressive strength of artificially cemented sand. *Journal of Geotechnical and Geoenvironmental Engineering*, ASCE, 136(5):759-763.
- Consoli, N.C.; Cruz, R.C. & Floss, M.F. (2011). Variables controlling strength of artificially cemented sand: influence of curing time. *Journal of Materials in Civil Engineering*, ASCE, 136(5):759-763.
- Consoli, N. C.; Cruz, R.C.; Viana da Fonseca, A. & Coop, M.R. (2012a). Influence of cement-voids ratio on stress-dilatancy behavior of artificially cemented sand. *Journal of Geotechnical and Geoenvironmental Engineering*, ASCE, 138(1):100-109.
- Consoli, N.C.; Cruz, R.C.; Consoli, B.S. & Maghous, S. (2012b). Failure envelope of artificially cemented sand. *Géotechnique*, 62(6):543-547.
- Consoli, N.C.; Ruver, C.A. & Schnaid, F. (2013). Uplift performance of anchor plates embedded in cement-stabilized backfill. *Journal of Geotechnical and Geoenvironmental Engineering*, ASCE, 139(3):511-517.
- Consoli, N.C.; Faro, V.P.; Schnaid, F.; Maghous, S. & Born, R.B. (2016). Crosswise-loaded pile tests on residual soil site. *Géotechnique Letters*, 6(3):216-220.
- Del Pino Jr, A.; Segantini, A.A.S. & Carvalho, D. (2002). Análise de estacas escavadas carregadas transversalmente, em solo colapsível, com umidade natural e após sua inundação. XII COBRAMSEG, São Paulo, ABMS, v. 3, pp. 1493-1501.
- Faro, V.P. (2014). Lateral Loading in Deep Foundations Associated to Cement Treated Soil Layers: Conception, Load Tests and Design Guidelines. Ph.D. Thesis, Federal University of Rio Grande do Sul, Brazil (in Portuguese).
- Faro, V.P.; Consoli, N.C.; Schnaid, F.; Thomé, A. & Lopes Jr., L.S. (2015). Field tests on laterally loaded rigid piles in cement treated soils. *Journal of Geotechnical and Geoenvironmental Engineering*, 141(6):06015003.

- Ferreira, C.V.; Lobo, A.S.; Albiero, J.H.; Carvalho, D. & Albuquerque, P.J.R. (2006). Comportamento de estaca carregada lateralmente, implantada em solo reforçado com solo-cimento. Proc. X Congresso Nacional de Geotecnia, Portugal, pp. 1089-1098.
- Higgins, W.; Vasquez, C.; Basu, D. & Griffiths, D.V. (2013). Elastic solutions for laterally loaded piles. Journal of Geotechnical and Geoenvironmental Engineering, ASCE, 139(7):1096-1103.
- Leroueil, S. and Vaughan, P.R. (1990). The general and congruent effects of structure in natural soils and weak rocks. Géotechnique, 40(3):467-488.
- Medero, G.M.; Schnaid, F. & Gehling, W.Y.Y. (2007). Oedometer behavior of an artificial cemented highly collapsible soil. Journal of Geotechnical and Geoenvironmental Engineering, 134(1):9-15.
- Miranda Jr., G. (2006). Estacas Submetidas a Esforços Horizontais em Solos Colapsáveis do Interior de São Paulo, nas Condições Natural, Melhorada e Inundada. Tese de Doutorado, Universidade Estadual de Campinas, p. 303.
- Miguel, M.G. (1996). Execução e Análise de Provas de Carga Horizontal em Estacas em Solo Colapsível. Dissertação de Mestrado, Escola de Engenharia de São Carlos, Universidade de São Paulo, p. 162.
- Poulos, H.G. & Davis, E. (1980). Pile Foundations Analysis and Design. John Wiley & Sons Inc., New York, p. 397.
- Rollins, K.M.; Herbst, M.; Adsero, M. & Brown, D. (2010). Jet-grouting and soil mixing for increased lateral pile group resistance. Proceedings GeoFlorida 2010: Advances in Analysis, Modeling & Design, ASCE, Orlando, Florida, pp. 1563-1572.
- Schnaid, F. & Huat, B.B.K. (2012). Sampling and testing of tropical residual soils. In: Handbook of Tropical Residual Soils Engineering. CRC Press, London, pp. 65-112.
- Simons, N.E. & Menzies, B.K. (1975). A Short Course in Foundation Engineering. Newnes-Butterworths, London, p. 159.
- Thomé, A.; Donato, M.; Consoli, N.C. & Graham, J. (2005). Circular footings on a cemented layer above weak foundation soil. Canadian Geotechnical Journal, 42(6):1569-1584.
- Verruijt, A. & Kooijman, A.P. (1989). Laterally loaded piles in a layered elastic medium. Géotechnique, 39(1) 39-49.

List of Symbols

- A_{mob} : Area under compression mobilized at the pile shaft
 D : Diameter of pile
 D_{cem} : Diameter of cement treated layer
 G_o : Initial shear modulus
 H : Horizontal load
 $H_{25\text{ mm}}$: Horizontal load at a top displacement of 25 mm
 L : Length of pile
 L_{cem} : Thickness of cement treated layer
 L_{crit} : Critical embedment depth
 L_n : LVDT reading at a specified time interval t
 L_{n-1} : LVDT reading immediately previous to L_n
 L_1 : First LVDT taken just after loading application
 δ : Horizontal displacement

Anchored Retaining Walls in Granite Residual Soils I. Parametric Study

N. Raposo, A.T. Gomes, M.M. Fernandes

Abstract. This work aims to be a contribution for a better knowledge of anchored earth retaining structures, providing preliminary guidelines for their correct design, by establishing starting points. It also constitutes the introduction to a second paper in which an innovative solution for preliminary design is presented. Starting from an extensive parametric study using PLAXIS on a typical moderate to high strength soil, the study begins by evaluating the influence of parameters such as the excavation depth, the stiffness of the retaining wall and the anchors, the initial prestress, and the soil properties (stiffness, strength, coefficient of earth pressure at rest and bedrock depth). For each parameter influence laws are derived, which will allow the implementation of the simplified design method in a companion paper.

Keywords: forces and displacements, residual soil, anchored wall, hardening soil model.

1. Introduction

The design of anchored walls to support deep excavations comprises difficulties and challenges since it depends on multiple variables, concerning the soil (strength, stiffness, at-rest state of stress), the retaining structure and the geometry of the cut.

The purpose of the parametric study presented in this paper, based on the work of Raposo (2007), is to evaluate the behavior of these structures. The study covers a wide range of geometries, as well as structural and soil parameters.

Subsequently, influence laws are derived, characterizing the effect of each individual variable under analysis. Using these influence laws, the results can be used to interpolate (or extrapolate) the same parameters for similar excavations.

The work is focused on excavations executed in soils with moderate to high strength, taking as reference the granite residual soils, similar to the ones found in the city of Porto, Portugal (Viana da Fonseca et al., 1997). In such ground, because of the frequent presence of batholiths in the soil mass, diaphragm walls are avoided and the most common solution for the retaining wall is cast in place concrete piles, often with spacing larger than their diameter (Matos Fernandes, 2010; Viana da Fonseca & Quintela, 2011).

The tool used to accomplish the parametric study is the finite element method, through the commercial software Plaxis. This method was chosen because it allows evaluating, very accurately and promptly, the influence of the variation of a particular parameter, or of a set of parameters, on the overall behavior of complex soil-structure interaction problems. The possibility of using analytical

models, similar to those of Saribas & Erbatur (1996) or Matos Fernandes et al. (2002), was considered, since they are more intuitive. However, due to the difficulty of applying them to highly hyperstatic structures such as the ones studied in this paper, this option was abandoned.

Given the nature of the soil and the type of retaining wall mentioned above, the water table was considered at the base of the excavation (Raposo & Topa Gomes, 2011). Thus, drained conditions were assumed and the analyses were performed in effective stresses.

2. Base Excavation #A00

2.1. General properties of the base excavation and the numerical model

The excavation used as the starting point for the parametric study (base excavation #A00) is 15.0 m deep and 30.0 m wide, performed in granite residual soils, as shown in Fig. 1. The length of the excavation was assumed to be much greater than its width, allowing the use of a plane strain model.

Two distinct geotechnical layers were considered: a surface layer of granite residual soil (W5) and a substratum, comprising highly weathered granite (W4). Although it may seem insufficient to consider only two layers for characterizing a given soil mass, it is shown in the Appendix how the adopted constitutive model allows the variation of mechanical properties in depth, especially in terms of stiffness, thereby improving the agreement between the numerical model and the reality.

The retaining structure consists of concrete piles with a diameter of 0.60 m and 1.20 m spacing between axes, presenting a flexural stiffness equivalent to that of a diaphragm wall 0.40 m thick. For the Young modulus, E , a value of

Nuno Raposo, Ph.D., Adjunct Professor, Department of Civil Engineering, Viseu Polytechnic Institute, Viseu, Portugal. e-mail: nraposo@ipv.pt.
António Topa Gomes, Ph.D., Assistant Professor, Faculty of Engineering (FEUP), University of Porto, Porto, Portugal. e-mail: atgomes@fe.up.pt.
Manuel de Matos Fernandes, Ph.D., Full Professor, Faculty of Engineering (FEUP), University of Porto, Porto, Portugal. e-mail: mfern@fe.up.pt.
Submitted on December 20, 2016; Final Acceptance on July 14, 2017; Discussion open until April 30, 2018.
DOI: 10.28927/SR.403229

Coulomb failure envelope, for the heavily weathered granite; and the hardening soil model for the granite residual soil. Table 1 contains the required parameters for both models, as well as the values considered for the calculation named “base excavation #A00” (Topa Gomes, 2009; Viana da Fonseca *et al.*, 1997). The first model is probably familiar to the majority of the readers. The latter is described in the Appendix.

2.2. Base excavation #A00 results

Figure 2 shows the displacement of the wall and of the ground surface for the final excavation phase, displaying a typical pattern for this type of geotechnical works (Matos Fernandes, 2010, 2015). In conjunction with the horizontal displacements, there is also a small heave of the wall, as a result of soil expansion, due to the considerable mean stress reduction occurred during the excavation. The maximum horizontal displacement, of about 30 mm, occurs near the excavation base, at 12 m depth. The top of the wall moves about 6 mm towards the excavation side.

As for surface displacements, the subsidence basin extends up to the external model boundary. This is a common limitation of the finite element models. Local instrumentation in several excavation works has revealed that the subsidence basin is much more concentrated near the wall than what Fig. 2 shows (Clough & O’Rourke, 1990; Kung, 2010). This difference results from two main contributions: first, soil stiffness for small strains is much higher and thus it would be necessary to use a model incorporating soil stiffness at very small deformations, such as the one proposed by Puzrin & Burland (1996) or the Hardening Soil model with small-strain stiffness implemented in Plaxis (Brinkgreve *et al.*, 2011), to reliably reproduce behaviour

in points considerably away from the wall; second, real excavations seldom present a length that may be assumed as infinite, and so 2D models tend to overestimate the in-plane deformation deformation, as they do not include the attenuation resulting from the settlement distribution over a length greater than the real excavation length. In real excavations this effect may be significant, reducing the settlements up to half of the value calculated for a plane strain condition.

Focussing the attention on the bending moments along the wall height, after the completion of the excavation, Fig. 3a shows an absolute maximum of 193 kNm/m. As for the horizontal displacements, such value also occurs near the bottom of the excavation, at 13.4 m depth. This maximum bending moment is compatible with the wall resistance, requiring an amount of reinforcement close to 0.6% of the piles cross section area. Comparing Fig. 3a with Fig. 3b, which shows the bending moments envelope, it can be concluded that the last excavation phase is dominant in the majority of the sections, particularly with regard to positive moments.

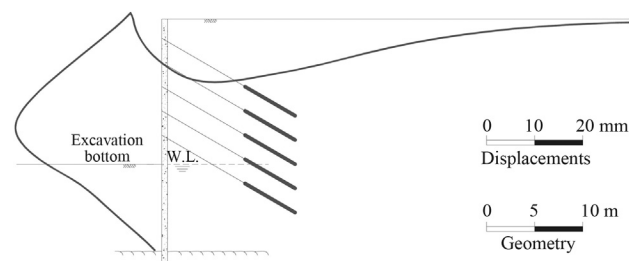


Figure 2 - Displacements of the wall and ground surface at the end of the excavation.

Table 1 - Parameters considered in the base excavation #A00.

Parameter		Granite residual soil	Highly weathered granite
Constitutive model	-	Hardening soil	Elastic perfectly plastic
Unit weight (kN/m ³)	γ_{unsat}	20.0	22.0
Saturated unit weight (kN/m ³)	γ_{sat}	21.5	23.0
Effective cohesion (kPa)	c'	12	100
Effective friction angle (°)	ϕ'	33	42
Dilatancy angle (°) *	Ψ	3	12
Secant stiffness in triaxial drained tests (MPa)	E_{50}^{ref}	22.5	400
Tangent stiffness in primary oedometer loading (MPa)	E_{oed}^{ref}	22.5	-
Exponent for stress-level dependency of stiffness	m	0.7	-
Unloading and reloading stiffness (MPa)	E_{ur}^{ref}	67.5	-
Poisson's ratio for unloading and reloading	ν_{ur}	0.26	0.2
Coefficient of earth pressure at rest	K_0	0.40	0.331
Failure ratio (q/q_a)	R_f	0.9	-

*The dilatancy angle was considered as $\Psi = \phi' - 30$.

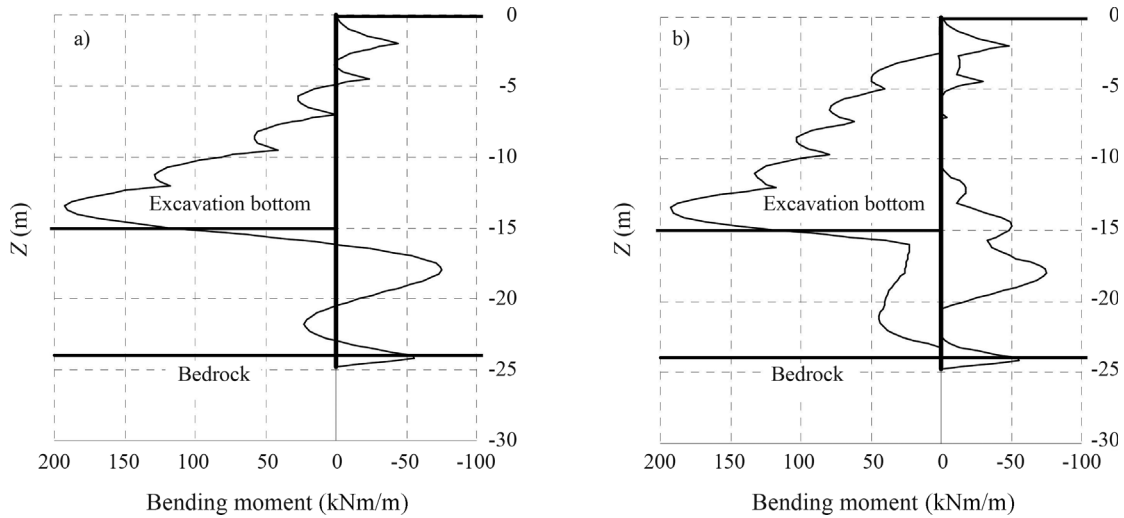


Figure 3 - Wall bending moments: a) final excavation stage; b) envelope.

Figure 4a shows the apparent earth pressure diagram, constructed from the horizontal projections of the anchor forces obtained at the end of the excavation works. This diagram is quite similar to the applied prestress diagram, although slightly higher. Figure 4b allows analyzing the evolution of the forces in the anchors during the various construction stages. The forces are represented as a percentage of the applied prestress. Without exception, these forces increase in excavation phases and decrease in stages where prestress forces are applied to the anchors below. This situation is typical of cases where the prestress forces are correctly designed. It is also important to underline that these variations are modest, validating the hypothesis that the prestress forces are reasonably adequate.

3. Parametric study organization

3.1. Parameters studied

The object of the parametric study are excavations in geotechnical conditions similar to those described in 2.1, with a retaining structure analogous to that in Fig. 1. The effects of a few parameters with proved influence on the behaviour of the excavation are analysed. Table 2 presents the various parameters of this study, as well as the respective symbols. To facilitate the comparison between different excavations, some parameters were made dimensionless.

Two of the parameters may not be so familiar to the reader: the prestressing index and the support system stiffness index.

The prestressing index (ξ) measures, in a dimensionless form, the horizontal force applied to the wall by the

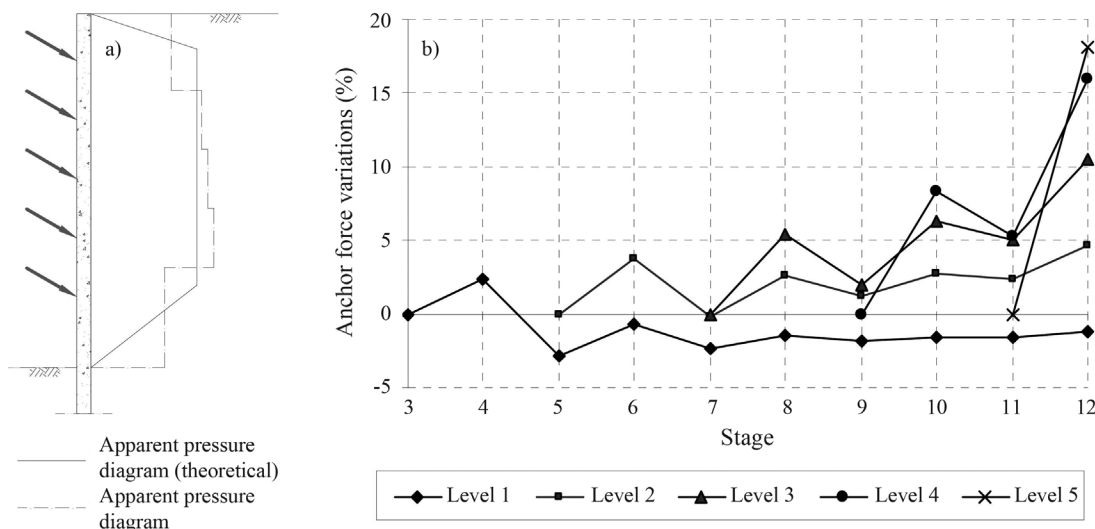


Figure 4 - Anchor forces: a) apparent earth pressures at the end of the excavation; b) anchor forces variation during construction.

grid of anchors. Therefore, the prestress force to be applied to each anchor, F_a , is defined by the equation:

$$F_a = \frac{\xi \gamma h h_a l_a}{\cos \alpha} \quad (1)$$

where ξ represents the prestressing index, γ represents the soil unit weight, h represents the maximum excavation depth, h_a and l_a represent the average height and width of influence of each anchor, respectively, and α the tilt angle of the anchors. The influence height for the first level of anchors extends up to the surface and the influence height for the last level of anchors extends to the bottom of the excavation.

In structures supported by various levels of prestressed anchors or struts, the stiffness of the support system, ρ_s , was defined by Mana (1978) as:

$$\rho_s = \frac{EI}{h_M^4 \gamma} \quad (2)$$

where EI represents the wall bending stiffness and h_M represents the maximum vertical spacing between consecutive supports. For this purpose, the soil below the base of the excavation acts as an additional support, located exactly at the base of the excavation. This definition of support system stiffness index is based on Goldberg *et al.* (1976), introducing additionally the soil unit weight, in order to make the parameter dimensionless. There are other alternatives to evaluate the stiffness of the support structure, such as the flexibility number in terms of displacements, defined by

Table 2 - Parametric study parameters.

Parameter	Symbol	Variation range
Bedrock depth	D/h	1.2 to 2.0
Prestressing index	ξ	0.1 to 0.3
Support system stiffness index	ρ_s	40 to 1600
Excavation depth (m)	h	10 to 25
Soil stiffness (MPa)	E_{50}	15 to 60
Effective friction angle ($^\circ$)	ϕ'	30 to 40
Effective cohesion (kPa)	c'	0 to 30
Coefficient of earth pressure at rest	K_0	0.4 to 0.6

Table 3 - Parametric study - base excavations.

Excavation	h (m)	ρ_s	ξ	D/h	E_{50} (MPa)	ϕ' ($^\circ$)	c' (kPa)	K_0
#A00	15	100	0.15	1.6	22.5	33	12	0.40
#B00	15	100	0.15	1.6	37.5	37	21	0.60
#C00	25	350	0.20	1.2	22.5	33	12	0.40
#D00	25	350	0.20	1.2	37.5	37	21	0.60

Addenbrooke *et al.* (2000), but since it is not dimensionless, it is discarded in favour of the definition of Mana (1978).

3.2. Designation and organization of the calculations

In the parametric study 158 calculations were performed. The designation of each of the calculations, as shown in Fig. 5, consists of three characters: the first corresponds to the series, the second to a certain parameter (subseries) and the third is an id of the calculation, corresponding to a predefined value of the parameter under study.

Each series corresponds to a particular set of calculations, created from the same base excavation. Comparing any calculation to the base excavation of the corresponding series, only one parameter differs. Each series consists of subgroups designated subseries. A subseries is a set of calculations (varying in number from four to six) where all parameters, except the parameter under study, remain constant.

The study begins by defining a base excavation, called #A00, which was presented in 2.1. This is the starting point of the series #A**. In parallel, three additional base excavations are defined, #B00, #C00 and D00, whose main characteristics are listed in Table 3.

Regarding the stiffness of the support system, the adopted values, between 100 and 350, correspond to a retaining structure constituted by 0.60 m and 0.80 m diameter piles, with spacing between, respectively, 1.20 m and 1.10 m. These values of the support system stiffness index can also correspond to diaphragm walls 0.40 m and 0.60 m thick.

The use of these four series has the intention of checking the validity of the influence curves, derived from each subseries, when taking different starting points in terms of geometry, prestress, stiffness of the support system and soil properties. As shown in Fig. 6, the base excavations corre-

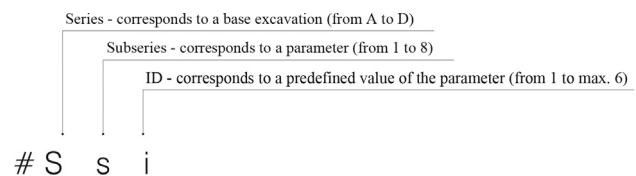


Figure 5 - Designation and organization of the calculations.

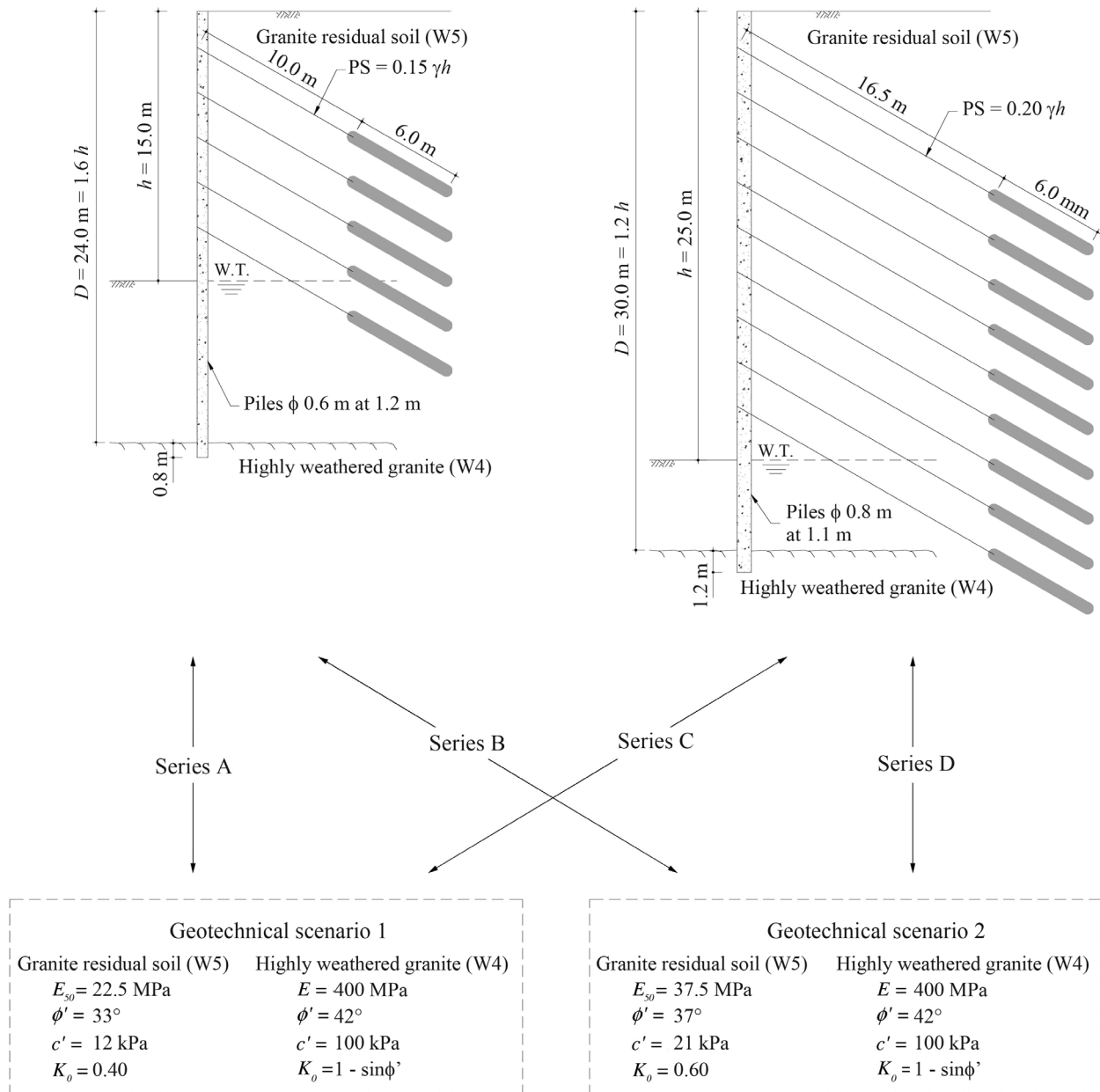


Figure 6 - Base excavations properties.

spond to two geotechnical scenarios and two different geometries and wall properties.

The subseries correspond to the variation of a particular parameter, of the soil or of the wall, according to Table 4. A maximum of 6 calculations was performed for each parameter, with a total of 158 different calculations.

For each subseries, several calculations were performed varying the parameter under study within reasonable limits. As an example, Table 5 presents the variation of the bedrock depth for the subseries # A1*. It involved five additional calculations, besides the base excavation #A00, in a total of six calculations with different values for the bedrock depth.

Table 4 - Parametric study - Subseries.

Subseries	Parameter under study	Number of calculations
##1*	Bedrock depth (D/h)	5
##2*	Prestressing index (ξ)	4
##3*	Support system stiffness index (ρ_s)	5
##4*	Excavation depth (h)	6
##5*	Soil stiffness (E_{50})	5
##6*	Effective friction angle (ϕ')	4
##7*	Effective cohesion (c')	5
##8*	Coefficient of earth pressure at rest (K_0)	4

Table 5 - Parametric study of bebrock depth – subseries #A1*.

Excavation	D/h
#A11	1.2
#A12	1.3
#A13	1.4
#A00	1.6
#A14	1.8
#A15	2.0

3.3. Normalization procedure

The variables of the parametric study on which the attention is focused have, above all, a practical interest: maximum bending moment in the wall, maximum force on the anchors and maximum horizontal wall and surface displacements.

The analysis of the calculations of a given subseries is not particularly problematic, since among the various calculations of that subseries only one parameter is changed. Therefore the differences in the results are a direct consequence of the changes in the parameter under study. However, when the calculations of two or more subseries are being compared, there are always differences in several parameters. These differences create difficulties when trying to determine the influence of a certain parameter. Hence, it is necessary to separate the effects of the parameters.

Taking as an example Fig. 7a, it can be noticed the difficulty in drawing conclusions about the influence of the maximum excavation depth on the maximum horizontal displacements of the wall.

To improve the comparability of results for the various subseries, a normalization procedure was introduced, defining a reference value for the variable under analysis. Thus, the maximum horizontal displacement of the wall, obtained in each calculation is divided by the maximum horizontal displacement obtained in the reference excavation of each subseries. This procedure consists, in its essence, in changing the vertical scale, so that the results of the several subseries intersect at a common point.

Figure 7b illustrates the normalization procedure using the data represented in Fig. 7a. The 15 m deep excavation has been taken as reference. To understand the effect of normalization attention should be given to the changes in the vertical scale. With these changes it is no longer possible to obtain from the figure an absolute value of the wall horizontal displacement. However, Fig. 7b allows determining the variation of the wall horizontal displacement as a consequence of the changes in the excavation depth. In this example, it can be verified that the increase of the maximum excavation depth from 15 m to 25 m causes an increase of the maximum horizontal displacement of the wall varying from 150% to 250%, depending on the subseries under study.

After normalization of the results, it is possible to use the method of least squares to define a function that best fits the results of several subseries, designated in this example β_h . A few types of functions were considered: linear, quadratic, exponential, logarithmic and power. In each case, the function type selected was the one leading to the best correlation coefficient.

This normalization procedure was performed for all parameters of the study, both for the maximum wall bending moments and horizontal displacements.

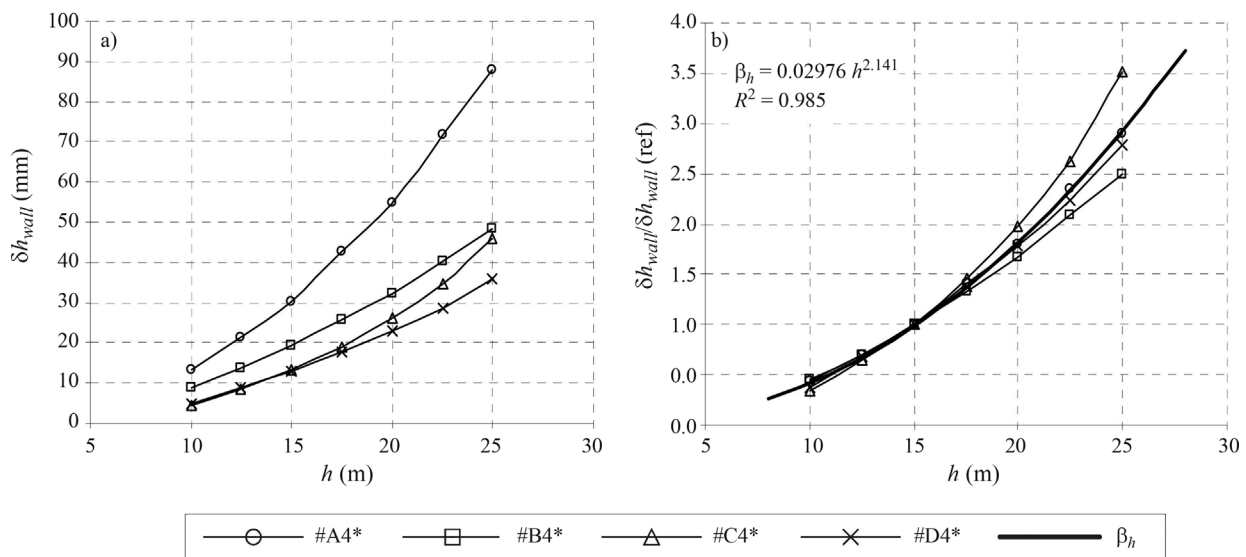


Figure 7 - Influence of excavation depth on the wall horizontal movements: a) results before normalization; b) results after normalization.

4. Summary and Analysis of the Results of the Parametric Study

Figures 8 to 15 present the main results of the parametric study. Each figure has two graphs, corresponding to the maximum bending moment of the wall, on the left, and to the maximum horizontal displacement of the wall, on the right. To facilitate the understanding and future use of the results, the previously presented normalization procedure was applied to all the results.

All graphs comprise four curves, corresponding to the variation of each parameter from the four base excavations. An additional curve, α_i or β_i , was added, corresponding to the least squares approximation of all the calculations in the graph. The Greek letter α was used to denote the curve that best fits the normalized maximum bending moments,

whereas the Greek letter β was used to denote the curve that best approximates the normalized maximum horizontal displacements of the wall. In each graph the mathematical equation and the correlation coefficient, R^2 , are displayed.

In general, for all the parameters it was possible to establish two curves, α and β , which approximate the results of the several subseries with reasonable accuracy, allowing the definition of the influence factor for each parameter on the maximum horizontal displacements and the maximum bending moments of the wall. In most cases the correlation coefficients, R^2 , are higher than 0.90, although presenting smaller values in a few particular situations.

The most puzzling situation occurs regarding the influence factor of the prestressing index on the wall bending

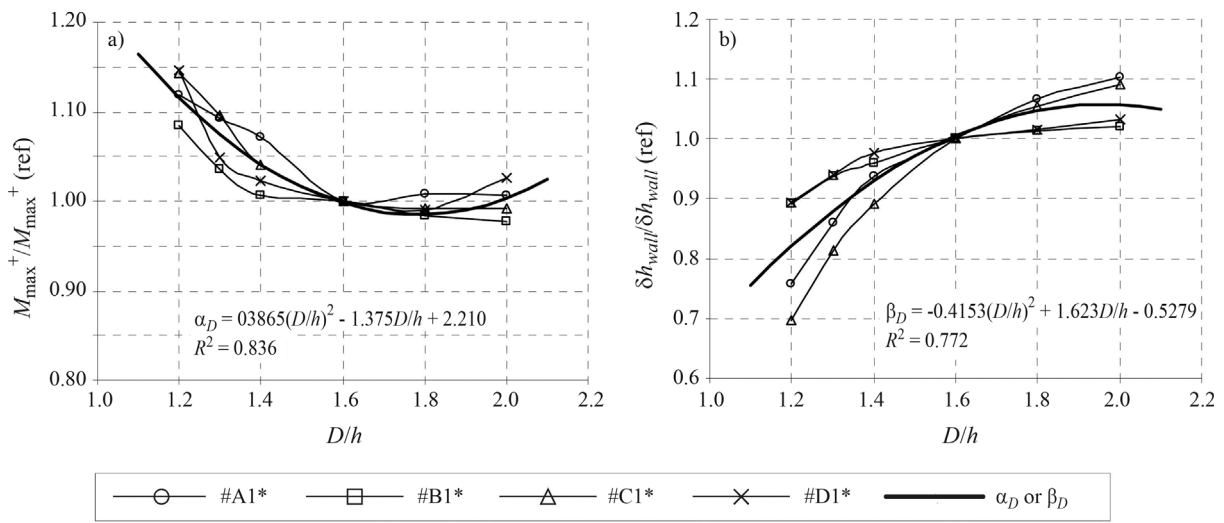


Figure 8 - Influence of bedrock depth: a) maximum bending moments; b) maximum horizontal displacements of the wall.

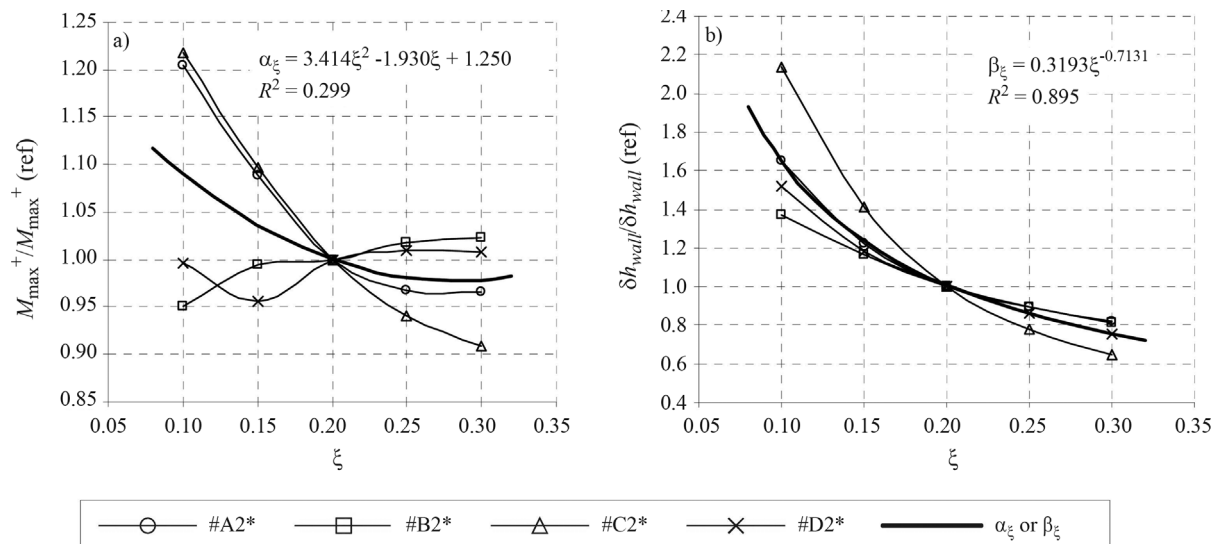


Figure 9 - Influence of prestressing index: a) maximum bending moments; b) maximum horizontal displacements of the wall.

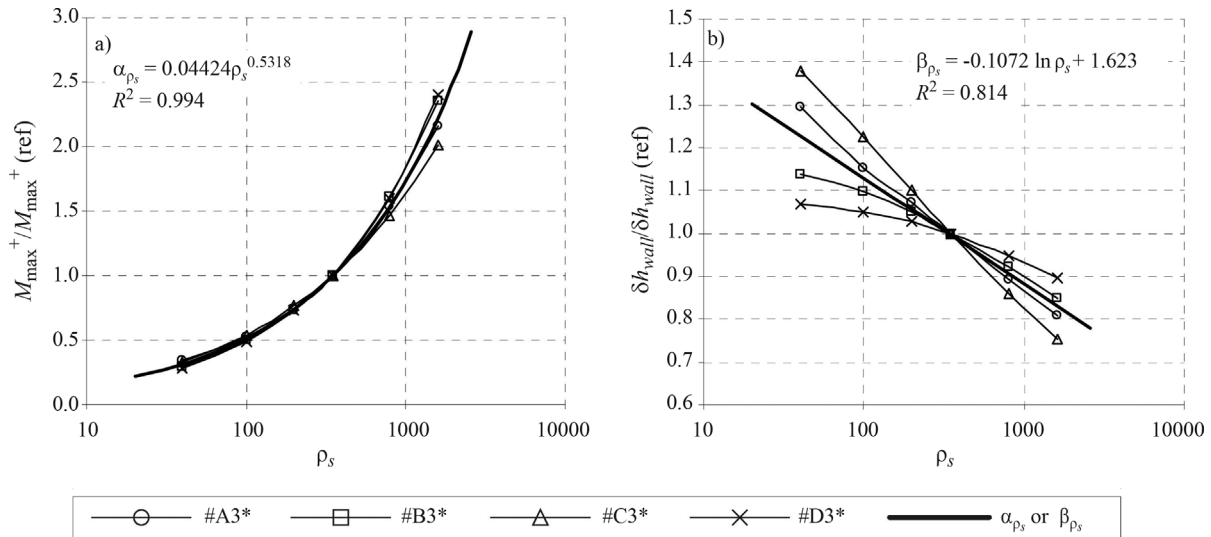


Figure 10 - Influence of support system stiffness index: a) maximum bending moments; b) maximum horizontal displacements of the wall.

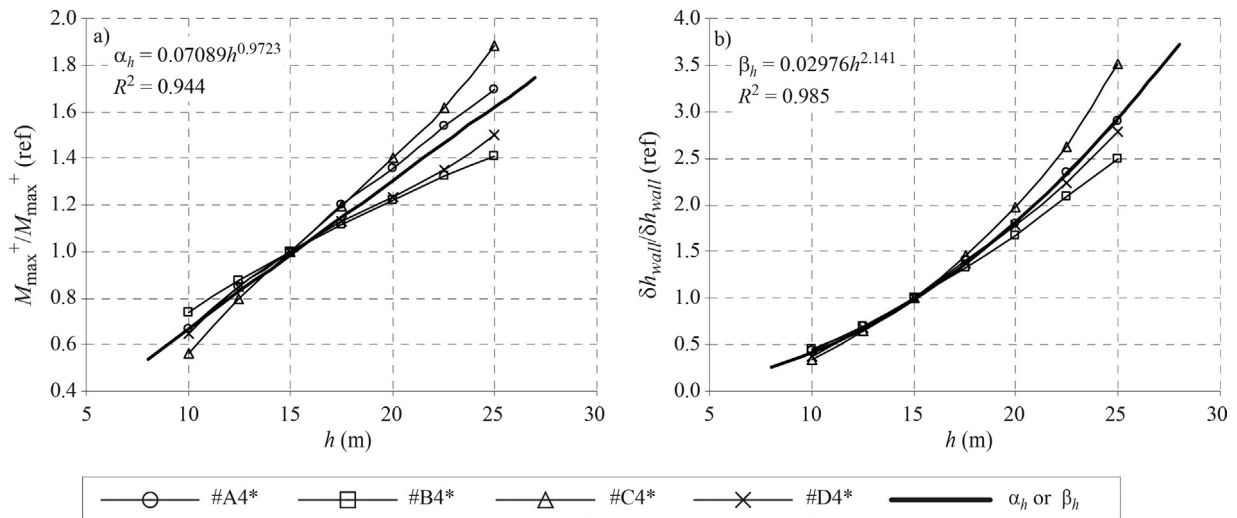


Figure 11 - Influence of maximum excavation depth: a) maximum bending moments; b) maximum horizontal displacements of the wall.

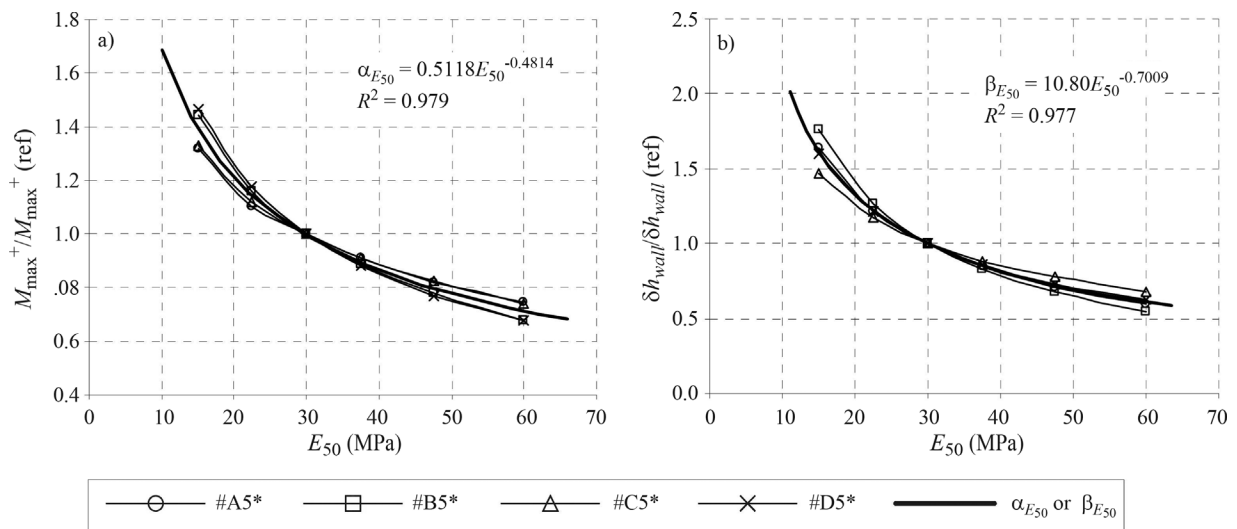


Figure 12 - Influence of soil stiffness: a) maximum bending moments; b) maximum horizontal displacements of the wall.

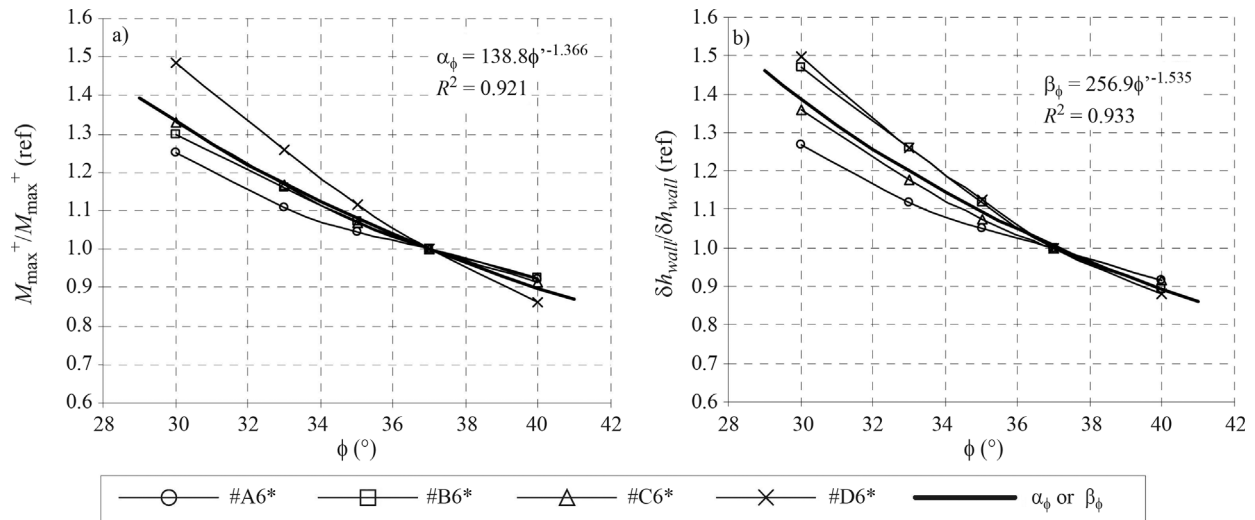


Figure 13 - Influence of soil effective friction angle: a) maximum bending moments; b) maximum horizontal displacements of the wall.

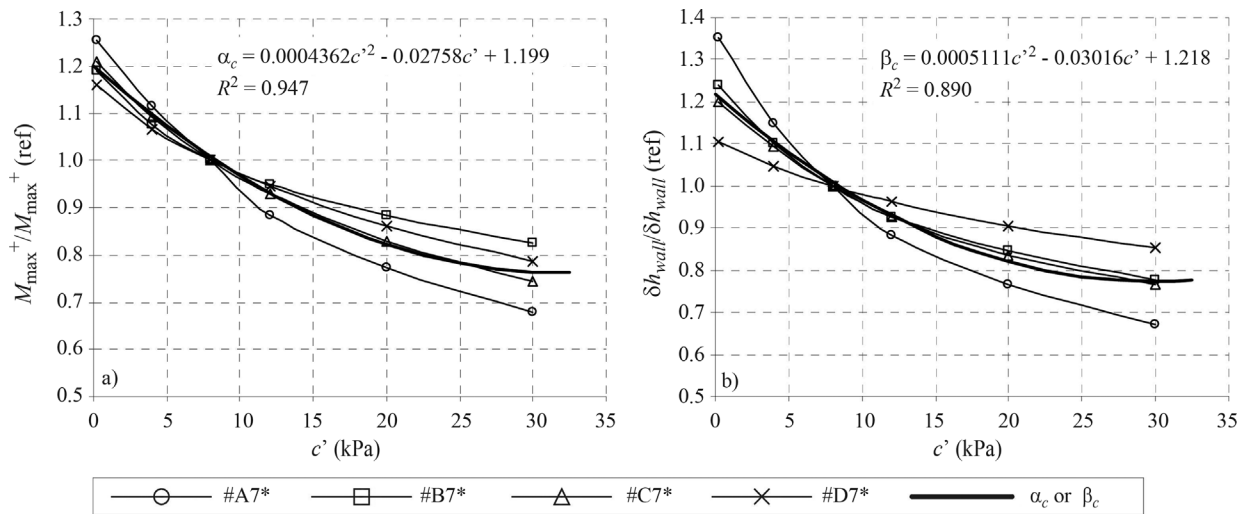


Figure 14 - Influence of soil effective cohesion: a) maximum bending moments; b) maximum horizontal displacements of the wall.

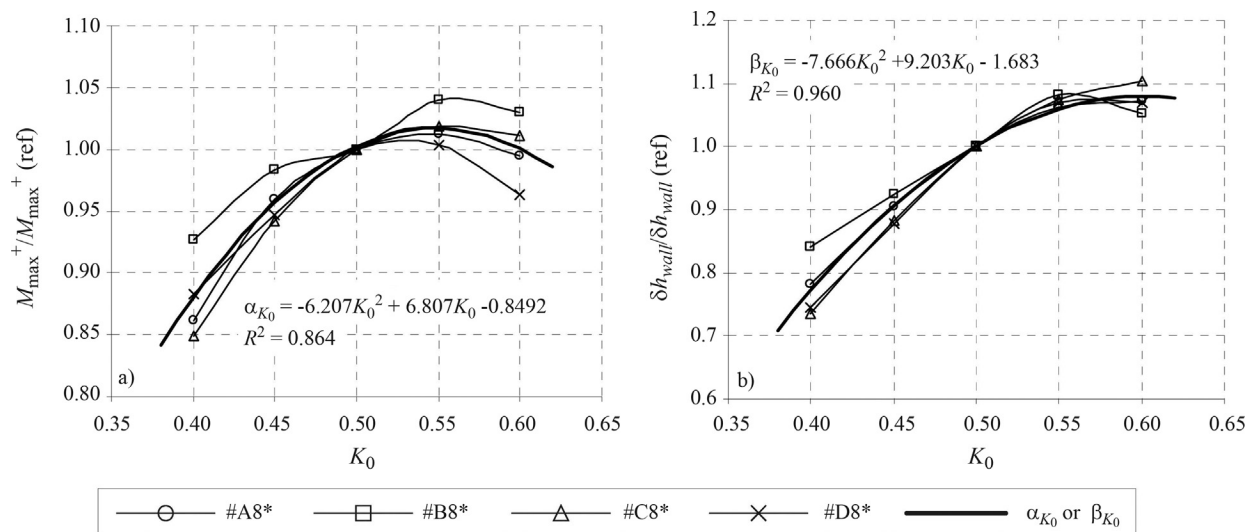


Figure 15 - Influence of soil coefficient of earth pressure at rest: a) maximum bending moments; b) maximum horizontal displacements of the wall.

moments, as illustrated by Fig. 9a, due to the fact that the considered factor is highly influenced by the adopted geotechnical scenario. In the calculations belonging to the subseries #A2 and #C2, increasing the prestressing index from 0.1 to 0.3 leads, in both cases, to reductions in the maximum bending moment close to 25%. In the calculations belonging to subseries #B2 and #D2, the same increase in the prestressing index has a very discrete influence on the maximum bending moment of the wall, leading to its slight increase. A detailed analysis of these results showed that this difference in behaviour is mainly due to the soil strength. The less resistant and stiff the soil is, the more favourable the prestressing. This effect is also found when analysing the maximum horizontal displacements of the wall, although with less intensity. Figure 9b shows that variations in the prestressing index have greater influence on excavations executed in less resistant and more deformable soils.

Table 6 summarizes the results of the parametric study, indicating the degree of importance of each parameter with regard to the maximum wall bending moment and horizontal displacement. Some of the parameters were classified as having moderate influence, by not having a particular influence over the analysed results.

The effect of the studied parameters on the maximum bending moment may be quite distinct from its effect on the maximum displacement. The best example of this fact is the support system stiffness index, which has a moderate influence on the displacement but considerably affects the maximum bending moment. Moreover, the support system stiffness index influences the displacement and the bending moments in opposite ways, as shown in Fig. 10.

During the parametric study of the different variables, in addition to the stresses and displacements of the wall, surface ground displacements were also calculated. A strong correlation between the displacements of the wall and the ground surface displacements was noticed.

In Fig. 16, where the maximum horizontal displacements of the ground surface are plotted against the maximum horizontal displacements of the wall, it becomes clear that the former are approximately half of the latter. Despite the large amount of calculations, based on quite diverse geotechnical conditions and different excavation geometries, the results show a significant consistency, as is proved by the high correlation coefficient obtained using the method of the least squares and assuming that the value at the origin is null.

The good correlation between the maximum horizontal surface displacements and the maximum horizontal wall displacements allows the use of the equation presented in Fig. 16 to estimate the former, at least for preliminary design situations.

Figure 17 shows a histogram indicating the variations of the force in the ground anchors, calculated as a percentage of the prestress force applied. Note that only one value

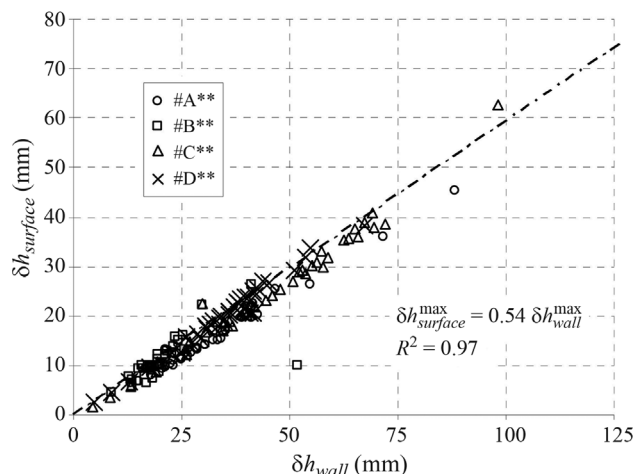


Figure 16 - Maximum horizontal surface movements vs. maximum horizontal displacements of the wall.

Table 6 - Degree and type of influence of the several parameters over bending moments and horizontal wall displacements.

Parameter	Symbol	Degree and type of influence over bending moments	Degree and type of influence over displacements
Bedrock depth	D/h	C ↓	C ↑
Prestressing index	ξ	C ↓	A ↓
Support system stiffness index	ρ_s	A ↑	B ↓
Excavation depth	h	A ↑	A ↑
Soil stiffness	E_{50}	B ↓	A ↓
Effective friction angle	ϕ'	B ↓	B ↓
Effective cohesion	c'	B ↓	B ↓
Coefficient of earth pressure at rest	K_0	C ↑	C ↑

A – Very important; B – Important; C – Moderate.

↑ – Grows with parameter increase; ↓ – Reduces with parameter increase.

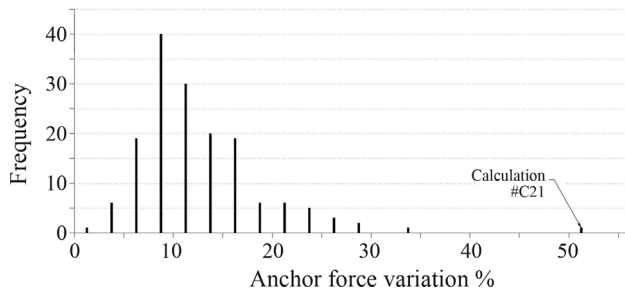


Figure 17 - Histogram with the variation of anchor forces, as a percentage of prestressing force (sample: 158 excavations).

per excavation is shown, corresponding to the most stressed anchor. In the majority of the excavations increments of 10% to 20% were obtained.

Regarding this point, calculation #C21 is in fact a singular case, by having a maximum increase of the anchor force of 57%. This abnormally high value is due to the small prestress used, corresponding to $0.1 \gamma h$, in conjunction with not so favourable geotechnical conditions. These facts lead to high stresses and large wall displacements, corresponding to a scenario in which the design could be considered inappropriate.

5. Conclusions

The parametric study aims to be a contribution towards understanding the effect of some of the variables that rule the behaviour of anchored retaining walls and their interaction with the supported ground.

The influence laws for each parameter and the results of all performed calculations allow a preliminary evaluation of the behaviour of anchored excavations.

On average, it appears that the maximum wall bending moment increases when the bedrock depth increases, the prestressing index reduces, the support system stiffness index increases, the maximum excavation depth increases, the soil stiffness decreases, the friction angle and soil cohesion decrease and the coefficient of earth pressure at rest increases. The parameter that most affects the maximum bending moment of the wall is the stiffness of the support system.

Concerning the maximum horizontal displacement of the wall, it was found that it increases when both the bedrock depth and the maximum excavation depth increase, the prestressing index and the support system stiffness index reduce, the friction angle and soil cohesion decrease and the coefficient of earth pressure at rest increases. The maximum excavation depth is particularly important in controlling the maximum horizontal displacement of the wall.

The comparative study of the maximum horizontal displacements of the wall *vs.* the maximum horizontal surface displacements allows concluding that the former can

be estimated from the latter within a quite reasonable degree of confidence.

The overall attained results seem to be quite satisfactory, contributing to an alternative and economic method for the preliminary design of anchored retaining structures, to be presented in a companion paper.

6. Appendix: Hardening Soil Model

In this appendix a brief description of the hardening soil model is presented. Detailed information about this soil model can be found in Brinkgreve (2002).

In most geotechnical problems, there is usually reasonable information about the soil strength parameters, but reduced information concerning its stiffness. This situation results, fundamentally, from the complexity of the stress-strain relations of the soils, in particular the dependence of soil stiffness on the confining stress, the stress path and the strain level (Topa Gomes, 2009; Viana da Fonseca, 2003).

For the reasons listed above, it becomes difficult to establish a single stiffness that can be used in an elastic perfectly plastic constitutive model. In geotechnical problems such as the ones studied in this work, the hardening soil model has the ability to simulate the soil behaviour much closer to reality, especially when referring to the simulation of loading and unloading cycles due to successive excavation and anchor prestressing stages. Being an elastoplastic model, its yield surface is not fixed in the principal stress space. During the expansion of the yield surface, irreversible plastic deformation occurs.

Distinction can be made between two main types of hardening, namely shear hardening and compression hardening. Shear hardening is used to model plastic strains due to primary deviatoric loading. Compression hardening is used to model plastic strains due to primary compression in oedometer loading and isotropic loading. Both types of hardening are contained in the hardening soil model (Brinkgreve, 2002).

When subjected to primary deviatoric loading, soil shows decreasing stiffness and, simultaneously, irreversible plastic strains develop. In the special case of a drained triaxial test, the observed relationship between the axial strain (ϵ_1) and the deviatoric stress (q) can be reasonably approximated by a hyperbola. Such a relationship, initially formulated by Kondner (1963) and Kondner & Zelasko (1963), was later used in the well-known hyperbolic model by Duncan & Chang (1970). The hardening soil model, however, supersedes the hyperbolic model in three relevant issues (Brinkgreve, 2002): i) it uses the theory of plasticity, rather than the theory of elasticity; ii) it includes soil dilatancy; iii) it introduces the yield cap, which corresponds to compression yielding, and creates a closed elastic region.

Among the main characteristics of this constitutive model, the following should be highlighted: i) the ability to change soil stiffness according to the confining stress (by means of the input parameter m); ii) the consideration of

plastic deformations caused by shear stress (E_{50}); iii) the consideration of plastic deformations caused by isotropic stress (E_{oed}); iv) the use of different values for soil stiffness according to the stress path (for unloading and reloading E_{ur} and v_{ur} are used instead of the stiffness parameters listed above); v) the use of an yield criterion according to Mohr-Coulomb (c' and ϕ'); vi) the control of the yield surface by means of the dilatancy angle (Ψ').

In a drained triaxial test, during primary loading, the relationship between axial strain (ε_1) and deviatoric stress (q), illustrated by Fig. 18, can be described by the following equation:

$$\varepsilon_1 = \frac{1}{2E_{50}} \frac{q}{1 - \frac{q}{q_a}} \quad \text{for } q < q_f \quad (3)$$

where q_a represents the asymptote of the hyperbola and q_f the maximum deviatoric stress (yield stress obtained in the test). Calculating the derivative of Eq. (3) with respect to q , results in an initial Young modulus of $2E_{50}$.

The value of q_f can be derived from the Mohr-Coulomb failure criterion:

$$q_f = (c' \cot \phi' + \sigma'_3) \frac{2 \sin \phi'}{1 - \sin \phi'} \quad (4)$$

When the deviatoric stress equals q_p , the yield stress is reached and perfectly plastic flow occurs, as described by the Mohr-Coulomb criterion. The ratio between the ultimate deviatoric stress, q_p , and the hyperbola asymptote, q_a , determines the input parameter R_f . In cases where there are not enough tests to estimate this parameter, Brinkgreve (2002) suggests the use of 0.9.

The secant Young modulus (E_{50}) for a deviatoric stress equal to one half of q_f depends on the confining stress σ'_3 . It can be calculated by the equation:

$$E_{50} = E_{50}^{ref} \left(\frac{c' \cos \phi' + \sigma'_3 \sin \phi'}{c' \cos \phi' + p'^{ref} \sin \phi'} \right)^m \quad (5)$$

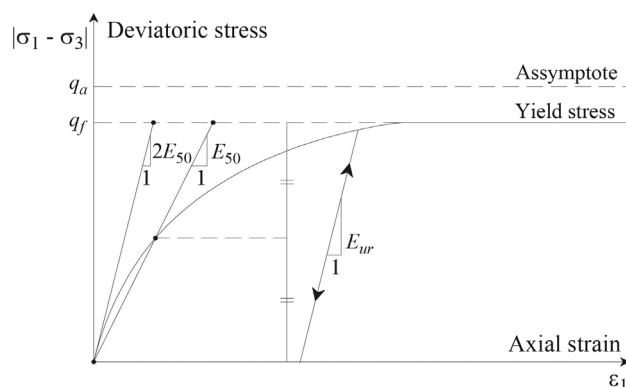


Figure 18 - Hyperbolic stress-strain relation in primary loading for a standard drained triaxial test, adapted from Brinkgreve (2002).

where E_{50}^{ref} is the reference Young modulus of the soil in primary loading, determined for a confining pressure p'^{ref} , which is usually 100 kPa. It should be noted that in Eqs. (4) and (5) the value σ'_3 is positive for compressive stress, consistent with the usual Soil Mechanics sign convention.

The dependency of E_{50} with respect to the stress level is given by the exponent m . This parameter can be considered equal to 1.0 for soft clayey soils. In numerous studies performed over sands and silts, this parameter ranges between 0.5 and 1.0 (Von Soos, 1990). In the case of Porto granite residual soils, values of m between 0.5 and 0.6 are common (Topa Gomes, 2009; Viana da Fonseca, 2003).

To reproduce the soil behaviour during loading and unloading cycles, the hardening soil model uses different stiffness parameters, depending whether it is a primary loading or a reloading stress path. This is a great improvement when compared to simpler soil models. The dependency of the Young modulus for unloading or reloading, E_{ur} , upon the confining pressure p'^{ref} , is expressed by the following equation:

$$E_{ur} = E_{ur}^{ref} \left(\frac{c' \cos \phi' + \sigma'_3 \sin \phi'}{c' \cos \phi' + p'^{ref} \sin \phi'} \right)^m \quad (6)$$

where E_{ur}^{ref} is the reference Young modulus of the soil in an unloading or reloading stress path, determined for a confining pressure p'^{ref} .

The hardening soil model allows an independent control of distortional and volumetric strain. This variable is controlled by the tangent oedometer modulus, given by:

$$E_{oed} = E_{oed}^{ref} \left(\frac{c' \cos \phi' + \sigma'_1 \sin \phi'}{c' \cos \phi' + p'^{ref} \sin \phi'} \right)^m \quad (7)$$

where E_{oed}^{ref} is the reference oedometer Young modulus, determined for a confining pressure p'^{ref} , as shown in Fig. 19. In this case σ'_1 is used instead of σ'_3 , since this is the only principal stress controlled.

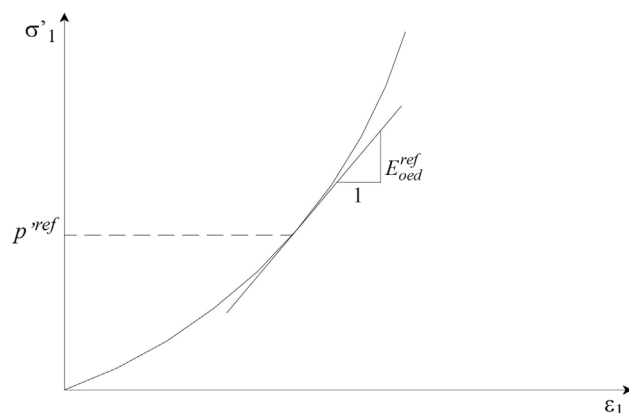


Figure 19 - Definition of E_{oed}^{ref} in oedometer test results.

Acknowledgments

This work was financially supported by: Project POCI-01-0145-FEDER-007457 – CONSTRUCT - Institute of R&D in Structures and Construction funded by FEDER funds through COMPETE2020 - Programa Operacional Competitividade e Internacionalização (POCI) – and by national funds through FCT - Fundação para a Ciência e a Tecnologia.

References

- Addenbrooke, T.I.; Potts, D.M. & Dabee, B. (2000). Displacement flexibility number for multipropped retaining wall design. *Journal of Geotechnical and Geoenvironmental Engineering*, 126(8):718-726.
- Brinkgreve, R. (2002). *Plaxis: Finite Element Code for Soil and Rock Analyses: 2D-Version 8: [user's Guide]*. Balkema, Delft, Netherlands.
- Brinkgreve, R.; Engin, E.; Swolfs, W.; Waterman, D.; Chesaru, A.; Bonnier, P. & Galavi, V. (2011). *Plaxis 3D 2011 Part 3 - Material Models Manual*. Plaxis bv, Delft, Netherlands.
- Clough, G.W. & O'Rourke, T.D. (1990). Construction induced movements of insitu walls. *ASCE Conference on Design and Performance of Earth Retaining Structures*. Cornell University, Ithaca, pp. 439-470.
- Duncan, J.M. & Chang, C.-Y. (1970). Nonlinear analysis of stress and strain in soils. *Journal of Soil Mechanics and Foundations Division, ASCE* 96(5):1629-1653.
- Goldberg, D.T.; Jaworski, W.E. & Gordon, M.D. (1976). *Lateral Support Systems and Underpinning, Vol. 1*. Federal Highway Administration, Washington D. C.
- Guerra, N.M.C.; Josefino, C.S. & Fernandes, M.M. (2007). Methods of two-dimensional modelling of soil anchors. *Proc. Applications of Computational Mechanics in Geotechnical Engineering V*, Guimarães, Taylor & Francis, London, pp. 257-268.
- Kondner, R.L. (1963). Hyperbolic stress-strain response: Cohesive soils. *Journal of the Soil Mechanics and Foundations Division, ASCE* 89(1):115-144.
- Kondner, R.L. & Zelasko, J.S. (1963). A hyperbolic stress-strain formulation for sands. *Proc. 2nd Pan-American Conference on Soil Mechanics and Foundation Engineering, Brasil*, pp. 289-324.
- Kung, G.T.-C. (2010). *Finite Element Analysis of Wall Deflection And Ground Movements Caused by Braced Excavations*. Finite Element Analysis, Sciyo.
- Mana, A.I. (1978). *Finite Element Analyses of Deep Excavation Behavior in Soft Clay*. PhD Thesis, Stanford University.
- Matos Fernandes, M.; Vieira, C. & Sousa, J. (2002). Flexible cantilever retaining walls: design according to Eurocode 7 and classical methods. *Foundation Design codes and soil investigation in view of international harmonization and performance based design*, 10-12 April 2002, Kamakura, Japan, 117-125, A. A. Balkema.
- Matos Fernandes, M. (2010). Deep urban excavations in Portugal: Practice, design, research and perspectives. *Soils and Rocks*, 33(3):115-142.
- Matos Fernandes, M. (2015). New developments in the control and prediction of the movements induced by deep excavations in soft Soils - Pacheco Silva Lecture. *Soils and Rocks*, 38(3):191-215.
- Matos Fernandes, M.; Cardoso, A.S.; Topa Gomes, A. & Borges, J.L. (2012). Deep excavations in urban areas - Finite element modelling for three geotechnical scenarios and retaining solutions. *Innovative Numerical Modelling in Geomechanics*. Taylor & Francis, London.
- Puzrin, A.M. & Burland, J.B. (1996). A logarithmic stress-strain function for rocks and soils. *Geotechnique*, 46(1):157-164.
- Raposo, N.P. (2007). *Preliminary Design of Anchored Earth Retaining Structures (in Portuguese)*. MSc Thesis, Universidade do Porto.
- Raposo, N.P. & Topa Gomes, A. (2011). Water table lowering effects on excavations. *Geotechnical Aspects of Underground Construction in Soft Ground*, May, 16 to 18, Rome.
- Saribas, A. & Erbatur, F. (1996). Optimization and sensitivity of retaining structures. *Journal of Geotechnical Engineering*, 122(8):649-656.
- Topa Gomes, A. (2009). *Elliptical Shafts by the Sequential Excavation Method. The Case of Metro do Porto (in Portuguese)*. PhD Thesis, Universidade do Porto.
- Van Langen, H. & Vermeer, P.A. (1991). Interface elements for singular plasticity points. *International Journal for Numerical and Analytical Methods in Geomechanics*, 15(5):301-315.
- Viana da Fonseca, A. (2003). Characterising and deriving engineering properties of a saprolitic soil from granite in Porto. *International Workshop on Characterisation and Engineering Properties of Natural Soils*, 2-4 December 2002, Singapore, pp. 1341-1378.
- Viana da Fonseca, A.; Matos Fernandes, M. & Cardoso, A.S. (1997). Interpretation of a footing load test on a saprolitic soil from granite. *Géotechnique*, 47(3):633-651.
- Viana da Fonseca, A. & Quintela, J.R. (2011). Modelling the behaviour of a retaining wall in residual soils for a cut and cover construction of a deep station in Metro do Porto. *Geomechanics and Geoengineering*, 6(4):265-281.
- Von Soos, P. (1990). *Properties of Soil and Rock*. *Grundbau Taschenbuch Part 4*, 4th ed. Ernst & Sohn, Berlin.
- Wood, D.M. (2004). *Geotechnical Modelling*. Spon Press, New York.

Anchored Retaining Walls in Granite Residual Soils II.

A Method for Preliminary Design

N. Raposo, A.T. Gomes, M.M. Fernandes

Abstract. In a companion paper, an extensive parametric study regarding anchored retaining structures was presented, contributing to better understand the behaviour and most relevant parameters regarding their design. Based on those results, a novel and simple methodology for preliminary design is presented, providing an alternative procedure for preliminary design and implementation of the observational method. The methodology consists on the following four steps: definition of the properties of the excavation to be analysed – target excavation; selection, among all the excavations simulated in the parametric study, of the reference excavation, that acts as a starting point; calculation of all the correction factors; prediction of the bending moments and movements of the target excavation. The paper finishes with the application of the proposed methodology to several examples of increasing complexity, allowing to show how the method is applied and simultaneously demonstrating its potential for practical purposes.

Keywords: forces and displacements, residual soil, anchored wall, preliminary design.

1. Introduction

In a companion paper (Raposo et al., 2017) it was presented a parametric study analyzing a large number of excavations supported by anchored walls. The geotechnical conditions assumed correspond to granite residual soils.

Based on that parametric study, this paper presents a simple numerical method that permits to estimate, with a reasonable approximation, the relevant results for a preliminary design of anchored walls used to support deep excavations in similar geotechnical conditions.

The task to be accomplished consists in obtaining a quick estimate for the maximum bending moment in the wall and the maximum horizontal displacement of the wall just on the basis of the parametric study results, that is, without analyzing the excavation using the finite element method or other numerical tool.

A strategy similar to the one followed by Mana (1978) and (Mana & Clough, 1981) was adopted, with innovations regarding the mathematical process.

As the maximum bending moment and the maximum horizontal displacement of the wall were calculated as function of eight variables, for which typically six different values were considered, a conventional interpolation procedure would have required more than one million analyses ($6^8 = 1679616$).

Having this in mind, an alternative method was developed, resulting in a large reduction of the total number of calculations to 158 (Raposo, 2007).

The paper presents some examples of gradually increasing complexity, highlighting the application of the de-

veloped approach. The results seem to prove the utility of the method but show, as well, its limitations.

2. Procedure for Applying the Proposed Method

2.1. General description

The proposed methodology was devised for preliminary design purposes and thus it is necessarily simple. The main aspiration is the possibility of obtaining the maximum bending moments and wall displacements, parameters that assume vital importance in the design of retaining structures. The idea is that of obtaining these parameters from accumulated experience in similar calculations. The method may easily be adapted to different geotechnical scenarios and geometrical conditions, which constitutes a great advantage. It has also the significant benefit of being an alternative procedure with respect to finite element calculations, providing an additional check for designers.

In simple terms, the method consists in the following four steps:

- A. Definition of the *target excavation*. The *target excavation* is the excavation whose preliminary design is required and should be characterized by the following parameters: excavation depth; bedrock depth; strength, stiffness and initial stress state of the ground; stiffness and prestress of the retaining structure. Table 1 presents the definition of the parameters and the variation range adopted in the parametric study (presented in the companion paper).
- B. Selection of the *reference excavation*. The *reference excavation* is to be chosen among the various excava-

Nuno Raposo, Ph.D., Adjunct Professor, Department of Civil Engineering, Viseu Polytechnic Institute, Viseu, Portugal. e-mail: nraposo@ipv.pt.
António Topa Gomes, Ph.D., Assistant Professor, Faculty of Engineering (FEUP), University of Porto, Porto, Portugal. e-mail: atgomes@fe.up.pt.
Manuel de Matos Fernandes, Ph.D., Full Professor, Faculty of Engineering (FEUP), University of Porto, Porto, Portugal. e-mail: mfern@fe.up.pt.
Submitted on March 4, 2017; Final Acceptance on September 1, 2017; Discussion open until April 30, 2018.
DOI: 10.28927/SR.403243

tions previously calculated and should be as similar as possible to the *target excavation*, having in mind the ground and retaining wall characteristics. The concept of close similarity depends on the fact that different parameters have different impact on the results. The *reference excavation* may be one of the four *base excavations* whose characteristics are shown in Table 2, with results summarized in Table 3, or any other excavation previously calculated.

Table 1 - Parameters and variation range used to characterize the excavations.

Parameter	Symbol	Variation range
Excavation depth (m)	h	10 to 25
Support system stiffness ⁽¹⁾	ρ_s	40 to 1600
Prestressing index ⁽²⁾	ξ	0.1 to 0.3
Bedrock depth	D/h	1.2 to 2.0
Soil stiffness (MPa)	E_{s0}	15 to 60
Effective friction angle (°)	ϕ'	30 to 40
Effective cohesion (kPa)	c'	0 to 30
Coefficient of earth pressure at rest	K_0	0.4 to 0.6

⁽¹⁾The stiffness of the support system is calculated by the expression:

$$\rho_s = \frac{EI}{h_M^4 \gamma} \quad (1)$$

where EI represents the wall bending stiffness, h_M is the maximum vertical spacing between consecutive supports and γ the unit weight of soil. Taking as an example a wall made of concrete piles ($E = 30$ GPa) with a diameter of 0.60 m and 1.20 m separation between axes, with a maximum vertical spacing between consecutive supports of 3 m, in a soil with a unit weight of 20 kN/m³, the stiffness of the support system would be:

$$\rho_s = \frac{EI}{h_M^4 \gamma} = \frac{30 \times 10^6 \times \pi \times \left(\frac{0.60^4}{64}\right) / 1.2}{3^4 \times 20} = 100 \quad (2)$$

⁽²⁾The prestressing index (ξ) measures, in a dimensionless form, the horizontal force applied to the wall by the grid of anchors. The prestress force to be applied to each anchor, F_a , is defined by the equation:

$$F_a = \frac{\xi \gamma h h_a l_a}{\cos \alpha} \quad (3)$$

where h represents the maximum excavation depth, h_a and l_a are the average height and width of influence of each anchor, respectively, and α the tilt angle of the anchors. Taking as an example an excavation with a prestressing index of 0.15, executed in a soil with a unit weight of 20 kN/m³, down to 15 m depth, supported by ground anchors with a tilt angle of 30 degrees, spaced 3.0 m horizontally and 2.5 m vertically, the prestress force to be applied to each anchor should be:

$$F_a = \frac{\xi \gamma h h_a l_a}{\cos \alpha} = \frac{0.15 \times 20 \times 15 \times 3 \times 2.5}{\cos 30} = 390 \text{ kN} \quad (4)$$

Table 2 - Parametric analysis – *base excavation* properties.

Excavation	h (m)	ρ_s	ξ	D/h	E_{s0} (MPa)	ϕ' (°)	c' (kPa)	K_0
#A00	15	100	0.15	1.6	22.5	33	12	0.40
#B00	15	100	0.15	1.6	37.5	37	21	0.60
#C00	25	350	0.20	1.2	22.5	33	12	0.40
#D00	25	350	0.20	1.2	37.5	37	21	0.60

Table 3 - Parametric analysis – results of the *base excavations*.

Excavation	M_{\max} (kNm/m)	δh_{wall} (mm)	$\delta h_{\text{surface}}$ (mm)	$\delta v_{\text{surface}}$ (mm)	$PS_{\max}^{(1)}$ (kN/m)
#A00	193	30.4	14.2	13.1	153
#B00	132	19.4	9.9	5.1	146
#C00	685	46.0	24.2	24.0	332
#D00	437	36.0	21.0	14.0	325

⁽¹⁾ PS_{\max} is the maximum axial force in the anchors divided by the horizontal influence distance, l_a , of each anchor.

- C. Calculation of the correction factors. For each of the base variables, the factors that allow scaling the results of the *reference excavation* must be calculated. This task is accomplished using the influence curves defined in Table 4 and Table 5.
- D. Multiplication of the correction factors by the results obtained in the *reference excavation*. With this operation the predictions for the maximum bending moment and maximum horizontal displacement of the wall are obtained.

2.2. Prediction of the bending moments

The maximum bending moment can be predicted through the following expression:

$$M_{\max} = M_{ref} \times cm_h \times cm_D \times cm_{\xi} \times cm_{\rho_s} \times cm_{E_{s0}} \times cm_{\phi} \times cm_c \times cm_{K_0} \quad (5)$$

which is the maximum bending moment in the *reference excavation* multiplied by the correction factors for the several parameters involved in the problem.

The correction factors for the bending moments are obtained by dividing the influence factors for the *target excavation* by the respective influence factors for the *reference excavation*, according to the equation:

$$cm_i = \frac{\alpha_i(\text{target excavation})}{\alpha_i(\text{reference excavation})} \quad (6)$$

where variable i represents a generic parameter and α_i is the influence factor for the bending moment relative to variable i . As referred in the companion paper, α_i corresponds to the value of the function that best defines the average influence

Table 4 - Influence factors for the maximum bending moments of the wall.

Influence factor	Equation	Influence factor range	Impact grade
α_{ρ_s}	$0.04424\rho_s^{0.5318}$	0.286 to 2.405	A (8.41)
α_h	$0.07089h^{0.9723}$	0.562 to 1.886	A (3.36)
$\alpha_{E_{50}}$	$0.5188E_{50}^{-0.4814}$	0.678 to 1.468	B (2.17)
α_s	$0.0004362c'^2 - 0.02752c' + 1.199$	0.679 to 1.255	B (1.85)
α_ϕ	$138.8\phi^{-1.366}$	0.861 to 1.485	B (1.72)
α_ξ	$3.414\xi^2 - 1.930\xi + 1.250$	0.908 to 1.218	C (1.34)
α_{K_0}	$-6.207K_0^2 + 6.807K_0 - 0.8492$	0.850 to 1.040	C (1.22)
α_D	$0.3865(D/h)^2 - 1.375(D/h) + 2.210$	0.978 to 1.147	C (1.17)

Table 5 - Influence factors for the maximum horizontal displacements of the wall.

Influence factor	Equation	Influence factor range	Impact grade
β_h	$0.02976h^{2.141}$	0.375 to 3.508	A (9.35)
β_ξ	$0.3193\xi^{-0.7131}$	0.651 to 2.137	A (3.28)
$\beta_{E_{50}}$	$10.80E_{50}^{-0.7009}$	0.544 to 1.761	A (3.24)
β_c	$0.0005111c'^2 - 0.03016c' + 1.218$	0.670 to 1.352	B (2.02)
β_{ρ_s}	$-0.1072 \ln(\rho_s) + 1.623$	0.752 to 1.379	B (1.83)
β_ϕ	$256.9\phi^{-1.535}$	0.880 to 1.495	B (1.70)
β_D	$-0.4153(D/h)^2 + 1.623(D/h) - 0.5279$	0.698 to 1.103	C (1.58)
β_{K_0}	$-7.666K_0^2 + 9.203K_0 - 1.683$	0.736 to 1.103	C (1.50)

of variable i on the maximum bending moment of the wall. Naturally, if one parameter is the same in the base and in the *target excavation*, it is not necessary to calculate the corresponding correction factor, as the influence factors are the same and thus their ratio is 1.

Table 4 contains a list of the equations that allow the calculation of the different influence factors for the bending moment, to be included in Eq. (6). These equations result from an extensive parametric study presented in the companion paper (Raposo *et al.*, 2017).

Considering the application of the method, it is crucial to know which parameters are more relevant, *i.e.*, those whose variation has greater consequences on the wall maximum bending moment.

The definition of the impact grade of each parameter was performed by analysing the range of the influence factor. This range, shown in the third column of Table 4, was defined from the extreme values of the parametric study done by Raposo *et al.* (2017) and not from the equation defining the influence factor. The ratio between the upper and lower limits of the range is presented inside brackets in the last column of Table 4. Taking this numerical classification as a starting point, a qualitative scale from A to C was defined, aiming to simplify the interpretation of the table,

with A corresponding to a relevant impact and C to a reduced impact. It should be noticed that the minimum theoretical value of this ratio is 1, corresponding to a variable with no influence on the wall maximum bending moment.

2.3. Prediction of the maximum horizontal displacements of the wall and the ground surface

The prediction of the maximum wall displacement is performed through a methodology similar to the one presented for the maximum wall bending moment, using the following expression:

$$\delta h_{wall} = \delta h_{wall}^{ref} \times cd_h \times cd_D \times cd_\xi \times cd_{\rho_s} \times cd_{E_{50}} \times cd_\phi \times cd_c \times cd_{K_0} \quad (7)$$

which consists of multiplying the horizontal displacement of the wall, obtained in the *reference excavation*, by the several correction factors corresponding to the different variables.

As for the bending moments, the correction factors are obtained dividing the influence factors for the *target excavation* by the respective factors for the *reference excavation*, as expressed by the following equation:

$$cd_i = \frac{\beta_i(\text{target excavation})}{\beta_i(\text{reference excavation})} \tag{8}$$

where i represents the generic parameter and β_i the displacement influence factor for parameter i .

Table 5 presents the equations of the displacement influence factors and information on the range of each influence factor. In the rightmost column of the table is presented a classification regarding the impact grade of each parameter, *i.e.*, its ability to influence the maximum horizontal displacement of the wall. Again, the impact grade of each parameter was determined by the range of the influence factor, similarly to the procedure adopted for the maximum wall bending moment.

In the parametric study described in the companion paper (Raposo et al., 2017), a global analysis of the displacements was performed and it was clear the correlation between the maximum horizontal displacement of the wall and the maximum horizontal displacements of the surface. Having in mind the strong correlation between these two variables, the maximum horizontal displacement of the surface of the supported ground may be estimated by the following equation:

$$\delta h_{\text{surface}}^{\text{max}} = 0.54 \delta h_{\text{wall}}^{\text{max}} \tag{9}$$

2.4. Validation of the proposed method

Once the *reference excavation* is chosen, the use of the method is simple and can be easily implemented in a spreadsheet. With Eqs. (5) and (7), respectively, the maximum wall bending moment and maximum horizontal displacement of the wall can be easily predicted. Table 4 and Table 5 present all the necessary equations for determining the correction factors.

Before applying the method, it was necessary to validate it within the range of excavations used. For this purpose, an automatic procedure was implemented in a spreadsheet and, for all the 158 calculated excavations, a prediction of the results was performed using the proposed method. It should be mentioned that in this case the choice of the *reference excavation* was relatively evident as any calculation was defined varying just one parameter with respect to its *base excavation*. In such conditions the *reference excavation* was assumed to be the *base excavation*.

The accuracy of the method was evaluated through the calculation of a parameter named relative deviation, Rd , which consists on the deviation between the predicted and calculated results, as follows:

$$Rd = \frac{pv - cv}{cv} \tag{10}$$

where pv corresponds to the predicted value using the proposed method and cv to the calculated value using the finite element method.

Table 6 presents the maximum and minimum values of Rd obtained in the 158 calculations performed. Negative values mean that the predicted value is lower than the calculated value. Although certain values seem too large, they result from the reduced magnitude of the variables involved. This is the case of the calculation corresponding to the maximum Rd , in which the predicted value for the maximum wall displacement is 7.1 mm while the calculated value is 4.5 mm. The value of Rd is 60%, although the real difference is only 2.6 mm, which can be considered small for practical purposes.

Table 6 also presents the average of the obtained Rd for two different situations: the column defined as Absolute Average is obtained using the modulus of Rd ; the column defined as Average is obtained using the real value of Rd , which may be positive or negative. The Absolute Average is necessarily bigger than the real average, where positive and negative Rd values tend to compensate each other. If the Average Rd was significantly different from zero, some incongruence in the method would have occurred.

Although the maximum Rd achieves relevant values, the Absolute Average is significantly lower, assuming the values of 4.2% for the maximum wall bending moment and 7.8% for the maximum horizontal displacement of the wall. These values certify the accuracy of the procedure presented in this paper. Additionally, the average of the Rd values is very close to zero, constituting a preliminary validation for the proposed methodology.

Finally, it must be referred that the accuracy in predicting bending moments is much higher than the accuracy in predicting displacements, either of the wall or of the ground. This result was expected, as the influence factors regarding the maximum horizontal displacements of the wall are bigger than the ones referring to the bending moments. The product of the eight values that measure the impact grade regarding the bending moments (Table 4) is 373.2, while the same product for the maximum horizontal displacements of the wall (Table 5) is 1479.9, proving the higher variability of the latter.

2.5. Alternative methodology for selection of the Reference Excavation

An alternative procedure to overcome the difficulty of choosing the *reference excavation* is based not in the selection of a single *reference excavation*, but in using all the four *base excavations* as starting points for the parametric study. These excavations were presented in Table 2 and are

Table 6 - Relative deviation between predicted and calculated values.

	Maximum	Minimum	Absolute average	Average
M_{max}	38.9%	-11.4%	4.2%	0.4%
δh_{wall}	60.0%	-22.3%	7.8%	0.5%

described in detail in the companion paper. Starting from the four base excavations, it is possible to make four different predictions. The average of those predictions should be close to the value obtained through calculations using the Finite Element Method.

This strategy presents two great advantages: it eliminates the difficulty of choosing the *reference excavation* and attenuates local disturbances in the functions expressing the maximum bending moment and horizontal displacement of the wall, resulting in very satisfactory predictions. The main disadvantage results from the attempt to approximate these functions from excavations amply different from the *target excavation*, transforming the method in a purely mathematical process, and thus totally neglecting the necessary engineering judgment for this type of problems.

3. Examples

3.1. Strategy for choosing the examples

Although the description of the method has been thoroughly explained in the previous sections, some examples are performed for its full understanding, with the additional advantage of contributing to the validation of the proposed methodology.

The selection of the examples follows a strategy of increasing difficulty in the choice of the *reference excavation*, allowing the reader to understand and master the proposed methodology.

Example 1 is intended to be as simple as possible. In such conditions, it shall be almost coincident with one of the *reference excavations*, varying just one parameter. The simplicity of the example should not create any difficulty in selecting the *reference excavation* and lead to satisfactory results.

Example 2 corresponds to an additional step in the difficulty of selecting the *reference excavation*, particularly focusing the doubt on two *reference excavations*. An example was created whose geometry is coincident with geometry 1, presented in the companion paper, but the geotechnical properties of the excavated soil are in between the properties adopted for geotechnical scenarios 1 and 2. In such conditions, the doubt in selecting the best *reference excavation* arises.

Example 3 intends to demonstrate the application to an excavation where both the geometrical conditions and the geotechnical scenario are significantly different from any of the *reference excavations*. This situation can lead to some difficulty in choosing the best *reference excavation* and so, taking advantage of the situation, alternative methodologies for selecting the reference excavation are discussed.

The purpose of Example 4 is to show an extra capability of the proposed method, which is the possibility of im-

proving itself by integrating results from new calculations or even real monitoring results.

All the predictions performed in the previous examples result from interpolations based in the several calculations performed. Naturally, extrapolating out of the calculated ranges might lead to results with reduced confidence or even to poor results. The purpose of Example 5 is to show the risk of applying the method to excavations clearly different from the ones previously used to define the influence functions and, particularly, the risk of predicting results for situations out of the validated range of each parameter.

Table 7 presents the values of the several parameters characterizing the excavations adopted as examples, as well as the parameters of the excavations #A00 to #D00, chosen as *reference excavations*.

3.2. Example 1

In the first, necessarily simple, example, the proposed preliminary design method will be used to estimate the maximum wall bending moment and maximum wall horizontal displacement for the excavation nominated #Ex1. As can be observed in Table 7 and Fig. 1, this excavation is identical to the *reference excavation* #A00, except for the parameter ρ_s (support system stiffness), justifying the choice of excavation #A00 as *reference excavation*. In such conditions, only the correction factor regarding the support system stiffness needs to be calculated, as all the other factors are equal to one.

Using the equations presented in Table 4, it is possible to determine the following values of factors α_{ρ_s} for the *target excavation* (#Ex1) and for the *reference excavation* (#A00), respectively:

$$\alpha_{\rho_s, =180} = 0.04424 \times 180^{0.5318} = 0.700 \quad (11)$$

and

$$\alpha_{\rho_s, =100} = 0.04424 \times 100^{0.5318} = 0.512 \quad (12)$$

Table 7 - Main characteristics of the excavations used in the examples.

Excavation	h (m)	ρ_s	ξ	D/h	E_{s0} (MPa)	ϕ' (°)	c' (kPa)	K_0
#A00	15	100	0.15	1.6	22.5	33	12	0.40
#B00	15	100	0.15	1.6	37.5	37	21	0.60
#C00	25	350	0.20	1.2	22.5	33	10	0.40
#D00	25	350	0.20	1.2	37.5	37	20	0.60
#Ex1	15	180	0.15	1.6	22.5	33	12	0.40
#Ex2	15	100	0.15	1.6	30.0	35	16.5	0.50
#Ex3	17.5	250	0.17	1.25	30.0	35	15	0.55
#Ex4	17.5	250	0.24	1.25	30.0	35	15	0.55
#Ex5	30	700	0.15	1.4	70.0	40	40	0.50

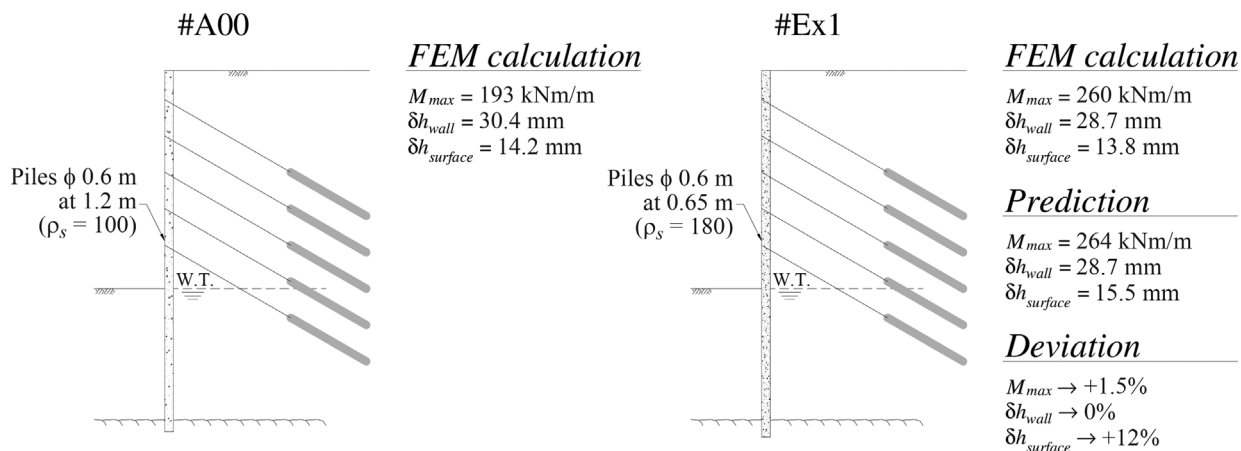


Figure 1 - Example 1: Excavation characteristics and results.

The ratio of these two values results in the correction factor for the maximum bending moment, cm_{ps} , of 1.367. Considering the maximum bending moment obtained in calculation #A00 (193 kNm/m, as shown in Fig. 1) and using Eq. (5), the estimated bending moment for excavation #Ex1 is 264 kNm/m.

Adopting the same procedure for the maximum horizontal displacement of the wall, the coefficients β_{ps} for both excavations are obtained using the equation presented in Table 5:

$$\beta_{p_s=180} = -0.1072 \ln(180) + 1.623 = 1.066 \quad (13)$$

and

$$\beta_{p_s=100} = -0.1072 \ln(100) + 1.623 = 1.129 \quad (14)$$

The ratio of these two values corresponds to the correction factor regarding the maximum horizontal displacement of the wall, whose value is 0.944. Using Eq. (7), a horizontal displacement for excavation #Ex1 of 28.7 mm is obtained, which is roughly 5.6% lower than the one corresponding to excavation #A00.

The predicted maximum horizontal displacements at the surface, obtained using Eq. (9), is equal to 15.5 mm.

Figure 1 presents a summary of the predicted and calculated values. The relative difference, Rd , is lower than 2% in the case of the bending moments. Curiously, for the horizontal displacements of the wall, the prediction coincides with the calculations. Regarding the horizontal displacements of the surface, the difference between the prediction and the calculation is 12% of the latter. This difference is typically higher than the differences in the bending moments and the horizontal displacement of the wall, as a second order estimation is used.

3.3. Example 2

In the previous example, the selection of the *reference excavation* was obvious as excavation #A00 was totally coincident with Example 1, except for the support

system stiffness. In Example 2, as can be seen in Fig. 2, the geometric conditions are coincident with the *reference excavations* #A00 and #B00, while the geotechnical properties, namely E_{s0} , ϕ' , c' and K_0 , are exactly the mean values of the geotechnical properties of the two *reference excavations* (#A00 and #B00).

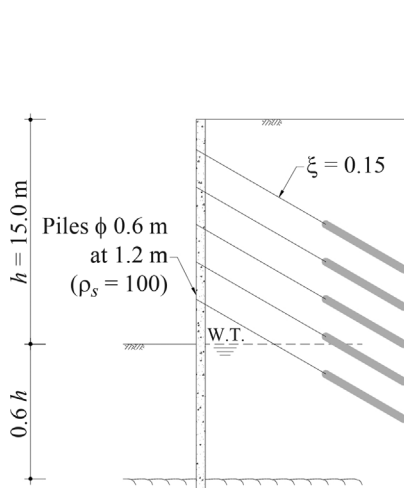
In such conditions, both excavations, #A00 and #B00, could be properly adopted as *reference excavations*. Figure 2 illustrates the results obtained for Example 2 adopting as *reference excavation* either excavation #A00 or excavation #B00.

Similarly to what was done in example 1, the equations presented in Table 4 were used to calculate the influence factors α_s , while the equations presented in Table 5 were used to calculate the factors β_s . Table 8 presents all influence and correction factors for Example 2, excavation #A00 and excavation #B00. The last column of the table shows the product of the several correction factors and, thus, it is an indirect measure of the difference between the chosen *reference excavation* and Example 3.

The predictions obtained are, in any situation, quite satisfactory, reaching a maximum Rd of 6.9% in the case of the maximum horizontal wall displacement. Regarding the bending moments, the deviations are both below 2.4%, which may be considered as an excellent result for preliminary design purposes.

Although *reference excavations* #A00 and #B00 could, apparently, be equally adopted, from the results presented in Fig. 2 it is clear that the quality of the prediction is dependent on the chosen *reference excavation*. Particularly for example 2, excavation #A00 is a better reference for predicting the maximum horizontal displacements of the wall, while excavation #B00 is preferable for predicting the maximum wall bending moments. The justification for this apparent contradiction is related to the impact grade of each parameter, as seen in Table 4 and Table 5.

Having in mind the previous results, it is clear that the *reference excavation* should be as similar as possible to the



Soil properties

#A00	#Ex2	#B00
$E_{50} = 22.5$ MPa	$E_{50} = 30.0$ MPa	$E_{50} = 37.5$ MPa
$\phi' = 33^\circ$	$\phi' = 35^\circ$	$\phi' = 37^\circ$
$c' = 12$ kPa	$c' = 16.5$ kPa	$c' = 21$ kPa
$K_0 = 0.40$	$K_0 = 0.50$	$K_0 = 0.60$

FEM calculation

#A00	#Ex2	#B00
$M_{max} = 193$ kNm/m	$M_{max} = 167$ kNm/m	$M_{max} = 132$ kNm/m
$\delta h_{wall} = 30.4$ mm	$\delta h_{wall} = 26.1$ mm	$\delta h_{wall} = 19.4$ mm
$\delta h_{surface} = 14.2$ mm	$\delta h_{surface} = 12.7$ mm	$\delta h_{surface} = 9.9$ mm

Predictions of Ex2 results

Based on #A00	Based on #B00
$M_{max} = 163$ kNm/m (-2.4%)	$M_{max} = 169$ kNm/m (+1.2%)
$\delta h_{wall} = 27.3$ mm (+4.6%)	$\delta h_{wall} = 24.3$ mm (-6.9%)
$\delta h_{surface} = 14.7$ mm (+15.7%)	$\delta h_{surface} = 13.1$ mm (+31%)

Figure 2 - Example 2: Excavation characteristics and results.

Table 8 - Example 2: influence factors and correction factors.

	h	ρ_s	ξ	D/h	E_{50}	ϕ'	c'	K_0	Product
α_i (#Ex2)	0.987	0.512	1.037	0.998	0.995	1.079	0.863	1.003	-
α_i (#A00)	0.987	0.512	1.037	0.998	1.143	1.170	0.931	0.880	-
cm_i (#A00)	1.000	1.000	1.000	1.000	0.871	0.923	0.927	1.139	0.849
α_i (#B00)	0.987	0.512	1.037	0.998	0.894	1.001	0.812	1.000	-
cm_i (#B00)	1.000	1.000	1.000	1.000	1.113	1.079	1.062	1.002	1.278
β_i (#Ex2)	0.981	1.129	1.235	1.006	0.996	1.096	0.860	1.002	-
β_i (#A00)	0.981	1.129	1.235	1.006	1.218	1.199	0.930	0.772	-
cd_i (#A00)	1.000	1.000	1.000	1.000	0.817	0.914	0.925	1.299	0.897
β_i (#B00)	0.981	1.129	1.235	1.006	0.852	1.006	0.810	1.079	-
cd_i (#B00)	1.000	1.000	1.000	1.000	1.169	1.089	1.061	0.929	1.255

target excavation, favouring the parameters with higher impact grade. This observation confirms the difficulty in choosing the best reference excavation, given the fact that the concept of “as similar as possible” may not be evident.

3.4. Example 3

In the third example, the target excavation is designated #Ex3, whose characteristics are presented in Table 7 and illustrated in Fig. 3. In this case, the choice of the reference excavation is not immediate as all the parameters differ from those of all of the four Base Excavations and, thus, any of them could be used as reference. Table 9 presents the influence factors and correction factors for example 3.

Considering the results presented in Fig. 3, it is not clear which is the best reference excavation. For the maximum wall bending moments, the best reference would be excavation #D00, but excavations #A00 and #C00 can also conduce to very satisfactory predictions, with Rd values lower than 1.5%. Excavation #B00 leads to a higher Rd , and can be considered the worst reference excavation for predicting bending moments in example 4.

Concerning the maximum wall horizontal displacements, excavations #A00 and #D00 give very satisfactory results. On the other hand, the predictions based on excavations #B00 and #C00 are quite different from the results obtained with the numerical calculations.

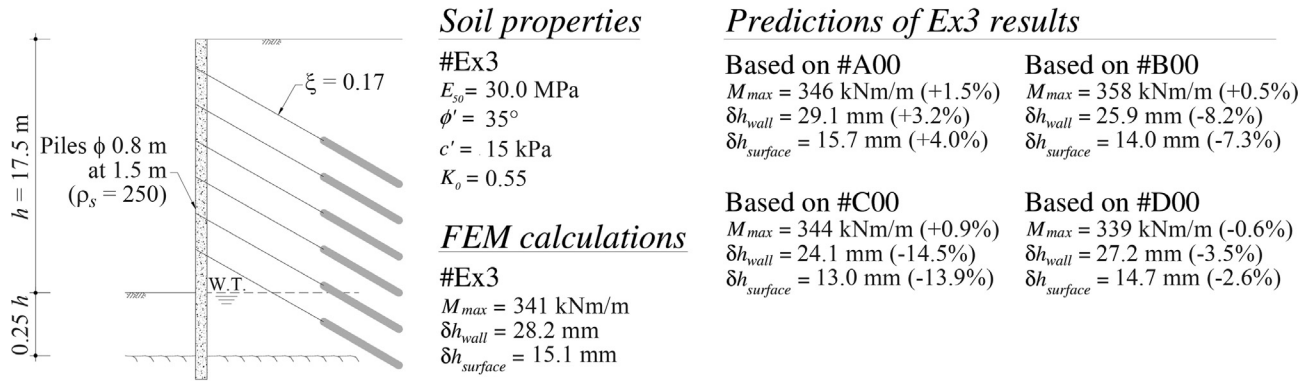


Figure 3 - Example 3: Excavation characteristics and results.

Table 9 - Example 3: influence factors and correction factors.

	h	ρ_s	ξ	D/h	E_{50}	ϕ'	c'	K_o	Product
α_i (#Ex3)	1.146	0.834	1.021	1.094	0.995	1.079	0.883	1.017	-
α_i (#A00)	0.987	0.512	1.037	0.998	1.143	1.170	0.931	0.880	-
cm_i (#A00)	1.162	1.628	0.984	1.096	0.871	0.923	0.949	1.155	1.797
α_i (#B00)	0.987	0.512	1.037	0.998	0.894	1.001	0.812	1.000	-
cm_i (#B00)	1.162	1.628	0.984	1.096	1.113	1.079	1.088	1.017	2.709
α_i (#C00)	1.621	0.997	1.001	1.115	1.143	1.170	0.967	0.880	-
cm_i (#C00)	0.707	0.836	1.020	0.981	0.871	0.923	0.914	1.155	0.501
α_i (#D00)	1.621	0.997	1.001	1.115	0.894	1.001	0.822	1.000	-
cm_i (#D00)	0.707	0.836	1.020	0.981	1.113	1.079	1.075	1.017	0.776
β_i (#Ex3)	1.365	1.031	1.130	0.852	0.996	1.096	0.881	1.060	-
β_i (#A00)	0.981	1.129	1.235	1.006	1.218	1.199	0.930	0.772	-
cd_i (#A00)	1.391	0.913	0.915	0.847	0.817	0.914	0.947	1.373	0.956
β_i (#B00)	0.981	1.129	1.235	1.006	0.852	1.006	0.810	1.079	-
cd_i (#B00)	1.391	0.913	0.915	0.847	1.169	1.089	1.087	0.982	1.338
β_i (#C00)	2.928	0.995	1.006	0.822	1.218	1.199	0.968	0.772	-
cd_i (#C00)	0.466	1.036	1.123	1.037	0.817	0.914	0.910	1.373	0.525
β_i (#D00)	2.928	0.995	1.006	0.822	0.852	1.006	0.819	1.079	-
cd_i (#D00)	0.466	1.036	1.123	1.037	1.169	1.089	1.075	0.982	0.756

In any case, the predicted values are very satisfactory having in mind that the proposed method aims to be used for preliminary design purposes. Independently of the *reference excavation*, the maximum Rd is 5.0% for the maximum bending moment, and 14.5% for the maximum horizontal wall displacements. These values are totally acceptable for preliminary design.

Despite the overall good results of the predictions, the method could be improved if the choice of the reference excavation was the most adequate, as it plays a vital role in the predictions.

As can be observed from the values in Fig. 3, the estimated values are close to the values obtained using the Finite Element Method, with the maximum difference around 8%. As the relative errors are negative, this means that the estimated values are lower than those obtained by the finite element calculations.

Example 3 is a typical case in which the predictions may be performed in a totally automatic mode, *i.e.*, without the need for choosing a *reference excavation*, as explained in section 2.5.

Considering the results obtained using the Finite Element Method as correct, the maximum error resulting from

the use of the proposed method, presented in brackets in Table 10, is lower than 10% for both bending moment and displacement. Apparently, using the automatic procedure, based on the use of the four *reference excavations* simultaneously, it is possible to have results with similar or better accuracy than using a single *reference excavation*.

3.5. Example 4

The main purpose of the fourth example is to illustrate another capability of the proposed method: the possibility to progress by integrating new results (or monitoring data from real construction sites).

Suppose that the actual bending moments and displacements of excavation #Ex3 are known. Admit now that it is important to evaluate the effect of increasing the anchor prestressing, which would result in a different excavation, nominated from now on #Ex4. Admit that the prestress will be increased from 167 kN/m to 233 kN/m. This increase corresponds to a variation in the prestressing index from 0.17 to 0.24, as shown in Fig. 4.

Using the method presented in this paper, it is only necessary to determine the correction factors corresponding to the prestressing index (cm_ξ and cd_ξ) and to multiply

each of them by the bending moments and horizontal displacements of the wall for excavation #Ex3, respectively.

Table 11 presents the influence factors and correction factors for the problem. Bearing in mind the values for the correction factors cm_ξ and cd_ξ , the increase in prestress from 167 kN/m to 233 kN/m, maintaining all the other characteristics of the excavation, will produce a reduction of the bending moment of around 4% (cm_ξ is equal to 0.964) and a reduction of the maximum horizontal displacement of the wall close to 20% (cd_ξ is equal to 0.782).

Both, the predicted values and the values obtained with the Finite Element Method, were included in Fig. 4, together with the difference between them. As can be observed, the deviations obtained are minimal.

This example proves that the accuracy of the methodology used in the predictions can improve itself by incorporating new data, creating a kind of Bayesian knowledge.

3.6. Example 5

The final example intends to illustrate the risk of using the proposed methodology in conditions significantly different from the ones validated with the several calculations performed. The excavation in this example has 3 parameters outside the studied range. Fig. 5 presents the geotechnical and geometric characteristics of #Ex5. The excavation depth increased to 30 m, 5 m more than the maximum excavation tested, the cohesion of the ground is assumed to be 40 kPa, while the assumed validation range for this parameter had a maximum of 30 kPa, and the soil stiffness is characterized by an E_{50} of 70 MPa, a value also

Table 10 - Example 3: Estimated and calculated values.

Reference excavation	M_{max} (kNm/m)	δh_{wall} (mm)	$\delta h_{surface}$ (mm)
#A00	346 (+1.5%)	29.1 (+3.2%)	15.7 (+4.0%)
#B00	358 (5.0%)	25.9 (-8.2%)	14.0 (-7.3%)
#C00	344 (+0.9%)	24.1 (-14.5%)	13.0 (-13.9%)
#D00	339 (-0.6%)	27.2 (-3.5%)	14.7 (-2.6%)
Average	347 (1.8%)	26.6 (-5.7%)	14.4 (-4.6%)
FEM	341	28.2	15.1

Table 11 - Example 4: influence factors and correction factors.

α_ξ (#Ex4)	0.983	β_ξ (#Ex4)	0.883
α_ξ (#Ex3)	1.021	β_ξ (#Ex3)	1.130
cm_ξ (#Ex4, #Ex3)	0.964	cd_ξ (#Ex4, #Ex3)	0.782

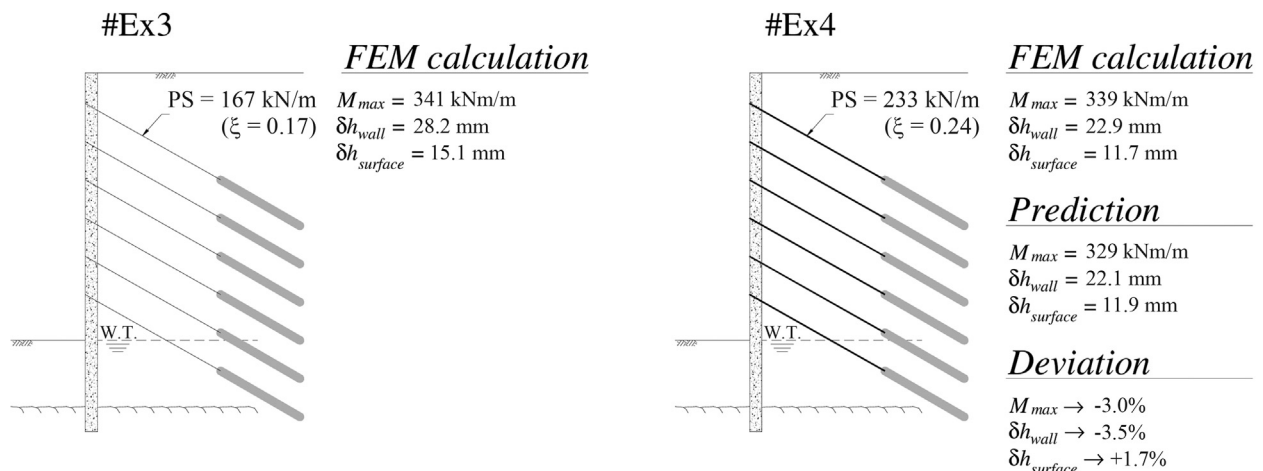


Figure 4 - Example 4: Excavation characteristics and results.

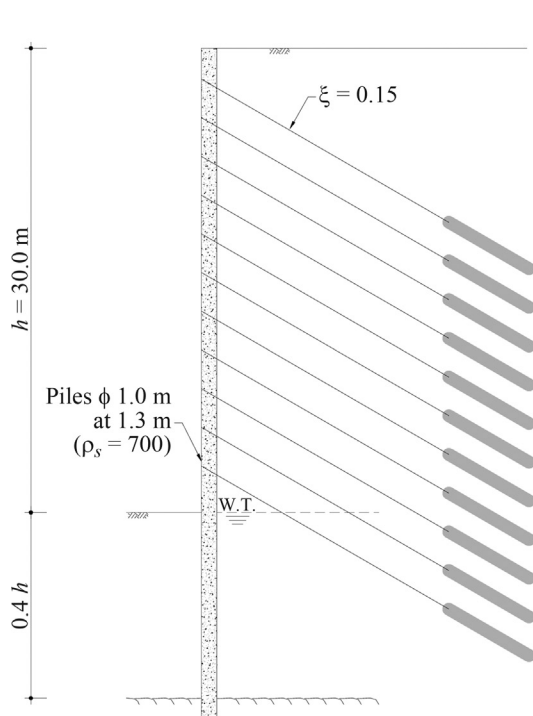


Figure 5 - Example 5: Excavation characteristics and results.

higher than the maximum Young modulus previously used. All the remaining parameters were within the validation ranges used.

Although the parameters out of the validation range were not significantly outside the range, the results presented in Fig. 5 clearly show that the obtained R_d are markedly higher than the equivalent deviations in the previous examples. In this case these R_d values are always above 10% and, in most of the situations, above 20%. Extreme values of 40% are obtained.

The example presented proves that the proposed methodology has to be used with caution and extrapolations should be avoided. In any case, preliminary design information may be obtained and the evolutionary characteristic of the method allows future developments in order to enlarge the range of geotechnical and geometrical scenarios.

4. Final Considerations

This paper proves the utility of a novel procedure that may be used for the preliminary design of earth retaining structures. Although the calculations performed for validation have indicated that this method is capable of predicting the maximum bending moment and maximum wall displacements with appreciable accuracy, it is imperative to emphasize that, in particular situations, relevant discrepancies may occur between the estimated values and those calculated through the Finite Element Method.

A particular example of what was referred in the previous paragraph is related to the support system stiffness. Although in its conceptual definition the distance between

Soil properties

#Ex5
 $E_{s0} = 70 \text{ MPa}$
 $\phi' = 40^\circ$
 $c' = 40 \text{ kPa}$
 $K_0 = 0.50$

FEM calculations

#Ex5
 $M_{max} = 390 \text{ kNm/m}$
 $\delta h_{wall} = 29.8 \text{ mm}$
 $\delta h_{surface} = 15.2 \text{ mm}$

Predictions of Ex5 results

Based on #A00
 $M_{max} = 480 \text{ kNm/m (+23\%)}$
 $\delta h_{wall} = 39.4 \text{ mm (+32\%)}$
 $\delta h_{surface} = 21.3 \text{ mm (+40\%)}$

Based on #C00
 $M_{max} = 476 \text{ kNm/m (+22\%)}$
 $\delta h_{wall} = 32.7 \text{ mm (+10\%)}$
 $\delta h_{surface} = 17.7 \text{ mm (+16\%)}$

Based on #B00
 $M_{max} = 497 \text{ kNm/m (+27\%)}$
 $\delta h_{wall} = 35.1 \text{ mm (+18\%)}$
 $\delta h_{surface} = 18.9 \text{ mm (+25\%)}$

Based on #D00
 $M_{max} = 470 \text{ kNm/m (+21\%)}$
 $\delta h_{wall} = 36.8 \text{ mm (+23\%)}$
 $\delta h_{surface} = 19.9 \text{ mm (+31\%)}$

anchors is included, the numerous tests performed proved that, in certain cases, this parameter is not enough to guarantee the quality of the estimation. The conclusion to be extracted from the results is that the critical spacing is the one referring to the distance between the last level of anchors and the bottom of the excavation. It was also noticed that, when the critical spacing differs from the value of 3.0 m, the value adopted for all the excavations, the estimated values may significantly diverge from the calculated ones.

Despite this handicap, the method presents its own utility. It is only necessary to consider another correction factor that takes the above mentioned aspects into consideration. One of the great advantages of the proposed method is its ability to evolve, being possible to include or exclude parameters at any moment in order to take into account any particular aspect.

The vital phase in the application of the proposed methodology is the definition of the geometrical parameters of the excavation and respective ground properties. The consecutive use of the method will increment its accuracy and confidence. Even having in mind that access to finite element codes is nowadays easy, the method may be used for an additional and different check.

The illustrated examples contribute for clarifying how to use the procedure, but also demonstrate the good results and accuracy of the methodology.

In spite of the global quality of the results, not only in the presented examples but also in many other calculations performed, it is important to refer that the method can make predictions by extrapolating from previous results, being

possible that important differences may occur in particular situations. Anyhow, these errors may be modest when compared to the difficulty in accurately defining parameters such as stiffness or the initial stress state of the ground, making the method appropriate for preliminary design purposes.

5. Appendix A –Mathematical Formulation of the Proposed Method

In order to clarify the *modus faciendi* of the proposed method for estimating forces and displacements, this section is devoted to its detailing and explanation.

From a mathematical point of view, this problem consists in determining the value of an unknown function, knowing the values of the variables the function depends on. In order to explain the adopted procedure, the function $Z(x, y)$, will be used as an example. This function, represented in Fig. 6, has the following analytical equation:

$$Z(x, y) = (x^2 - 2x + 3)(\log(y - 9) + 0.3) + 0.2x + 4 \quad (15)$$

The starting step consists in the definition of two points, from now on designated as “base points”. The choice of these points did not follow any specific rule but they should be located as much apart as possible within the studied domain.

Figure 7 shows the base points used in this example. The adopted points, in this case, correspond to the squares identified by 1 and 2, and have the following coordinates:

Base point 1: $(x = 1, y = 2)$;

Base point 2: $(x = 2.5, h = 16)$.

Picking each of the base points, the function was computed assuming for x all the possible values in the range $\{0, 0.5, 1, 1.5, 2, 2.5, 3\}$, resulting in the points shown in Fig. 7. Using the method of least squares, these points can be approximated by two curves that reflect the influence of parameter x . For function $Z(x, y)$, defined by Eq. (15), the

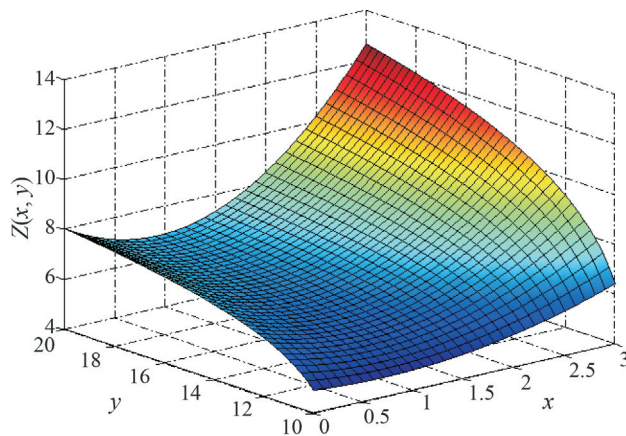


Figure 6 - Three-dimensional representation of the function $Z(x, y)$.

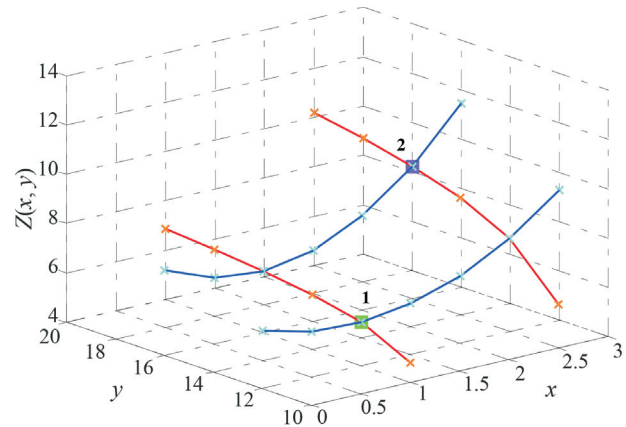


Figure 7 - Base points and one-dimensional analysis.

curves represented in Fig. 7 by the lines with constant y correspond to:

$$f_{y=12}(x) = 0.7771x^2 - 1.354x + 6.331 \quad (16)$$

and

$$f_{y=16}(x) = 1.145x^2 - 2.090x + 7.435 \quad (17)$$

These curves can be placed in the same vertical plane, as shown in Fig. 8a, and then n with respect to any point in the domain. Setting $x = 1.5$ as the normalization reference value, as shown in Fig. 8b, it is possible to determine an average normalized influence curve for variable x , in this case defined by the following equation:

$$f_{med}(x) = 0.1450x^2 - 0.2639x + 1.064 \quad (18)$$

Adopting the same method for variable y , the following equation is obtained:

$$g_{med}(y) = 0.5763 \log(y - 9) + 1 \quad (19)$$

After determining the average influence curves for each variable, it is possible to estimate the value of $Z(x, y)$ in any point of the domain. It is, of course, possible to estimate values of $Z(x, y)$ using values of x or y out of their domain of variation, but that procedure should be avoided as it can produce significant errors.

In order to calculate $Z'(x, y)$, the function that represents the estimated value for $Z(x, y)$ in any point with coordinates (x, y) , a scalar α should be multiplied by both functions of the average influence of each of the variables, $f_{med}(x)$ and $g_{med}(y)$, as defined by the following equation:

$$Z'(x, y) = \alpha f_{med}(x) g_{med}(y) \quad (20)$$

Factor α is determined from a known point of the function $Z(x, y)$ in such a way that $Z'(x, y)$ matches $Z(x, y)$ in that point. Eq. (20) may be rewritten as:

$$Z'(x, y) = Z(a, b)c(x)c(y) \quad (21)$$

where $c(y)$ is equal to $f_{med}(x)/f_{med}(a)$ and $c(x)$ corresponds to $g_{med}(y)/g_{med}(b)$.

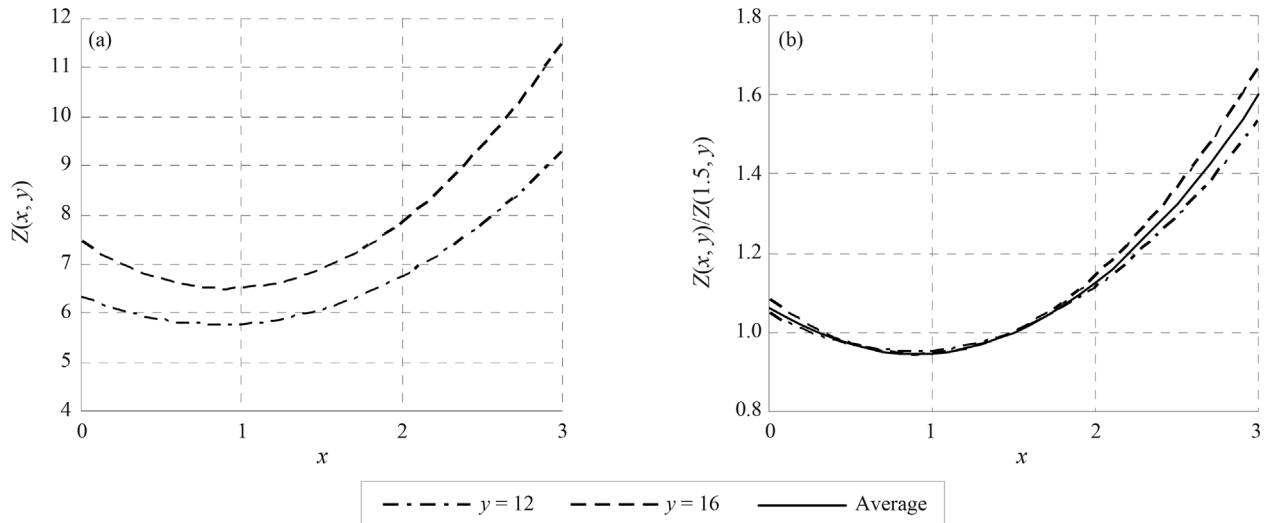


Figure 8 - Parametric analysis for variable x .

Equation (21) clarifies the procedure adopted in the proposed preliminary design method and shows how, starting from a known value of the function $Z(a, b)$, the value for the function in another point can be estimated, by multiplying it by the corrective factors $c(x)$ and $c(y)$, each corresponding to a variable in the function.

Figure 9 shows the overlapping of the function $Z(x, y)$, defined by the opaque surface, and the function $Z'(x, y)$, defined by the grid. To define the function $Z'(x, y)$ the two functions were forced to coincide at point (2.5, 16), corresponding to base point 2, and shown in Fig. 9 by a square. The parameter α assumed, in this case, the value 4.75. In certain areas of Fig. 9 the grid representing the function $Z'(x, y)$ is not visible as it is below the surface representing the function $Z(x, y)$.

Raposo (2007) presents a detailed description of the methodology briefly presented in the preceding paragraphs. A similar procedure was adopted for the functions maximum bending moment and maximum horizontal dis-

placement of the wall. For this purpose, individual analysis of each variable were performed starting from 4 different *base excavations*.

Acknowledgments

This work was financially supported by: Project POCI-01-0145-FEDER-007457 – CONSTRUCT - Institute of R&D in Structures and Construction funded by FEDER funds through COMPETE2020 - Programa Operacional Competitividade e Internacionalização (POCI) – and by national funds through FCT - Fundação para a Ciência e a Tecnologia.

References

- Mana, A.I. (1978). Finite Element Analyses of Deep Excavation Behavior in Soft Clay. PhD Thesis, Stanford University.
- Mana, A.I. & Clough, G.W. (1981). Prediction of movements for braced cuts in clay. *Journal of Geotechnical and Geoenvironmental Engineering* 107(GT6), p. 759-777.
- Raposo, N.P. (2007). Pré-Dimensionamento de Estruturas de Contenção Ancoradas. MSc Thesis, Universidade do Porto.
- Raposo, N.P.; Topa Gomes, A. & Matos Fernandes, M. (2017). Anchored Retaining Walls in Granite Residual Soils; I - Parametric Study. *Soils and Rocks* 40(3):229-242.

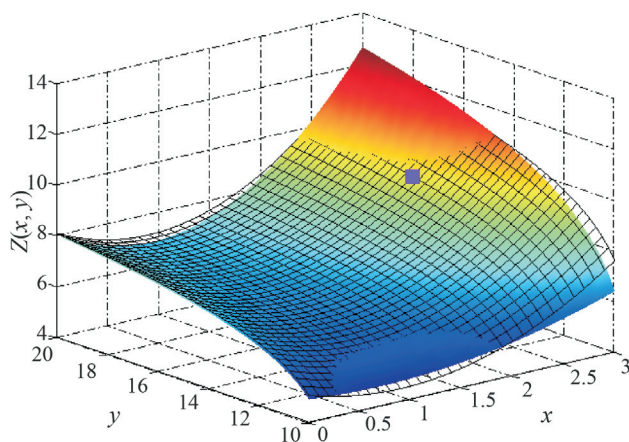


Figure 9 - Function $Z'(x, y)$, function $Z(x, y)$ and base point 2.

Influence of Traverse Velocity and Pump Pressure on the Efficiency of Abrasive Waterjet for Rock Cutting

P.B. Arab, T.B. Celestino

Abstract. This paper presents investigations on the behavior of four types of rocks (syenite, granite, marble and sandstone) subjected to abrasive waterjet cutting. The influence of traverse velocity and pump pressure on the efficiency of cutting is analyzed. Moreover, the influence of the physical-mechanical behavior of the rocks on their removal process is investigated. It was found that, in general, the removed volume of rock and the cutting rate tend to increase with the decrease of traverse velocity and with the increase of pump pressure. Moreover, the opposite trend was observed in the analysis of the specific energy of cutting. Optimum conditions of cutting efficiency were found when cutting the studied rocks with a traverse velocity of 200 mm/min and a pump pressure of 400 MPa. Finally, the marble and the sandstone presented the lowest resistance to abrasive waterjet cutting while the syenite and granite presented the highest resistances.

Keywords: Abrasive waterjet, efficiency of cutting, physical-mechanical behavior, rock cutting.

1. Introduction

Abrasive waterjet (AWJ) consists in a versatile and non-conventional cutting technique which has been effectively applied to rock cutting since the late 1980s. In geotechnics, it is also frequently applied in mineral extraction, hydrodemolition and well drilling (Summers, 1995). Until the early 1980s, AWJ machining was considered economically unfeasible, yet researchers made efforts in order to develop technologies which ensured its growth into a full-scale viable production process (Akkurt *et al.*, 2004). The AWJ action involves high impact forces which lead to the generation and propagation of cracks through the affected area of the rock. Cracking occurs along with erosion in order to disaggregate the target, producing a kerf. At the top of the kerf the cracking process is more intense, while at the bottom what predominates is erosion because of AWJ energy loss with increasing depth. AWJ rock cutting is a complicated process due to the turbulent action of the jet and the complexity of the rock material, which is generated in uncontrolled environment without human interference. Moreover, it is composed by different types of minerals with distinct behaviors. Because of that, some researchers have been discouraged to continue developing studies with focus on rock behavior, giving preference to working with a single type of rock, mainly granites, or “rock-like” materials like concrete (Momber *et al.*, 1999; Momber & Kovacevic, 1999; Lauand *et al.*, 2001; Aydin *et al.*, 2012; Karakurt *et al.*, 2012; Aydin *et al.*, 2013; Oh & Cho, 2016). Even presenting mechanical similarities, concrete is similar only to a restricted range of rocks, thus the phenomena involved in AWJ rock cutting must focus on varied rocks as materials studied. Therefore, the present study aims to contribute with an experimental analysis of the behavior of four differ-

ent types of rocks when subjected to AWJ cutting. The influence of traverse velocity (v_T) and pump pressure (P) on the efficiency of cutting is investigated. The traverse velocity is the velocity with which the AWJ machine nozzle runs across the target surface, *i.e.* the rock surface.

2. Experimental Study

2.1. The abrasive waterjet machine

The machine used in this research is a Flow Mach 2C and the tests performed involved a pressure range from 100 to 400 MPa and a traverse velocity from 100 to 400 mm/min. Figure 1 presents a flowchart which summarizes the machine operating system. Tap water is filtered and maintained under little pressure inside the booster pump to ensure that the intensifier pump is kept fed. The intensifier pump consists of two circuits: the oil circuit and the water circuit. The oil circuit drives the intensifier piston so that it may push the water and amplify its pressure. At the initial condition of the water, the oil is kept in a reservoir and a hydraulic pump maintains it under low pressure. Then, the pressurized water goes through the attenuator, which damps pressure fluctuations assuring a steady water flow through the plumbing to the cutting head. The water passes through the orifice, which is responsible for converting pressurized water into a waterjet. The abrasive material (almandine garnet) joins the waterjet by suction due to the effect of the waterjet and the water and abrasive material are mixed and homogenized inside the nozzle, before leaving the machine and hitting the target as an abrasive waterjet. When the jet leaves the target, it is collected in a water tank.

Paola Bruno Arab, D.Sc., Assistant Professor, Centro de Engenharias, Universidade Federal de Pelotas, Pelotas, RS, Brazil. e-mail: paola.arab@gmail.com.
Tarcísio Barreto Celestino, D.Sc., Professor, Departamento de Geotecnia, Universidade de São Paulo, São Carlos, SP, Brazil. e-mail: tbcelest@usp.br.

Submitted on December 19, 2016; Final Acceptance on September 11, 2017; Discussion open until April 30, 2018.

DOI: 10.28927/SR.403255

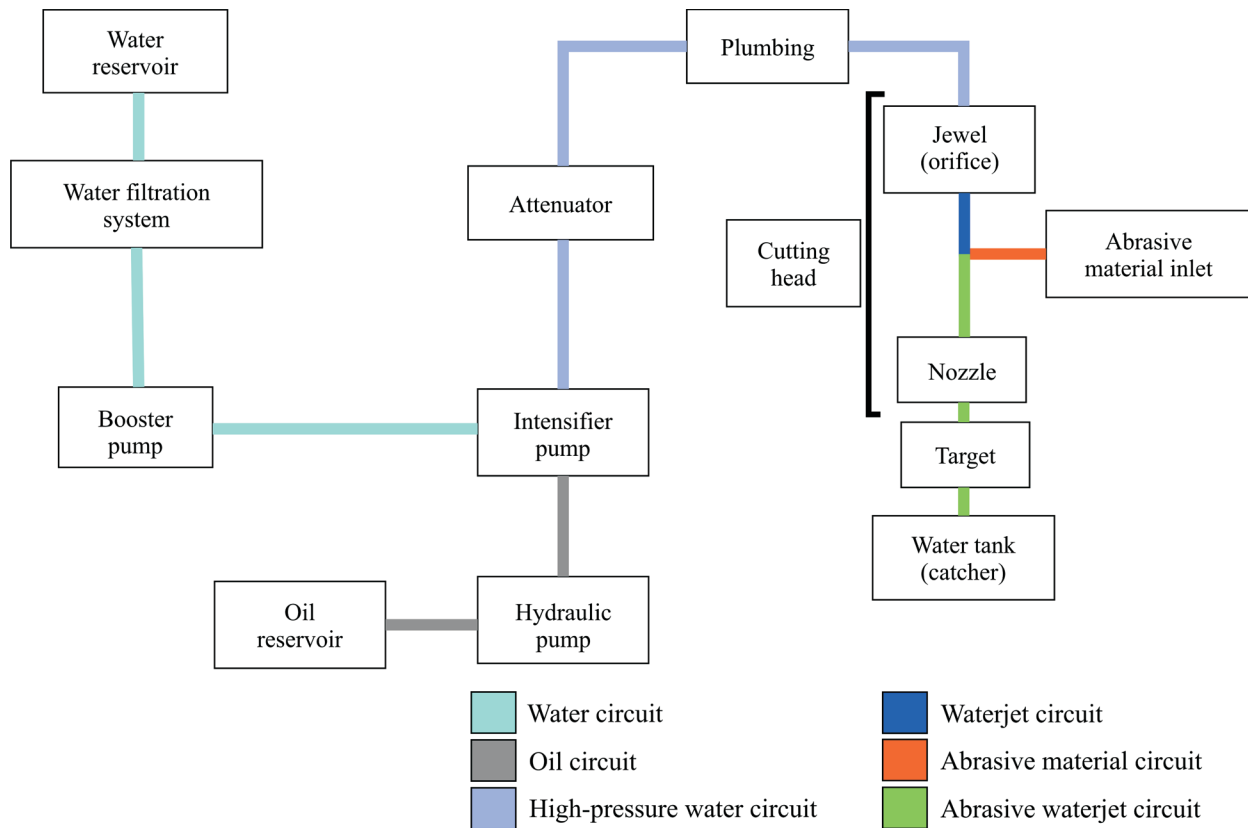


Figure 1 - Flowchart of the AWJ machine operating system.

2.2. Tested rocks

Four types of Brazilian rocks were selected based on their distinct physical-mechanical characteristics: syenite, granite, marble and silicified sandstone. Rock blocks were collected in single batches at quarries in the States of São Paulo and Espírito Santo. The main properties and mineralogical compositions of the specimens are shown in Table 1. The tensile strength and the Schmidt hardness were determined based on the ISRM Suggested Methods (1978, 2009). The compressive strength and the Young's modulus were determined according to the ISRM Suggested Methods (1979), while the dry density, porosity and Amsler wear were determined according to the Brazilian standards NBR 12766 (ABNT, 1992a) and NBR 12042 (ABNT, 1992b). Thin sections of the rocks were examined for determination of the mineralogical composition and texture.

2.3. Rock specimens for cutting tests

Rock blocks were cut and rectified as rectangular prisms with minimum dimensions of 100 x 100 x 160 mm. The machine parameters were adjusted so that the specimens were not cut through. The intention was to generate kerfs in order to investigate parameters related to the volumes of the kerfs. For the same type of rock and the same

conditions of cutting, five tests were performed to increase the reliability of the results.

2.4. Tests performed

According to Momber (2004) the most important machine parameters which influence the cutting performance of brittle materials are traverse velocity (v_r), pump pressure (P) and abrasive flow rate (m_a). In the present study, the first two parameters were investigated.

The experimental program involved tests with two main different conditions: variation of traverse velocity and variation of pump pressure. The other parameters were kept constant during the experiments (Table 2). Data analysis was made through scatter diagrams and basic regression. For the analysis of pump pressure data, second order polynomial curves fitted adequately. However, it was observed that the scatter diagrams for traverse velocity data showed more complex behavior, which could not be described by basic functions in consistency with reality. Therefore, fitting for these cases is not shown.

The volumes of the kerfs were determined by filling them with mercury. Eq. 1 describes the calculation of the mercury volume inside a kerf, which corresponds to the volume of removed rock. V is the volume of the kerf (cm^3), m_{Hg} is the mass of mercury (g), m_s is the mass of the syringe

Table 1 - Main properties and mineralogical compositions of the rocks studied.

Features		Syenite	Granite	Marble	Sandstone
Physical and mechanical	Dry density (g/cm ³)	2.71	2.61	2.82	2.31
	Porosity (%)	0.064	0.182	0.313	2.830
	Amsler abrasion wear (mm/1000 m)	0.86	0.68	7.96	1.53
	Tensile strength (MPa)	13.20	10.17	4.22	12.11
	Compressive strength (MPa)	257.17	182.41	69.75	191.85
	Schmidt hardness	47.60	46.90	39.10	41.20
	Young's modulus (GPa)	75.34	73.91	54.84	34.72
Mineralogical composition (%)	Alkali feldspar	40	45	-	traces
	Plagioclase	20	16	-	-
	Quartz	-	35	-	100
	Augite	12	-	-	-
	Nepheline	12	-	-	-
	Biotite	2	2	-	-
	Hornblende	1	-	-	-
	Apatite	5	traces	-	-
	Olivine	3	-	-	-
	Opaque minerals	5	2	-	-
	Calcite/Dolomite	-	-	100	-
	Lithic fragments	-	-	-	traces
	Epidote	-	-	traces	-
	Zircon	traces	traces	-	-

Table 2 - Machine parameters adopted in the tests.

Machine parameters	Test 1 (v_t variation)	Test 2 (P variation)
Pump pressure - P (MPa)	400	100, 200, 300, 400
Nozzle angle (°)	90	90
Traverse velocity - v_t (mm/min)	100, 200, 300, 400	200
Stand-off distance - h_s (mm)	5.00	5.00
Orifice diameter - d_o (mm)	0.33	0.33
Nozzle diameter - d_f (mm)	1.02	1.02
Abrasive flow rate - m_A (g/min)	408.23	408.23
Abrasive diameter - d_A (mesh)	80	80

(g) and 13.58 corresponds to the specific mass of mercury (g/cm³):

$$V = \frac{m_{Hg} - m_s}{13.58} \quad (1)$$

The main results obtained from the cutting tests are summarized in Table 3. The specific energy of cutting (SE_c) is defined as the ratio between the total amount of energy provided by the AWJ machine and the removed volume of rock (V_R). The total amount of energy was calculated ac-

ording to the procedure presented in Momber & Kovacevic (1999). The cutting rate (CR) is the ratio between the volume of the kerf and the time elapsed during the cutting process. Each result presented in Table 3 is the average of results of 5 tests.

3. Results and Discussion

Figure 2 presents the relationship between the removed volume of rock and the traverse velocity. A general trend of decrease of the removed volume of rock with the

Table 3 - Results obtained from the AWJ cutting tests.

Rock	v_f (mm/min)	P (MPa)	V_R (cm ³)	CR (cm ³ /min)	SE_c (J/cm ³)
Syenite	100	400	17.04	11.36	144.09
Syenite	200	400	17.31	19.39	84.73
Syenite	300	400	8.27	16.54	99.00
Syenite	400	400	4.98	13.28	123.71
Syenite	200	100	2.40	3.20	101.87
Syenite	200	200	6.16	8.22	95.56
Syenite	200	300	9.38	12.50	100.73
Granite	100	400	15.29	10.19	160.63
Granite	200	400	18.30	17.77	92.15
Granite	300	400	7.69	15.39	106.79
Granite	400	400	5.17	13.78	118.81
Granite	200	100	2.49	3.32	98.65
Granite	200	200	4.29	5.71	137.43
Granite	200	300	8.05	10.73	115.45
Marble	100	400	29.36	19.57	83.77
Marble	200	400	28.78	37.56	43.60
Marble	300	400	18.09	36.20	45.27
Marble	400	400	8.57	22.85	71.93
Marble	200	100	3.21	4.28	74.70
Marble	200	200	9.89	13.19	59.68
Marble	200	300	18.33	24.44	50.60
Sandstone	100	400	29.62	19.75	82.91
Sandstone	200	400	33.24	39.34	43.60
Sandstone	300	400	15.07	30.14	54.33
Sandstone	400	400	9.41	25.08	65.78
Sandstone	200	100	4.01	5.35	59.86
Sandstone	200	200	10.87	14.49	54.30
Sandstone	200	300	18.22	24.29	50.97

increase of traverse velocity is observed, in spite of the results obtained for 100 mm/min. An optimum traverse velocity exists around 200 mm/min for the rocks studied. Low values of removed volume are observed for traverse velocity of 100 mm/min. Lower velocities imply higher exposure time of an area to the action of the AWJ. Thus, a larger loss of energy is expected mainly due to damping effects regarding larger accumulation of water and abrasive material inside the kerf, which reduces the impact of the AWJ. In contrast, at higher velocities (300 and 400 mm/min) water and abrasive material do not have time enough to accumulate inside the kerf, thus losses are smaller. However, as the exposure time is too short, there is not enough time to remove a considerable amount of rock. In addition, since the removed volume is larger at 100 mm/min than beyond 300 mm/min, it may be inferred that the exposure time

plays a more important role in the removal of rock than the damping effects. At higher traverse velocities, the range of rock removal is small, while at lower traverse velocities the removal of the less resistant rocks (*i.e.* the marble and sandstone) is more efficient.

Figure 3 presents the influence of the pump pressure (P) on the removed rock volume. For the rocks studied, the removed volume increases with the increase of pump pressure. A steeper gradient is observed for the marble and sandstone, indicating a lower resistance of these rocks to removal due to the action of the AWJ. Curve fitting the data points adopting second degree polynomial equations resulted in R^2 higher than 0.99 (Eq. 2 to 5):

$$\text{Syenite: } V_R = 2.6 \times 10^{-5} P^2 + 0.027P - 0.344 \quad (2)$$

$$\text{Granite: } V_R = 9.4 \times 10^{-5} P^2 - 0.012P + 2.975 \quad (3)$$

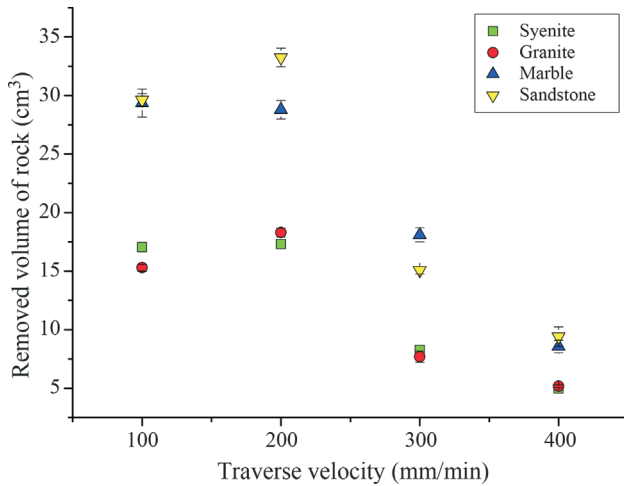


Figure 2 - Influence of traverse velocity on the removed volume of rock.

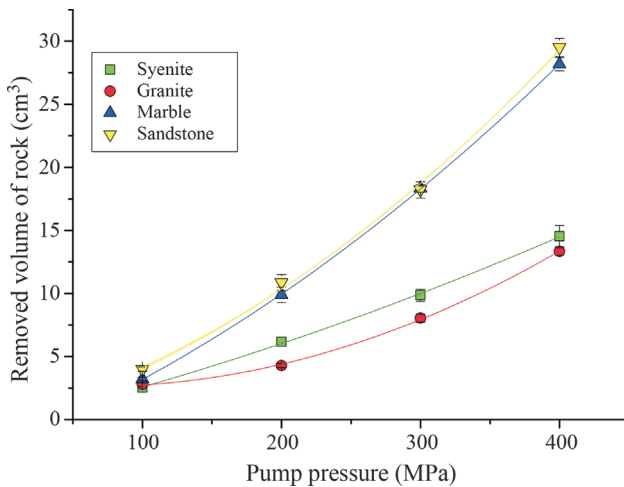


Figure 3 - Influence of pump pressure on the removed volume of rock.

$$\text{Marble: } V_R = 7.9 \times 10^{-5} P^2 + 0.044P - 1.983 \quad (4)$$

$$\text{Sandstone: } V_R = 1.1 \times 10^{-4} P^2 + 0.032P - 0.192 \quad (5)$$

Momber & Kovacevic (1999) state that for brittle materials there is a threshold pressure under which the AWJ is no longer able to remove material. Those authors estimate this critical value by a linear fit of the erosion depth vs. the applied pump pressure data regarding kerf depth. In contrast, Engin (2012) investigated the correlation between the erosion depth and the applied pump pressure regarding AWJ cutting of granites and a nonlinear correlation below 100 MPa was observed. In the case of the present study, it seems that the relationship between the removed volume of rock (V_R) and the pump pressure is also not linear. A linear extrapolation would suggest a lower threshold pressure for the syenite and granite. However, this is not consistent with

the fact that these rocks are more resistant to AWJ removal when compared to the marble and sandstone. Bortolussi *et al.* (1988) observed that even with 34 MPa an AWJ is able to cut granite samples up to 5 mm depth with machine parameters similar to those adopted in this study. Therefore, more tests would have to be performed between 0 and 100 MPa in order to determine the threshold pressure with certainty.

Figure 4 presents the influence of traverse velocity on the specific energy of cutting (SE_C), *i.e.* the total energy provided by the machine per removed volume of rock. In spite of the results for a traverse velocity of 100 mm/min, the specific energy of cutting increases linearly with the increase of the traverse velocity. This means that with traverse velocity of 200 mm/min the AWJ machine expends less energy in kerf generation. Moreover, as already discussed, much energy is lost because of damping effects at very low traverse velocities, which explains the large expenditure of energy when cutting rocks with 100 mm/min.

Figure 5 presents the relationship between the pump pressure and the specific energy of cutting. The general trend is the decrease of the specific energy of cutting with the increase of pump pressure. The granite presented a different behavior with a specific energy peak at 200 mm/min, which may be influenced by the variability of the rock. It is interesting to notice that the range of specific energy values is larger for the tests with varying traverse velocity in comparison to the tests with varying pump pressure. Eq. 6 through 9 are the results of polynomial curves fitting the data from the rocks studied. R^2 values were much better for the marble and sandstone.

$$\text{Syenite: } SE_C = -2.5 \times 10^{-4} P^2 + 0.093P + 87.441 \quad (6)$$

$$R^2 = 0.91$$

$$\text{Granite: } SE_C = -1.7 \times 10^{-3} P^2 + 0.861P + 21.763 \quad (7)$$

$$R^2 = 0.61$$

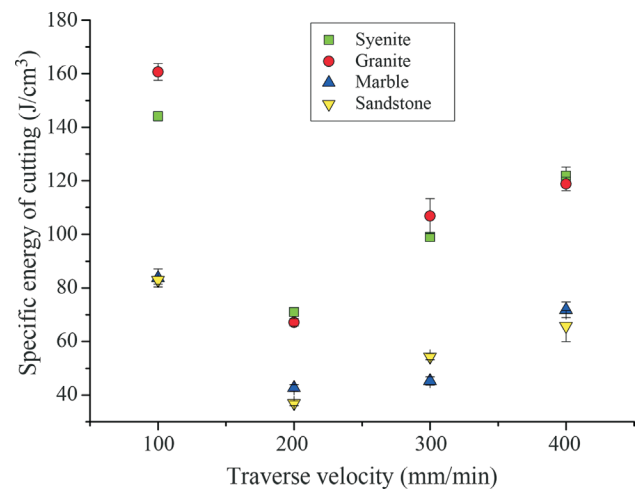


Figure 4 - Influence of traverse velocity on the specific energy of cutting.

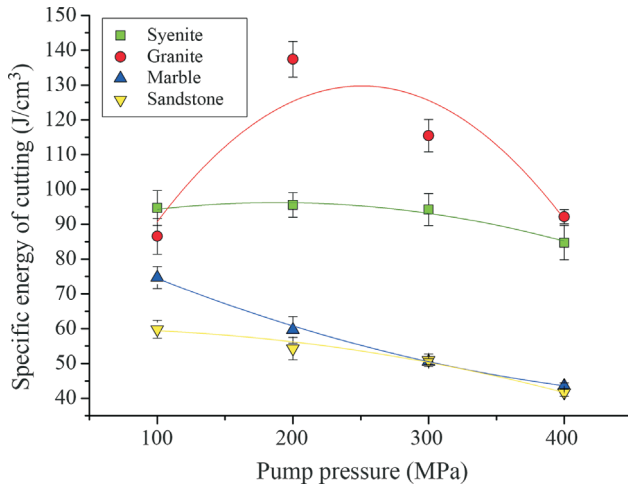


Figure 5 - Influence of pump pressure on the specific energy of cutting.

Marble: $SE_c = 1.7 \times 10^{-4} P^2 - 0.186P + 91.411$ (8)

$R^2 = 0.99$

Sandstone: $SE_c = -1.4 \times 10^{-4} P^2 + 0.009P + 59.898$ (9)

$R^2 = 0.97$

Figure 6 shows the relationship between the cutting rate and the traverse velocity. In spite of the results for 100 mm/min, the cutting rate decreases with the increase of the traverse velocity. Again, the traverse velocity of 200 mm/min is the optimum condition for cutting with the highest cutting rates. At 100 mm/min the rock removal is complicated by the large amount of water and abrasive material inside the kerf, damping the impact and useful power of the AWJ.

Figure 7 presents the relationship between the cutting rate and the pump pressure. The cutting rate increases with the increase of the pump pressure. As observed in other re-

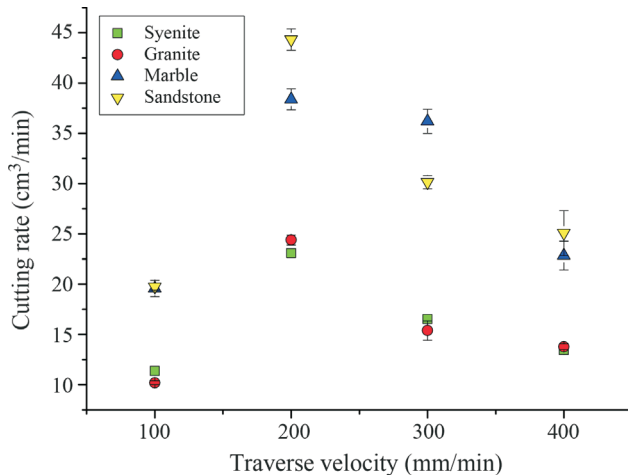


Figure 6 - Influence of traverse velocity on the cutting rate.

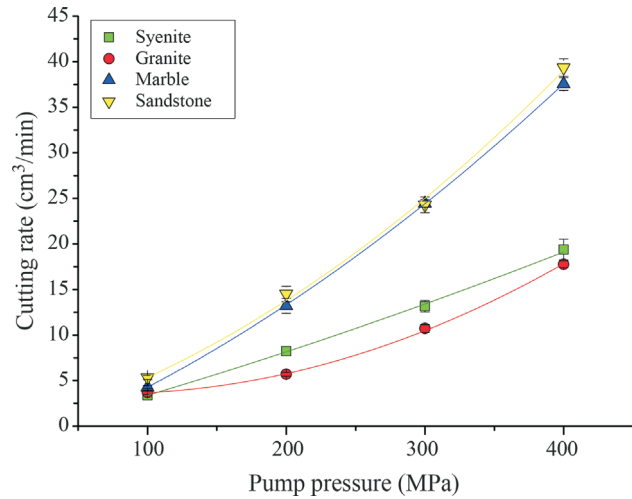


Figure 7 - Influence of pump pressure on the cutting rate.

lationships, a steeper gradient is observed for the marble and sandstone because of their lower resistance to rock removal. Eq. 10 through 13 describe the fitted curves for this relationship.

Atici & Ersoy (2009) state that a good indication of the cutting performance can be assessed by analyzing the relationship between the specific energy of cutting and the cutting rate. When the lowest specific energy is associated to the highest cutting rate, then the most efficient condition is achieved. Also, the specific energy of cutting is directly related to the costs of production/cutting. In the case of this study, the most efficient condition is observed when cutting rocks with a traverse velocity of 200 mm/min and a pump pressure of 400 MPa. In this condition, the removed volume of rock is also larger for all rocks studied.

Syenite: $CR = 2.3 \times 10^{-5} P^2 + 0.0407P - 0.9149$ (10)

$R^2 = 0.99$

Granite: $CR = 1.3 \times 10^{-4} P^2 - 0.019P + 4.2271$ (11)

$R^2 = 0.99$

Marble: $CR = 1.03 \times 10^{-4} P^2 + 0.0593P - 2.6807$ (12)

$R^2 = 0.99$

Sandstone: $CR = 1.4 \times 10^{-4} P^2 + 0.0422P - 0.2565$ (13)

$R^2 = 0.99$

The marble and the sandstone presented similar behavior regarding the response to the AWJ cutting and the same can be stated for the syenite and the granite. The marble is easily cut by the AWJ due to two main reasons: primarily it is practically a monomineralic rock composed by calcite, a mineral which presents three perfect cleavage directions. Thus, the abrupt impact of the AWJ on the surface of this rock leads to the generation of a dense network of cracks through its cleavage planes, easily disaggregating it.

Secondly, since much of the rock is removed by erosion, the process is facilitated because calcite hardness is 3 according to the Mohs scale. In the case of the sandstone, a different situation occurs. Although it is a sedimentary rock, its tensile and uniaxial compressive strength are very high due to its silica cement and the lack of weak structures like cleavage. However, when subjected to high impact like during AWJ cutting, fast propagation of cracks occurs due to its high brittleness (high UCS strength, but low rigidity), easily generating kerfs.

Finally, both syenite and granite present similar properties and both are igneous rocks. Their lower cutting rate and higher AWJ specific energy, in comparison to the other rocks studied, are a result of their higher strength and rigidity. These rocks have a main difference regarding their strength: while the granite presents quartz, the syenite has an imbricated structure. Both features increase strength and may compensate for weaker features like the presence of phenocrysts in the granite and the lack of quartz in the syenite.

4. Conclusions

The effects of traverse velocity and pump pressure on cutting parameters related to cutting efficiency were investigated for different types of rocks. The condition with which the best cutting efficiency is achieved is cutting with a traverse velocity of 200 mm/min and a pump pressure of 400 MPa. The removed volume of rock and the cutting rate both decrease from 200 mm/min to 400 mm/min and also to 100 mm/min, thus an optimum traverse velocity exists around 200 mm/min. The opposite trend is observed for the specific energy of cutting. Both the removed rock volume and the cutting rate increase with the increase of pump pressure and, in general, the opposite trend is observed for the specific energy of cutting. The mineralogical composition of the rocks and their physical-mechanical behavior play a major role on how the studied rocks are disaggregated in order to generate kerfs. It was found that the marble and sandstone present a lower and similar resistance to AWJ cutting and the syenite and granite present a higher and similar resistance to AWJ cutting.

Acknowledgments

The authors are grateful to CNPq (Conselho Nacional de Desenvolvimento Científico e Tecnológico) for financial support throughout this research.

References

ABNT (1992a). NBR 12.766: Rochas para Revestimento: Determinação de Massa Específica Aparente, Porosidade Aparente e Absorção D'água Aparente - Método de Ensaio.

ABNT (1992b). NBR 12.042: Materiais Inorgânicos - Determinação do Desgaste por Abrasão.

Akkurt, A.; Mustafa, K.K.; Ulvi, S.C. & Fevzi, E. (2004). Effect of feed rate on surface roughness in abrasive water jet cutting applications. *Journal of Materials Processing Technology*, 147(1):389-396.

Atici, U. & Ersoy, A. (2009). Correlation of specific energy of cutting saws and drilling bits with rock brittleness and destruction energy. *Journal of Materials Processing Technology*, 209(5):2602-2612.

Aydin, G.; Karakurt, I. & Aydiner, K. (2012). Performance of abrasive waterjet in granite cutting: influence of the textural properties. *Journal of Materials in Civil Engineering*, 24(7):944-949.

Aydin, G.; Karakurt, I. & Aydiner, K. (2013). Prediction of the cut depth of granitic rocks machined by abrasive waterjet (AWJ). *Rock Mechanics and Rock Engineering*, 46(5):1223-1235.

Bortolussi, A.; Yazici, S. & Summers, D.A. (1988). The use of waterjets in cutting granite. *Proc. 9th Int. Symp. on Jet Cutting Tech.*, Sendai, paper E3, 15 p.

Engin, I.C. (2012). A correlation for predicting the abrasive water jet cutting depth for natural stones. *South African Journal of Science*, 108(9-10):1-11.

ISRM (1978). Suggested Methods for Determining Tensile Strength of Rock Materials. *International Journal of Rock Mechanics and Mining Sciences & Geomechanics Abstract*, 15(3):99-103.

ISRM (1979). Suggested methods for determining the uniaxial compressive strength and deformability of rock materials. *International Journal of Rock Mechanics and Mining Sciences & Geomechanics Abstract*, 16(2):135-140.

ISRM (2009). Suggested Method for Determination of the Schmidt Hammer Rebound Hardness: Revised Version. *International Journal of Rock Mechanics and Mining Sciences*, 46(3):627-634.

Karakurt, I.; Aydin, G. & Aydiner, K. (2012). An experimental study on the depth of cut of granite in abrasive waterjet cutting. *Materials and Manufacturing Processes*, 27(5):538-544.

Lauand, C.T.; Martín, C.G.R.; Hennies, W.T. & Agus, M. (2001). Performance of abrasive waterjet in granite cutting: influence of the textural properties. *WJTA American Waterjet Conference*, pp. 427-449.

Momber, A.W. (2004). Wear of rocks by water flow. *International Journal of Rock Mechanics and Mining Sciences*, 41(1):51-68.

Momber, A.W. & Kovacevic, R. (1999). An energy balance of high-speed abrasive water jet erosion. *Proceedings of the Institution of Mechanical Engineers, Part J: Journal of Engineering Tribology*, 213(1):463-472.

Momber, A.W.; Mohan, R.S. & Kovacevic, R. (1999). On-line analysis of hydro-abrasive erosion of pre-cracked materials by acoustic emission. *Theoretical and Applied Fracture Mechanics*, 31(1):1-17.

Oh, T.M. & Cho, G.C. (2016). Rock cutting depth model based on kinetic energy of abrasive waterjet. *Rock Mechanics and Rock Engineering*, 49(3):1-14.

Summers, D.A. (1995). *Waterjetting Technology*. 1st ed. Chapman & Hall, London, 624 p.

List of Symbols

AWJ: abrasive waterjet

CR: cutting rate

d_o : orifice diameter

d_a : abrasive diameter

d_f : nozzle diameter

h_s : stand-off distance

m_a : abrasive flow rate

m_{Hg} : mass of mercury

m_s : mass of the syringe

P : pump pressure

R^2 : coefficient of determination

SE_c : specific energy of cutting

V : volume of the kerf

V_R : removed volume of rock

v_T : traverse velocity

Rainfall Effects on Pore Pressure Changes in a Coastal Slope of the Serra do Mar in Santa Catarina

A.A.M. González, L.B. Passini, A.C.M. Kormann

Abstract. This research aims to describe how rainfall can cause changes in the piezometric pore pressure and soil matric suction in a densely instrumented slope by the South BR-101 (Brazilian Numbered Highway), in the area of Morro do Boi, in the State of Santa Catarina, South Region of Brazil. The slope presented a history of instability movements instigated by intense rainfall, with debris accumulation on the highway and traffic interruption. The analyzed data are measured by six vibrating wire piezometers and eight electrical tensiometers attached to a datalogger, two conventional slope inclinometers and a rain gauge with an internal datalogger. A total of 2,552 readings corresponding to the vibrating wires and electrical resistance instruments, 29 inclinometers records and 7,143 rainfall records were collected over the first ten months of slope monitoring. The analysis results demonstrated that during the monitoring period there were no heavy rains. Three monitoring periods were identified by the frequency and intensity of rainfalls. The soil pore pressure monitoring instruments showed significant variations in the high frequency period and low intensity rainfall, and little variation in low frequency period and high intensity rainfall, which demonstrates greater runoff and little infiltration during the occurrence of more significant rainfall.

Keywords: field instrumentation, geotechnical monitoring, natural slope, pore pressure, rainfall.

1. Introduction

The Serra do Mar is a mountain range which constitutes the most prominent orographic feature of the Atlantic edge of the South American continent, with approximately 1,000 km length, extending from the state of Rio de Janeiro to the state of Santa Catarina (Almeida & Carneiro, 1998). In these accentuated-relief regions, there are important Brazilian highways which are exposed to risks associated with mass movements, a consequence of the natural and anthropic conditioning (Montoya, 2013).

Although literature indicates that mass movements can be a result of many different factors, such as climatological and hydrological processes, geological characteristics, topography, vegetation, anthropogenic actions (garbage deposits, deforestation, changes in drainage or poor surface and deep drainage, cutting and embankment with expressive angles, overloading, design and change the route of highway) or of all these factors combined (Fernandes *et al.*, 2001; Rahardjo *et al.*, 2008; Zuquette *et al.*, 2013; Carvalho *et al.*, 2015), the role of rain in the events that cause slope instability is widely known (Brand, 1984; Brand *et al.*, 1984; Lim *et al.*, 1996; Rahardjo *et al.*, 2001; Chen & Lee, 2004; Rahardjo *et al.*, 2008; Zuquette *et al.*, 2013).

Significant rainfall can promote such mass movements (Chen & Lee, 2004; Kormann *et al.*, 2011; Gerscovich *et al.*, 2011; Sestrem & Kormann, 2013; Montoya, 2013; Zuquette *et al.*, 2013; Sestrem *et al.*, 2015; Kormann *et al.*, 2016), which frequently have been responsible for major human and economic losses (Bandeira & Coutinho, 2015), and also for damage to the highway network infrastructure.

The effects of rainfall on slope stability are a theme of interest as parameters and warning systems can be generated from rainfall data to prevent human and material losses (Montoya, 2013; Bandeira & Coutinho, 2015). The infiltration of rainfall into the ground develops positive pore pressures by raising the water table and reducing suction levels (Chen & Lee, 2004; Rahardjo *et al.*, 2001, 2008, 2016; Gerscovich *et al.*, 2011; Advincula, 2016), and also generates a preferential flow through the fractures of the bedrock. Therefore, the infiltration resulting from rainfall and the subsequent variations in pore pressure determine the safety level of a slope (Gerscovich *et al.*, 2011; Montoya, 2013; Carvalho *et al.*, 2015).

This article aims to describe, analyze and discuss monitoring data from a research study on a highway slope, with a history of mass movements prompted by significant rainfalls, during the period from May/2012 to March/2013 (González, 2013).

Andrés Miguel González Acevedo, Ph.D. Student, Programa de Pós-Graduação em Geologia, Universidade Federal do Paraná, Curitiba, PR, Brazil. e-mail: andresmgonzalez@gmail.com.

Larissa de Brum Passini, Ph.D., Associate Professor, Programa de Pós-Graduação em Engenharia de Construção Civil, Universidade Federal do Paraná, Curitiba, PR, Brazil. e-mail: larissapassini@hotmail.com.

Alessander Christopher Moraes Kormann, Ph.D., Associate Professor, Programa de Pós-Graduação em Engenharia de Construção Civil, Universidade Federal do Paraná, Curitiba, PR, Brazil. e-mail: alessander@ufpr.br.

Submitted on April 6, 2017; Final Acceptance on September 21, 2017; Discussion open until April 30, 2018.

DOI: 10.28927/SR.403263

2. Materials and Methods

2.1. Description of the study area

The slope, herein described as the object of study, is located on the BR-101 southern lane, between km 140+700 m and km 140+950 m, being delimited by the coordinates S 27°01'30" and S 27°02'30", W 48°35'30" and W 48°36'30", close to the cities of Camboriú and Itapema, in the state of Santa Catarina (SC), Brazil (Fig. 1), on the geomorphological feature known as Morro do Boi (Sestrem, 2012; González, 2013).

According to Sestrem (2012), the slope had a history of instability characterized by movement and the consequent accumulation of debris on the highway and traffic disruption. An occurrence of mass movement – with the breakdown of this rocky slope and the removal of the soil top layer, causing soil and rock blocks to fall down on the highway lane – was recorded during the rainfall that occurred between November 20th and 24th, 2008. Besides this slope, several other highway points had ruptures in slopes resulting from the intense rainfall, which took place in the state of Santa Catarina during this period (CIRAM, 2016). These rainfalls fell on areas such as the Greater Florianópolis, Vale do Itajaí and North Coast of the state of Santa Catarina (Zuquette *et al.*, 2013). Regions such as Blumenau and Joinville experienced around 1000 mm of rain in that month. The region of Vale do Itajaí has been subject to a total rainfall of approximately 600 mm between November 21st and 24th, 2008, according to CIRAM (2016).

The slope under study was stabilized (with nails, metallic mesh and a cap beam of root piles), in order to minimize future inconvenience to road users, after the catastrophic event of 2008. The need to better understand the mechanisms that may trigger accidents motivated the investigation and instrumentation of the slope (Fig. 2) to

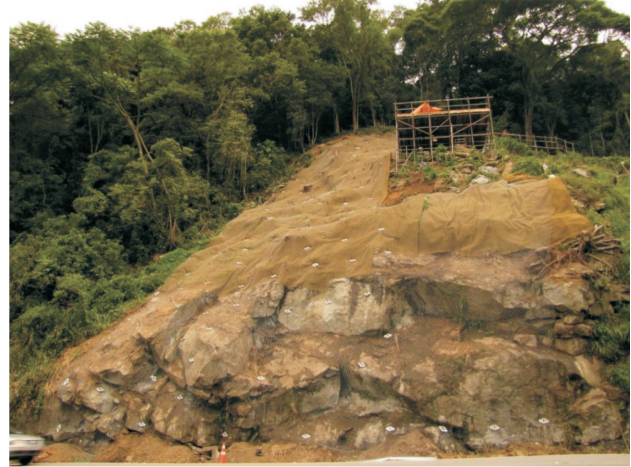


Figure 2 - Stabilized slope and installation of geotechnical monitoring (Sestrem, 2012).

monitor the stabilization solution adopted (Kormann *et al.*, 2016).

2.2. Lithological and geological aspects

The study area is characterized by the presence of two main lithological types: Morro do Boi's Migmatites and Nova Trento's Intrusive Suite granites. The suite is represented by an intrusive body in Morro do Boi's Migmatites, aligned in the NE-SW direction (CPRM, 2014).

According to CPRM (2014), the Morro do Boi's Migmatites extends in the northeast - southwest (NE-SW) direction, in a strip ranging in width from 1.0 to 1.5 km and to the south and east of the city of Camboriú. Its structure is mainly stromatic, often folded, where dark gray metabasic rock xenoliths are common, ranging from homogeneous bodies of massive aspect to finely banded.

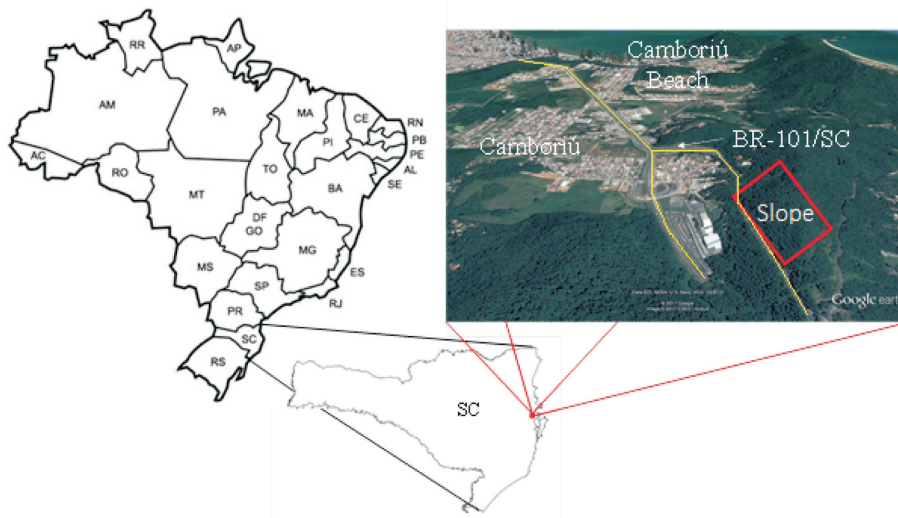


Figure 1 - Location of the study area.

A major fracture system occurs in the body of Morro do Boi's Migmatites generated by NE-SW and NW-SE direction shearing and by sub-horizontal fractures, having as main effect the subdivision of the massif in blocks, which reduces its mechanical resistance. Additionally, due to the continuity and interconnection of fractures, the water easily flows within the massif. In complement to these conditions, there is a layer of silty sand soil on the slope.

2.3. Geotechnical characterization

The soil ranges from mature residual to young in depth, in areas of the slope which were not transported. However, in part of the monitored area, the top soil was identified as colluvial. Through field tests performed on the slope, including three holes of SPT (Standard Penetration Test) and five SM (Standard Penetration Test and rotary drilling), it was observed a superficial layer of silty sand soil with a thickness of around 3.0 m, complemented in some regions by the presence of blocks of rock. There is also a highly weathered layer of rock with a thickness of about 3.0 m over a layer of moderately weathered rock found at 6.0 m depth and with a thickness of around 3.0 m, which overlies the Migmatite, found from approximately 9.0 m depth. The depths of the field investigations were approximately of 12.38 m for the SM-01, 13.00 m for SM-02, 8.20 m for SM-03, 9.25 m for SM-04 and 10.70 m for SM-05.

The colluvium superficial soil presented N_{SPT} from approximately 9 to 40 blows, increasing in depth along the drilling hole, characteristics of a medium compact to com-

pact material. Below that layer, refusal was achieved, being false results due to the presence of rock blocks at some points. Through the SM field investigations, high percentages of RQD (Rock Quality Designation) were obtained from the samples with continuous recovery, characterizing an excellent quality of the rocky massif (RQD of 90% to 100%). As for the moderately weathered rock layer, the mean RQD values obtained were 60%, of reasonable quality.

During the geotechnical surveys it was also possible to observe the water level position, which was equal to 5.35 m for SM-01, 6.12 m for SM-02, 3.50 m for SM-03, 4.60 for SM-04 and 4.60 m for SM-05. Based on such water level depths, the quotas for the installation of pore pressure monitoring instruments were determined, specifically with respect to the deepest piezometers. A geological-geotechnical profile of the slope, which resulted from the compilation of the geotechnical investigation carried out in it, is presented in Fig. 3, including geotechnical monitoring instrumentation, such as inclinometers (INCL), piezometers (PIEZ) and tensiometers (TENS).

According to Massad (2003), in regions of humid tropical climate, the lithotypes which correspond to gneiss metamorphic rocks or with banded appearance give rise to predominantly silty and micaceous soil. For this purpose, soil characterization procedures were carried out to confirm that the weathered Migmatites found in the region result in this type of soil.

To evaluate and characterize the superficial soil properties in the monitored area of the slope, laboratory tests

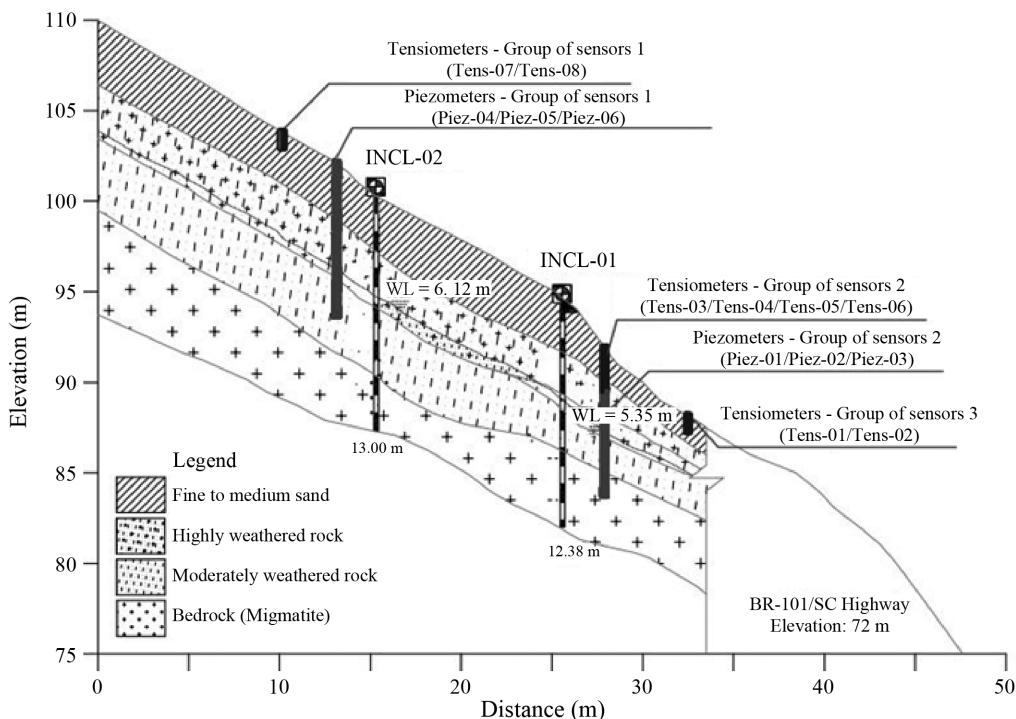


Figure 3 - Sketch of the geological and geotechnical slope profile with instrumentation (WL = water level).

were carried out on four deformed samples collected from non-deformed blocks, in the top slope layer (Lazarim, 2012). Among the performed tests are: soil density – employing the procedure described by DNER-ME Standard 093 (1994) –, Atterberg limits – following the procedures described in the standards NBR 6459 (liquid limit) and NBR 7180 (plastic limit) (ABNT, 2016 b,c) – and particle size analysis of the material – according to the procedure described in NBR 7181 (ABNT, 2016 a).

The laboratory tests classified the top soil as silty sand, with particle density of approximately 2.66 g/cm^3 , average liquid limit of 32%, average plastic limit of 27% and average plasticity index of 5% (Table 1). With respect to particle size analysis (Fig. 4), the average percentages obtained were 4% clay, 27% silt, 61% sand and 8% gravel (Table 2). Direct shear strength tests for samples of colluvium soil collected at depths of 0.25 m to 1.27 m, presented mean friction angle of 34° and mean cohesive intercept of 2 kPa. The average specific natural weight for this material was equal to 16.20 kN/m^3 (Lazarim, 2012; Gonzalez, 2013). In addition, in situ permeability tests were executed at the colluvium surface soil, with values ranging between 4.47×10^{-7} and 1.71×10^{-6} m/s, in agreement with the granulometric analysis, according to Pretto (2014).

2.4. Geotechnical instrumentation

According to Kormann *et al.* (2016), the equipments selected were based mainly on their applications and history of use in the academic scientific environment and the geotechnical practice of slope monitoring (Dunnicliff,

Table 1 - Atterberg limits and particle density.

Sample ID	Atterberg Limits			Particle density (g/cm^3)
	LL (%)	LP (%)	IP (%)	
01	32.2	26.6	5.6	2.61
02	35.3	28.7	6.6	2.63
03	28.4	25.3	3.1	2.69
04	31.8	26.9	4.9	2.70
Average	31.9	26.9	5.1	2.66

Table 2 - Grain-size analyses.

Sample ID	Particle size distribution			
	Clay (< 0.002 mm)	Silt (0.002-0.06 mm)	Sand (0.06-2.0 mm)	Gravel (2.0-60 mm)
01	7.0	25.0	59.3	8.7
02	0.0	30.0	69.7	0.3
03	8.0	22.0	57.4	12.6
04	2.0	31.0	55.3	11.7
Average	4.3	27.0	60.4	8.3

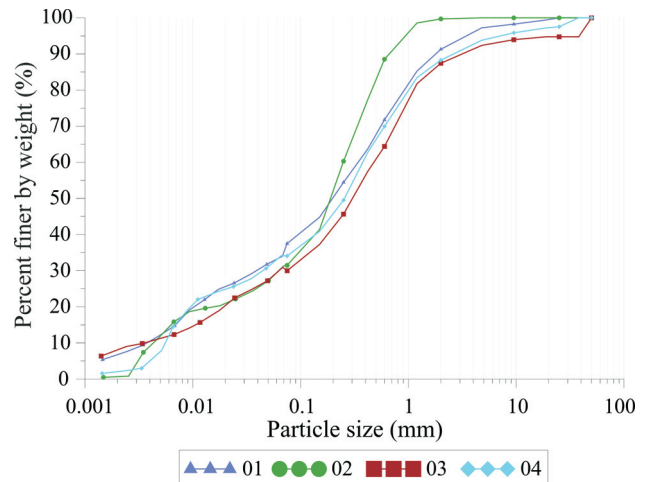


Figure 4 - Grain-size distribution.

1988; Silveira, 2006; Dixon and Spriggs, 2007; Eberhardt, 2008), being: inclinometers, piezometers, tensiometers and rain gauge (Lim *et al.*, 1996; Li *et al.*, 2005; Marinho, 2005; Cerqueira, 2006; Zhan *et al.*, 2007; Bonzanigo *et al.*, 2007; Simeoni & Mongiovì, 2007; Leung *et al.*, 2011; Tommasi *et al.*, 2013; Bicalho *et al.*, 2015).

The slope geotechnical instrumentation aimed to observe the parameter changes such as positive pore pressure and matric suction, in order to check the oscillations of the water table and piezometric level, as well as the occurrence of negative pressure at the top soil. Therefore, six (06) vibrating wire piezometers were installed and eight (08) electrical resistance tensiometers were distributed in islands (Sestrem, 2012) or groups (Sestrem *et al.*, 2015) connected to a datalogger for storing the resulting data. Additionally, two casings with inclinometers were installed to monitor possible horizontal movements of the soil mass as a result of the changes in the above parameters. A rain gauge was also installed to register the intensity of local rainfall and thus relate the monitored parameter variations with the recorded rainfall. A sketch of the instruments installed in the slope is presented in Fig. 5, showing the three islands and including topographic values.

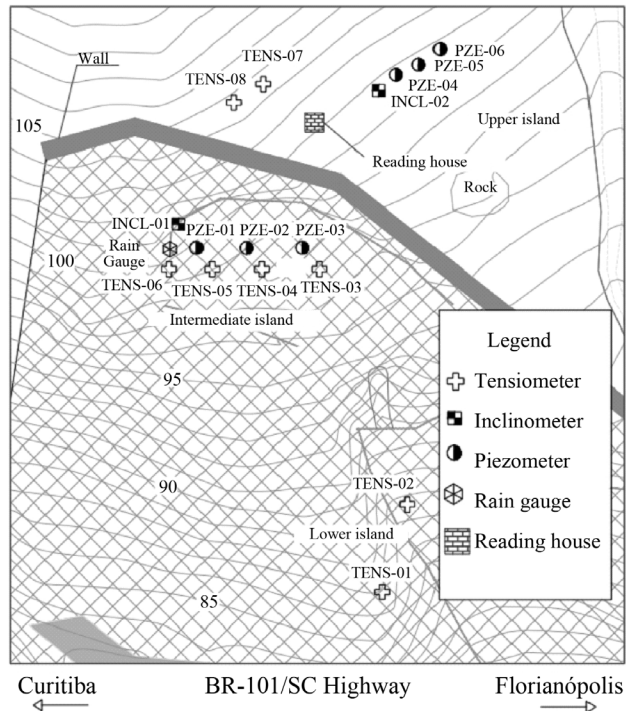


Figure 5 - Sketch of the instruments installed in the slope.

2.4.1. Piezometers

The piezometers are installed in two islands consisting of three instruments each; the upper island (Group 1) with depths of 8.60 m (PZE-04), 7.20 m (PZE-05) and 3.70 m (PZE-06) and the intermediate island (Group 2) with depths of 8.65 m (PZE-01), 6.40 m (PZE-02) and 3.90 m (PZE-03). It is important to note that these instruments were placed at an equivalent depth between the islands, with the deepest ones installed in the interface of rock and weathered rock layer, and the most superficial ones in the highly weathered rock layer.

For the determination of positive pore pressures, vibrating wire standard piezometers were used (Fig. 6a). Among the sensors available, it was selected the Geokon model 4500S (reading capacity ranging from -100 kPa to 350 kPa). These sensors present readings as frequency, the square of the vibration frequency being proportional to the pressure applied to the steel diaphragm (membrane), according to GEOKON (2012).

Prior to installation, a saturation procedure was necessary to prevent the presence of air bubbles inside the instrument. This procedure initially consisted of removing the porous tip and subjecting it to boiling. Then it was transferred to a larger vessel without the contact with the water being lost, so that it was repositioned in the body of the piezometer. The sensor was then stored and sealed. As a result, each instrument was read zero with the tip positioned at the bottom of the bottle with water.

The stages of installation of the piezometers began with the hole drilling. Then, the piezometer was positioned at the reading depth of interest. A bulb of sand (coarse and washed) with a height of 1.00 m was added to then remove the survey coating. Then, a seal with bentonite of 0.50 m thickness was realized, aiming to waterproof the region of the readings. Finally, the hole was filled to the surface. The cable was initially connected to a mobile reader unit for determination of preliminary readings. After that, all the cables were connected to multiplexers, these being finally connected to the datalogger, thus finalizing the automation of the readings.

2.4.2. Tensiometers

As for tensiometers, they were distributed into three islands, all in colluvial soil; at the upper island (Group 1) with depths of 1.00 m (TENS-07) and 2.00 m (TENS-08), in the intermediate island (Group 2) with depths of 0.50 m (TENS-03), 1.00 m (TENS-05), 2.00 m (TENS-06) and 3.00 m (TENS-04), and in the lower island (Group 3) with depths of 1.00 m (TENS-01) and 2.00 m (TENS-02). Installation depths of piezometers and tensiometers followed the water level found at the geotechnical surveys, in order to obtain records of the increases and decreases of the positive and negative pore pressure values, as well as the advancing wetting front through the soil.

For the determination of negative pore pressures, conventional tensiometers were used, model model 2725A from Soil Moisture (Fig. 6b), composed by the following components: porous ceramic cup, plastic tube body and a vacuum meter. Measurement of the negative pressure (vacuum) was automated by means of a transducer coupled to the tensiometer. The instrument reading capacity ranged from 0 kPa to - 100 kPa.

Prior to installation, the tensiometers were prepared and assembled in laboratory where initially the porous stones were submitted to a saturation procedure. To this end, they were immersed in a container containing water and subjected to the removal of air in a desiccator with silica and vacuum pump. In parallel to this, the inside of the tensiometer tube was washed with water and detergent. This procedure aimed to remove particles and possible fat spots that might favor the formation of air bubbles and, therefore, alter the suction values read. After saturation of the porous stone tips and cleaning of the interior of the tensiometer tubes, they were fitted according to the desired lengths. All the connection threads between the tube extensions were installed with o-rings to ensure complete sealing of the tensiometer, preventing the entry of air and the formation of bubbles, avoiding the phenomenon of cavitation (expansion of air bubbles), according to Soil Moisture (2011).

After being assembled, the tubes were subjected to a suction process, with the ceramic tip being immersed in a vessel with boiled water and the other end connected to a

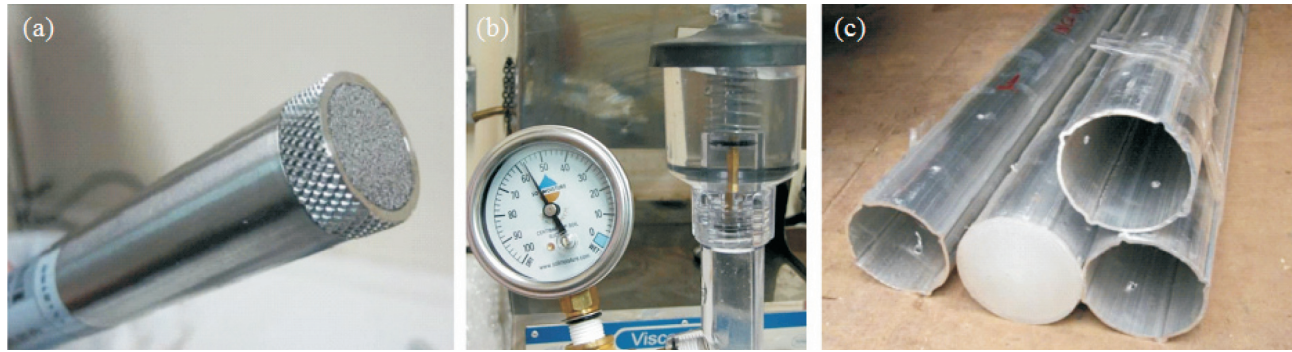


Figure 6 - Instrumentation: (a) vibrating wire standard piezometers, (b) conventional tensiometers and (c) conventional inclinometer tubes (Sestrem, 2012).

pump. This procedure allowed the removal of as much trapped air as possible in the wells (Jones *et al.*, 1981 *apud* Marinho, 2005).

Once the tubes were completely filled by water, they were connected to the reservoirs, which were also filled with boiled water. Then the upper end of the reservoir was pressed so as to inject water into the tube to fill it completely and eliminate any remaining bubbles. Once assembled and tested, they were prepared for transportation to the field. In order to avoid the loss of saturation of the porous stones, in addition to possible leaks, they were immersed in water and protected with a plastic bag, according to the recommendations provided by the manufacturer.

For field installation, it was applied a hand drill. Prior to the positioning of the instrument in the drilling, its tip was placed in contact with a mixture of water and previously sieved local soil (#40). This mixture was also used to fill the hole, ensuring the system sealing and avoiding infiltrations into the tensiometer.

It was also necessary to verify the calibration of the analog tensiometer, an accessory supplied by the manufacturer hermetically sealed at sea level. When installed at a higher elevation, as in the case of the present work, the pointer on the gauge display may have a reading other than zero, resulting from a lower atmospheric pressure.

Finally, the portion of the tensiometers positioned above the soil surface was protected with a 100 mm diameter PVC tube filled with soil from the site, trying to avoid possible problems, such as accidental impacts and bending of the tensiometer tube. In addition, all tensiometers received additional concrete-based protection and an external metal shield of 300 mm diameter.

2.4.3. Inclinometers

For the monitoring of horizontal displacements in the slope, two conventional inclinometer tubes were installed (Fig. 6c), anchored in Migmatites, at a depth of 12.38 m (INCL-01) and 13.00 m (INCL-02), placed in the middle and upper islands, respectively. They were installed into the drilling holes of SM-01 and SM-02, respectively.

The installation sequence of each inclinometer started with placing the access tube in a hole with a diameter of 100 mm, with the respective depth of INCL-01 and INCL-02. An aluminum tube with a diameter of 80 mm and four diametrically opposed slots was used to guide the instrument (torpedo) during the readings. The tube was inserted in the hole, maintaining the alignment of the grooves according to the main axes of displacements of the slope, that is, a plane perpendicular and another parallel to the highway. After complete installation of the pipe/tube, the space between it and the walls of the bore was filled with cement grout and bentonite (1:10) upwardly through the injection hose. Finally, a protective box with padlock was installed at the surface, and a concrete base was also executed, in order to prevent any damage caused by work operations and vandalism.

2.4.4. Rain gauge

The rain gauge installed (Fig. 7) with tipper buckets was model TB4/0.2 from Hydrological Services, whose readings are obtained by a datalogger model ML1-FL. This system has a maximum reading intensity of 700 mm/h and a resolution of 0.2 mm, being able to record in its memory the date and time of the occurrence of rain, with a storage capacity of up to 100 thousand events with a resolution of 1 second, according to Hydrological Services (2011).

The chosen pluviograph has its operation based on a tipping system. Whereby, a metal bucket of 200 ± 0.3 mm in diameter accumulates the precipitations and, when its capacity is reached (0.20 mm) tipping occurs. At this point, the data collector system records the date and time of this occurrence. Between the bucket and the measuring system, there is also a metal screen with the purpose of preventing the passage of objects that could obstruct the system (leaves, branches). The data collector has a reading capacity for rains with intensities between 0 and 500 mm/h (lower than that of the datalogger), temperature range from -20 to $+70$ °C, and accuracy of $\pm 2\%$ for intensities between 25 and 300 mm/h $\pm 3\%$ for intensities between 300 and 500 mm/h, according to Hydrological Services (2011).



Figure 7 - Instrumentation: rain gauge installed.

The definition of the position of the pluviograph considered that it should guarantee a representative reading of the pluviometric indices at the site. It was positioned as close to ground level as possible, avoiding sloping terrain. In addition, there was the need to position it in an area protected from strong winds and obstacles. Another problem that could occur was the absorption of rainwater from the soil around the sensor. Thus, to avoid such interference, it was decided to install the instrument at a distance of approximately 1.20 m from the ground. It was chosen to position it within the stabilized area. It should be emphasized that care with vegetation that grows in this location should be taken, thus not only serving the pluviometer, but also making it possible to read the inclinometer installed in the same local area (INC-01).

The installation began by driving a vertical nail at the chosen location (of the same model used for the stabilization solution) so that its tip was approximately 40 cm above the surface. A circular base was then positioned on such bar, leaving it centered in concrete. Finally, the pluviograph was installed on three screws that allowed leveling, by means of the adjustment of the nuts guided by the bubble level contained in the equipment. After the pluviograph was installed, a test operation was performed in which the hopper tip was initially pressed a few times to check if each movement was being logged, and whether the tilt mechanism was operating freely. According to Hydrological Services (2012), the instrument is factory calibrated and the only maintenance procedure required is cleaning, whereby the following items must be checked: trap filter, siphon, bucket interior, upper surface of set screws, fastening screws (which must be lubricated after cleaning) and screens against insects.

2.5. Instrumentation data

The slope instrumentation data collected during the first ten months of monitoring – from May 1st, 2012 until March 1st, 2013 – were compiled and analyzed. The automatic data collection from the piezometers and tensiometers provided readings every hour and, later, these

readings were grouped so that the results were converted into daily average values. The readings of the tipping bucket rain gauge (PLUV-01), located in the intermediate island, were registered every time it reached 0.20 mm of rain, and the data was stored in an independent datalogger.

During the monitoring period, 7143 rain gauge readings, 2552 readings from piezometers and tensiometers and 29 total readings from both inclinometers were collected.

The obtained data were classified as continuous time series data, which can be interpreted with specific technical statistics. This classification was based on the characteristics of the obtained data, which showed a sequence at regular time intervals during a specific period (Latorre & Cardoso, 2001).

The data interpretation was based on several graphical representations of the time series to determine an ascending or descending trend, the influence of time – stationarity – and any discordant observations – outliers – (Gonzalez, 2013).

The time series were compared with the rain events, for example, to establish a relation between the positive and negative variation of pore pressure parameters and the rainfall events that occurred in the analysis location. It is important to observe that for the analysis of time series, the first step is to model the phenomenon to be studied for describing its behavior and thus evaluate which factors influenced its variations and behavior (Latorre & Cardoso, 2001).

For the definition of rain intensity, the classification system by CIRAM (2016) was considered, whereby the intervals for accumulated rainfall per hour (mm/h) were classified and defined, in a general manner. In this classification, the authors considered: drizzle rain (C_{mFra}) for rainfalls between 0.25 mm/h and 1.00 mm/h; light rain (C_{Fra}) for rainfalls between 1.00 mm/h and 4.00 mm/h; moderate rain (C_{Mod}) for rainfalls between 4.00 mm/h and 16.00 mm/h; heavy rain (C_{Fo}) for rainfalls between 16.00 mm/h and 50.00 mm/h, and violent rain (C_{mFO}) for rainfalls equal to or greater than 50.00 mm/h.

With respect to the classification of accumulated daily rainfall (mm/day), intervals were determined based

Table 3 - Daily rainfall determined by means of the quantile technique.

Classification per day	Daily accumulated rainfall (P, mm/day)
Dry day (D_s)	$P < 0.20$
Drizzle (C_{mFra})	$0.20 < P < 0.60$
Light Rain (C_{Fra})	$0.60 < P < 3.20$
Moderate Rain (C_{Mod})	$3.20 < P < 13.00$
Heavy Rain (C_{Fo})	$13.00 < P < 45.60$
Violent Rain (C_{mFo})	$P > 45.60$

on the definition of quantiles, evaluating the history of rainfall by the probability of occurrence (Xavier & Xavier, 1987; Leite *et al.*, 2011; Souza *et al.*, 2012). The analysis was performed with an updated database of the rain gauge installed in the study area, as shown in Table 3.

3. Results and Discussion

The time series resulting from the monitoring of geotechnical instrumentation were analyzed initially considering the independent variable (rain) and the relationship of this parameter with the variations in positive pore pressure and suction values, according to Lim *et al.* (1996) e Rahardjo *et al.* (2008).

3.1. Rainfall events

Through the data series, three different rain periods were observed, delimited by the intensity and magnitude of the events. The first period – between the months of May and July, 2012 – was characterized by magnitudes of 196.60 mm, 203.40 mm and 260.00 mm, although with moderate intensities – around 19.40 mm/h, 11.60 mm/h and 14.60 mm/h. It means that rainfall events resulted in prolonged rain over the days, with the most significant ones classified as moderate and heavy rain, according to the classification of CIRAM (2016).

In the second period – between August and November, 2012 – the accumulated rainfalls per month had a lower magnitude, with 49.20 mm for August and 61.80 mm for September, with peaks of 4.00 mm/h and 11.60 mm/h, respectively. These events were considered moderate rain-

falls, according to CIRAM (2016). It was observed that October had an outstanding record, in which isolated rains of great intensity and magnitude reached 174.20 mm accumulated rainfall with a peak of 13.40 mm/h. In this month, two significant events were recorded – which influenced the instrumentation readings behavior, hence an increase in the month-accumulated value: they occurred on October 11th, with an 80.60 mm accumulated rainfall, and on the 22nd, with 40.40 mm accumulated.

It is important to highlight that – due to failure in the instrument between November 8th and December 12th, 2012 – November recorded only 0.40 mm, hence November to the beginning of December were without valid records.

In the third period – between the months of December, 2012 and February, 2013 – the rains had great magnitude with intensity that reached 112.00 mm in 14 days of rainfall recorded for December and with a peak of 29.60 mm/h. For January the record was 109.60 mm in 17 days of rainfall and a peak of 38.00 mm/h. For February the record was 216.60 mm in 22 days, reaching a volume peak of 38.00 mm/h. The precipitation related to these three months was characterized as heavy rainfall, according to CIRAM (2016).

In order to observe in detail the magnitude and behavior of rainfall, without generalizing the monthly accumulated values, it is shown in Fig. 8 the rain distribution throughout the monitoring period based on daily rainfall values. Furthermore, it is presented the water level readings at the slope during the same period of time, where the records were made once a month manually. It can be observed water level variation ranging from 6.98 m to 9.80 m in INCL-01 and 9.05 m to 9.97 m in INCL-02. Unexpectedly, water level depths were deeper than the values determined during the geotechnical survey, as equal to 5.35 m for SM-01 (INCL-01) and 6.12 m for SM-02 (INCL-02).

In this study, 263 out of 304 days had records during the monitoring period. These rainfall events were classified according to the quantiles technique (Xavier & Xavier, 1987; Leite *et al.*, 2011; Souza *et al.*, 2012), with the results shown in Table 4.

It is possible to observe that 44.11% of the rainfall events were classified under the category Dry Day (D_s) and

Table 4 - Results of the classification of rainfall events during the monitoring period according to the quantile technique.

Classification	Daily accumulated rainfall (P, mm/day)	Events (days)	Events (%)
D_s	$P < 0.20$	116	44.11
C_{mFra}	$0.20 < P < 0.60$	38	14.45
C_{Fra}	$0.60 < P < 3.20$	44	16.73
C_{Mod}	$3.20 < P < 13.00$	33	12.55
C_{Fo}	$13.00 < P < 45.60$	24	9.13
C_{mFo}	$P > 45.60$	8	3.04

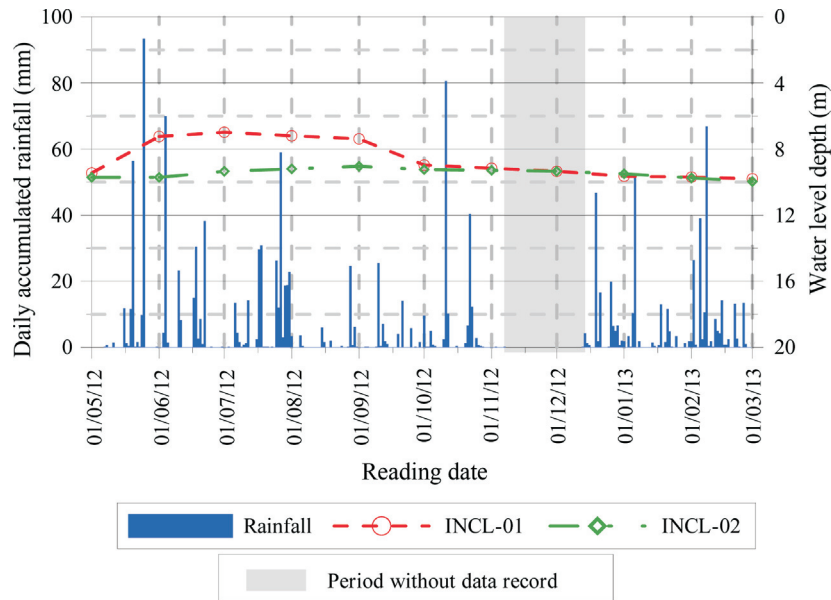


Figure 8 - Daily rainfall accumulation and water level monitoring at the study site.

the others from Drizzle (C_{mFra}) to Strongest Rain (C_{mFo}), ranging from 3.04% to 16.73%.

Surface runoff basically occurs when the rainfall intensity overcomes the infiltration capacity. Under this concept, evaporation and evapotranspiration during the rain are negligible. Considering the in situ permeability test, with values between 4.47×10^{-7} and 1.71×10^{-6} m/s for the surface soil layer, it is possible to establish the equivalence to 1.61 mm/h to 6.16 mm/h of rainfall intensity. In this range and by the rainfall classification made by CIRAM (2016), moderated rainfall will have surface runoff.

3.2. Piezometers

As for piezometers installed at the intermediate island, it was observed a behavior of significant variations during the first (May to July) and second (August to November) monitoring periods, until the readings stabilization in the third period (December to February) as shown in Fig. 9. On the other hand, the piezometers installed at the upper island did not show significant variations in readings behavior, as shown in Fig. 10. The daily accumulated rainfall and the total accumulated rainfall during the monitoring period can be observed and compared with the piezo-

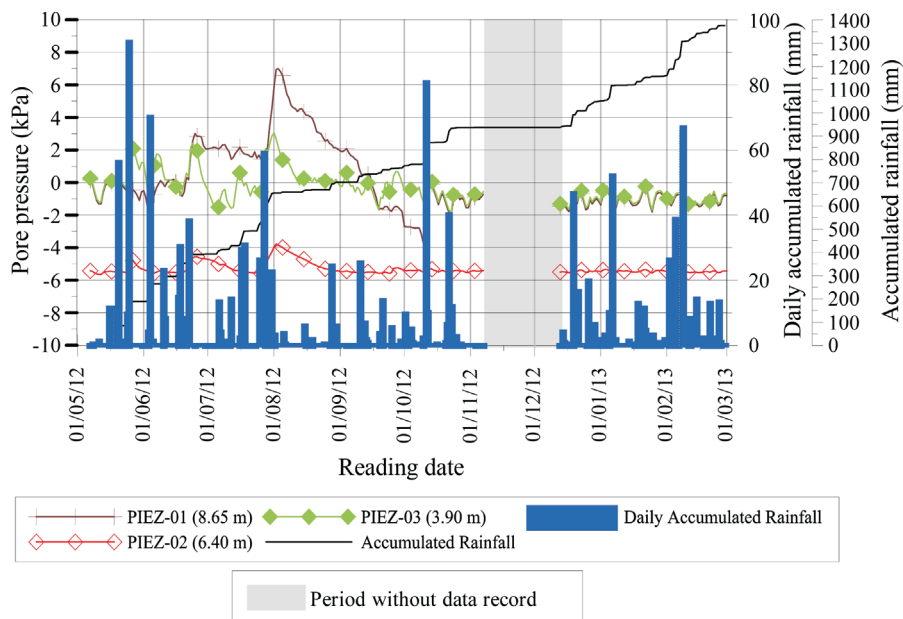


Figure 9 - Readings of piezometers installed at the intermediate island.

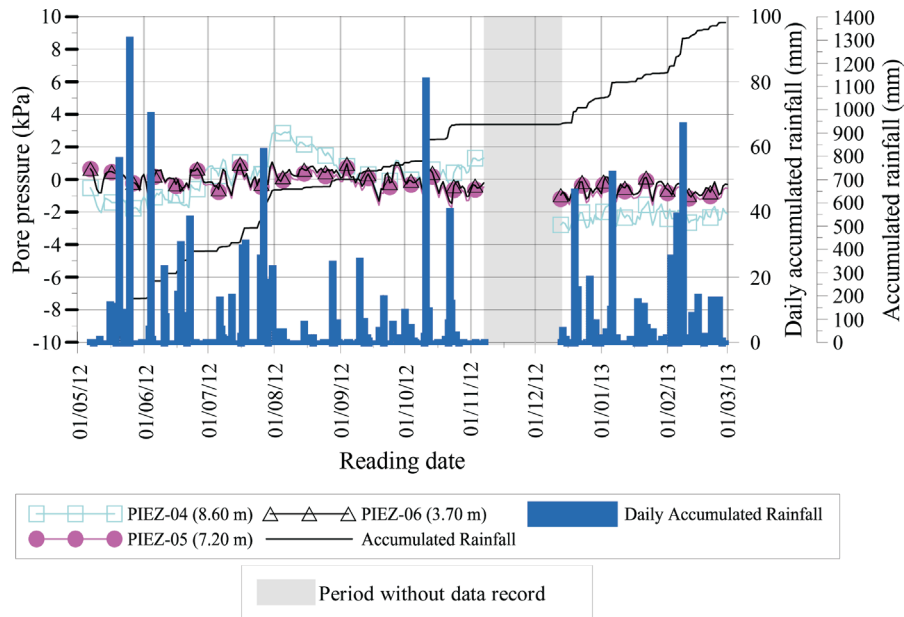


Figure 10 - Readings of piezometer installed at the upper island.

meter records (Figs. 9 and 10). In general, the piezometer presented good agreement with the daily accumulated rainfall, showing an increase in positive pore pressure as the rainfall occurs and a decrease during the period with less rain.

The instruments placed at greater depths showed the greatest pore pressure variations, with peaks up to 7.00 kPa, minimum reading equal to -3.80 kPa and an average reading of 0.17 kPa for the piezometer PZE-01 (installed at a depth of 8.65 m), as can be observed in Fig. 9. The maximum reading was equal to 2.90 kPa for the piezometer PZE-04 (installed at a depth of 8.60 m), while the minimum reading was equal to -3.10 kPa with an average reading of -0.53 kPa, as can be observed in Fig. 10. These high rise behaviors were justified by the water table level increase during continuous rainfall periods which occurred from July 15th to 31st, 2012. As the water level depth recordings were deeper than the values determined during the geotechnical survey, the deeper instruments were reading intentionally the capillary fringe. Furthermore, these instruments could capture an eventual elevation of the water table following the occurrence of a very intense rainfall as happened in 2008.

The piezometers installed at an intermediate depth, such as PZE-02 (6.40 m) and PZE-05 (7.20 m), as well as the most superficial ones, PZE-03 (3.90 m) and PZE-06 (3.70 m), presented lower readings variation. The records of such instruments varied around zero, even though they were located in sites with different slopes and elevations, demonstrating that the wetting front was parallel to the slope and that the instruments were located above the water level. Conversely, the values corresponding to PZE-02 pre-

sented reduced reading intervals, characterizing abnormal behavior (Fig. 9).

3.3. Tensiometers

The tensiometers showed a variation trend similar for them all during the first monitoring period (May to July) until the beginning of August, with values between 0 to 10 kPa. After the initial phase, it was observed a change in the data provided by the instrument closer to the surface. More specifically, there was an increase in the suction values for the TENS-03, located at a 0.50 m depth at the intermediate island, with minimum and maximum readings equal to 3.20 kPa and 77.97 kPa, respectively (Fig. 11). As the slope conditions changed over time due to the vegetation growth, the instrument installed closer to the surface became more susceptible to reading changes after rain events, which reflected on the quick variation on the suction records, as can be noticed by the difference between slope vegetation covering in April 2012 and March 2013 from Fig. 12.

The most significant rainfall event for the decrease of suction in the TENS-03 (0.50 m depth) was February 7th to 11th, 2013. In this period, the suction measured decreased 66.6 kPa in five days and the previously daily accumulated rainfall associated was 66.80 mm (February 8th). Like this episode, there were two significant decreases of suction in this instrument. In January 2013, between 4th and 14th, there was a decrease of 42.72 kPa in eleven days with an associated daily accumulated rainfall of 52 mm (January 6th). The last event occurred, from October 11th to 14th, 2012, in which the suction measured decreased 39.2 kPa in four

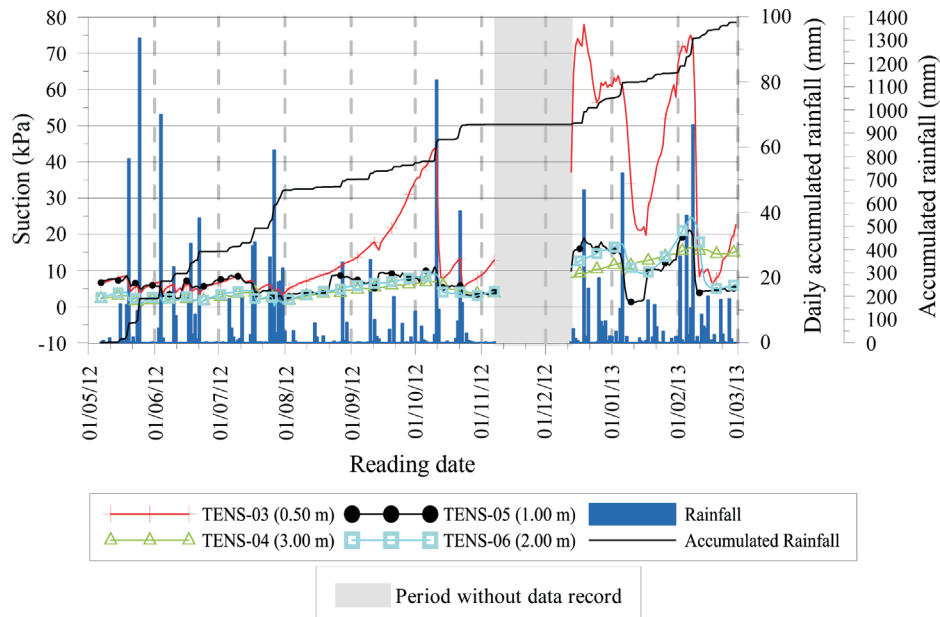


Figure 11 - Readings of tensiometers installed at the intermediate island.



Figure 12 - Slope vegetation covering in (a) April 2012 and (b) March 2013.

days with previously daily accumulated rainfall of 80.60 mm (October 11th).

The other tensiometers also installed at the intermediate island (Fig. 11) had records with small ranges between minimum and maximum values, yet with higher variations starting from November, 2012. The minimum and maximum readings of the tensiometer installed at the greatest depth, TENS-04 (3.00 m), were 0.12 kPa and 16.66 kPa, respectively, with an average of 6.32 kPa, from May, 2012 to March, 2013. TENS-05 (1.00 m) had minimum and maximum readings of 1.09 kPa and 21.13 kPa, respectively, and an average reading of 7.38 kPa. TENS-06 (2.00 m) recorded a minimum reading of 0.17 kPa, a maximum of 24.84 kPa and an average of 6.78 kPa.

The reading variations of the instruments can be interpreted according to their location on the slope, that is, their

positioning in the islands. For example: TENS-01 (1.00 m) and TENS-02 (2.00 m), installed at the lower island (Fig. 13), starting the reading variations in December, 2012 – month with intense yet disperse rainfalls. TENS-01 showed increases in the suction levels going from minimum readings of 4.04 kPa to maximum readings of 79.46 kPa with an average of 53.15 kPa. TENS-02 presented minimum readings of 9.77 kPa to a maximum reading of 68.84 kPa and an average of 38.70 kPa. These measurements were associated with their location on the steeper portion of the slope, which is more exposed to sunlight.

On the other hand, at the upper island (Fig. 14), the TENS-07 (1.00 m) and TENS-08 (2.00 m) presented low and constant suction values, ranging from 3.36 kPa to 13.32 kPa for TENS-07 and from -3.58 kPa and 6.42 kPa

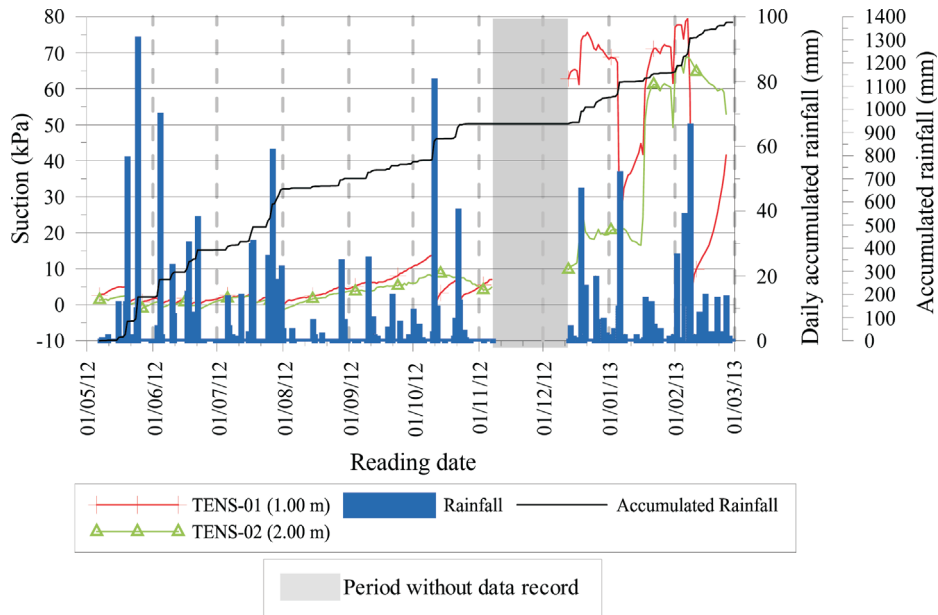


Figure 13 - Readings from tensiometers installed at the lower island.

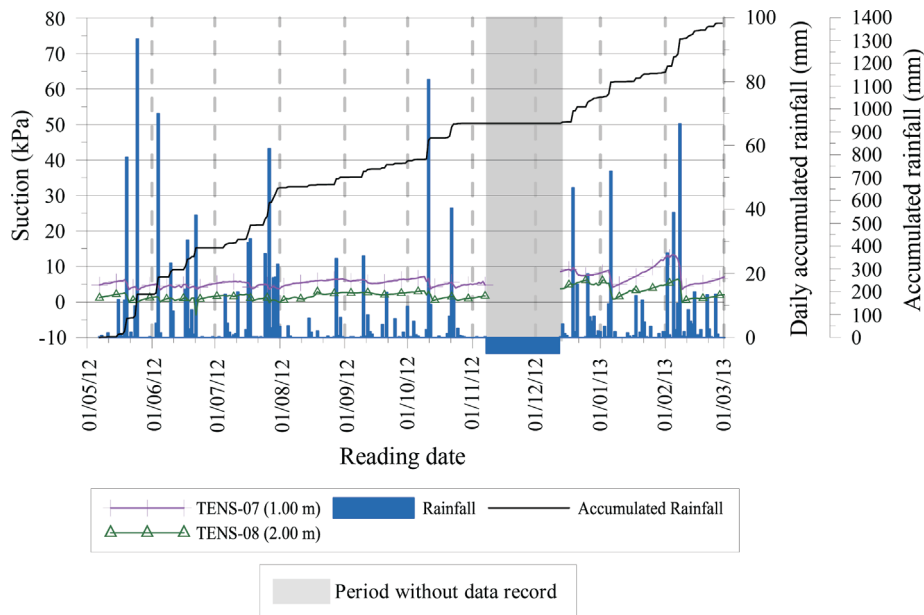


Figure 14 - Readings of tensiometers installed at the upper island.

for TENS-08, with average values of 5.97 kPa and 2.09 kPa, respectively. This island is less exposed to sunlight so that the local humidity can be much more preserved.

The daily accumulated rainfall and the total accumulated rainfall during the monitoring period can be observed and compared with the tensiometers records (Figs. 11, 13, 14), where the daily accumulated rainfall shows more influence than the total accumulated rainfall in tensiometers variation readings. Overall, the tensiometers presented an

increase in the negative pore pressure (suction) during the period with less rain and a decrease as the rainfall occurs.

It can be observed that, in the instruments located at 1.00 m depth and less (TENS-03 at 0.50 m depth according to Fig. 11), daily accumulated rainfall over 40 mm caused also variations to the readings. In TENS-05 (Fig. 11), TENS-01 (Fig. 13) and TENS-07 (Fig. 14), for example, the events occurred in January and February, 2013, had similar effect, with abrupt falls after rainfall events, but with different range. As the instruments are installed at

deeper layers from the soil surface, they do not suffer such significant variations.

In the data presented (Figs. 9, 10, 11, 13 and 14) it can be observed that the records were interrupted during the period of November 8th to December 12th, 2012, usually resulting from problems with the acquisition at the datalogger system.

3.4. Inclinometers

As for the monitoring of horizontal movements of the soil mass, INCL-01 located at the middle portion of the slope (intermediate island), presented stable accumulated reading values of less than +/-2 mm between the base and the top (Fig. 15). There have been two perceivable yet subtle areas of horizontal displacement accumulation, at depths of 2.5 m and 5.0 m, however, they were not significant.

INCL-02 located at the upper island (Group 1), also presented stability in its readings, with accumulated displacements lower than +/-2 mm (Fig. 16). The distortions observed in both instruments can be attributed to: (i) accommodation of the top silty sand soil layer as a consequence of hole drilling for tube installation, and (ii) torpedo readings.

The axes of the inclinometer tubes corresponded to the direction in which its casings were positioned in relation to the slope. Therefore, axes A and B corresponded to movements which are perpendicular and parallel to the slope, respectively.

In slope stability studies, the movement's magnitude and relevance are considered according to the horizontal displacement speed, with creep being the slowest process, with displacement rates of 15 mm/year (Cruden & Varnes, 1993). For both inclinometers (INCL-01 and INCL-02), the accumulated horizontal displacement measured over the slope monitoring period did not reach what is considered to be a soil creep phenomenon. The data point out the stability of the monitored slope, attesting to the adequacy of the stabilization structure implanted *in situ*.

4. Conclusions

The analysis of rainfall readings in this study demonstrates that, during the monitoring period, there were not any events of great magnitude (highest record equal to 260 mm in July, 2012), as opposed to those recorded in 2008, which accumulated approximately 1000 mm in November. There were also no heavy rain events during the monitoring period, which led to little significant variations of rainfall readings.

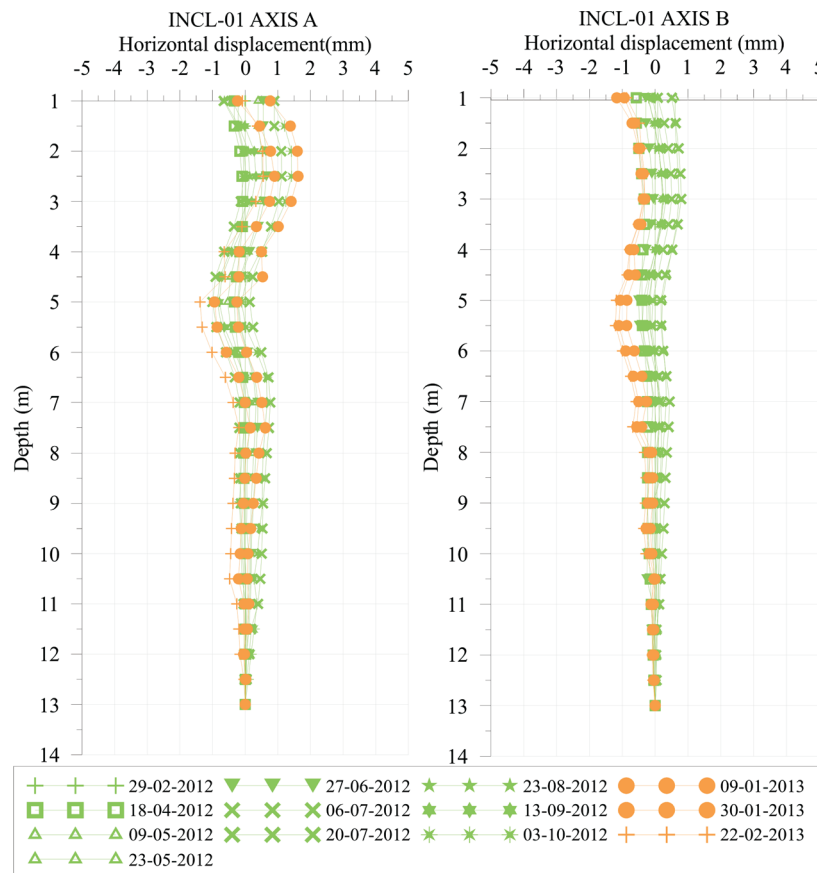


Figure 15 - Readings of accumulated displacements from INCL-01 at the intermediate island.

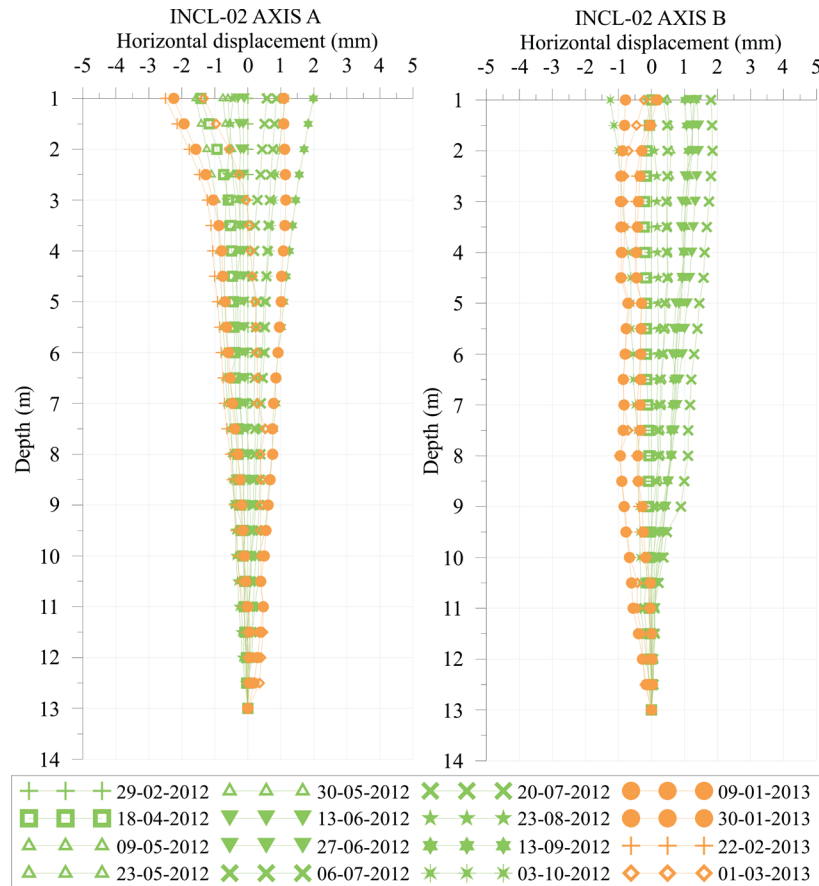


Figure 16 - Readings of accumulated displacements from INCL-02 at the upper island.

Throughout the first three months of monitoring (from May to July, 2012), it was possible to note low intensity rainfalls which lasted for long periods. Starting from the months of August and September, 2012, the events were scattered, with low rainfall values. This can be characterized as a drier period in relation to the previous quarter. In the last months of monitoring (December, 2012 to February, 2013), the rainfalls had higher hourly intensity during reduced periods of time. The records measured were equal to 38 mm/h in January and February. This type of rain events tends to produce greater runoff and less water infiltration in the soil. Consequently, the positive pore pressure levels remained relatively stable.

The piezometer and tensiometer responses were in accordance with the daily accumulated rainfall; for example, an increase of piezometric levels and a decrease of suction values were observed after rain periods and, additionally, a decrease of positive pore pressure values and a suction increase were observed after periods without rainfall records. It is worth to highlight that the local soil type, characterized as silty sand, and the high fracture of the underlying rock, contribute to allow a faster drainage of the slope, thus reducing the increase of positive pore pressures. The piezometers showed a certain tendency towards stabilization of readings as a result of a few events of great inten-

sity and heavy rainfalls. The piezometers installed at greater depths showed more significant readings, especially during July, 2012, which was characterized by low intensity rainfalls that lasted for long periods. This corresponded to an increase of the piezometric level, as a result of infiltration and rainfall accumulation.

Due to the vegetation growth over the monitoring period, the suction values tended to increase for the tensiometers installed closer to the surface, in the intermediate and lower slope islands (Groups 2 and 3). It was also verified that the suction readings in the study area decrease with location depth, which corresponds to the expected humidity profile for the active, non-saturated zone. As for the horizontal displacements, the readings analyses indicate stability, with values ranging up to ± 2 mm.

Acknowledgments

The authors would like to thank the ANTT – Brazilian National Agency for Transportation – and the Autopista Litoral Sul – Grupo Arteris for their support to this research and for making viable the study presented in this work.

References

Advincula, M.R.E. (2016). Evaluation of the Pore Pressure Increase Effect on the Strength Characteristics of Three

- Tropical Soils. PhD Thesis, PUC-Rio, Rio de Janeiro, Brazil, 278 p. In Portuguese.
- Almeida, F.F.M. & Carneiro, C.D.R. (1998). Origin and evolution of the Serra do Mar. *Brazilian Journal of Geosciences*, 28(2):135-150. In Portuguese.
- ABNT (2016a). Soil – Grain Size Analysis - NBR 7181. Brazilian Association of Technical Standards, Rio de Janeiro, Brazil, 12 p. In Portuguese.
- ABNT (2016b). Soil – Liquid Limit Determination - NBR 6459. Brazilian Association of Technical Standards, Rio de Janeiro, Brazil, 5 p. In Portuguese.
- ABNT (2016c). Soil – Plasticity Limit Determination - NBR 7180. Brazilian Association of Technical Standards, Rio de Janeiro, Brazil, 3 p. In Portuguese.
- Bandeira, A.P.N. & Coutinho, R.Q. (2015). Critical rainfall parameters: Proposed landslide warning system for the metropolitan region of Recife, PE, Brazil. *Soils and Rocks*, 38(1):27-48.
- Bicalho, K.V.; Vivacqua, G.P.D.; Cui, Y.-J.; Froumentin, M.; Mercadier, D. & Tang, A.M. (2015). Experimental investigation of soil-atmosphere interaction in an instrumented embankment constructed with two treated clays. *Soils and Rocks*, 38(2):149-162.
- Bonzanigo, L.; Eberhardt, E. & Loew, S. (2007). Long-term investigation of a deep-seated creeping landslide in crystalline rock. Part I. Geological and hydromechanical factors controlling the Campo Vallemaggia landslide. *Canadian Geotechnical Journal*, 44(10):1157-1180.
- Brand, E.W. (1984). Landslides in southeast Asia: a state-of-the-art report. *Proceedings of the 4th International Symposium on Landslides*, Canadian Geotechnical Society, Toronto, v. 1. pp. 17-59.
- Brand, E.W.; Premchitt, J. & Phillipson, H.B. (1984). Relationship between rainfall and landslides in Hong Kong. *Proceedings of the 4th International Symposium on Landslides*, v. 1. Canadian Geotechnical Society: Toronto; pp. 377-384.
- Carvalho, J.C.; Gitirana Junior, G.F.N.; Machado, S.L.; Mascarenha, M.M.A. & Silva Filho, F.C. (2015). Unsaturated Soils in the Geotechnical Context. *Brazilian Association of Soil Mechanics and Geotechnical Engineering (ABMS)*, São Paulo, 759 p. In Portuguese.
- Cerqueira, J.L.R.P. (2006). Radiometeorological Study of the Amazon Region. PhD. Thesis, Graduate Program in Electrical Engineering. Pontifical Catholic University of Rio de Janeiro, Rio de Janeiro, Brazil, 261 p. In Portuguese.
- Chen, H. & Lee, C. (2004). Geohazards of slope mass movement and its prevention in Hong Kong. *Engineering Geology* 76:3-25.
- CIRAM (2016). The rains of November 2008 in Santa Catarina: a case study aimed at improving the monitoring and prediction of extreme events. (Technical Note). Information Center for Environmental Resources and Hydrometeorology of Santa Catarina. Ed. Maria Assunção Silva Dias, INPE. São José dos Campos, SP, Brazil, 67 p. Available in: http://www.ciram.com.br/ciram_arquivos/arquivos/gtc/downloads/NotaTecnica_SC.pdf Accessed in: 07/06/16. In Portuguese.
- CPRM (2014). Geological map of the State of Santa Catarina. Scale 1:500.000. – Mineral Resources Research Company. Geological Survey of Brazil. 1 p. Available in: http://geobank.cprm.gov.br/pls/publico/geobank.download.downloadlayouts?p_webmap=N Accessed in: 06/15/16. In Portuguese.
- Cruden D.M. & Varnes D.J. (1993). Landslide types and processes. In: Turner A.K. & Schuster R.L. (eds) *Landslides: Investigation and Mitigation*. Washington, DC, USA, National Research Council, Transportation and Research Board Special Report 247, pp. 36-75.
- Dixon, N. & Spriggs, M. (2007). Quantification of slope displacement rates using acoustic emission monitoring. *Canadian Geotechnical Journal*, 44(8):966-976.
- DNER (1994). Soils - Determination of Particle Density: Test method - DNER ME-093 (Road Standard). National Department of Highways. Rio de Janeiro, Brazil, 4 p. In Portuguese.
- Dunnicliff, J. (1988). *Geotechnical instrumentation for monitoring field performance*. 1st ed. John Wiley and Sons, Inc. New York, USA, 577 p.
- Eberhardt, E. (2008). Twenty-ninth Canadian Geotechnical Colloquium: The role of advanced numerical methods and geotechnical field measurements in understanding complex deep-seated rock slope failure mechanisms. *Canadian Geotechnical Journal* 45(4):484-510.
- Fernandes, N.F.; Guimarães, R.F.; Gomes, R.A.T.; Vieira, B.C.; Montgomery, D.R. & Greenberg, H. (2001). Geomorphological Conditions of Slope Slips: Evaluation of methodologies and application of model of prediction of susceptible areas. *Brazilian Journal of Geomorphology*, 2(1):51-71. In Portuguese.
- GEOKON (2012). *Introduction Manual: Vibrating Wire Piezometer - Model 4500S Products*. Geokon, Inc., Lebanon, NH, USA. 39 p. Available in: <http://geokon.com/products/>. Accessed in 10/10/11.
- Gerscovich, D.M.S; Vargas Jr., E.A. & de Campos, T.M.P. (2011) Analysis of a Landslide in a Residual Soil Slope in Rio de Janeiro, Brazil. *Soils and Rocks*, 34(2):139-149.
- González, A.A.M. (2013). Study of Series of Readings Obtained Through the Monitoring of the Geotechnical Instrumentation Implanted in a Coastal Slope. Master's Thesis, Construction Engineering Graduate Program, Federal University of Paraná, 188 p. In Portuguese.
- Hydrological Services (2011). *Introduction Manual: Tipping Bucket Rain Gauge - Model TB4*. Hydrological Services Pty Ltd., Liverpool, NSW, Australia, 17 p. Available in: <http://www.hydroserv.com.au/products/tb4.asp>. Accessed in 02/05/11.
- Kormann, A.C.M.; Sestrem, L.P. & Asakawa, S. (2011). Stability and performance evaluations of road slope pro-

- tection systems on an instrumented coastal slope. In: VI Workshop Resources for Technological Development, Brasília, Federal District, Brazil, pp. 8-9. In Portuguese.
- Kormann, A.C.M.; Sestrem, L.P.; Lazarim, T.P.; Passini, L.B. & Asakawa, S.S. (2016). Integration of geological-geotechnical models and instrumentation data: A challenging case of a reinforced slope in a Brazilian coastal hillside. *Geotechnical Journal*, 138(1):61-84. In Portuguese.
- Latorre, M.R.D.O. & Cardoso, M.R.A. (2001). Analysis of time series in epidemiology. *Brazilian Journal of Epidemiology*, 4(3):145-152. In Portuguese.
- Lazarim, T.P. (2012). Geotechnical characterization and retroanalysis of the rupture of a road slope - BR-101, Santa Catarina. Completion of course work. Department of Civil Engineering. Federal University of Paraná, 69 p. In Portuguese.
- Leite, M.L.; Adacheski, P.A. & Virgens Filho, J.S. (2011). Analysis of the frequency and intensity of rainfall in Ponta Grossa, State of Parana, in the period between 1954 and 2001. *Acta Scientiarum. Technology*, 33(1):57-64. In Portuguese.
- Leung, A.K.; Sun, H.W.; Millis, S.W.; Pappin, J.W.; Ng, C.W.W. & Wong, H.N. (2011). Field monitoring of an unsaturated saprolitic hillslope. *Canadian Geotechnical Journal*, 48(3):339-353.
- Li, A.G.; Yue, Z.Q.; Tham, L.G.; Lee, C.F. & Law, K.T. (2005). Field-monitored variations of soil moisture and matric suction in a saprolite slope. *Canadian Geotechnical Journal*, 42(1):13-26.
- Lim T.T.; Rahardjo H.; Chang M.F. & Fredlund D.G. (1996). Effect of rainfall on matric suctions in a residual soil slope. *Canadian Geotechnical Journal*, 33(4):618-628.
- Marinho, F.A.M. (2005). *Unsaturated Soils: Theoretical, Experimental and Applied Aspects*. Text (Free Teaching), Polytechnic School of the University of São Paulo, 201 p. In Portuguese.
- Massad, F. (2003). *Earthworks: Basic Geotechnical Course*. 1ª ed. Oficina de Textos. São Paulo, 203 p. In Portuguese.
- Montoya, C.A.H. (2013). *Uncertainties, Vulnerability and Risk Assessment Due to Road Slipping*. PhD. Thesis. Department of Civil and Environmental Engineering, University of Brasilia, 250 p. In Portuguese.
- Pretto, J.H.F. (2014). *Stress x Strain Analysis of a Natural Slope. Case Study: Morro do Boi – Balneário Camboriú/SC*. Master's Thesis. Construction Engineering Graduate Program. Federal University of Paraná, 129 p. In Portuguese.
- Rahardjo, H.; Krisnanto, S. & Leong, E.C. (2016). Effectiveness of capillary barrier and vegetative slope covers in maintaining soil suction. *Soils and Rocks*, 39(1):51-69.
- Rahardjo, H.; Leong, E.C. & Rezaur, R.B. (2008). Effect of antecedent rainfall on pore-water pressure distribution characteristics in residual soil slopes under tropical rainfall. *Hydrological Processes*, 22(4):506-523.
- Rahardjo, H.; Leong, E.C. & Rezaur, R.B. (2001). The effect of antecedent rainfall on slope landslides. *Geotechnical and Geological Engineering*, 19(3):371-379.
- Sestrem, L.P. (2012). *Design and Implementation of an Instrumentation Plan to Evaluate the Geotechnical Conditions of a Coastal Slope*. Master's Thesis, Construction Engineering Graduate Program, Federal University of Paraná, 195 p. In Portuguese.
- Sestrem, L.P. & Kormann, A.C.M. (2013). *Implementation of an automated monitoring system for monitoring a coastal road slope*. In: Proc. 8º Brazilian Congress of Highways and Concessions. Santos, São Paulo, 11 p. In Portuguese.
- Sestrem, L.P.; Kormann, A.C.M.; Pretto, J.H.F. & Marinho, F.A.M. (2015). Precipitation influence on the distribution of pore pressure and suction on a coastal hillside. *Soils and Rocks*, 38(1):81-92.
- Silveira, J.F.A. (2006). *Instrumentation and Safety of Earth Dams and Rockfill*. 1ª ed. Oficina de Textos, São Paulo, 413 p. In Portuguese.
- Simeoni, L. & Mongiovì, L. (2007). Inclinometer monitoring of the Castelrotto Landslide in Italy. *Journal of Geotechnical and Geoenvironmental Engineering, ASCE*, 133(6):653-666.
- SOILMOISTURE (2011). *Operation Instructions: Tensiometer*. Soilmoisture Equipment Corp., Santa Barbara, CA, USA. 12 p. Available in: <http://www.soilmoisture.com/PDF%20Files/tensiom.pdf>. Accessed in: 02/05/11.
- Souza, W.M.; Azevedo, P.V. & Araújo, L.E. (2012). Classification of daily precipitation and impacts of rainfall-related disasters in the city of Recife-PE. *Brazilian Journal of Physical Geography*, 5(2):250-268. In Portuguese.
- Tommasi, P.; Boldini, D.; Caldarini, G. & Coli, N. (2013). Influence of infiltration on the periodic re-activation of slow movements in an overconsolidated clay slope. *Canadian Geotechnical Journal*, 50(1):54-67.
- Xavier, T.M.B.S. & Xavier, A.F.S. (1987). Classification and dry or rainy periods and calculation of pluviometric indices for the Northeast Region of Brazil. *Brazilian Journal of Engineering*, 5(2):7-30. In Portuguese.
- Zhan, T.L.T.; Ng, C.W.W. & Fredlund, D.G. (2007). Field study of rainfall infiltration into a grassed unsaturated expansive soil slope. *Canadian Geotechnical Journal*, 44(4):392-408.
- Zuquette, L.V.; Pejon, O.J.; Lima, R.E.; Dantas-Ferreira, M. & Guimarães, V. (2013). A preliminary assessment of the distribution and consequences of natural and some anthropogenic hazards in Brazil. *Soils and Rocks*, 36(1):67-95.

Development of a Cyclic Simple Shear Apparatus

M.B. Corte, L. Festugato, N.C. Consoli

Abstract. Considering the increasing incidence of cyclic loadings on engineering structures and the enhancement of design analysis, soil testing under cyclic conditions has renewed its importance. Laboratory tests are conducted to simulate as near as possible field conditions. Assumed conditions aid on the choice of the tests to be conducted in order to determinate the relevant geotechnical parameters to each situation observed on the field. The simple shear test is highlighted among the typical tests in Geomechanics. This is the only laboratory test capable of submitting the specimen to plane strain conditions under constant volume while allowing the rotation of principal stresses. Such conditions are representative of situations such as the adjacent shear mechanism to the shaft of piles or under offshore platforms. In this sense a simple shear testing apparatus was developed. Contrasting with commercial equipment where confinement is made by means of a rigid membrane, specimens are confined by cell pressure in the developed apparatus. Consolidation can be conducted under isotropic or anisotropic paths and shearing, under monotonic and cyclic conditions (either stress or strain controlled). Validation tests were conducted on the equipment using an well-known material. The results obtained were satisfactory, validating the developed apparatus.

Keywords: cyclic loading, laboratory testing, monotonic loading, simple shear test.

1. Introduction

The direct simple shear apparatus has been successfully employed to characterize static and dynamic soil properties for many years (Duku *et al.*, 2007). This test is often preferred when the continuous rotation of the principal stress directions during shearing is a field condition. In the conventional apparatus, initial stresses can be applied to simulate at-rest field conditions when wire reinforced membranes are used to minimize lateral distortion of specimens (Bjerrum & Landva, 1966). A few of the most common applications of the simple shear testing are the vertical shear wave propagation through a soil column, the mode of shearing to a pile shaft (Randolph & Wroth, 1981) and under an offshore gravity base platform (Andersen *et al.*, 1980). Advantages and limitations of simple shear tests relative to other types of laboratory tests have been described by many authors (*e.g.* Lucks *et al.*, 1972; Saada *et al.*, 1983; Vucetic & Lacasse, 1982; Airey & Wood, 1984; Budhu & Britto, 1987; Boulanger *et al.*, 1993).

Most simple shear apparatuses, in order to impose no lateral distortion, enclose the soil in a rubber-reinforced membrane (Kjellman, 1951, Bjerrum & Landva, 1966). A near K_0 condition is assumed to be obtained in this type of equipment. Differently, recent devices, such as the University of Western Australia (UWA) equipment, enclose specimen in an unreinforced latex membrane inside a pressurized cell (Mao & Fahey, 2003). The vertical and cell pressures are controlled independently. With the equipment software routine, total vertical stress and sample height are kept constant during shearing. In order to achieve

such conditions, the vertical loading ram is locked and the cell pressure varies to keep total vertical stress constant. Once height and volume are constant (undrained tests), average cross-sectional area is likely to remain constant. The UWA equipment is frequently called as simple shear apparatus.

This paper describes the design of a simple shear apparatus, based on the UWA apparatus. The equipment was designed, manufactured and calibrated at the Federal University of Rio Grande do Sul. Tests were carried out using a well-known uniform sand to validate the equipment.

2. Previous Work

Simple shear tests have been used for many engineering and geology purposes, such as the study of mechanical behavior of sands (De Alba *et al.*, 1976, Mao & Fahey, 2003), clays (Chu & Vucetic, 1992, Boulanger *et al.*, 1993) and mine tailings (Wijewickreme *et al.*, 2005, Wijewickreme *et al.*, 2010, Festugato *et al.*, 2013, Festugato *et al.*, 2015), and the modeling of folding and fracture patterns (Price & Torok, 1989). The equipment development started with an apparatus by Kjellman (1951) to overcome some of the shortcomings of the traditional direct shear test, which suffers from non-uniform stress distribution throughout the specimen. Typically, the test consists of a circular specimen, consolidated to a stress level under K_0 conditions.

There are a number of different configurations in which direct simple shear devices were developed (Doherty & Fahey, 2011). Each tries to solve the most difficult problem of the test: to apply normal and shear stresses at the lateral boundaries of the specimen while preventing vertical

Marina Bellaver Corte, D.Sc. Student, Federal University of Rio Grande do Sul, Porto Alegre, RS, Brazil, e-mail: marinabellaver@gmail.com.
Lucas Festugato, D.Sc., Senior Lecturer, Federal University of Rio Grande do Sul, Porto Alegre, RS, Brazil, e-mail: lucas@ufrgs.br.
Nilo Cesar Consoli, Ph.D., Professor, Federal University of Rio Grande do Sul, Porto Alegre, RS, Brazil, e-mail: consoli@ufrgs.br.
Submitted on April 3, 2017; Final Acceptance on November 24, 2017; Discussion open until April 30, 2018.
DOI: 10.28927/SR.403279

and horizontal deformation. During shearing, the different designs try to keep volume and dimensions of the cross-sectional area of the specimen constant (Franke *et al.*, 1979).

Roscoe (1953) resolved the problem by enclosing a square-shaped specimen within rigid metallic walls (Cambridge apparatus). The sidewalls parallel to the directions of the shear deformation are fixed relative to the base, while the walls perpendicular to the deformation are attached to the base by hinges. The movable lid remains parallel to the base during the shear phase as well as during consolidation. Authors as Roscoe & Burland (1967), Ansell & Brown (2008), Peacock & Seed (1968) and Finn *et al.* (1971) have improved aspects of the equipment developed by Roscoe (1953). Once the specimen is enclosed by a sealed rubber membrane, a sand specimen can be fully saturated with water through backpressure, so the pore water pressure can be measured during undrained simple shear tests.

Another configuration of simple shear was developed by the Norwegian Geotechnical Institute (NGI) to study quick clays (Bjerrum & Landva, 1966). In this device, a cylindrical specimen is enclosed by a rubber membrane reinforced by a spiral winding of steel wire. The steel spiral is supposed to prevent any change in the diameter of the specimen during the test, while allowing for vertical strains during consolidation. Undrained shear tests conducted using backpressure to saturate specimens are not possible with this type of equipment. That is because pore water pressure and a sufficiently high backpressure would lead to bulging of the reinforced rubber membrane (Franke *et al.*, 1979). The constant volume of the specimen is obtained by adjusting the vertical load to maintain a constant height. The change in vertical stress is then assumed to correspond to the change in pore water pressure of an equivalent test with pore water pressure measurements. Casagrande (1976), DeAlba *et al.* (1976) and Ansell & Brown (1978) made some adjustments to the equipment.

The aim of all these apparatuses was to apply a simple shear mode of deformation to a soil specimen, but the need for the ends of the specimen to extend during shearing means that complementary shear stresses are not generated on the ends (Boylan & Long, 2009). Because of this, the shear stress is non-uniform across the top and bottom of the specimen, falling to zero at the corners. The resulting unbalancing couple has to be counteracted by an opposite couple generated by a non-uniform distribution of normal stress on the top and bottom of the specimen surface (Airey *et al.*, 1985).

These apparatus devices have been criticized as they only measure the total vertical normal stress and the total horizontal shear stress on the specimen during shearing and give no idea of the uniformity of these stresses and true stress state in the specimen (Perazzolo, 2008). To overcome these shortcomings, researchers (*e.g.* Budhu, 1984, Airey & Wood, 1984) have developed apparatuses, that

surround the test specimen with an array of load cells to measure the complete state of stress around the specimen. Radiographic techniques were used to monitor lead shot embedded in the test specimen to give a measure of the internal strains, the uniformity of strains and allow the development of ruptures to be monitored (Budhu, 1984). Research conducted by Airey & Wood (1984) on kaolin showed that direct simple shear tests in a routine apparatus with only the total horizontal shear stress and total vertical stress measured underestimated the simple shear values measured in an elaborately instrumented apparatus by only 10%. It has been suggested on the basis of experimental results that simple shear tests on clay can be presented with more confidence than those conducted on sand (Airey & Wood, 1984).

Mao & Fahey (2003) presented the simple shear apparatus manufactured in the University of Western Australia (UWA). In this equipment, the sample is enclosed in an unreinforced latex membrane and contained in a pressurized cell, very similar to a triaxial apparatus. The vertical and cell pressures are controlled independently. A feedbacked system allows total vertical stress to be kept constant during shearing phase while maintaining a constant sample height. This is achieved by locking the vertical loading ram, and using the feedback system to vary the cell pressure to keep the total vertical stress constant. As the height and volume are both constant (for undrained tests), the average cross-sectional area is likely to remain constant also.

As a number of different simple shear apparatuses have been developed over the past few decades, Doherty & Fahey (2011) investigated two different aspects of the devices. The different total stress paths followed by devices that impose constant cross-sectional area using a stiff external boundary, and those that use a constant total stress lateral boundary condition were explored. This was done by conducting finite element analysis of a single cubic element. The authors observed that this element might be subjected to perfect simple shear using four different boundary condition types. Each boundary condition type results in the same effective stress path, but different total stress paths and excess pore pressures. However, significant differences in total stress path and excess pore pressures occur among the four boundary condition types.

3. Description of the Apparatus

The simple shear device of the Federal University of Rio Grande do Sul (UFRGS) was designed to confine samples with a membrane through confining pressure. In the developed apparatus, sample height is kept constant during shearing and total vertical stress is constant. The maximum horizontal displacement a sample can achieve during shearing is 25 mm, while in UWA equipment the maximum displacement is 10 mm.

Figure 1 presents the basic definitions of the simple shear apparatus. In Fig. 1, σ_y is the vertical stress, σ_x is the horizontal stress, D is the diameter of the specimen, h represents the height of the specimen, τ_{xy} is the shear stress, ϵ_x is the horizontal strain, ϵ_y is the vertical strain and γ_{xy} is the shear strain.

Shear stress τ refers to the shearing loads in the horizontal direction, while the strain caused by shearing, γ , is the ratio between the horizontal displacement and height of the specimen. The principal stresses of can be determined through Eq. 1 and 2, being dependent on the vertical and horizontal effective stresses, σ'_v and σ'_H .

$$\begin{aligned} \sigma'_v &= CP + q - PP \\ \sigma'_H &= CP - PP \end{aligned} \quad (1)$$

where CP is the confining pressure, PP is the pore pressure and q is the deviator stress.

The principal effective stresses ($\sigma'_1, \sigma'_2, \sigma'_3$) can be obtained from the equation:

$$\begin{aligned} \sigma'_{1,3} &= \frac{\sigma'_v + \sigma'_H}{2} \pm \sqrt{\left(\frac{\sigma'_v - \sigma'_H}{2}\right)^2 + \tau^2} \\ \sigma'_2 &= \sigma'_H \end{aligned} \quad (2)$$

where σ'_v and σ'_H are the effective vertical and horizontal stresses and τ is the shear stress on the horizontal plane (Mao & Fahey, 2003).

q and p' can be obtained from Eq. 3 and 4 respectively.

$$q = \sigma'_1 - \sigma'_3 \quad (3)$$

$$p' = \frac{(\sigma'_1 + \sigma'_2 + \sigma'_3)}{3} \quad (4)$$

The principal requirement of the apparatus design was that all test phases could be controlled and monitored

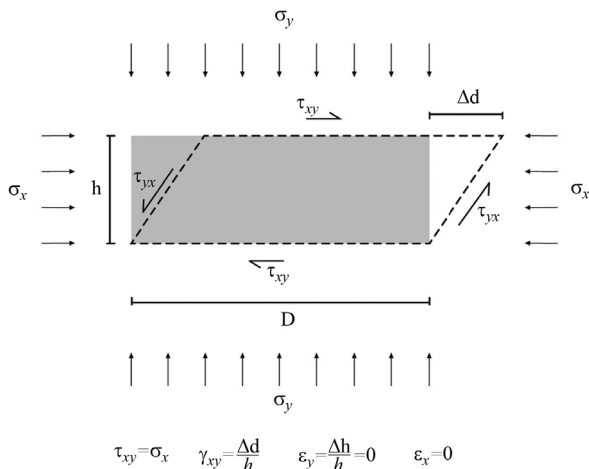


Figure 1 - Basic definitions of the simple shear apparatus.

by software. Also, the instrumentation should be as close as possible to the soil sample.

A schematic view of the apparatus and instrumentation is shown in Fig. 2. The specimen is cylindrical and three different diameter samples can be tested in the developed equipment: 50, 75 and 100 mm (the validation tests performed in this research used 100 mm diameter samples). The sample height is usually not higher than half of the diameter to ensure uniform stress distribution. To confine the sample, a latex membrane is used. The specimen is enclosed both top and bottom by two steel plates. These plates present 8 mm salient edges that contain the porous stone and the sample during shearing. Hoses are connected to each plate to allow drainage. This group of pieces is called shear cell, and its schematic view is shown in Fig. 3. The two plates and the specimen are placed in the equipment and connected to pins linked to the load cell.

The horizontal displacement system, vertical force application system, confining pressure and backpressure system, instrumentations and control system are described in the next sections.

3.1. Horizontal displacement system

The horizontal displacement is applied with a servo motor system. The rotation of the motor is converted into horizontal displacement through a recirculating ball screw. A piston is linked to the ball screw and connected to the load cell, responsible for measuring the shear stress supported by the sample. The load cell is involved by metal pieces connected at the bottom to a slider and a rail system that allows horizontal displacement, and at the top to the shear box, linked to the load cell through a rigid pin. In addition, a linear displacement transducer is connected to this piece assembly to measure horizontal displacements.

3.2. Vertical force application system

The same configuration of servo motor system is used to apply vertical force on the top of specimen. The rotation of the motor is converted into vertical translation through a recirculating ball screw. A piston is linked to the ball screw and connected to a load cell, responsible to measure the vertical force applied to the sample. A linear transducer is fixed to the reaction system used to impose constant height during shearing. Linear guides guide the system up and down movement.

3.3. Confining and back pressures

The apparatus was design to receive air as fluid to apply confining pressure. The air was used as confining fluid to allow all the instrumentations be placed inside the chamber without the need of waterproof instruments, also the large volume of fluid required to fill the chamber contributed to this option.

Compressed air is received by a proportional valve, which sends the pressure requested by the control system to

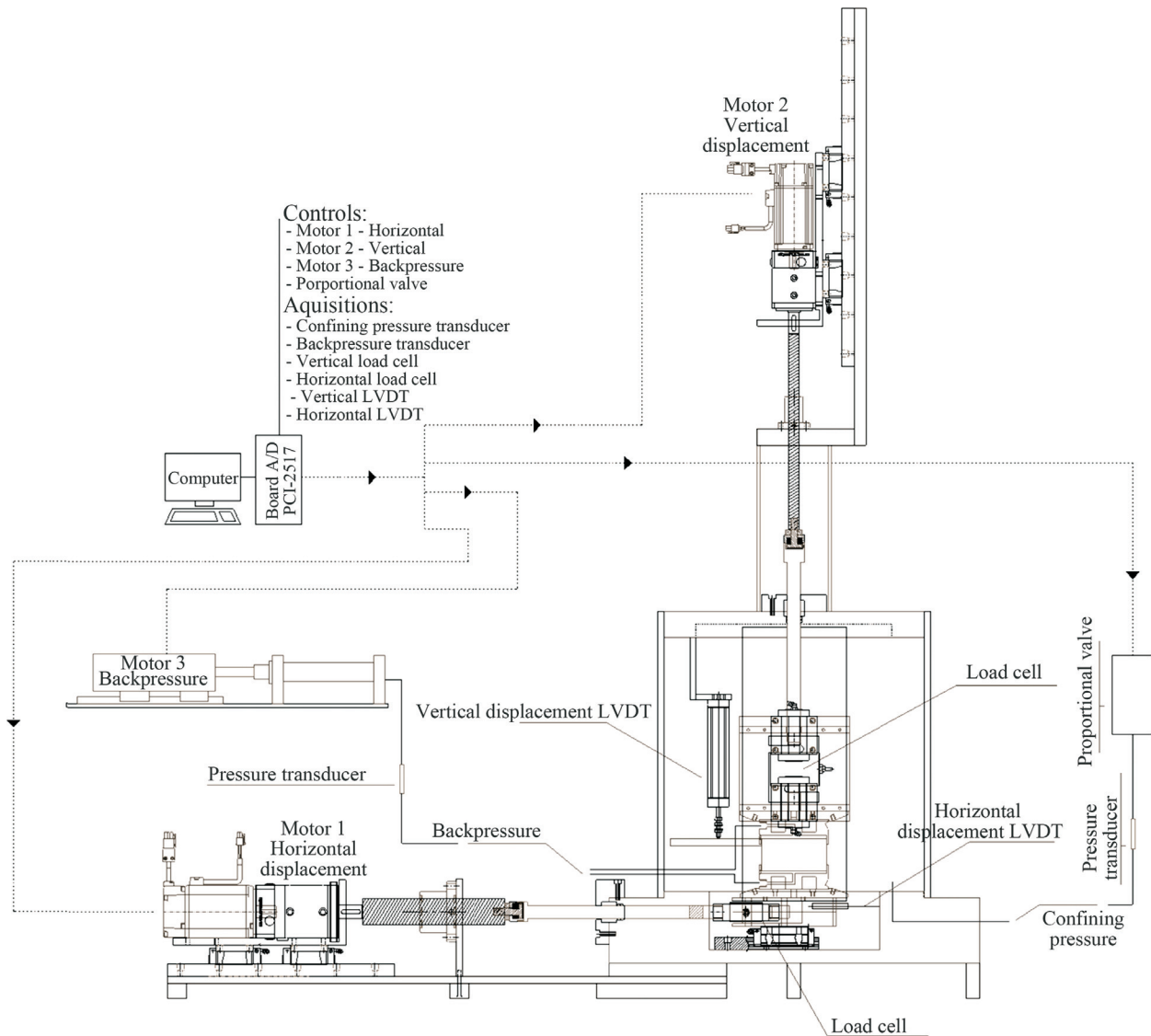


Figure 2 - Schematic view of the apparatus.

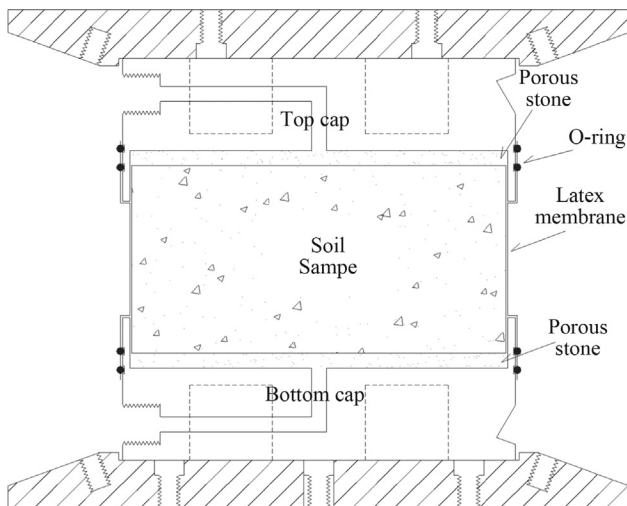


Figure 3 - Schematic view of the shear cell.

the chamber. The pressure imposed on the system is measured and checked by a pressure transducer located at the top of the chamber.

The application of backpressure was based on the consolidation systems used in triaxial tests. Water is pressurized by a piston moving inside a cylinder. The piston is actuated by a ball screw and a servomotor guided by sliders and rails.

This system is responsible for applying backpressure and measuring volume change. A pressure transducer linked to the system controls the backpressure imposed to the specimen. As the volume of the cylinder and the position of the servomotor are known, it is possible to measure any volume change in the specimen. Digital limitations of movement are used to prevent the piston to exceed the limits of the cylinder. The servomotor stops when the digital limitation is triggered.

3.4. Instrumentation and control system

The digital control system for the simple shear device serves two purposes. The first is to provide control signals to the drives that control the three servomotors of the equipment (horizontal displacement, vertical force and backpressure system) and the proportional valve (confining pressure). The second purpose is to acquire data from the load cells, linear transducers and pressure transducers.

A PCI-2517 board was used to control the test and measure the instrumentation. This enables guaranteed sampling frequencies with an internal feedback loop of 1 kHz. Differential analog input channels are used for the two load cells, two LVDTs and two pressure transducers.

The board has four analog output channels with resolution of 16 bits. Accuracy of analog input is 0.031%. The board channels control the three motors and the proportional valve. The proportional valve is from Norgren. It has a total error smaller than 1% and the response time is smaller than 100 ms, maximum pressure is 10 bar. The servomotors used in the apparatus are from Delta Instruments. They have a power of 0.74 kW, torque of 2.39 Nm and maximum rotation of 3000 rpm.

A LabVIEW algorithm was implemented to control and read the instrumentation during tests. The simple shear device operates under strain control or stress control which requires two different shear routines.

In strain controlled tests, the reading of the horizontal LVDT is required to set the direction and way of motion of the servomotor. In stress controlled tests, the servomotor operates according to the measurement of the horizontal load cell. In addition, the confining pressure transducer governs the operation of the pressure valve. Differing from the confining pressure, the backpressure is applied with a servo-controlled motor, which allows the measurement of volume change of sample during tests. Instrumentation is read and recorded every 20 ms.

Before conducting any test with the apparatus, all measuring instruments, such as load cells, pressure transducers and LVDTs were calibrated. The servo-controlled motors were also calibrated, so routine test could be conducted through a linear velocity, instead of an angular one. Figure 4 presents the developed simple shear apparatus.

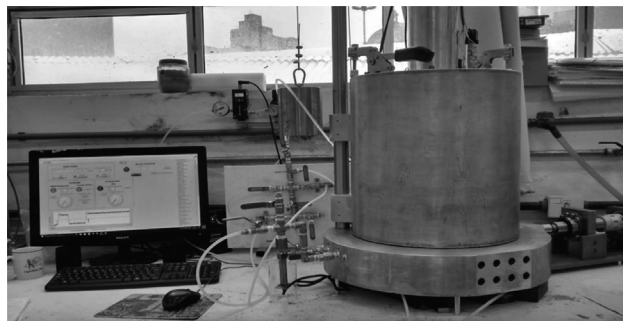


Figure 4 - Simple shear apparatus developed.

4. Test Procedure

Once the size of the specimen is chosen, the corresponding plates are positioned on the equipment. The sample is positioned between the bottom and top caps and the latex membrane is placed. The set is positioned in the apparatus. The vertical piston is positioned in order to touch the set. With the entire fixation finished, the chamber is closed and all the zeros of the test are read.

The phases of percolation (upwards water flow is established through the sample), saturation (incremental steps of backpressure are imposed to achieve saturation) and consolidation (sample is conducted to the effective stress state desired before shearing) are conducted with the according software specific routine. Once the first steps of the test are concluded, the sample is ready to be sheared. The routines of monotonic, strain controlled or stress controlled loading are then opened and conducted.

5. Materials and Methods

5.1. Materials and specimen preparation

Oso rio sand was chosen due to its widely known behavior and extensive investigation in the past 20 years at the Federal University of Rio Grande do Sul (UFRGS, Brazil) using distinct laboratory testing, such as plate load tests (Casagrande, 2001, Consoli *et al.*, 2003a, 2009, Spinelli, 1999), ring shear tests (Casagrande, 2005, Consoli *et al.*, 2003b, 2007), direct shear tests (Marcon, 2005), isotropic compression tests (Consoli *et al.*, 2005) and triaxial compression tests (Consoli *et al.*, 1998, 2002, 2004, Festugato 2008, 2011, Sachetti, 2014).

The sand is classified as uniform fine sand. Quartz corresponds to 99% of the mineralogical composition. Oso rio sand has a specific gravity of solids of 2.62; uniformity coefficient, C_u , of 2.1; curvature coefficient, C_c , 1.0; its effective diameter, D_{10} , is 0.09 mm; mean diameter, D_{50} , 0.16 mm, minimum void ratio, e_{min} , 0.6 and maximum void ratio, e_{max} , 0.9.

Specimens were prepared with a split mold. The sand was manually mixed with 10% of water and compacted in two layers by tamping inside the mold at a relative density of 50%. The size of the specimens was fixed with diameter of 100 mm and 50 mm height. The latex membrane was positioned inside the mold, which has a hollow tube to apply vacuum. A vacuum pump was used to approximate the latex membrane to the mold during sample compaction. O-rings were used for sealing. Once the specimen was prepared, the top cap was positioned and the set was put in the apparatus. Figure 5 presents the method of preparation of specimens and the test procedure.

5.2. Simple shear testing

The main focus of the tests was to validate the equipment. Thus, tests were carried out with monotonic and cyclic loading. Specimens were tested with relative density of



Figure 5 - Specimen preparation and test procedure: (a) insertion of saturated porous stone on top and bottom cap; (b) placing of saturated filter paper; (c) preparation of latex membrane inside split mold; (d) vacuum application; (e) compaction of soil specimen; (f) finalization of specimen preparation and cleaning of the membrane surface; (g) insertion of the top cap; (h) insertion of specimen on the simple shear apparatus; (i) specimen after shearing.

50%. The initial effective stresses were 50, 100 and 150 kPa for monotonic loading and 100 kPa for cyclic loading. For all tests the backpressure was 300 kPa and the confining pressure was changed according to the initial effective stress. This range of effective stresses was chosen so that the results observed in this research could be compared against previous works that studied similar levels of effective stresses (Casagrande, 2005, Festugato, 2008, Marcon, 2005). Shearing was performed under undrained conditions. For monotonic tests, the displacement rate of 0.1 mm/s was adopted based on previous work of Festugato *et al.* (2013). Cyclic testing was conducted under strain controlled conditions with initial effective stress of 100 kPa, a shear strain amplitude of $\pm 2.5\%$ and frequency of 0.1 Hz (Festugato *et al.*, 2013). Monotonic simple shear tests were analyzed through shear stress-shear strain, pore pressure variation-shear strain, variation of vertical effective stress-shear strain curves and stress paths. Cyclic simple shear tests were studied through shear stress-shear strain curves; shear stress, shear strain, variation of pore pressure and variation effective vertical against the number of cycles curves, and stress paths. From the curves, strength and stiffness parameters are defined: effective internal friction angle, γ' , and shear modulus, G , respectively.

6. Simple Shear Test Results

In order to demonstrate the performance of the simple shear apparatus, tests were conducted on Osório sand specimens. The obtained results were compared to results of other authors.

6.1. Monotonic test results

The monotonic tests were performed under undrained conditions, with constant displacement speed of 0.1 mm/min, equivalent to a shear strain rate constant of approximately 0.2%/min.

Figure 6 presents results of the monotonic test at the initial effective vertical stress of 50, 100 and 150 kPa. The sandy matrix under undrained simple shear conditions presents slightly pronounced strength peak, followed by a shear stress reduction associated with the increase of pore pressure (Fig. 7).

The shear stress rises up to a level around 50 kPa falling to about 40 kPa until 10% strain for the specimen tested with an initial vertical effective stress of 50 kPa. After this fall, the sand specimen regains strength.

The specimen tested with 100 kPa initial vertical effective stress exhibited similar behavior to the 50 kPa test. Under undrained monotonic simple shear conditions, the

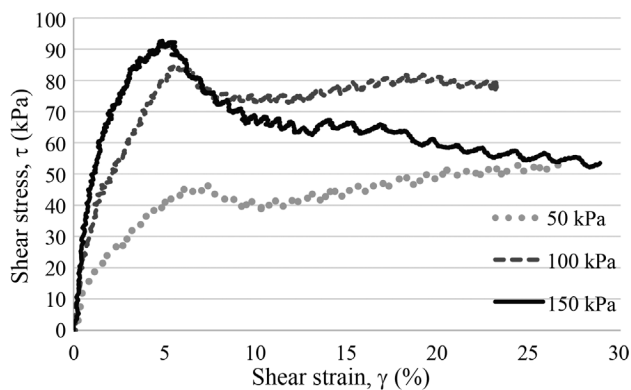


Figure 6 - Shear stress vs. shear strain for $\sigma'_v = 50, 100$ and 150 kPa.

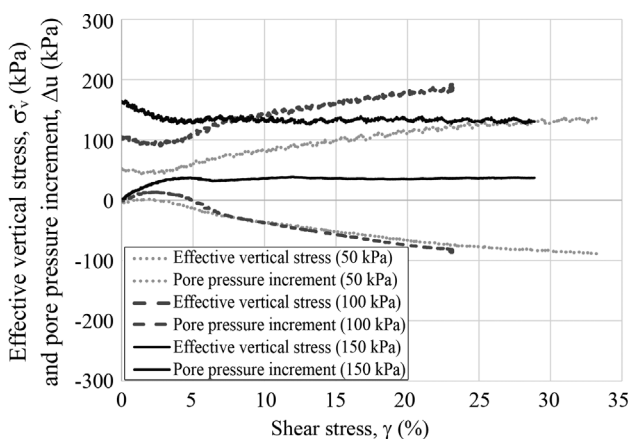


Figure 7 - Effective vertical stress and pore pressure increment vs. shear strain for $\sigma'_v = 50, 100$ and 150 kPa.

sandy soil presented a slightly pronounced strength peak. The shear stress increased up to a level of 85 kPa falling to about 80 kPa at 22% strain. Analogous behavior was observed for 150 kPa initial effective vertical stress.

The variation of pore pressure and effective vertical stress is presented in Fig. 7. For the test conducted with initial effective vertical stress of 50 kPa, the variation of pore pressure increases to around 7 kPa at 3% strain. After that, the pore pressure increment decreases until the end of the test when it comes to -90 kPa. In response to pore pressure variation, to guarantee plane strain conditions with constant volume, effective vertical stress initially at 50 kPa is reduced to 43 kPa at 3% strain. It then undergoes a gradual increase, reaching 140 kPa at a strain of 33%.

In the test of 100 kPa initial effective vertical stress, the pore pressure increment increased up to 15 kPa, reducing afterwards to -90 kPa upon reaching the deformation 20% and continued to reduce until the end of the test. In response to increasing pore pressure, to guarantee conditions of plane strain with constant volume, the effective vertical stress initially at 100 kPa reduced to 85 kPa, reaching afterwards 190 kPa at 20% strain.

With an initial effective stress of 150 kPa, pore pressure increases to a value of 36 kPa and remains constant until the end of the test. Effective vertical stress reduces to 114 kPa in response.

In Fig. 8 the results are presented as p' vs. q . Results show the same behaviors for all tests until the maximum value of q is reached in each test.

The ratio between shear stress and effective vertical stress vs. shear strain is presented in Fig. 9. It was observed the expected behavior. For all monotonic tests, as strength of cohesionless materials is essentially derived from friction, shear stress normalized by the vertical effective stress is shown to be similar.

6.2. Cyclic test results

Cyclic simple shear tests were conducted with the initial effective vertical stress of 100 kPa. Due to a problem in data acquisition, the first readings were not recorded by the software. The data obtained starts for Test 1 at vertical effective stress of 65 kPa and for Test 2 of 85 kPa. Cyclic loading was performed under strain controlled conditions. The frequency was 0.1 Hz and the shear strain amplitude was $\pm 2.5\%$.

Figure 10 shows the shear stress-effective vertical stress curves obtained for the two cyclic tests. Initial load

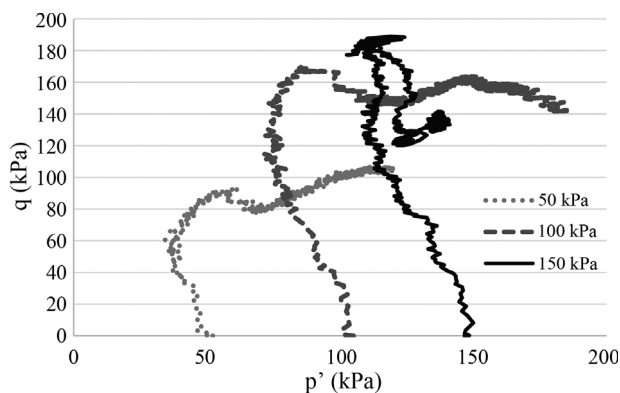


Figure 8 - p' vs. q for $\sigma'_v = 50, 100$ and 150 kPa.

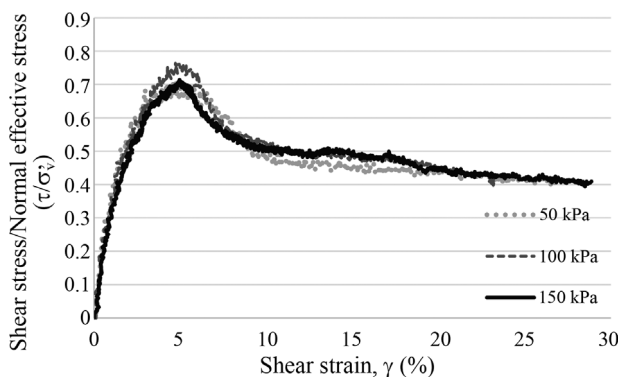


Figure 9 - Shear stress/Normal effective stress vs. shear strain for $\sigma'_v = 50, 100$ and 150 kPa.

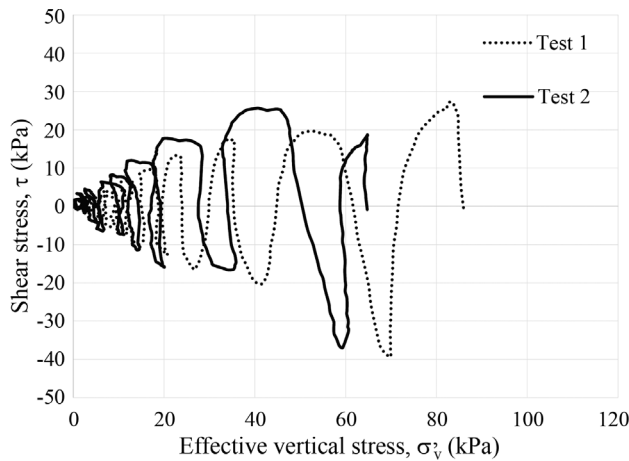


Figure 10 - Shear-stress for cyclic tests, $\sigma'_v = 100$ kPa.

cycles present higher values of strength. With increasing number of cycles, strength decreases with the reduction of effective vertical stress. The decrease of the effective vertical stress during the test can be seen in Fig. 11. This reduction is quite pronounced during the test. This decrease is a response to the pore pressure variation. It is observed the increase in pore pressure increment with increasing cycles, resulting in reduction of the effective vertical stress. Although the pore pressure during cyclic test has presented distinct behavior between Test 1 and Test 2, both tests resulted in the same strength envelope (Fig. 12).

6.3. Comparison of results

The studied sand behavior was analyzed through testing at different initial effective vertical stresses. For monotonic tests, initial effective vertical stress were carried with 50, 100 and 150 kPa. Cyclic tests were conducted with 100 kPa initial effective vertical stress. Figure 12 gathers the shear stress-shear strain curves of the three monotonic tests and the cyclic tests. The strength peaks for monotonic tests are observed at shear strains varying from 5 to 7%. After these peaks, the strength falls. Such behavior is expected

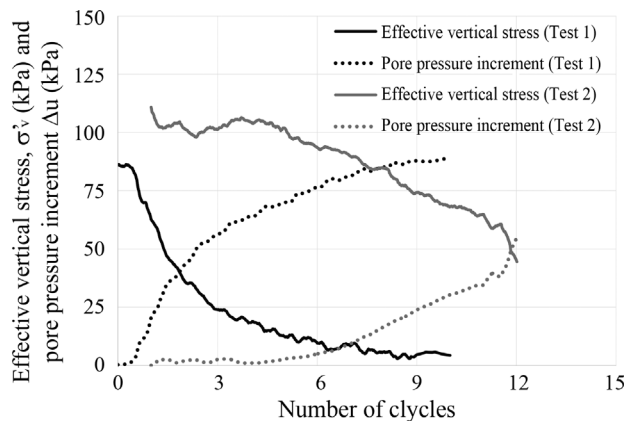


Figure 11 - Variation of initial effective stress, $\sigma'_v = 100$ kPa.

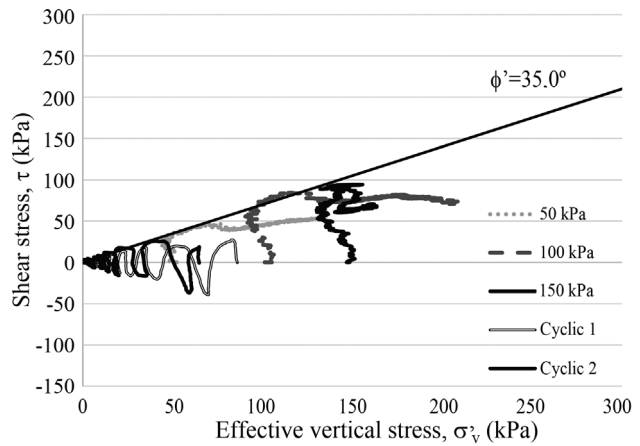


Figure 12 - Strength envelope for cyclic and monotonic tests.

for medium dense sands (Atkinson, 1993, Wood, 1990, Lambe & Whitman, 1979). In the initial cycles of testing, it is verified that the stress path of cyclic tests did not reach the failure envelope. After the third cycle, the stress path reaches the failure envelope. The test was conducted until the effective vertical stress was reduced to zero for both tests.

To analyze the strength parameter, a straight line was fitted to the points of maximum shear stress. The internal friction angle of 35° was obtained and the cohesive intercept was zero.

The shear modulus (G) variation with shear strain is presented in Fig. 13. It can be observed that the three analyzed stresses had very similar shear modulus variation trend. As shear strain evolves the shear modulus degrades. Atkinson & Sallfors (1991) and Mair (1993) observed also a stiffness degradation for a wide range of shear strain.

6.4. Validation of the apparatus

In order to validate the developed apparatus, the strength parameters derived from the testing of this study were compared against literature results (Table 1). It was found compatibility of the results obtained for the Osório sand with previous studies on this same material. Four dis-

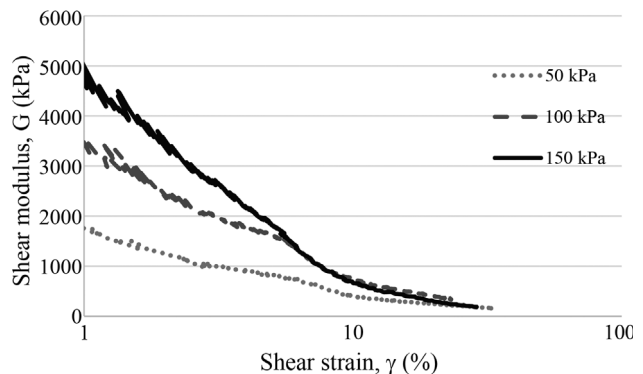


Figure 13 - Variation of modulus (G) with shear stress.

Table 1 - Tests analyzed to compare the strength parameters.

Reference	Test	Dr (%)	e (%)	σ'_v (kPa)	ϕ' (°)
Casagrande (2005)	Triaxial	50	0.75	20 100 200 e 400	33.5
Festugato (2008)	Triaxial	50	0.75	50 100 e 200	37.0
Marcon (2005)	Triaxial	67	0.71	50 100 e 200	35.9
Marcon (2005)	Direct shear	67	0.71	50 100 e 200	34.9
This study	Simple Shear	50	0.75	50 100 e 150	35.0

tinct researches were evaluated. Three of these performed triaxial tests (Casagrande, 2005, Festugato, 2008, Marcon, 2005) and one of them carried out direct shear tests (Marcon, 2005).

Drained triaxial tests conducted by Marcon (2005) found the friction angle was 35.9°. The mean void ratio in the study was 0.71 with relative density of 67% and the initial confining stresses were 50, 100 and 200 kPa. The author also conducted direct shear tests under normal stresses of 50, 100 and 200 kPa, obtaining a friction angle of 34.9°.

Casagrande (2005) examined the behavior of Osório sand with relative density of 50% carrying out consolidated drained triaxial tests. The author used confining pressures of 20, 100, 200 and 400 kPa and obtained a friction angle of 33.5°.

Festugato (2008) carried out drained triaxial tests with Osorio sand (at relative density of 50%) under the confining pressures of 50, 100 and 200 kPa. The effective friction angle was of 37.0°.

Such testing results are presented in Table 1 along with the current study data.

Through the results comparison, it can be seen that the effective internal friction angle obtained through the simple shear equipment is consistent with the reference values found in the literature. There was a slight variation of the values, which can be explained by the different stress paths performed.

7. Conclusions

A simple shear apparatus has been developed to test soil samples. The apparatus uses internal monitoring instruments. Shear stress can be applied considering monotonic or cyclic loading. Cyclic loading can be conducted under strain or stress controlled conditions.

The results of the simple shear tests presented in this paper indicate that the equipment has consistent and adequate quality results. When results of the simple shear tests are compared against results on this same Osorio sand from literature, values are comparable. Unlike usual triaxial tests, the simple shear test presents the advantage of allowing the simulation of complete rotation of the stress state by imposing a plane strain condition.

Despite the limited number of performed tests, the observed results were consistent and presented good agreement. A sound indication of that is the same strength enve-

lope limiting all stress paths. The results presented in Table 1, show very low variety from the internal friction angle obtained on the simple shear. From literature, minimum value found was 33.5° and maximum was 37°, the average was 35.3°. Simple shear tests performed obtained a strength parameter of 35°. The shear strength parameter ϕ' obtained in triaxial tests showed minimum variations compared with the value found with the simple shear apparatus. When compared to the direct shear test, the internal friction angle obtained through the simple shear tests varied very little.

It was observed that the behavior of the proportional valve, with an associated pressure transducer, showed optimum performance, maintaining the confining pressure with little variation. The behavior of the servomotor assembly and the associated pressure transducer was suitable for the requirements. Pressures were kept stable throughout the tests without leaks.

Load cells and displacement transducers showed expected performance. Small oscillations could be found during the analysis of the results, due to electromagnetic induction created by the drivers of the engines. These oscillations did not affect the results. The calibration of the engines was adequate and their behavior was satisfactory to perform simple shear tests.

The preparation of specimens, assembly and completion of simple shear tests showed no major difficulties. The developed equipment allowed the evaluation of soil behavior when subjected to cyclic loading. All analyzes obtained in this type of device were made in effective shear stresses.

Due to the reasons cited above, the equipment developed was considered satisfactory for the execution of simple shear tests. New researches will be developed using this same equipment.

Acknowledgments

The authors express their thankfulness to the Brazilian Research Council (CNPq/MCT) and CAPES/MEC for their financial support.

References

- Airey, D.W. Budhu, M. & Wood, D.M. (1985). Some aspects of the behavior of soils in simple shear. Proc. 11th Int. Conf. on Soil Mech. and Found. Engn., ISSMFE, San Francisco, v. 2, p. 185-213.

- Airey, D.W. & Wood, D.M. (1984). Discussion on specimen size effect in simple shear test. *Journal of Geotechnical Engineering*, 111(2):439-442.
- Andersen, K.H.; Pool, J.H.; Brown, S.F. & Rosenbrand, W.F. (1980). Cyclic and static laboratory tests on Drammen clay. *Journal of Geotechnical Engineering (ASCE)*, 106(5):499-529.
- Ansell, P. & Brown, S.F. (1978). A cyclic simple shear apparatus for dry granular materials. *Geotechnical Testing Journal*, 1(2):82-92.
- Atkinson, J. (1993). *An Introduction to the Mechanics of Soils and Foundations*. McGraw-Hill Book Co, New York, 337 p.
- Atkinson, J.H. & Sallfors, G. (1991) Experimental determination of soil properties. In: *Proceedings of the 10th ECSMFE*, Florence, v. 3, p. 915-956.
- Bjerrum, L. & Landva, A. (1966). Direct simple shear tests on a Norwegian quick clay. *Géotechnique*, 16(1):1-20.
- Boulanger, R.W.; Chan, C.K.; Seed, R.B. & Sousa, J. (1993). A low-compliance bi-directional cyclic simple shear apparatus. *Geotechnical Testing Journal (ASTM)*, 16(1):36-45.
- Boyland, N. & Long, M. (2009). Development of a direct simple shear apparatus for peat soils. *Geotechnical Testing Journal*, 32(2):126-138.
- Budhu, M. (1984). Nonuniformities imposed by simple shear apparatus. *Canadian Geotechnical Journal*, 20(1):125-137.
- Budhu, M. & Britto, A. (1987). Numerical analysis of soils in simple shear devices. *Soils and Foundations*, 27(2):31-41.
- Casagrande, A. (1976). *Liquefaction and Cyclic Deformation of Sands - A Critical Review*. Harvard Soil Mechanics Series, Harvard University, Cambridge, 88p.
- Casagrande, M.D.T. (2005). *Fiber Reinforced Soils Behavior Under Large Strain*. PhD Thesis, Civil Engineering Post-Graduate Program, Federal University of Rio Grande do Sul, Porto Alegre, 217 p (in Portuguese).
- Casagrande, M.D.T. (2001). *Behaviour Study of Fiber Reinforced Soil to be Used on Shallow Foundations*. Dissertation, Civil Engineering Post-Graduate Program, Federal University of Rio Grande do Sul, Porto Alegre, 95p (in Portuguese).
- Chu, H.H. & Vucetic, M. (1992). Settlement of compacted clay in a cyclic direct simple shear device. *Geotechnical Testing Journal*, 15(4):371-379.
- Consoli, N.C.; Montardo, J.; Prietto, P.D.M. & Pasa, G. (2002). Engineering behavior of a sand reinforced with plastic waste. *J. Geotech. Geoenviron. Engng, ASCE*, 128(6):462-472.
- Consoli, N.C.; Vendruscolo, M.A. & Prietto, P.D.M. (2003a). Behavior of plate load tests on soil layers improved with cement and fiber. *J. Geotech. Geoenviron. Engng, ASCE*, 129(1):96-101.
- Consoli, N.C.; Heineck, K.S. & Casagrande, M.D.T. (2003b). Large strain behaviour of polypropylene fiber-reinforced sandy soil. *Proc. 12th Pan-Am. Conf. Soil Mech. Geotech. Engng, Boston, USA, v. 2*, p. 2201-2206.
- Consoli, N.C.; Montardo, J.; Donato, M. & Prietto, P.D.M. (2004). Effect of material properties on the behavior of sand - Cement-fibre composites. *Ground Improvement, ISSMGE 8(2):77-90*.
- Consoli, N.C.; Casagrande, M.D.T. & Coop, M.R. (2005). Effect of fiber reinforcement on the isotropic compression behavior of a sand. *J. Geotech. Geoenviron. Engng, ASCE 131(11):1434-1436*.
- Consoli, N. C.; Casagrande, M. D. T.; Thomé, A.; Dalla Rosa, F. & Fahey, M. (2009). Effect of relative density on plate tests on fibre-reinforced sand. *Géotechnique*, 59(5):471-476.
- Consoli, N.C.; Prietto, P.D.M. & Ulbrich, L.A. (1998). Influence of fiber and cement addition on behavior of sandy soil. *J. Geotech. Geoenviron. Engng, (ASCE) 124(12):1211-1214*.
- Consoli, N.C.; Casagrande, M.D.T. & Coop, M.R. (2007). Performance of a fibre-reinforced sand under large shear strains. *Géotechnique*, 9(57):751-756.
- De Alba, P.; Chan, C.K. & Seed, H.B. (1976). Sand liquefaction in large scale simple shear tests. *Journal of Geotechnical Engineering, ASCE*, 102(9):909-927.
- Doherty, J.P. & Fahey, M. (2011). A three-dimensional finite element study of the direct simple shear test. *Proceedings. 2nd Int. Symp. on Frontiers in Offshore Geotechnics, ISFOG2, Perth, Western Australia, v. 1*, p. 341-346.
- Duku, P.M.; Stewart, J.P.; Whang, D.H. & Venugopal, R. (2007). Digitally controlled simple shear apparatus for dynamic sil testing. *Geotechnical Testing Journal*, 30(5):368-377.
- Festugato, L. (2008). *Behaviour of a soil micro-reinforced with a distinct aspect ratio*. Dissertation, Civil Engineering Post-Graduate Program, Federal University of Rio Grande do Sul, Porto Alegre, 145 (in Portuguese).
- Festugato, L. (2011). *Hidration mechanical behavior and cyclic shear response of fiber reinforced cemented materials*. PhD Thesis, Civil Engineering Post-Graduate Program, Federal University of Rio Grande do Sul, Porto Alegre, 221 p (in Portuguese).
- Festugato, L.; Consoli, N.C. & Fourie, A. (2015). Cyclic shear behavior of fibre-reinforced mine tailings. *Geosynthetics International*, 22(2):196-206.
- Festugato, L.; Fourie, A. & Consoli, N.C. (2013). Cyclic shear response of fibre-reinforced cemented paste back-fill. *Géotechnique Letters*, 3(1):5-12.
- Finn, W.D.; Pickering, D.J. & Bransby, P.L. (1971). Sand liquefaction in triaxial and simple shear tests. *Journal of the Soil Mechanics and Foundations Division, 97(4):639-659*.

- Franke, E.; Kiebusch, M. & Schuppener, B. (1979). A new direct simple shear device. *Geotechnical Testing Journal*, 2(4):190-199.
- Kjellman, W. (1951). Testing the shear strength of clay in Sweden. *Géotechnique*, 2(3):225-232.
- Lambe, T.W. & Whitman, R.V. (1979). *Soil Mechanics*, SI Version. John Wiley & Sons, New York, 553 p.
- Lucks, A.S.; Christian, J.T.; Brandow, G.E. & Hoeg, K. (1972). Stress conditions in NGI simple shear test. *Journal of Soil Mechanics and foundations Division (ASCE)*, 98(1):155-160.
- Mair, R.J. (1993) Unwin memorial lecture 1992. Developments in geotechnical engineering research: application to tunnels and deep excavation. *Proceedings of the ICE - Civil Engineering* 97(1):27-41.
- Mao, X. & Fahey, M. (2003). Behaviour of calcareous soils in undrained cyclic simple shear. *Géotechnique*, 53(8):715-727.
- Marcon, L.P. (2005). Comparative Mechanical Study of Two Osorio Sands. Dissertation, Civil Engineering Post-Graduate Program, Federal University of Rio Grande do Sul, Porto Alegre, 148p (in Portuguese).
- Peacock, W.H. & Seed, H.B. (1968). Sand liquefaction under cyclic loading simple shear conditions. *Journal of the Soil Mechanics and Foundations Division, ASCE*, 94(3):689-708.
- Perazzolo, L. (2008). Apparatus for Simple Shear Tests. PhD Thesis, Programa de Pós-Graduação em Engenharia Civil, Universidade Federal do Rio Grande do Sul, Porto Alegre. 143p (in Portuguese).
- Price G.P. & Torok, P.A. (1989). A new simple shear deformation apparatus for rocks and soil. *Tectonophysics*, 158:291-309.
- Randolph, M.F. & Wroth, C.P. (1981). Application of the failure state in undrained simple shear shaft capacity of driven piles. *Géotechnique*, 31(1):143-157.
- Roscoe, K.H. (1953). An apparatus for the application of simple shear to soil samples. *Proceedings, Third International Conference on Soil Mechanics and Foundation Engineering*. Zurich, Switzerland, p. 186-191.
- Roscoe, K.H. & Burland, J.B. (1967). On the generalized stress-strain behavior of 'wet' clay, in *Engineering Plasticity (J. Heyman and F.A. Leckie, eds.)*, Cambridge University Press, Cambridge, United Kingdom, p. 535-609.
- Saada, A.S.; Fries, G. & Ker, C.C. (1983). Stress induced in short cylinders subject to axial deformation. *Soils and Foundations*, 23(1):114-118.
- Sachetti, A.S. (2014). New Approach for Prediction of Shear Stress on Cemented Sand. Dissertation, Civil Engineering Post-Graduate Program, Federal University of Rio Grande do Sul, Porto Alegre, 138p (in Portuguese).
- Spinelli, L.F. (1999). Behaviour of Shallow Foundations Assented on Cemented Soils. Dissertation, Civil Engineering Post-Graduate Program, Federal University of Rio Grande do Sul, Porto Alegre, 133 p (in Portuguese).
- Vucetic, M. & Lacasse, S. (1982). Specimen size effect in simple shear test. *Journal of Geotechnical Engineering (ASCE)*, 108(12):1567-1585.
- Wijewickreme, D; Sanin, M.V. & Greenaway, R.G. (2005). Cyclic shear response of fine-grained mine tailings. *Canadian Geotechnical Journal*, (42):1408-1421.
- Wijewickreme, D, Khalilim A. & Wilson, G.W. (2010). Mechanical response of highly gap-graded mixtures of waste rock and tailings. Part II: Undrained cyclic and post-cyclic shear response. *Canadian Geotechnical Journal*, 47:566-582.
- Wood, D.M. (1990). *Soil Behaviour and Critical State Soil Mechanics*. Cambridge University Press, Cambridge, 448 p.

The Undrained Strength of Soft Clays Determined from Unconventional and Conventional Tests

S.G.F.P. Lemos, P.J.M. Pires

Abstract. The laboratory fall cone test, considered an unconventional test, was performed to estimate the undrained shear strength of undisturbed samples of Brazilian coastal soft clays with different plasticity index values. The undrained shear strength determined by laboratory fall cone test was compared with the strength determined by conventional field and laboratory tests commonly used to estimate this parameter in cohesive soils: piezocone test, field vane test, unconfined compression test, unconsolidated undrained triaxial compression test and laboratory vane test. The fall cone test undrained shear strength results presented good agreement with the laboratory vane test strength results and reasonable agreement with unconfined compression test strength results. The strength results obtained by laboratory tests were compared with the continuous strength profile estimated from the piezocone test calibrated using the field vane test, and presented good agreement with fall cone test and laboratory vane test strength results. The normalised undrained shear strength was compared with some empirical correlations reported in the literature based on plasticity index, being verified some behaviour similarity.

Keywords: fall cone test, soft clays, undrained shear strength.

1. Introduction

The properties of the soil are crucial to perform a geotechnical engineering design. Estimating geotechnical parameters is complex because of the difficulty in obtaining reliable experimental data and because of the natural variability of the subsoil. In soft cohesive soils, the determination of these parameters is considered to be even more complex, as it is necessary to understand not only the soils strength properties but also its deformability properties and hydraulic conductivity. For short-term stability analyses in these soils, the undrained shear strength S_u is the most important design parameter (Shogaki, 2006).

Many factors affect the shear strength of clays, such as the types of minerals, humidity, stress history, draining during shear, load rate and soil structure, and it is not justifiable to attempt to attribute a unique shear-strength value to any given clay (Sridharan *et al.*, 1971). Moreover, according to Lunne *et al.* (1997b), there is no unique value for S_u *in situ*; this value depends on the mode of rupture, the anisotropy of the soil, the deformation rate and the stress history.

The standard tests to determine the shear strength of soils are typically classified as either laboratory or field tests. Field tests generally supply measurements of the soil strength that can be acquired more rapidly and in greater quantity than the measurements afforded by laboratory tests. However, they provide less precise measurements and, in some cases, are based on empirical correlations (Alshibli *et al.*, 2011).

The conventional tests to determine S_u in the laboratory are unconfined compression test (UCT), unconsolidated undrained triaxial compression test (UUT) and laboratory vane test (LVT), and *in situ* are piezocone test (CPTU), field vane test (FVT) and pressuremeter test (Kempfert & Gebreselassie, 2010). S_u depends on the testing method, among other factors, thus to understand the relations between the strengths determined by each test and the reliability of these determinations is important when S_u is a relevant parameter (Watabe & Tsuchida, 2001).

The fall cone test (FCT), considered unconventional test in many countries, was developed between 1914 and 1922 by the Geotechnical Commission of the Swedish State Railways and, compared with other test methods, it is considered to be a very simple method, which has led to its extensive use in Scandinavia (Hansbo, 1957). Although it was originally developed to estimate the strength of remoulded cohesive soils, it became widely used as a standard method of determining the liquid limit of clays (Koumoto & Houlsby, 2001), having already been included in the British, Swedish, Canadian and Japanese standards (Claveveau-Mallet *et al.*, 2012; Feng, 2000; Tanaka *et al.*, 2012).

The present study shows the result of five conventional and commonly applied tests for the S_u determination - CPTU, FVT, UCT, UUT and LVT - and compares these results with those of the fall cone test (FCT), also known as the Swedish cone test.

The strength results obtained by laboratory tests were compared with the strength profile obtained from CPTU

Silvia Gomes Fernandes Polido Lemos, Ph.D. Student, Programa de Pós-Graduação em Engenharia Civil, COPPE, Universidade Federal do Rio de Janeiro, Rio de Janeiro, RJ, Brazil. e-mail: polidolemos@gmail.com.

Patricio J.M. Pires, D.Sc., Associate Professor, Departamento de Engenharia Civil, Universidade Federal do Espírito Santo, Vitória, ES, Brazil. e-mail: patricio.pires@gmail.com.

Submitted on September 11, 2016; Final Acceptance on November 24, 2017; Discussion open until April 30, 2018.

DOI: 10.28927/SR.403291

with the cone factors (N_{ki} and $N_{\Delta u}$) calibrated using the FVT, considered a referential test to obtain reliable values of S_u (Schnaid & Odebrecht, 2012). The CPTU was adopted because it supplies a continuous profile of S_u . Also it has a strong theoretical foundation and several well-known and comprehensive publications are available concerning its interpretation (Robertson, 2009).

This study also compares the normalised undrained shear strength results with some empirical correlations reported in the literature based on the plasticity index (I_p).

2. Materials and Methods

2.1. Soil

The investigated site is located in the city of Vila Velha, Espírito Santo State, in the coastal region of Brazil, near to Rio de Janeiro, composed of recent fluvial, fluvial-marine and fluvial-lacustrine sediments. The soft clay deposits in Brazil found all along the coast-

line were originated in the Quaternary period. The local subsoil was formed by cycles of erosion and sedimentation which occurred during periods of regression and transgression of sea level, between the Pleistocene, 123000 years ago, and the Holocene, 5100 years before present (Suguio, 2010).

The investigated deposit is formed of a thick layer of soft clay, situated in an area near to a highway construction site, whose subsoil underwent rupture during the embankment operations. Standard penetration tests (SPT) and piezocone test (CPTU) performed locally indicate that the site (Fig. 1) is composed of a subsurface layer of a very soft organic clay, with water level 0.50 m below the surface, over a layer of very soft marine clay with thickness of 15.0 m, followed by a layer of sand. Fig. 1 also presents the clay layer SPT blow count (N_{value}) of zero values, low values of q_t and f_s , obtained from CPTU, and water content (w_n) values above the liquid limits (w_L) determined by characterization tests in SPT samples.

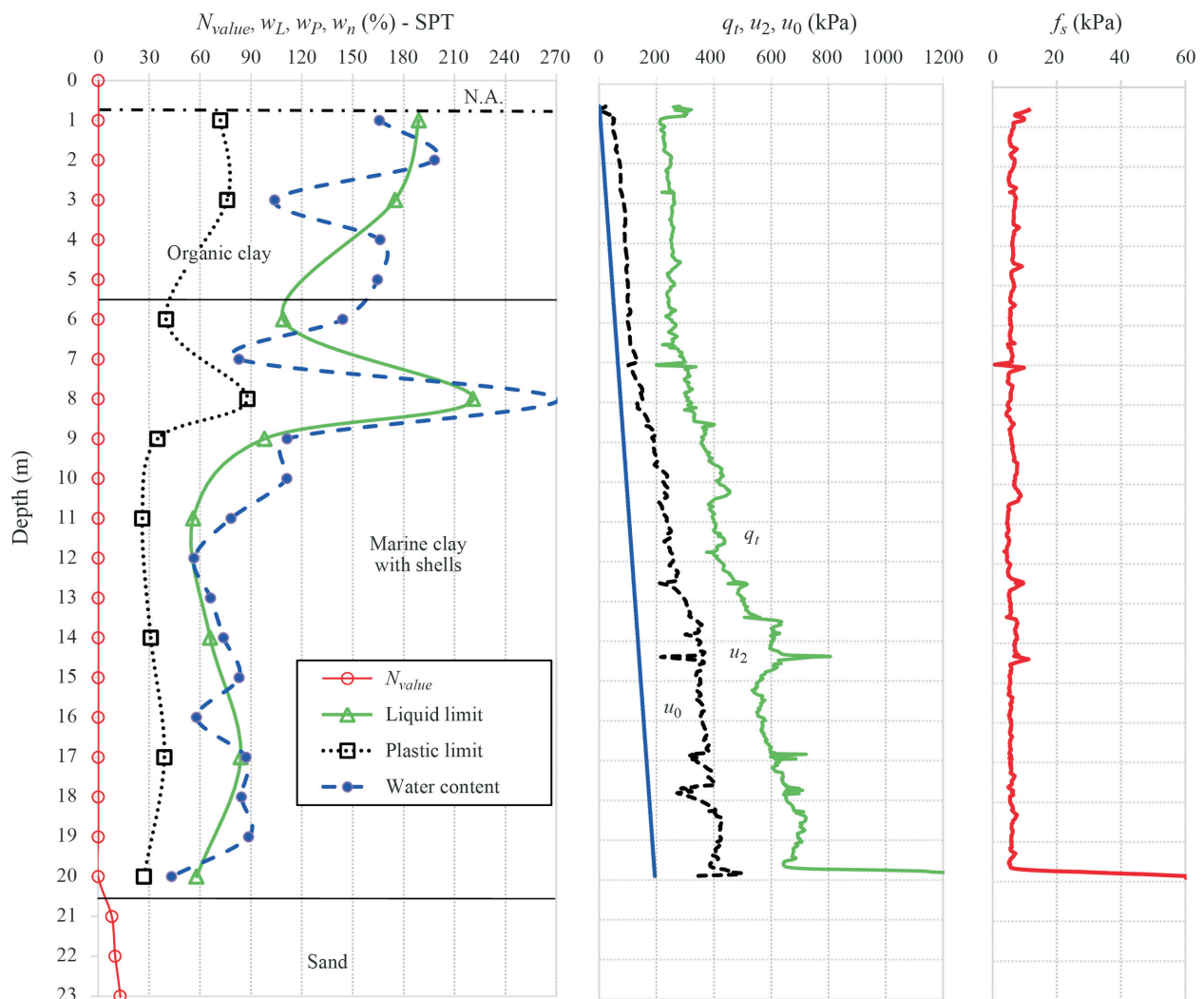


Figure 1 - Typical geotechnical profile.

2.2. Testing program

Piezocone test (CPTU) and field vane tests (FVT) were performed near to the Standard Penetration Test location whose results are indicated in Fig. 1. CPTU was performed between the depths of 0.50 and 20.0 m, with three dissipation tests being performed at depths of 6, 7 and 12 m. At depths between 7.0 and 12.0 were performed the field vane tests (FVT) and also collected six undisturbed samples. The sampling procedures, packaging and transport of the undisturbed samples followed the requirements of the Brazilian standard ABNT (1997).

The laboratory testing program comprised 24 fall cone tests (FCT), 12 vane tests (LVT), 6 unconfined compression tests (UCT) and 6 unconsolidated undrained triaxial tests (UUT).

The undisturbed sampling tubes were segmented as illustrated in Fig. 2, allowing the FCT tests to be performed on the faces of all segments. The FCT and LVT were performed with the soil sample kept in the segmented sampling tube. Subsequently the sample was extracted for moulding the specimens to UUT, UCT and oedometer (OCT) tests.

2.3. Fall cone test (FCT)

The test consists of dropping a standard cone onto the soil under its own weight and after 5 seconds measuring the penetration depth of the cone into the soil. From the penetration depth, the undrained shear strength in both undisturbed (S_u) and remoulded (S_{ur}) conditions can be estimated by the following equation:

$$S_{u(FCT)} = K \frac{W}{d^2} \quad (1)$$

where W is the mass of the cone in grams, d is the penetration depth of the cone in the soil in units of mm, and K is an

empirical constant that depends on the cone tip angle (β) and on the cone roughness (ξ).

Hansbo (1957) estimated the value of K by comparing the FCT results with FVT and LVT, with K equal to 1.0 and 0.30 for cone angles of 30° and 60° , respectively, that are used in the Canadian standard CAN (2006) to estimate S_u and S_{ur} (Claveveau-Mallet *et al.*, 2012). Wood (1985 *apud* 1990) found K mean values of 0.85 and 0.29 for cones angles of 30° and 60° , respectively, by comparing results between FCT and LVT. The European standard ISO (2004) indicates K values of 0.80 to 1.0 for cone angle of 30° and 0.27 for 60° .

Houlsby (1982) has presented a theoretical analysis of the cone test for strengths in the same range as those that have already been determined empirically. This analysis reinforces the use of empirical correlations and the relevance of certain variables in the determination of the constant K , such as the cone tip angle and its roughness.

Koumoto & Houlsby (2001) have analysed the cone penetration mechanism into the soil, introducing the concept of dynamic strength for static results. They compared their theoretical K values with those obtained experimentally by other authors, concluding that there was good agreement in the results obtained for a cone with an angle of 60° , whereas for a 30° cone, the theoretical values were slightly higher than those obtained experimentally.

The fall cone tests were performed on the faces of the soil sample kept in the segmented sampling tube following the recommendations of the European standard ISO (2004). The cone has a weight (W) of 80 g, a cone tip angle of 30° and a mean roughness of $0.4 \mu\text{m}$. Five measurements of the depth (d) were performed on each face of the segmented sample indicated in Fig. 2, keeping at least 25 mm distance between each point and from the edge of the sampler. Measurements higher than 10% of the mean value were ex-

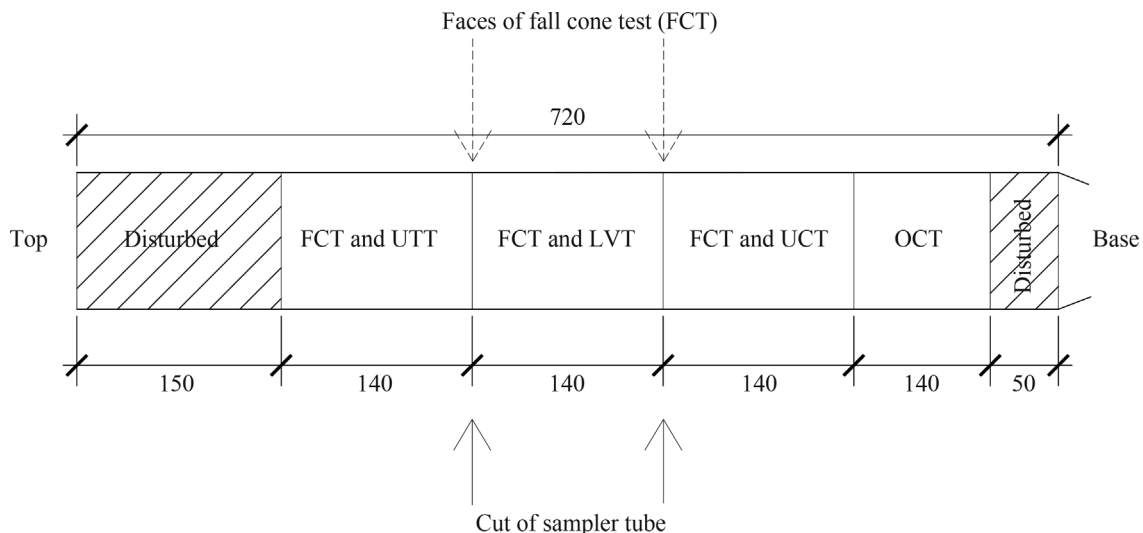


Figure 2 - Undisturbed sampling tubes segmentation for laboratory tests. Values in mm.

cluded from the estimate of S_u and a K value 0.80 was adopted, as recommended by the standard ISO (2004).

2.4. Conventional laboratory tests

2.4.1. Laboratory vane test (LVT)

The procedure to perform the LVT followed the recommendations of the American standard ASTM (2010), including those concerning the calibration of the springs. The vane has a height of 25.4 mm and a diameter of 12.7 mm, corresponding to the 2:1 ratio that is recommended to reduce the effects of the anisotropy on the shear strength. The vane was inserted into the soil sample kept in the segmented sampling tube, with a depth equal to twice its height, for measuring undisturbed strength (S_u). Two tests were performed for each segmented samples indicated in Fig. 2 in opposite faces. The remoulded conditions were created after the peak strength was reached. So the vane was manually rotated by ten complete turns, and the test was then repeated. The S_u and S_{ur} values were estimated based on the following equation, for the height of the vane being twice the diameter:

$$S_{u(LVT)} = 0.86 \frac{T}{\pi D^3} \quad (2)$$

where T is the maximum torque applied by the spring and D is the diameter of the vane in consistent units with strength. The relationship between vane torque T and spring deflection measurement in the test was established through the calibration procedure.

2.4.2. Unconfined compression test (UCT)

The UCT was performed following the recommendations of the American standard ASTM (2006). Specimens were moulded for each segmented sampling tube indicated in Fig. 2, except for sampling from 7.0 m depth that was highly fissured and was discarded. They were prepared with a constant height to diameter ratio of 2 and unconfined compression tests with controlled strain were performed. The $S_{u(UCT)}$ value was calculated as half of the unconfined compression strength (q_u).

2.4.3. Unconsolidated Undrained Triaxial Compression Test (UUT)

The UUT was performed in accordance with the recommendations of the American standard ASTM (2003). Specimens were moulded for each segmented sampling tube indicated in Fig. 2 with a constant height to diameter ratio of 2 and wrapped in a membrane. The specimen was inserted into a triaxial cell for the application of confining pressure followed by the application of an axial load. The $S_{u(UUT)}$ value was calculated as half of the deviator stress (σ_d), calculated without correction for membrane effects.

2.5. Conventional in situ tests

2.5.1. Field vane test (FVT)

The field vane tests were performed in accordance with the Brazilian standard ABNT (1989) using a steel vane retracted in the protective shoe for advancement without pre-drilling and the instrument is equipped with slip coupling. The vane prescribed by the Brazilian standard has a diameter of 65 mm, a height of 130 mm, and a vane thickness of 2 mm. The vane retracted in the protective shoe was inserted into the soil and once the desired depth was reached, it was pushed into the soil 0.50 m from the lower part of the protective shoe. Immediately was applied torque at a speed of $6 \pm 0.6^\circ/\text{min}$ and the torque curve vs. the applied rotation was recorded to determinate S_u . The remoulded conditions were created by rotating the vane rapidly through ten revolutions and the test repeated to determine S_{ur} . The $S_{u(FVT)}$ and $S_{ur(FVT)}$ values were estimated using Eq. 2, where T is the maximum value of torque corrected for rod friction measured by slip coupling.

2.5.2. Piezocone test (CPTU)

The cone test with porewater pressure measurements was performed following the recommendations of the American standard ASTM (2012). The penetrometer has a cross section area of 10 cm² and the filter element located at the base (measurement of u_2). The penetration was performed at a constant speed of 20 ± 5 mm/s, taking automatic measurements of the following parameters: cone resistance (q_c), friction sleeve resistance (f_s) and porewater pressure (u_2). The corrected cone total resistance (q_t) was calculated using the following equation:

$$q_t = q_c + u_2(1 - a_n) \quad (3)$$

where a_n is the ratio between the areas obtained through calibration, which, in this case, was equal to 0.75.

A large number of studies concerning the interpretation of the CPTU to obtain the undrained strength of clays can be found in the literature, representing two different interpretation approaches: one based on theoretical solutions and another based on empirical correlations, generally preferred as reported by Lunne *et al.* (1997b). The empirical approaches estimate S_u by three empirical cone factors, N_{kt} , $N_{\Delta u}$ and N_{ke} , generally used in combination with FVT data being given by the following equations (Danziger & Schnaid, 2000):

$$S_{u(CPTU)} = \frac{(q_t - \sigma_{vo})}{N_{kt(FVT)}} \quad (4)$$

$$S_{u(CPTU)} = \frac{(u_2 - u_0)}{N_{\Delta u(FVT)}} \quad (5)$$

$$S_{u(CPTU)} = \frac{(q_t - u_2)}{N_{ke(FVT)}} \quad (6)$$

In geotechnical engineering practice in Brazil, Eq. 4 is more used (Danziger & Schnaid, 2000; Almeida & Marques, 2014; Coutinho & Schnaid, 2010). In very soft clays, the Eq. 5 has more accuracy in u_2 and u_0 measurements than q_t (Robertson & Cabal, 2015).

3. Results and Discussion

3.1. Field test results

The undisturbed and remoulded strengths obtained through the field vane test (FVT) are presented in Table 1. According to Skempton & Northey (1952) classification, the soil deposit can be considered sensitive.

The N_{kt} and $N_{\Delta u}$ values obtained by Eqs. 4 and 5 and calibrated using the FVT are shown in Fig. 3(a). Typically N_{kt} varies from 10 to 20 (Lunne *et al.*, 1997b; Robertson, 2009). For Brazilian soft clays, Coutinho & Schnaid (2010) reported N_{kt} values between 9 and 18, Schnaid & Odebrecht (2012) between 10 and 20 for normally consolidated or slightly overconsolidated clays and Baroni (2016) between 6 and 18 for soft clays of Rio de Janeiro.

Table 1 - Vane test results.

Depth (m)	$S_{u(FVT)}$ (kPa)	$S_{ur(FVT)}$ (kPa)	$S_t = S_u/S_{ur}$
7.0	2.95	1.72	1.72
8.0	6.60	1.40	4.71
9.0	11.32	1.97	5.75
10.0	14.08	3.02	4.66
11.0	12.34	1.72	7.17
12.0	11.02	1.72	6.41

Although $N_{kt(FVT)}$ values of the studied deposit vary between 17 and 37, values at depths of 7 and 8 m do not have good agreement with the range reported in the literature, so N_{kt} equal to 20 was adopted as representative of the deposit, being slightly higher than Brazilian reported clays. Almeida *et al.* (2010) compared N_{kt} values from several regions of the Brazilian coast and considered the dispersion of the values to be significant, indicating the large variabil-

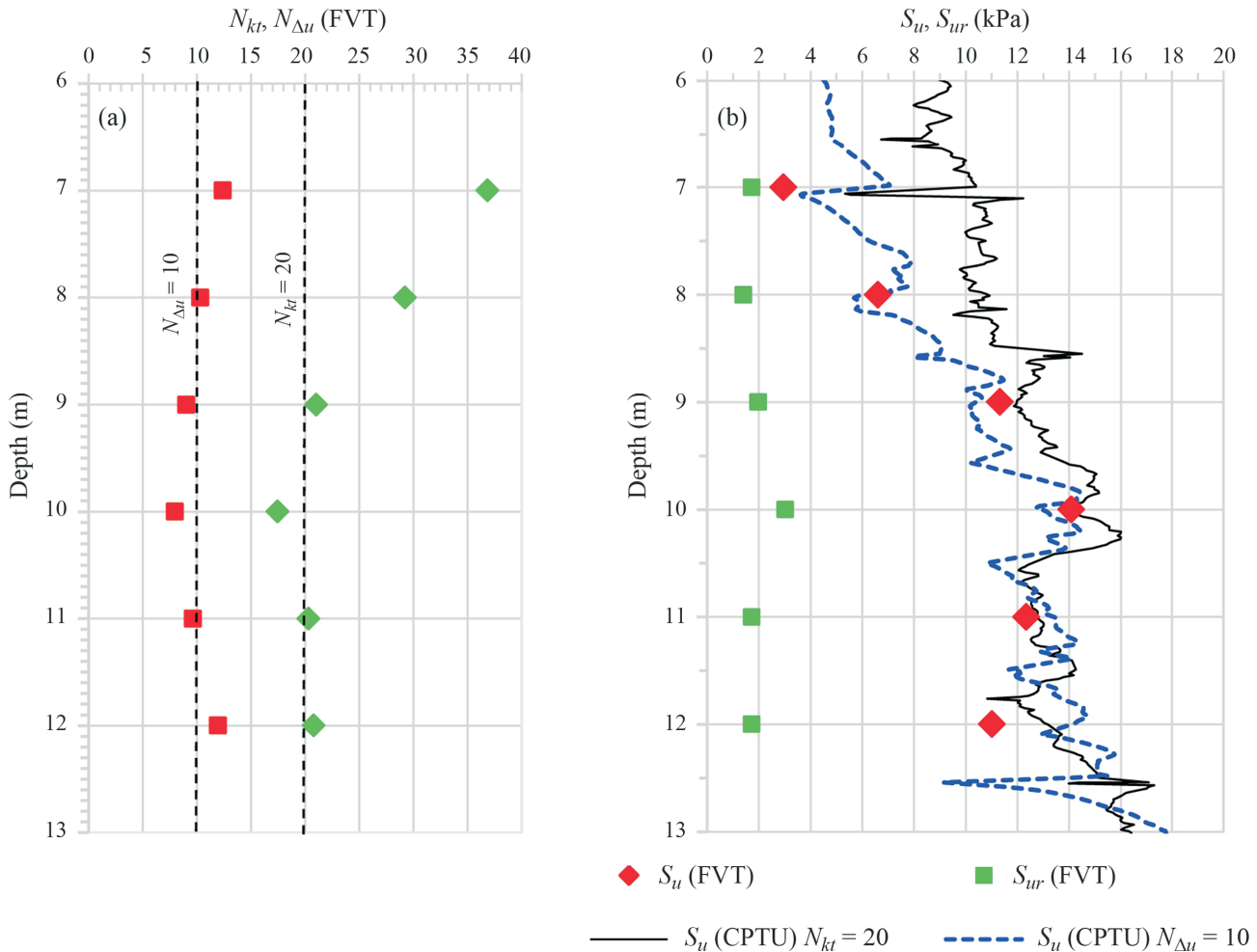


Figure 3 - (a) N_{kt} and $N_{\Delta u}$ values with depth, (b) Strength estimates by FVT and CPTU.

ity of the Brazilian coast soils and the importance of estimating the N_{kt} value for each deposit.

Roberson & Cabal (2015) reported $N_{\Delta u}$ values between 4 and 10. For Brazilian soft clays, Coutinho & Schnaid (2010) reported $N_{\Delta u}$ values between 7 and 9.5 and Coutinho & Bello (2014) between 7.5 and 11 for Recife soft clays. $N_{\Delta u(FVT)}$ equal to 10 was adopted as representative of the deposit, being similar to Brazilian reported clays.

Figure 3(b) shows the undrained shear strength values estimated by *in situ* tests. The S_u estimate from CPTU used the adopted cone factors N_{kt} and $N_{\Delta u}$, respectively, equal to 20 and 10. From 9.0 m depth there was a good agreement between the $S_{u(CPTU)}$ estimates by the two cone factors and between $S_{u(CPTU)}$ and $S_{u(FVT)}$ estimates.

3.2. Laboratory test results

Table 2 shows the quality classification of undisturbed samples based on the ratio between variation in the void ratio (Δe) and initial void ratio (e_o), proposed by Lunne *et al.* (1997a) modified by Coutinho (2007) for Brazilian clays. It is observed that samples numbers 2, 5 and 6 presented poor quality and numbers 3 and 4 presented good to excellent quality.

Overall, the results of tests performed on low-quality samples tend to underestimate S_u . Tanaka (1994, 2008) has observed for LVT tests performed on poor samples that quality of the sample has little influence on the results of S_u , but for UCT tests S_u was underestimated.

A summary of the soil properties obtained from undisturbed samples is presented in Table 3. The natural water content values are closer to the liquid limit and the samples can be subdivided into three groups depending on the I_p value: (1°) I_p greater than 60% and less than 100%, samples 1 and 2; (2°) I_p greater than 100%, samples 3 and 4; and (3°) I_p less than 50%, samples 5 and 6.

Table 3 - Properties of the soil studied.

Sample number	1	2	3	4	5	6
Depth (m)	7.0	8.0	9.0	10.0	11.0	12.0
Specific gravity of soils particles - G_s (kN/m ³)	27.3	27.5	27.6	26.9	27.0	27.2
Bulk unit weight - γ_{nat} (kN/m ³)	-	14.8	13.6	13.1	15.0	15.2
Clay fraction ≤ 0.002 mm (%)	40	46	52	49	38	36
Silt > 0.002 - 0.063 mm (%)	36	30	23	28	16	27
Sand > 0.063 - 2.0 mm (%)	24	24	25	23	46	37
Natural water content - w_n (%)	112	86	139	162	82	76
Liquid limit - w_L (%)	121	95	143	167	77	71
Plastic limit - w_p (%)	34	31	41	45	29	26
Plasticity index - I_p (%)	87	63	102	123	48	44
Void ratio - e_o	-	2.42	3.71	4.25	2.15	2.01
Over consolidation ratio - OCR (by OCT)	-	1.02	1.23	1.23	1.06	-

Table 2 - Quality classification of undisturbed samples by Coutinho (2007).

Sample number	$\Delta e/e_o$	Classification
2	0.10	Poor
3	0.07	Good
4	0.04	Excellent
5	0.10	Poor
6	0.18	Very poor

The X-ray diffraction measurements indicated that kaolinite and muscovite are the predominant clay minerals, being also detected the presence of quartz, illite and montmorillonite.

3.2.1 Strength results and comparison

Figure 4 shows the relationship between undrained shear strengths estimated from FCT and from conventional laboratories tests: LVT, UCT and UUT. For FCT and LVT it can be concluded that there was good agreement between the results, with a tendency for the $S_{u(LVT)}$ values to be slightly lower than those of the $S_{u(FCT)}$, as shown by regression lines ($R^2 = 0.84$). The same behaviour has also been observed by Rajasekaran & Narasimha Rao (2004) on marine clays treated with lime. Those authors concluded that the FCT test is a good alternative for estimating the undrained strength of clays.

The $S_{u(LVT)}/S_{u(FCT)}$ ratio had a mean of 0.92 with standard deviation of 0.17 and variation coefficient of 1.3%.

For FCT and UCT there was reasonable agreement between the S_u results, with a tendency for the $S_{u(UCT)}$ values to be higher than the $S_{u(FCT)}$, as shown by regression lines ($R^2 = 0.62$). The $S_{u(UCT)}/S_{u(FCT)}$ ratio had a mean of 1.14 with standard deviation of 0.34 and variation coefficient of 30%.

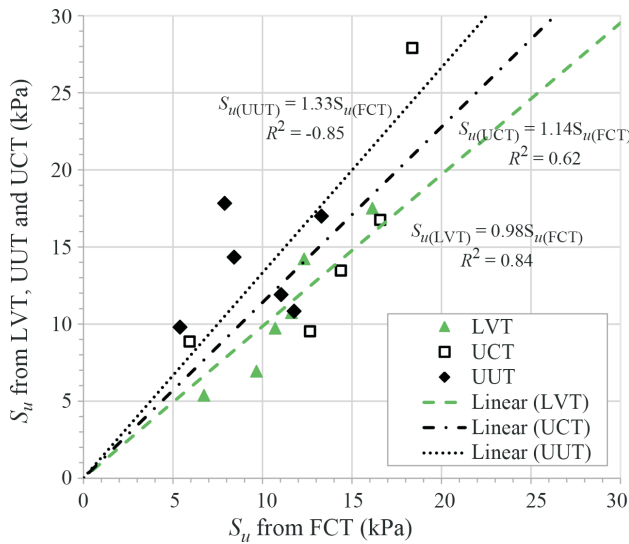


Figure 4 - Correlation between S_u values from FCT and conventional laboratory tests (LVT, UCT and UUT).

Tanaka *et al.* (2012) have compared S_u data estimated by UCT and FCT from four sites that have been extensively investigated in Japan (Atsuma, Takuhofu, Y-Ariake, & H-Osaka). These sites exhibit different characteristics but similar undrained shear strengths, varying between 20 and 80 kPa. In this study, the author recognised a tendency for the $S_{u(UCT)}$ values to be lower than the $S_{u(FCT)}$, except for the Y-Ariake site. It was observed that the differences could not be attributed to the quality of the samples, consistent with the study of Horng *et al.* (2011), which concluded that the effects of disturbances in the samples are similar for UCT and FCT.

Unexpectedly, the UUT results did not demonstrate good agreement with the FCT, as shown by regression lines ($R^2 = -0.85$). And the $S_{u(UUT)}/S_{u(FCT)}$ ratio had a mean of 1.51 with standard deviation of 0.51 and a variation coefficient of 34%.

Figure 5 shows the correlation between undrained shear strengths estimated from FCT and conventional *in situ* tests: FVT and CPTU. For these correlations there was observed larger discrepancy between S_u results and it was not possible to establish an adequate linear regression.

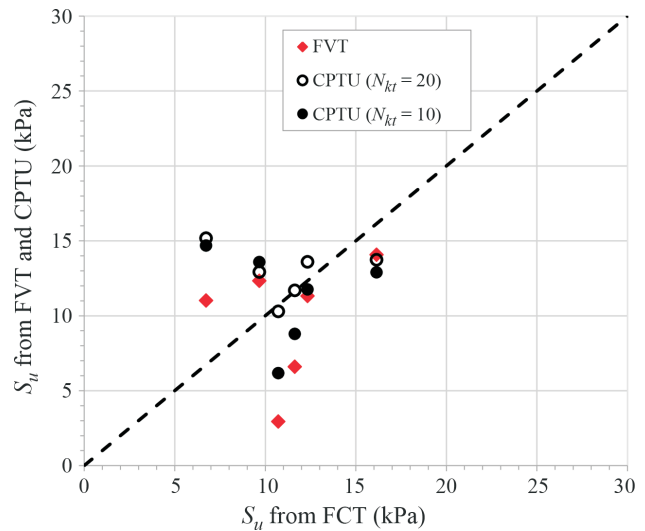


Figure 5 - Correlation between S_u values from FCT and conventional *in situ* tests (FVT and CPTU).

The $S_{u(FVT)}/S_{u(FCT)}$ ratio had a mean of 0.92 with standard deviation of 0.49 and variation coefficient of 53%. Despite the larger discrepancy, it was observed a tendency for the $S_{u(FCT)}$ values to be higher than the $S_{u(FVT)}$ values, similarly to Tanaka *et al.* (2012) results.

The $S_{u(CPTU-Nkt)}/S_{u(FCT)}$ ratio had a mean of 1.25 with standard deviation of 0.52 and variation coefficient of 41%. The $S_{u(CPTU-Nkt)}/S_{u(FCT)}$ ratio had a mean of 1.11 with standard deviation of 0.59 and variation coefficient of 53%.

It is difficult to judge whether variation in soil properties is caused by human factors or by the natural variability in the properties (Tanaka, 2008). The discrepancy observed in Figs. 4 and 5 can be considered to be predominantly attributable to the disturbance of the samples, as their quality was generally classified as poor. However, others important factors were observed in the samples and should be considered, such as the large vertical variability, indicated by liquid limit variations, the presence of shells (Fig. 6a), concrectionary materials (Fig. 6b) and thin layers of sand and mica (Fig. 6c). These factors may have influenced the



Figure 6 - Samples variability: (a) shells, (b) concrectionary material and (c) layers of fine sand and mica.

laboratory test results, particularly the FCT and LVT, and are also an indicative of horizontal variability.

Figure 7 may help to understand the larger discrepancy between S_u results presented in Fig. 5. It is observed that S_u estimated by CPTU ranged between 3.6 kPa to 17.6 kPa with considerable variations at certain depths, such as between 7.0 and 7.2 m. For correlations presented in Fig. 7, the mean value of $S_{u(CPTU)}$ in 1.0 m range was considered, thus it was not possible to verify by this analysis if there was good agreement between the FCT and CPTU results.

Despite the heterogeneity of the deposit and discarding the very discrepant values of $S_{u(UCT)}$ and $S_{u(UUT)}$, it can be visually observed in Fig. 7 that between the depths of 7.0 and 11.0 m there is a good agreement between the laboratory S_u results and $S_{u(CPTU)}$ estimated with N_{kt} cone factor. Between depths of 11.0 and 13.0 m the $S_{u(FCT)}$ and $S_{u(LVT)}$ do not present good agreement with $S_{u(CPTU)}$. These samples presented the lowest plasticity index (mean of 46) and the highest percentage of sand (mean of 42%). Maybe a drained behaviour can explain this greater variation among the S_u results. Larsson *et al.* (1987) observed that $S_{u(FCT)}$ values measured in specimens from greater depths than 10 and 15 m are often too low and the same behaviour occurs in clays of low plasticity and high sensitivity, which also can explain the lower $S_{u(FCT)}$ results between depths of 11.0 and 13.0 m.

3.2.2. Empirical correlations

Attempts to develop simple methods for estimating the undrained shear strength of soils based on physical indices, such as correlations based on plasticity index, have been conducted since the beginning of Soil Mechanics (Kempfert & Gebreselassie, 2010). However, several of the most well-known empirical correlations were established using data from soils obtained in countries of northern Europe and America, where the sediments were strongly influenced by the glaciers of the ice age period (Tanaka, 2000; Tanaka *et al.*, 2001).

Although the correlations developed in a given geological context are not universally applicable and should be

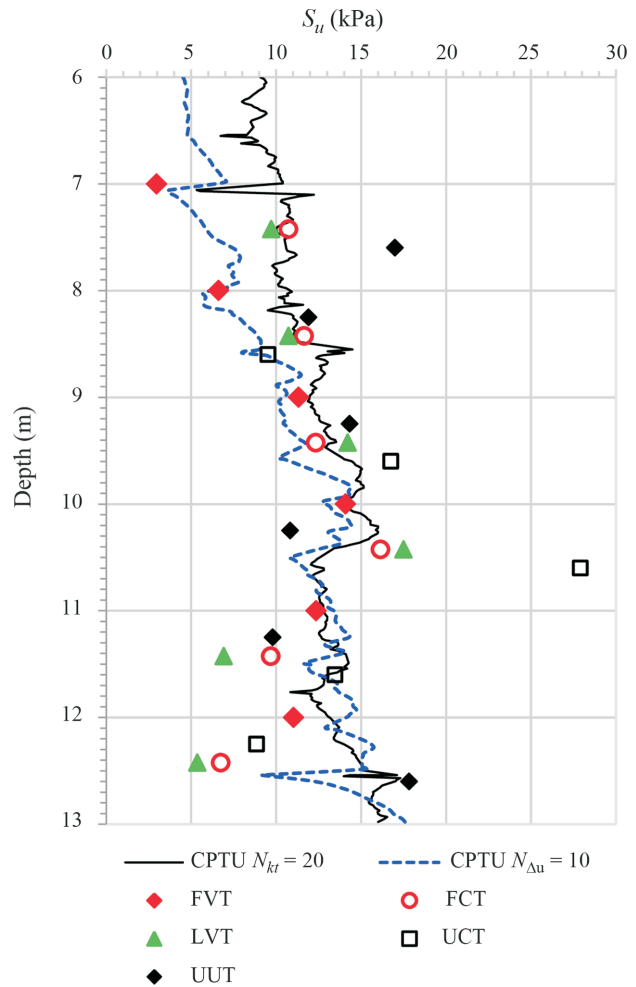


Figure 7 - Undrained shear strength estimated by conventional and unconventional tests.

used with caution, as well as be calibrated locally (Larsson & Ahnberg, 2005; Leroueil *et al.*, 2001), empirical correlations between the undrained shear strength (S_u) and the plasticity index (I_p) can be used to support and complement strength determinations (Larsson *et al.*, 1987). Some of these correlations are presented in Table 4.

Table 4 - Empirical correlations between normalised S_u and I_p (adapted from Kempfert & Gebreselassie, 2010).

Equation	Reference	Applicability
$S_u/\sigma'_{vo} = 0.0037I_p + 0.11$	Skempton (1957)	NC soils, $I_p > 10\%$
$S_u/\sigma'_p = 0.0024I_p + 0.2$	Leroueil <i>et al.</i> (1983)	Clays from eastern Canada, $I_p < 60\%$
$S_u/\sigma'_p = 0.003I_p + 0.14$	Lambe & Whitman (1969)	All clays
$S_u/\sigma'_p = 0.45(I_p/100)^{1/2}$	Bjerrum & Simons (1960)	NC clays
$S_u/\sigma'_p = 0.22$	Mesri (1975)	Soft clays
$S_u/\sigma'_p = 0.0043I_p + 0.129$	Wroth & Houlsby 1985	NC clays

σ'_{vo} : initial effective vertical stress; σ'_p : preconsolidation stress.

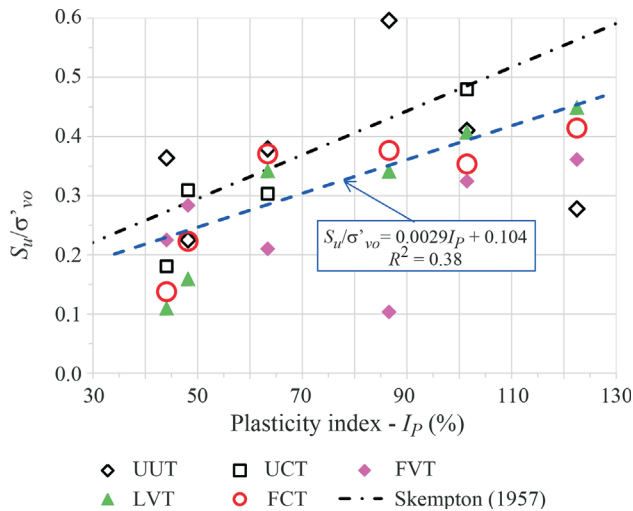


Figure 8 - Relationship between normalised undrained shear strength with effective vertical stress (S_u/σ'_{vo}) and plasticity index (I_p).

Many of these correlations indicate a tendency for S_u/σ'_p or S_u/σ'_{vo} increase with increasing of I_p . Figures 8 and 9 illustrates the relation between S_u/σ'_{vo} and S_u/σ'_p and I_p using the *in situ* test data (FVT) and laboratory test data (FCT, LVT, UUT, UCT) obtained in this study and the empirical correlations presented in Table 4.

Despite the large dispersion, it can be observed in Fig. 8 that exists a tendency for S_u/σ'_{vo} increase with increasing of I_p , as shown by linear correlation ($R^2 = 0.38$), similar to the Skempton linear correlation and being more accentuated for I_p lower than 70%. Baroni (2016) reported for Rio de Janeiro soft clays that there is not a tendency for S_u/σ'_{vo} increase with I_p .

Figure 9 was elaborated with S_u/σ'_p results of samples number 2 to 5 and presents the same behaviour of Fig. 8, a tendency for S_u/σ'_p increase with increasing of I_p and being more accentuated for I_p lower than 70%. The regression line presented the same behaviour of Bjerrum & Simons potential correlation. Similarly, Futai *et al.* (2008) have observed for clay deposits in Rio de Janeiro that the S_u/σ'_p ratio demonstrates a tendency to increase with increasing of I_p , similar behaviour of the Canada clays.

As reported by Tanaka (1994), the S_u/σ'_p ratios determined for various Japanese marine clays ranged between 0.25 and 0.35 and did not exhibit any significant relationship to I_p , being S_u values estimated by FVT and I_p values ranging between 20% and 150%. Chung *et al.* (2007) had also concluded for a specific Japanese marine clay deposit that the S_u/σ'_p ratio did not depend on I_p .

4. Conclusions

In the present study, the undrained shear strength (S_u) results from laboratory fall cone test (FCT) were compared

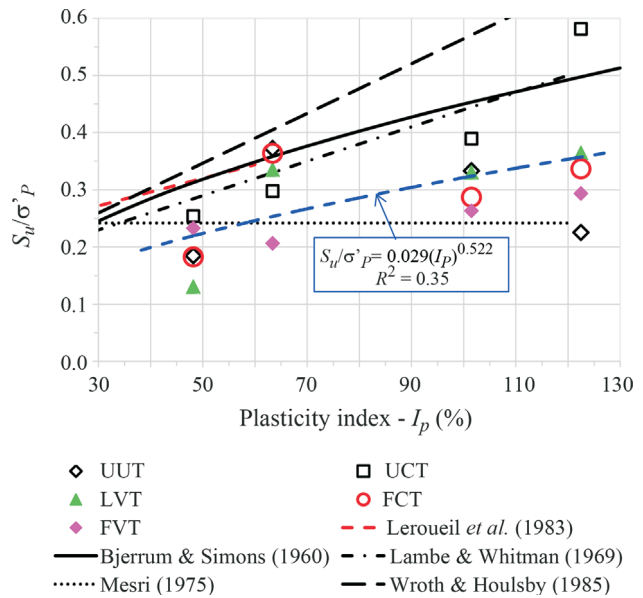


Figure 9 - Relationship between normalised undrained shear strength with preconsolidation stress (S_u/σ'_p) and plasticity index (I_p).

with the S_u results from conventional field and laboratory tests commonly used in geotechnical engineering to estimate this parameter in cohesive soils: CPTU, FVT, UCT, UUT and LVT. The normalised undrained shear strength estimates were compared with some empirical correlations based on plasticity index. The following conclusions result from this study:

- The S_u values determined by FCT presented good agreement with the S_u determined by LVT, with $S_{u(LVT)}/S_{u(FCT)} = 0.98$ obtained by linear regression (coefficient of determination $R^2 = 0.84$).
- For FCT and UCT there was reasonable agreement between the S_u results, with a tendency for the $S_{u(UCT)}$ values to be higher than the $S_{u(FCT)}$. The $S_{u(UCT)}/S_{u(FCT)} = 1.14$ was obtained by linear regression (coefficient of determination $R^2 = 0.62$).
- FCT and UUT did not demonstrate good agreement between the S_u results, with variation coefficient of 34% for the $S_{u(UUT)}/S_{u(FCT)}$ ratio.
- The S_u values determined by FCT did not present good agreement with the S_u determined by FVT, with variation coefficient of 53% for the $S_{u(FVT)}/S_{u(FCT)}$ ratio.
- Despite the considerable variations between $S_{u(CPTU)}$ values estimated with N_{kt} cone factor for certain depth ranges, there was a good agreement with $S_{u(FCT)}$ and $S_{u(LVT)}$ for depths until 11.0 m.
- The difference between S_u values determined through laboratory and *in situ* tests can be assigned to others important factors like the large vertical variability indicated by liquid limit variations and the presence of shells, concrectionary materials and thin layers of sand and mica

that may have influenced the laboratory test results, particularly the FCT and LVT.

- The normalized undrained shear strength data, S_u/σ'_p and S_u/σ'_{vo} , determined using the various test methods presented a tendency to increase with increasing of I_p , similar to some empirical correlations reported in the literature.

As a final contribution of this study, considering the simplicity and flexibility of the fall cone test (FCT) application and the possibility to collect a greater number of data, it would be appropriate to use this method to support and complement other strength determinations.

References

- ABNT (1997). Assessment of Undisturbed Low Consistency Soil Samples from Boreholes – Procedure. NBR 9820, Rio de Janeiro, 5 p. (in Portuguese).
- ABNT (1989). Soil – Field Vane Shear Test – Method of Test. NBR 10905, Rio de Janeiro, 9 p. (in Portuguese).
- Almeida, M.S.S. & Marques, M.E.S. (2014). Embankments on Soft Soils: Design and Performance. 2nd ed. Oficina de Textos, São Paulo, 256 p. (in Portuguese).
- Almeida, M.S.S.; Marques, M.E.S. & Baroni, M. (2010). Geotechnical parameters of very soft clays from CPTu. Proc. 2th International Symposium on Cone Penetration Test, California, USA.
- Alshibli, K.A.; Okeil, A.M.; Alramahi, B. & Zhang, Z. (2011). Reliability analysis of CPT measurements for calculating undrained shear strength. *Geotechnical Testing Journal*, 34(6):1-9.
- ASTM (2003). Standard Test Method for Unconsolidated-Undrained Triaxial Compression Test on Cohesive Soils. D2850-03a. ASTM International, West Conshohocken, Pennsylvania, USA, 6 p.
- ASTM (2006). Standard Test Method for Unconfined Compressive Strength of Cohesive Soil. D2166-06. ASTM International, West Conshohocken, Pennsylvania, USA, 6 p.
- ASTM (2010). Standard Test Method for Laboratory Miniature Vane Shear Test for Saturated Fine-Grained Soil. D4648/D4648M-10. ASTM International, West Conshohocken, Pennsylvania, USA, 7 p.
- ASTM (2012). Standard Test Method for Electronic Friction Cone and Piezocone Penetration Testing of Soils. D5778-12. ASTM International, West Conshohocken, Pennsylvania, USA, 20 p.
- Baroni, M. (2016). Geotechnical Behaviour of Extremely Soft Clays of the Jacarepaguá Lowlands, RJ. PhD Dissertation, COPPE, Federal University of Rio de Janeiro, 292 p. (in Portuguese).
- CAN (2006). Soils – Determination of Undrained Shear Strength and Determination of Sensitivity of Cohesive Soils using the Fall Cone Penetrometer. BNQ 2501-110. Canadian Standards Association and Bureau de Normalisation du Québec, National Standard of Canada, Ottawa, ON, CAN.
- ISO (2004). Geotechnical Investigation and Testing – Laboratory Testing of Soil – Part 6: Fall Cone Test. ISO/TS 17892-6. ISO, Geneva, CHE, 16 p.
- Chung, S.G.; Kim, G.J.; Kim, M.S. & Ryu, C.K. (2007). Undrained shear strength from field vane test on Busan clay. *Marine Georesources and Geotechnology*, 25:167-179.
- Claveveau-Mallet, D.; Duhaime, F. & Chapuis, R.P. (2012). Practical considerations when using the Swedish Fall Cone. *Geotechnical Testing Journal*, 35(4):1-11.
- Coutinho, R.Q. (2007). Characterization and engineering properties of Recife soft clays - Brazil. Proc. 2th International Workshop on Characterization and Engineering Properties of Natural Soils, Tan, Phoon, Hight and Leroueil (eds), Singapore, v. 3, pp. 2049-2100.
- Coutinho, R.Q. & Bello M.I.M.C.V. (2014). Geotechnical characterization of Suape soft clays, Brazil. *Soils and Rocks*, 37(3):257-276.
- Coutinho, R.Q. & Schnaid, F. (2010). CPT Regional Report for South America. Proc. 2th International Symposium on Cone Penetration Test, California, USA, v. 1, p. 313-333.
- Danziger, F.A.B. & Schnaid, F. (2000). Piezocone Tests: Procedures, recommendations and interpretation. Proc. SEFE IV, São Paulo, v. 3, pp. 1-51 (in Portuguese).
- Feng, T.W. (2000). Fall-cone penetration and water content relationship of clays. *Géotechnique*, 50(2):181-187.
- Futai, M.M.; Almeida, M.S.S. & Lacerda, W.A. (2008). Laboratory behavior of Rio de Janeiro soft clays. Part 2: strength and yield. *Soils and Rocks*, 31(2):77-84.
- Hansbo, S. (1957). A New Approach to the Determination of the Shear Strength of Clay by the Fall-Cone Test. Proceedings of Royal Swedish Geotechnical Institute, n. 14, Stockholm.
- Houlsby, G.T. (1982). Theoretical analysis of the fall cone test. *Géotechnique*, 32(2):111-118.
- Hornig, V.; Tanaka, H.; Hirabayachi, H. & Tomita, R. (2011). Sample disturbance effects on undrained shear strengths – Study from Takunoku site, Sapporo. *Soils and Foundations*, 51(2):203-213.
- Kempfert, H. & Gebreselassie, B. (2010). Excavations and Foundations in Soft Soils. Springer-Verlag Berlin Heidelberg r, Netherlands, 576 p.
- Koumoto, T. & Houlsby, G.T. (2001). Theory and practice of the fall cone test. *Géotechnique*, 51(8):701-712.
- Larsson, R. & Ahnberg, H. (2005). On the evaluation of undrained shear strength and preconsolidation pressure from common field tests in clay. *Canadian Geotechnical Journal*, 42:1221-1231.
- Larsson R.; Bergdahl, U. & Eriksson, L. (1987). Evaluation of shear strength in cohesive soils with special reference

- to Swedish practice and experience. *Geotechnical Testing Journal*, 10(3):105-112.
- Leroueil, S.; Demers, D. & Saihi, F. (2001). Considerations on stability of embankments on clay. *Soils and Foundations*, 41(5):117-127.
- Lunne, T.; Berre, T. & Strandvik, S. (1997a). Sample disturbance effects in soft low plastic Norwegian clay. *Proc. of the Conference on Recent Developments in Soil and Pavement Mechanics*, Rio de Janeiro, pp. 81-102.
- Lunne, T.; Robertson, P.K. & Powell, J.J.M. (1997b). *Cone Penetration Testing in Geotechnical Practice*. Taylor & Francis, New York, 352 p.
- Robertson, P.K. (2009). Interpretation of cone penetration tests – unified approach. *Canadian Geotechnical Journal*, 46:1337-1355.
- Robertson, P.K. & Cabal, F.L. (2015). *Guide to Cone Penetration Testing for Geotechnical Engineering*. 6th ed. Gregg Drilling & Testing Inc., Signal Hill, 133 p.
- Rajasekaran, G. & Narasimha Rao, S. (2004). Falling cone method to measure the strength of marine clays. *Ocean Engineering*, 31:1915-1927.
- Schnaid, F. & Odebrecht, E. (2012). *Field Tests and their Applications to Foundation Engineering*. 2nd ed. Oficina de Textos, São Paulo, 223 p. (in Portuguese).
- Shogaki, T. (2006). An improved method for estimating *in-situ* undrained shear strength of natural deposits. *Soils and Foundations*, 46(2):109-121.
- Skempton, A.W. & Northey, R.D. (1952). The sensitivity of clays. *Géotechnique*, 3(1):30-53.
- Sridharan, A.; Narasimha Rao, S. & Venkatappa Rao, G. (1971). Shear strength characteristics of saturated montmorillonite and kaolinite clays. *Soils and Foundations*, 11(3):1-22.
- Suguio, K. (2010). *Quaternary Geology and Environmental Changes*. 2nd ed. Oficina de Textos, São Paulo, 408 p. (in Portuguese).
- Tanaka, H. (1994). Vane shear strength of a Japanese marine clay and applicability of Bjerrum correction factor. *Soils and Foundations*, 34(3):39-48.
- Tanaka, H. (2000). Sample quality of cohesive soils: lessons from three sites, Ariake, Bothekennar and Drammen. *Soils and Foundations*, 40(4):57-74.
- Tanaka, H. (2008). Sampling and sample quality of soft clays. *Proc. 3rd International Conference on Site Characterization*, Taipei, pp. 139-157.
- Tanaka, H.; Hirabayashi, H.; Matsioka, T. & Kaneko, H. (2012). Use of fall cone test as measurement of shear strength for soft clay materials. *Soils and Foundations*, 52(4):590-599.
- Tanaka, H.; Locat, J.; Shibuya, S.; Soon, T.T. & Shiwakoti, D.R. (2001). Characterization of Singapore, Bangkok, and Ariake clays. *Canadian Geotechnical Journal*, 38:378-400.
- Watabe, Y. & Tsuchida, T. (2001). Comparative study on undrained shear strength of Osaka Bay pleistocene clay determined by several kinds of laboratory test. *Soils and Foundations*, 41(5):47-59.
- Wood, D.M. (1990). *Soil Behaviour and Critical State Soil Mechanics*. Cambridge University Press, Cambridge, 488 p.

SOILS and ROCKS

An International Journal of Geotechnical and Geoenvironmental Engineering

Publication of

ABMS - Brazilian Association for Soil Mechanics and Geotechnical Engineering

SPG - Portuguese Geotechnical Society

Volume 40, N. 3, September-December 2017

Author index

Albuquerque, P.J.R.	109	Lopes, F.R.	61, 197
Amin, M.M.	187	Lukiantchuki, J.A.	77
Antão, A.N.	133	Maher, A.	165
Arab, P.B.	255	Mahler, C.F.	31
Araújo Neto, C.L.	51	Marques, S.F.V.	147
Araujo, P.P.	187	Mascarenha, M.M.A.	3
Benetti, L.B.	17	Massad, F.	39
Bernardes, G.P.	77	Matos, F.A.	187
Born, R.B.	219	Melo, M.C.	51
Celestino, T.B.	255	Miranda Neto, M.I.	31
Consoli, N.C.	147, 155, 219, 279	Monteiro, V.E.D.	51
Cordão Neto, M.P.	3	Nóbrega, B.M.A.	51
Corte, M.B.	279	Novaes, J.F.	155
Cunha, R.P.	109	Nunes, A.L.L.S.	61, 197
Diambra, A.	147	Paiva, W.	51
Esquivel, E.R.	77	Passini, L.B.	17, 263
Faro, V.P.	219	Pires, P.J.M.	291
Fernandes, M.M.	229, 243	Porto, T.B.	177
Festugato, L.	147, 279	Queiroz, J.C.B.	187
Freitas Neto, O.	109	Raposo, N.	229, 243
Garcia, J.R.	109	Riyis, M.T.	93
Giacheti, H.L.	93	Romero, E.	3
Gomes, A.T.	229, 243	Salame, C.W.	187
Gomes, R.C.	177	Saldanha, R.B.	155
González, A.A.M.	263	Santos Josefino, C.M.	133
Guerra, N.M.C.	133	Santos Junior, O.F.	109
Hu, J.C.	123	Scheuermann Filho, H.C.	155
Ibraim, E.	147	Schnaid, F.	219
Janbaz, M.	165	Silva, P.C.R.	39
Janbaz, S.	165	Sousa, R.B.A.	51
Juvenio, E.L.	61, 197	Torres, A.C.A.	177
Kormann, A.C.M.	17, 263	Vieira, T.O.	187
Lemos, S.G.F.P.	291	Wang, H.F.	123
Lopes, B.C.F.L.	3	Zhao, J.	123

BUILDING A BETTER WORLD



TPF

PLANEGE CENOR



Engineering and Architectural Consultancy

Geology, Geotechnics, Supervision of Geotechnical Works
Embankment Dams, Underground Works, Retaining Structures
Special Foundations, Soil Improvement, Geomaterials



www.tpfplanegecenor.pt



- > **Prospecção Geotécnica**
Site Investigation
- > **Consultoria Geotécnica**
Geotechnical Consultancy
- > **Obras Geotécnicas**
Ground Treatment-Construction Services
- > **Controlo e Observação**
Field Instrumentation Services and Monitoring Services
- > **Laboratório de Mecânica de Solos**
Soil and Rock Mechanics Laboratory

Certificada ISO 9001 por



Geocontrole



Parque Oriente, Bloco 4, EN10
2699-501 Bobadela LRS
Tel. 21 995 80 00
Fax. 21 995 80 01
e.mail: mail@geocontrole.pt
www.geocontrole.pt


Geocontrole
Geotecnia e Estruturas de Fundação SA



COBA

GEOLOGY AND GEOTECHNICS

Hydrogeology • Engineering Geology • Rock Mechanics • Soil Mechanics • Foundations and Retaining Structures • Underground Works • Embankments and Slope Stability
Environmental Geotechnics • Geotechnical Mapping



- Water Resources Planning and Management
- Hydraulic Undertakings
- Electrical Power Generation and Transmission
- Water Supply Systems and Pluvial and Wastewater Systems
- Agriculture and Rural Development
- Road, Railway and Airway Infrastructures
- Environment
- Geotechnical Structures
- Cartography and Cadastre
- Safety Control and Work Rehabilitation
- Project Management and Construction Supervision



PORTUGAL

CENTER AND SOUTH REGION
Av. 5 de Outubro, 323
1649-011 LISBOA
Tel.: (351) 210125000, (351) 217925000
Fax: (351) 217970348
E-mail: coba@coba.pt
www.coba.pt

Av. Marquês de Tomar, 9, 6.º.
1050-152 LISBOA
Tel.: (351) 217925000
Fax: (351) 213537492

NORTH REGION

Rua Mouzinho de Albuquerque, 744, 1.º.
4450-203 MATOSINHOS
Tel.: (351) 229380421
Fax: (351) 229373648
E-mail: engico@engico.pt

ANGOLA

Praceta Farinha Leitão, edifício nº 27, 27-A - 2.º Dto
Bairro do Maculusso, LUANDA
Tel./Fax: (244) 222338 513
Cell: (244) 923317541
E-mail: coba-angola@netcabo.co.ao

MOZAMBIQUE

Pestana Rovuma Hotel. Centro de Escritórios.
Rua da Sé nº114. Piso 3, MAPUTO
Tel./Fax: (258) 21 328 813
Cell: (258) 82 409 9605
E-mail: coba.mz@tdm.co.mz

ALGERIA

09, Rue des Frères Hocine
El Biar - 16606, ARGEL
Tel.: (213) 21 922802
Fax: (213) 21 922802
E-mail: coba.alger@gmail.com

BRAZIL

Rio de Janeiro
COBA Ltd. - Rua Bela 1128
São Cristóvão
20930-380 Rio de Janeiro RJ
Tel.: (55 21) 351 50 101
Fax: (55 21) 258 01 026

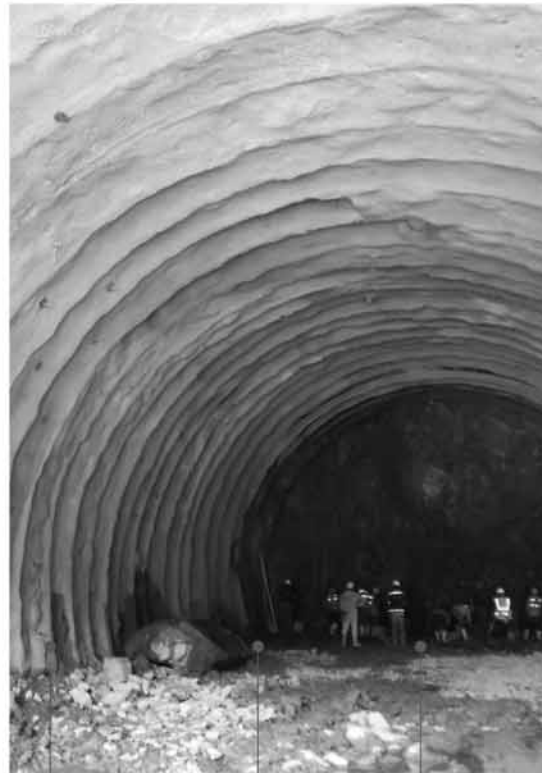
Fortaleza

Av. Senador Virgílio Távora 1701, Sala 403
Aldeota - Fortaleza CEP 60170 - 251
Tel.: (55 85) 3261 17 38
Fax: (55 85) 3261 50 83
E-mail: coba@esc-te.com.br

UNITED ARAB EMIRATES

Corniche Road - Corniche Tower - 5th Floor - 5B
P. O. Box 38360 ABU DHABI
Tel.: (971) 2 627 0088
Fax: (971) 2 627 0087

Much more support to your business.



Incotep - Anchoring Systems

Incotep anchoring Systems is a division of Açotubo Group, which engaged in the development of Anchoring Systems, used in geotechnical and structural applications where high quality prestressing systems are designed to meet diverse needs.

Know our solutions for your processes

- Self Drilling Injection Hollow Bar
- Cold Rolled Thread Bars and Micropiles
- Hot Rolled Thread Bars
- Incotep Tie Rods (Port and Dike Construction)

- Umbrella Tubes Drilling System
- Pipes for Root Piles, among others

www.incotep.com.br
+55 11 2413-2000

INCOTEP
Sistemas de Ancoragem

A company Açotubo Group





Conheça mais:
www.geobrugg.com/pt/taludes



Safety is our nature

TECCO® SYSTEM³ com fio de aço de alta resistência

**SISTEMA ECOLOGICAMENTE
CORRETO PARA ESTABILIZAÇÃO
DE TALUDES**

SPECIALISTS IN GEOTECHNICAL IN-SITU TESTS AND INSTRUMENTATION

GEOTECHNICAL SERVICES (onshore and offshore)

IN-SITU TESTS

- Seismic CPT
- Cone Penetration Testing Undrained-CPTu (cordless system)
- Vane Shear Testing (electrical apparatus)
- Pressuremeter Testing (Menard)
- Flat Dilatometer Test-DMT (Machetti)
- Standard Penetration Test-SPT-T

INSTRUMENTATION

- Instrumentation, installation and direct import
- Routine Monitoring
- Operation and Maintenance
- Engineering analyses
- Consultancy, design & geotechnical engineering services

SAMPLING

- Soil sampling and monitoring
- Groundwater sampling and monitoring
- Field and laboratory testing

ENVIRONMENTAL

- Environmental Services
- Soil and groundwater sampling and monitoring
- Field and laboratory testing



0800 979 3436

São Paulo: +55 11 8133 6030

Minas Gerais: +55 31 8563 2520 / 8619 6469

www.deltageo.com.br deltageo@deltageo.com.br

Whatever your geotechnical challenge

Reinforced soil slopes with Green Terramesh®

Dynamic Rockfall barriers

Rock slope protection with SteelGrid®

we can engineer a better solution

Reinforced Soil Walls with Terramesh® System

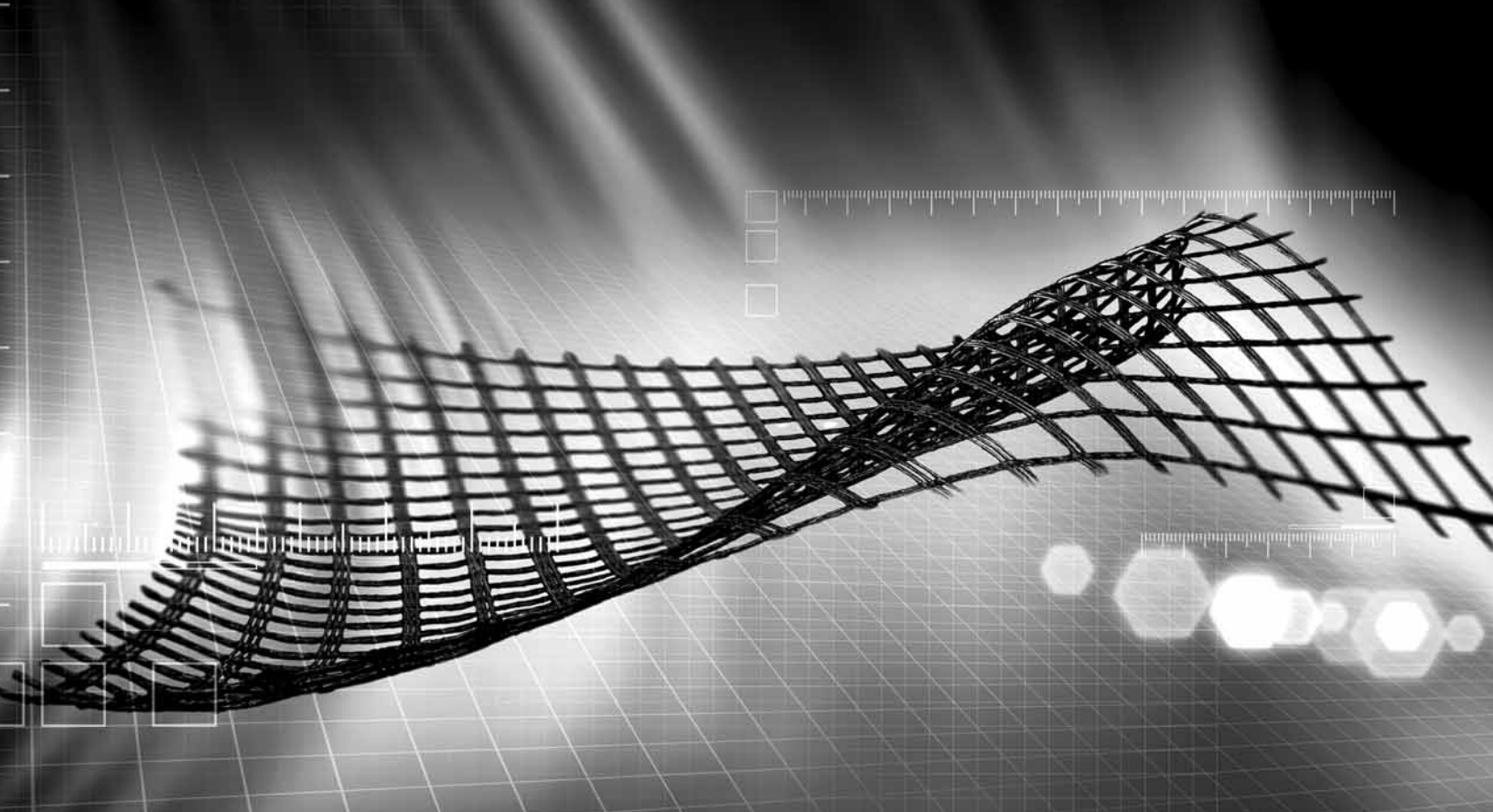
Follow us:



[/maccaferri](#) [/maccaferribr](#) [@Maccaferri_BR](#) [#MaccaferriWorld](#) [/maccaferriworld](#)

For technical data, software and more, visit:
www.maccaferri.com/br

MACCAFERRI



A strong, lasting connection.

With a history of over 150 years of pioneering in geosynthetics, we strive to create solutions for the most diverse engineering challenges.

Our business areas:



**Earthworks and
Foundations**



**Environmental
Engineering**



Roads and Pavements



Hydraulic Engineering

Talk to HUESKER Brasil:
www.HUESKER.com.br
HUESKER@HUESKER.com.br
+55 (12) 3903 9300

Follow HUESKER Brasil in social media:



HUESKER
Ideen. Ingenieure. Innovationen.



Geotechnic and Rehabilitation

TEIXEIRA DUARTE
ENGENHARIA E CONSTRUÇÕES, S.A.

• **Head Office**
Lagoas Park - Edifício 2
2740-265 Porto Salvo - Portugal
Tel.: [+351] 217 912 300
Fax: [+351] 217 941 120/21/26

• **Angola**
Alameda Manuel Van Dunen 316/320 - A
Caixa Postal 2857 - Luanda
Tel.: [+34] 915 550 903
Fax: [+34] 915 972 834

• **Algeria**
Parc Miremont - Rua A, Nº136 - Bouzareah
16000 Alger
Tel.: [+213] 219 362 83
Fax: [+213] 219 365 66

• **Brazil**
Rua Iguatemi, nº488 - 14° - Conj. 1401
CEP 01451 - 010 - Itaim Bibi - São Paulo
Tel.: [+55] 112 144 5700
Fax: [+55] 112 144 5704

• **Spain**
Avenida Alberto Alcocer, nº24 - 7° C
28036 Madrid
Tel.: [+34] 915 550 903
Fax: [+34] 915 972 834

• **Mozambique**
Avenida Julyus Nyerere, 130 - R/C
Maputo
Tel.: [+258] 214 914 01
Fax: [+258] 214 914 00

Instructions for Submission of Manuscripts

Category of the Papers

Soils and Rocks is the international scientific journal edited by the Brazilian Association for Soil Mechanics and Geotechnical Engineering (ABMS) and the Portuguese Geotechnical Society (SPG). The aim of the journal is to publish (in English) original research and technical works on all geotechnical branches.

According to its content the accepted paper is classified in one of the following categories: Article paper, Technical Note, Case Study or Discussion. An article paper is an extensive and conclusive dissertation about a geotechnical topic. A paper is considered as a technical note if it gives a short description of ongoing studies, comprising partial results and/or particular aspects of the investigation. A case study is a report of unusual problems found during the design, construction or the performance of geotechnical projects. A case study is also considered as the report of an unusual solution given to an ordinary problem. The discussions about published papers, case studies and technical notes are made in the Discussions Section.

When submitting a manuscript for review, the authors should indicate the category of the manuscript, and is also understood that they:

- assume full responsibility for the contents and accuracy of the information in the paper;
- assure that the paper has not been previously published, and is not being submitted to any other periodical for publication.

Manuscript Instructions

Manuscripts must be written in English. The text is to be typed in a word processor (preferably MS Word), **single column**, using ISO A4 page size, left, right, top, and bottom margins of 25 mm, Times New Roman 12 font, and line spacing of 1.5. All lines and pages should be numbered. The text should be written in the third person.

The first page of the manuscript must include the title of the paper followed by the names of the authors with the abbreviation of the most relevant academic title. The affiliation, address and e-mail must appear below each author's name. An abstract of 200 words follows after the author's names. A list with up to six keywords at the end of the abstract is required.

Although variations on the sequence and title of each section are possible, it is suggested that the text contains the following sections: Introduction, Material and Methods, Results, Discussions, Conclusions, Acknowledgements, References and List of Symbols. A brief description of each section is given next.

Introduction: This section should indicate the state of the art of the problem under evaluation, a description of the problem and the methods undertaken. The objective of the work should be clearly presented at the end of the section.

Materials and Methods: This section should include all information needed to the reproduction of the presented work by other researchers.

Results: In this section the data of the investigation should be presented in a clear and concise way. Figures and tables should not repeat the same information.

Discussion: The analyses of the results should be described in this section.

Conclusions: The content of this section should be based on the data and on the discussions presented.

Acknowledgements: If necessary, concise acknowledgements should be presented in this section.

References: References to other published sources must be made in the text by the last name(s) of the author(s), followed by the year of publication, similarly to one of the two possibilities below:

...while Silva & Pereira (1987) observed that resistance depended on soil density... or It was observed that resistance depended on soil density (Silva & Pereira, 1987).

In the case of three or more authors, the reduced format must be used, e.g.: Silva *et al.* (1982) or (Silva *et al.*, 1982). Two or more citations belonging to the same author(s) and published in the same year are to be distinguished with small letters, e.g.: (Silva, 1975a, b, c.). Standards must be cited in the text by the initials of the entity and the year of publication, e.g.: ABNT (1996), ASTM (2003).

Full references shall be listed alphabetically at the end of the text by the first author's last name. Several references belonging to the same author shall be cited chronologically. Some examples are listed next:

Papers: Bishop, A.W. & Blight, G.E. (1963). Some aspects of effective stress in saturated and unsaturated soils. *Geotechnique*, 13(2):177-197.

Books: Lambe, T.W. & Whitman, R.V. (1979). *Soil Mechanics*, SI Version. John Wiley & Sons, New York, 553 p.

Book with editors: Sharma, H.D.; Dukes, M.T. & Olsen, D.M. (1990). Field measurements of dynamic moduli and Poisson's ratios of refuse and underlying soils at a landfill site. Landva, A. & Knowles, G.D. (eds), *Geotechnics of Waste Fills - Theory and Practice*, American Society for Testing and Materials - STP 1070, Philadelphia, pp. 57-70.

Proceedings (printed matter or CD-ROM): Jamiolkowski, M.; Ladd, C.C.; Germaine, J.T. & Lancellotta, R. (1985). New developments in field and laboratory testing of soils. Proc. 11th Int. Conf. on Soil Mech. and Found. Engn., ISSMFE, San Francisco, v. 1, pp. 57-153. (specify if CD ROM).

Thesis and dissertations: Lee, K.L. (1965). *Triaxial Compressive Strength of Saturated Sands Under Seismic Loading Conditions*. PhD Dissertation, Department of Civil Engineering, University of California, Berkeley, 521 p.

Standards: ASTM (2003). *Standard Test Method for Particle Size Analysis of Soils - D 422-63*. ASTM International, West Conshohocken, Pennsylvania, USA, 8 p.

Internet references: Soils and Rocks available at <http://www.abms.com.br> and downloaded on August 6th 2003.

On line first publications must also bring the digital object identifier (DOI) at the end.

Figures shall be either computer generated or drawn with India ink on tracing paper. Computer generated figures must be accompanied by the corresponding digital file (.tif, .jpg, .pcx, etc.). All figures (graphs, line drawings, photographs, etc.) shall be numbered consecutively and have a caption consisting of the figure number and a brief title or description of the figure. This number should be used when referring to the figure in text. Photographs should be black and white, sharp, high contrasted and printed on glossy paper.

Tables shall be numbered consecutively in Arabic and have a caption consisting of the table number and a brief title. This number should be used when referring to the table in the text. Units should be indicated in the first line of the table, below the title of each column. Acronyms should be avoided. When applicable, the units should come right below the corresponding column heading. Additional comments can be placed as footnotes.

Equations shall appear isolated in a single line of the text. Numbers identifying equations must be flushed with the right margin. International System (SI) units must be used. The definitions of the symbols used in the

equations must appear in the List of Symbols. It is recommended that the symbols used are in accordance with Lexicon in 8 Languages, ISSMFE (1981) and the ISRM List of Symbols.

The text of the submitted manuscript (including figures, tables and references) intended to be published as an article paper or a case history should not contain more than 30 pages, formatted according to the instructions mentioned above. Technical notes and discussions should have no more than 15 and 8 pages, respectively. Longer manuscripts may be exceptionally accepted if the authors provide proper explanation for the need of the required extra space in a cover letter.

Discussion

Discussions must be written in English. The first page of a discussion should contain:

The title of the paper under discussion;

Name of the author(s) of the discussion, followed by their position, affiliation, address and e-mail. The author(s) of the discussion should refer to himself (herself/themselves) as the reader(s) and to the author(s) of the paper as the author(s).

Figures, tables and equations should be numbered following the same sequence of the original paper. All instructions previously mentioned for the preparation of article papers, case studies and technical notes also apply to the preparation of discussions.

Editorial Review

Each paper will be evaluated by reviewers selected by the editors according to the subject of the paper. The authors will be informed about the results of the review process. If the paper is accepted, the authors will be required to submit a version of the revised manuscript with the suggested modifications. If the manuscript is rejected for publication, the authors will be informed about the reasons for rejection. In any situation comprising modification of the original text, classification of the manuscript in a category different from that proposed by the authors, or rejection, the authors can reply presenting their reasons for disagreeing with the reviewer comments.

Submission

The author(s) must upload a digital file of the manuscript to the Soils and Rocks website.

Follow Up

The online management system will provide a password to the corresponding author, which will enable him/her to follow the reviewing process of the submitted manuscript at the Soils and Rocks website.

Volume 40, N. 3, September-December 2017**Table of Contents***MANUEL ROCHA LECTURE**Stress History of Soils from Cone Penetration Tests*

P.W. Mayne

203

*ARTICLES**Stabilised Soil Layers Enhancing Performance of Transverse-Loaded Flexible Piles on Lightly Bonded Residual Soils*

N.C. Consoli, V.P. Faro, F. Schnaid, R.B. Born

219

Anchored Retaining Walls in Granite Residual Soils I – Parametric Study

N. Raposo, A.T. Gomes, M.M. Fernandes

229

Anchored Retaining Walls in Granite Residual Soils II. A Method for Preliminary Design

N. Raposo, A.T. Gomes, M.M. Fernandes

243

Influence of Traverse Velocity and Pump Pressure on the Efficiency of Abrasive Waterjet for Rock Cutting

P.B. Arab, T.B. Celestino

255

Rainfall Effects on Pore Pressure Changes in a Coastal Slope of the Serra do Mar in Santa Catarina

A.A.M. González, L.B. Passini, A.C.M. Kormann

263

Development of a Cyclic Simple Shear Apparatus

M.B. Corte, L. Festugato, N.C. Consoli

279

The Undrained Strength of Soft Clays Determined from Unconventional and Conventional Tests

S.G.F.P. Lemos, P.J.M. Pires

291